CRANFIELD UNIVERSITY

ALESSANDRO GIULIANO

ENHANCED PIEZOELECTRIC ENERGY HARVESTING POWERED WIRELESS SENSOR NODES USING PASSIVE INTERFACES AND POWER MANAGEMENT APPROACH

SCHOOL OF APPLIED SCIENCES
Manufacturing & Materials Department

PhD Thesis
Academic Year: 2010-2014

Supervisor: Prof. Meiling Zhu

ABSTRACT

Low-frequency vibrations typically occur in many practical structures and systems when in use, for example, in aerospaces and industrial machines. Piezoelectric materials feature compactness, lightweight, high integration potential, and permit to transduce mechanical energy from vibrations into electrical energy. Because of their properties, piezoelectric materials have been receiving growing interest during the last decades as potential vibration-harvested energy generators for the proliferating number of embeddable wireless sensor systems in applications such as structural health monitoring (SHM). The basic idea behind piezoelectric energy harvesting (PEH) powered architectures, or energy harvesting (EH) more in general, is to develop truly “fit and forget” solutions that allow reducing physical installations and burdens to maintenance over battery-powered systems. However, due to the low mechanical energy available under low-frequency conditions and the relatively high power consumption of wireless sensor nodes, PEH from low-frequency vibrations is a challenge that needs to be addressed for the majority of the practical cases. Simply saying, the energy harvested from low-frequency vibrations is not high enough to power wireless sensor nodes or the power consumption of the wireless sensor nodes is higher than the harvested energy. This represents a main barrier to the widespread use of PEH technology at the current state of the development, despite the advantages it may offer.

The main contribution of this research work concerns the proposal of a novel EH circuitry, which is based on a whole-system approach, in order to develop enhanced PEH powered wireless sensor nodes, hence to compensate the existing mismatch between harvested and demanded energy. By whole-system approach, it is meant that this work develops an integrated system-of-systems rather than a single EH unit, thus getting closer to the industrial need of a ready-to-use energy-autonomous solution for wireless sensor applications such as SHM. To achieve so, this work introduces:

- Novel passive interfaces in connection with the piezoelectric harvester that permit to extract more energy from it (i.e., a complex conjugate

impedance matching (CCIM) interface, which uses a PC permalloy toroidal coil to achieve a large inductive reactance with a centimetre-scaled size at low frequency; and interfaces for resonant PEH applications, which exploit the harvester's displacement to achieve a mechanical amplification of the input force, a magnetic and a mechanical activation of a synchronised switching harvesting on inductor (SSHI) mechanism).

- A novel power management approach, which permits to minimise the power consumption for conditioning the transduced signal and optimises the flow of the harvested energy towards a custom-developed wireless sensor communication node (WSCN) through a dedicated energy-aware interface (EAI); where the EAI is based on a voltage sensing device across a capacitive energy storage.

Theoretical and experimental analyses of the developed systems are carried out in connection with resistive loads and the WSCN under excitations of low frequency and strain/acceleration levels typical of two potential energy-autonomous applications, that are: 1) wireless condition monitoring of commercial aircraft wings through non-resonant PEH based on Macro-Fibre Composite (MFC) material bonded to aluminium and composite substrates; and 2) wireless condition monitoring of large industrial machinery through resonant PEH based on a cantilever structure.

It is shown that under similar testing conditions the developed systems feature a high performance in comparison with other architectures reported in the literature or currently available on the market. Power levels up to 12.16 mW and 116.6 μW were respectively measured across an optimal resistive load of 66 and 277 kΩ for an implemented non-resonant MFC energy harvester on aluminium substrate and a resonant cantilever-based structure when no interfaces were added into the circuits. When the WSCN was connected to the harvesters in place of the resistive loads, data transmissions as fast as 0.4 and 15.8 s were also respectively measured. By use of the implemented passive interfaces, a maximum power enhancement of around 95% and 452% was

achieved in the two tested cases and faster data transmissions obtained with a maximum percentage improvement around 36% and 73%, respectively. By the use of the EAI in connection with the WSCN, results have also shown that the overall system's power consumption is as low as a few microwatts during non-active modes of operation (i.e., before the WSCN starts data acquisition and transmission to a base station).

Through the introduction of the developed interfaces, this research work takes a whole-system approach and brings about the capability to continuously power wireless sensor nodes entirely from vibration-harvested energy in time intervals of a few seconds or fractions of a second once they have been firstly activated. Therefore, such an approach has potential to be used for real-world energy-autonomous applications of SHM.

Keywords:

energy autonomous; self powered; complex conjugate impedance matching; synchronysed switching harvesting on inductor; SSHI; wireless sensor network; WSN; structural health monitoring; SHM

LIST OF PUBLICATIONS

1. Giuliano, A., Qasim, A. and Zhu, M. “Characterization of a Low-Frequency Strain Energy Harvester for a Self-Powered Wireless Sensor Network”, submitted to *IEEE/ASME Transactions on Mechatronics*.
2. Giuliano A. and Zhu, M. “A Passive Impedance Matching Interface Using a PC Permalloy Coil for Practically Enhanced Piezoelectric Energy Harvester Performance at Low Frequency”, *IEEE Sensor Journal*, vol. 14, no. 8, pp. 2773-81, 2014.
3. Marsic, V., Giuliano, A. and Zhu, M. (2013): “Low Power Consumption Wireless Sensor Communication System Integrated with an Energy Harvesting Power Source”, *Sensors & Transducers Journal*, vol. 18, Special Issue, pp.156-65.
4. Giuliano A. and Zhu, M. (2013): “Experimental Study of a Passive Impedance Matching Interface Based on a Centimeter-Size High Inductance Coil for Practically Enhanced Piezoelectric Energy Harvester Performance at Low Frequency”, *IEEE International Conference on Green Computing and Communications*, Beijing, China, 20-23 Aug 2013, pp. 1659-61.
5. Daniels, A., Giuliano, A., Zhu, M. and A. Tiwari, (2013): “Modeling, Validation and Design Analyses of a Piezoelectric Cymbal Transducer for Non-Resonant Energy Harvesting”, *IEEE International Conference on Green Computing and Communications*, Beijing, China, 20-23 Aug 2013, pp. 1665-67.
6. Giuliano, A., Marsic, V. and Zhu, M. (2012): “Implementation and Testing of an Elastic Strain Powered Wireless Sensing System for Energy-Autonomous Applications”, *IEEE International Conference on Green Computing and Communications*, Besançon, France, 20-23 Nov 2012, pp. 681-84.
7. Marsic, V., Giuliano, A., Zhu, M. and Williams, S. (2012): “Performance testing of a Low Power Consumption System Integrated with an Energy Harvesting Power Source”, *Sensordevices 2012: The Third International*

Conference on Sensor Device Technologies and Applications, Rome, Italy, 19-24 Aug 2012, pp. 112-18.

8. Zhu, M., Giuliano A. and Marsic, V. (2012): “Low-power consumption energy harvesting circuitry for smart energy-aware activation of wireless sensor systems”, UK Patent Application No. 1213807.9, Journal 6434, 12 Sept 2012.

ACKNOWLEDGEMENTS

My thanks go to all those people who have helped me throughout my academic years at Cranfield University. First and foremost, my thanks go to my supervisor Prof. Meiling Zhu for her careful guidance, technical help, humanity, and real-life example of success based on achievements. Without her support and trust I could have never experienced and joined worldwide top-level researchers and professional people from industries as well as governmental bodies. I would like to thank all the technical staff along with my office colleagues at the Manufacturing & Materials Department for their practical support and friendship that have helped me to complete my research work and understand more about international cultures and the world alike. I would like to show my gratitude to my colleague Alice Daniels, who first helped me to settle down in the UK, and Mr. Vlad A. Marsic for being a truly remarkable friend, in life as well as in the office. I would like to thank my girlfriend, Miss Brigitta Varro, who has been able to transform my life experience in a much more pleasant one and give me the best reason to never give up. My thanks for her patience and understanding during all those times when, responsibly or irresponsibly, I have preferred spending my time together with my paperwork rather than her. Special thanks go to my family: my parents and my brother, in particular, who has always been ready to support my choices with the right word at the right time. I would like to thank my housemates (David, Susie, Miks, Laurita, and Dr. Joao Duro) for their “latino” life-approach which, despite the nationality of origin, has constantly helped me to find a good reason for aiming or not aiming at something. Last but not least, my thanks go to all those students I have had the pleasure to get acquainted with or not during these years: people who have been consciously or unconsciously teaching me a lot by simply walking on campus around me, exchanging with me a glance or missing a smile during an usual cloudy day.

“Non est quod timeas ne operam perdideris, si tibi didicisti.”

Lucio Anneo Seneca

TABLE OF CONTENTS

LIST OF FIGURES

LIST OF TABLES

LIST OF ABBREVIATIONS

AC	Alternating Current
CCIM	Complex Conjugate Impedance Matching
CPU	Central Processing Unit
CU	Cranfield University
DC	Direct Current
DCM	Discontinuous Conduction Mode
DSSH	Double Synchronised Switch Harvesting
DS-SS	Direct-sequence spread spectrum
EAI	Energy-Aware Interface
EC	Electrochemical Capacitors
ELF	Extremely Low Frequency
EH	Energy Harvesting
ESR	Equivalent Series Resistance
ESSH	Enhanced Synchronised Switch Harvesting
FET	Field-Effect Transistor
FH-SS	Frequency-hopping spread spectrum
FSK	Frequency-shift keying
FSM	Finite State Machine
HVAC	Heating, Ventilation, and Air Conditioning
IC	Integrated Circuit
IEEE	Institute of Electrical and Electronics Engineers
IETF	Internet Engineering Task Force
ISM	Industrial, Scientific, and Medical
LAN	Local Area Network
LDO	Low Drop-Out
LEACH	Low Energy Adaptive Clustering Hierarchy
LiPON	Lithium Phosphorus Oxynitride
MAC	Media Access Control
MEC	Micro-Energy Cell
MECH	Maximum Energy Cluster Head
MEMS	Micro-Electro-Mechanical Systems

MFC	Macro-Fibre Composite
MPPT	Maximum Power Point Tracker
MsM	Magnetostrictive Material
NIC	Negative Immittance Converter
PACT	Power Aware Clustered Time division Multiple Access
PEG	Piezoelectric Energy Generator
PEH	Piezoelectric Energy Harvesting
PIC	Positive Impedance Converter
PMM	Power Management Module
PVDF	Polyvinylidene Fluoride
PWM	Pulse-Width Modulation
PZT	Lead Zirconate Titanate
RF	Radio Frequency
RAM	Random-Access Memory
ROM	Read-Only Memory
RISC	Reduced Instruction Set Computing
SB	Sensor Block
SECE	Synchronous Electric Charge Extraction
SHM	Structural Health Monitoring
SMAC	Sensor Media Access Control
SSDCI	Synchronised Switching and Discharging to a storage Capacitor through an Inductor
SSHI	Synchronised Switch Harvesting on Inductor
SSHI-MR	Synchronised Switch Harvesting on Inductor using Magnetic Rectifier
TDMA	Time division Multiple Access
VCVS	Voltage-Controlled Voltage Source
WCB	Wireless Communication Block
WLAN	Wireless Local Area Network
WSMB	Wireless Sensor Management Block
WSN	Wireless Sensor Network

1 INTRODUCTION

Energy harvesting (EH) is scavenging energy from ambient sources (e.g., solar light, heat, wind, vibration) in order to directly supply power to electronic devices or store energy into an electrical storage reservoir (usually a rechargeable battery or capacitor) for a later use. Although the EH concept is not new, its transition from watt to nano-watt scaled power has been progressing only in the last couple of decades with the advances of micro electromechanical systems. Such advances have significantly raised the promise that many low-power electronic devices can have a built-in EH functionality in the near future so as to become truly self-sufficient in energy supply, called energy-autonomous devices in this thesis. Vibration EH by use of piezoelectric materials, in particular, is a research field of growing interest due to the fact that mechanical vibrations are almost ubiquitous in the environment around us and piezoelectric transducers are compact, lightweight, and characterised by high integration potential for applications. However, the low amount of power that can be delivered from small-scale piezoelectric energy harvesters at the current state of the development is proving a barrier to the adoption of this technology. Device optimisation can be a way to increase the power density of piezoelectric energy harvesters, but the use of the “harvesting circuitry” connected to the harvesters to condition and/or manage the generated power is another effective way to enhance the overall performance of PEH systems.

This chapter introduces the context of this research work. It starts with an overview of the EH concept, including the research background with focus on self-powered wireless sensor applications, and then moves to the motivation and challenges of the research, the aim and objectives, the contribution and novelties, the adopted methodology and scope, and finally ends with outlining the structure of this thesis.

1.1 Research background

The rapid evolution of electronic devices and integration technologies, together with the development of wireless systems, have been removing structural

constraints and leading to the implementation of “smart” environments around us [1]. As a consequence, there has been a large proliferation of portable and remote sensing devices, such as wireless sensor networks (WSNs), which are more and more widely used in military, industrial, and civilian applications. Since power to these devices has to be supplied locally, the use of batteries has represented for years the most intuitive solution. However, even if battery-powered systems are power-cords independent, periodic battery recharging/replacement and displacement introduce additional costs and burdens to maintenance.

Different research studies are bringing about higher energy-density, smaller and lower cost batteries; nevertheless, for applications where power has to be supplied to locations that are difficult to be reached or to hazardous places, the use of batteries is not yet an option. In order to address these challenges, EH from surrounding sources may provide a truly “fit-and-forget” battery alternative, which is why in recent years there has been a significant growing interest in this field.

A variety of energy sources such as mechanical, thermal, radiant, and biochemical sources have been studied as potential alternatives in energy supply. Figure 1-1 shows the average power density levels that can up to date be achieved from a variety of ambient sources.

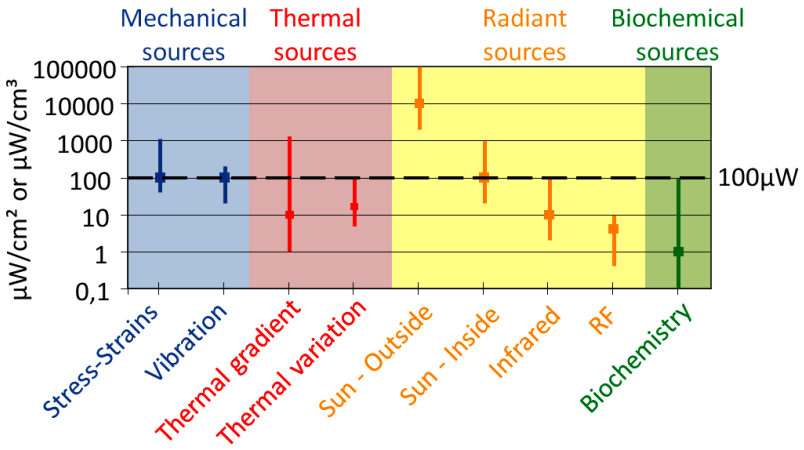

Figure 1-1 Potential EH sources and their average power density levels (Figure reprinted from [2])

Among energy harvesters, thermoelectric generators, vibration/kinetic driven power generators, and solar cells are more widely studied because of their ubiquity, high efficiency, and potentials to miniaturisation.

Thermal gradient can be conveniently converted to electricity, and there are many potential sources such as exothermally heated ocean water (85ºC), solar ponds (50ºC), natural lake thermoclines (10-20ºC), and utility power plant waste heat (15ºC) [3-4]. However, thermal energy is hard to control, cannot be used for medical implant, and the conversion efficiency is lower in comparison with solar and vibration energy sources.

From Figure 1-1, it can be observed that outdoor solar energy has the highest power density, but for indoor solar energy this is rather low. Although solar cells are a mature technology and a mature research area, solar lighting is not really suitable for embedded applications where no or not enough light is available [5]. Vibration energy shows a relatively high power density too and has been demonstrated to offer great potential [6-9].

Table 1-1 shows a comparison of the power densities achieved in some specific works reported in the literature.

Table 1-1 Comparison of power density for a number of ambient energy sources

Ambient source	Power density (μW/cm^3)	References
Solar	Outdoor:15000	[6]
	Indoor:10	[6]
Vibration	Electrostatic: 50~100	[7-8]
	Electromagnetic:119	[9]
	Piezoelectric: 250	[5]
	Magnetostrictive:606	[10]
Thermal	60 (at 5ºC gradient)	[11]

In order to convert mechanical energy from vibrations into electrical energy, electromagnetic, piezoelectric, electrostatic, and magnetostrictive transduction mechanisms have been typically used in literature [10] and a schematic representation of those is shown in Figure 1-2 Schematic representation of

typical electromechanical transducers: (a) electromagnetic, (b) piezoelectric, (c) electrostatic, (d) magnetostrictive (Figure adapted from [5], [10])

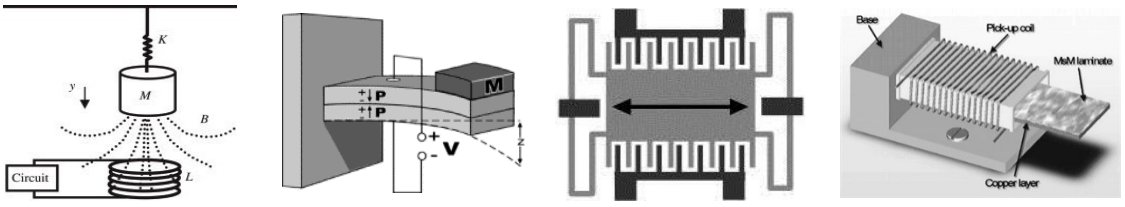

(a) **(b)** **(c)** **(d)**

Figure 1-2 Schematic representation of typical electromechanical transducers: (a) electromagnetic, (b) piezoelectric, (c) electrostatic, (d) magnetostrictive (Figure adapted from [5], [10])

From Table 1-1 it can be observed that the average power density for vibration energy harvesters is lower than what can be achieved from outdoor lighting, but higher with regards to indoor lighting or thermal sources.

The magnetostrictive transduction mechanism, in particular, permits to achieve relatively high power density due to the capability of magnetostrictive materials (MsMs), such as Metglas, to reach magnetomechanical coupling factors higher than 0.9. MsMs, however, perform well in the high frequency spectrum whilst most of the available ambient vibrations are in a range up to 200 Hz [5], [12]. PEH devices have been studied more intensively than other vibration harvesters as, further than high power density output, they offer advantages such as precise mechanical control, high integration potential and a simple configuration [5], [13-24]. Indeed, piezoelectric materials are usually integrated onto a host vibrating structure and electromechanically coupled to them. When strain occurs because of the deformation or bending of the vibrating structure, hence of the piezoelectric material, electric charge is generated.

Table 1-2 shows a comparison summary of the advantages and disadvantages of different vibration EH mechanisms.

Table 1-2 Summary of the comparison of advantages and disadvantages of different vibration EH mechanisms

Type	Advantages	Disadvantages
Electromagnetic	• No need of active material • No need of external voltage source	• Large form factor due to magnets and pick-up coil • Hard integration in MEMS environment
Electrostatic	• No need of smart material • Compatible with MEMS • Medium voltage output	• Need of an external voltage source • Need of structural constraints
Piezoelectric	• No need of external voltage source • High voltages output • Precise mechanical control • Compact configuration	• Depolarisation issue • Brittleness of bulk piezo-layers • Charge leakage • High output impedance
Magnetostrictive	• High coupling factor • No depolarisation issue • Large flexibility	• Non-linear effect • Need a vibration pick-up coil • Hard integration in MEMS environment • May need bias magnets

Examples of PEH systems have been reported in literature and mainly focussed on increasing the efficiency of the elctromechanical coupling so as to increase the generated electrical energy while keeping down the size of the active element. In order to make use of the harvested energy, PEH systems also include a power management module (PMM). The PMM is the link between the energy source of the system (i.e., the piezoelectric harvester) and the electrical load of the end-application (e.g., a wireless sensor node) as shown in the basic block diagram of a PEH powered wireless sensor system depicted in Figure 1-3.

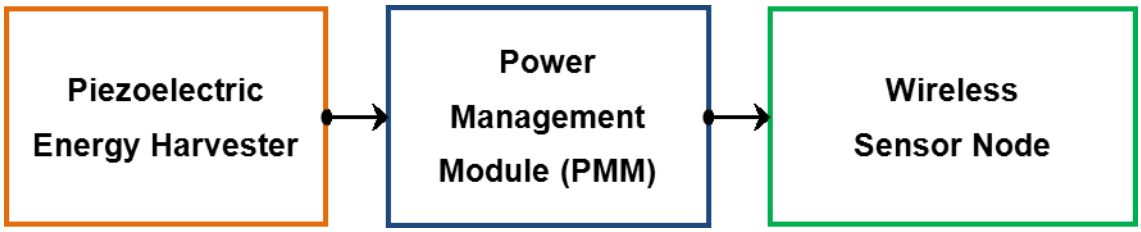

Figure 1-3 Basic block diagram of a PEH powered system

As shown in Figure 1-4, the PMM performs two important tasks, which are:

1. Conditioning of the piezoelectric-transduced signal;
2. Storage of the harvested energy.

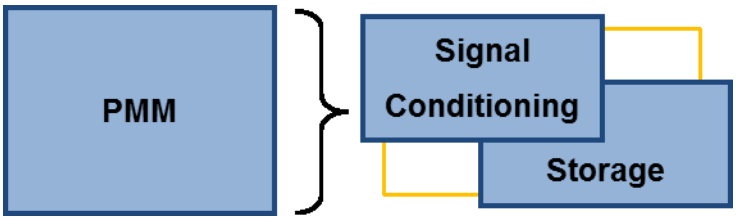

Figure 1-4 PMM internal block diagram

Since the electrical load of the end-application is typically an electronic device that requires a stabilised DC power supply, then conditioning the piezoelectric-transduced signal consists of: an AC/DC (Alternating Current-to-Direct Current) rectification stage as the harvester's electrical output is alternating being the deformation in vibrating structures also alternating; and a DC/DC regulation stage. Ambient sources are generally discontinuous and the spectrum of commonly occurring vibrations is characterised by high spikes, shortly damped to very-low levels that are difficult to harvest. Since at times ambient energy could not be present at all, electric-charge accumulators such as (super)-capacitors or batteries are also integrated into the PMM. They provide different energy performance in a number of footprints and configurations but, due to their lower charge leakage through time, batteries are preferable in applications where long-term energy storage is required. Once energy has been stored, it can supply the electrical load for the end-application all at once under higher peaks of power. For wireless sensor applications, the electrical load as depicted in Figure 1-5 consists of at least three functional blocks: the sensors block (SB), the wireless sensor management block (WSMB), and the wireless communication block (WCB).

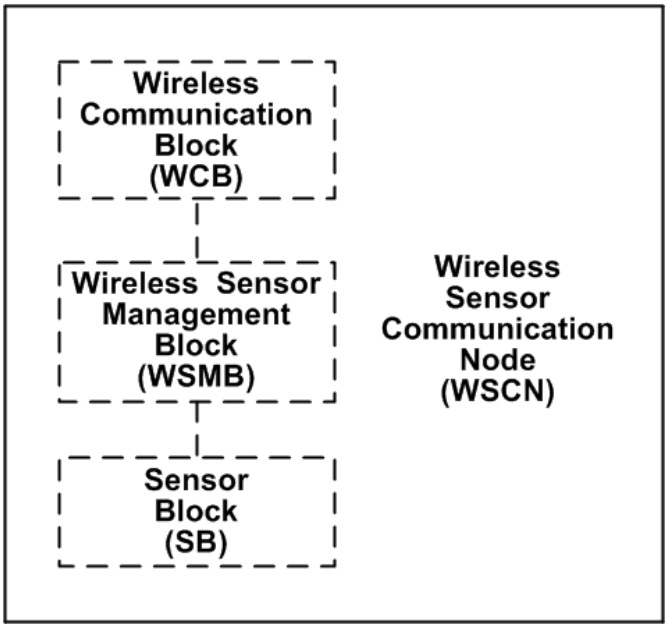

Figure 1-5 Block diagram of a wireless sensor communication node (WSCN)

The SB interacts with the external environment and transforms specific stimuli (e.g. temperature, acceleration, light intensity, pressure, etc.) in electrical signals. The WSMB takes data from the SB and, after processing, sends them to the WCB. The WCB transmits via air the data provided by the WSMB to a base station, which can be linked to internet or directly to the user. All together, the SB, the WSMB, and the WCB make a wireless sensor communication node (WSCN) that, in turn, makes the basis of a WSN.

One main limitation for supplying a WSN by EH is the mismatch between energy harvested and energy demanded. This is true especially in the case of low-frequency applications due to the low mechanical energy levels available for EH. In particular, PEH at low frequency is a relatively new topic and has not been the focal point in the research community although the low-frequency range of structural vibrations occurrs around structures such as in aerospace and industrial monitoring. As much as increasing the harvesting capability of the power generator, minimising the power consumption of the end-application load also needs further consideration towards the development of a whole energy-autonomous system-of-systems. In particular, the power consumption level of a WSCN is higher in the active phases of data acquisition and transmission when compared to the real-time EH capability of small-scale piezoelectric energy

harvesters. Although the active operation of the WSCN can be duty-cycled, this often depends on the intended application. In such a framework, this research work focusses on PEH for wireless sensor applications and, in particular, on the development of a novel EH circuitry for a practically enhanced system performance under low-frequency vibrations. The main target of this research relates to the application of energy-autonomous structural health monitoring (SHM) by use of self-powered WSCNs. As it has been shown by previous examples in the literature [25-26], self-powered systems can promote easy access to up-to-date asset information for better decision making on operations, service and maintenance, and improve reliability and safety of industrial businesses. There are actually widespread needs of such energy-autonomous systems for SHM in the railway, automotive, aircraft, marine, and military industries.

1.1.1 SHM applications

SHM is used to identify damage in structures to improve safety and reliability of mechanical systems. Monitoring has been a manual process in the majority of the cases and requires experienced people. Since lack of information cannot be avoided without increasing costs and time, a common trend has been to adopt objective protocols of damage detection, run in an automated manner, in place of subjective inspection run by a human operator according to a time-based maintenance schedule. The adoption of WSNs, capable to collect data such as temperature, light intensity, humidity, proximity, etc. and transmit them wirelessly to a central hub for remote analysis represent an effective solution to the demand of high technology industries for managing their products over life cycles. WSNs can perform local analysis and control for functions such as data logging, event detection, alarming, short message service notifications, and web-based network data visualisation. Therefore, WSNs can allow easy access to information for better decision-making in the maintenance process of high technology products and, furthermore, do not add weight or burdens to structures as running wires or cabling to main.

Most prior wireless structural monitoring systems have relied on continuous power supplied by batteries [27] but periodic replacing or recharging represents an additional maintenance task to be performed. A few studies on purely passive systems (which do not need any external power source) for SHM have been carried out. For instance, in [28], Guyomar *et al.* proposed a method of impact location estimation for SHM based on resistively shunted piezoelectric inserts. This method relies on the comparison of the electrical energy extracted by closely laid piezoelectric elements, which are considered as local electromechanical dampers and give insight of the energy flow. However, such a passive detection technique is based on testing upon an infinite lossless beam and it does not take into account the effects of simultaneous multiple impacts, which possibly lead to interferences of waves and cancellation of the energy at the location of a piezoelectric element. On the contrary, wireless sensors can constantly monitor through direct measurements and automatically report on the required information so as to identify early warning signs of structural failure [29].

Wireless sensor applications for SHM are thus interesting applications for the deployment of EH and vibration EH, in particular, being vibrations almost ubiquitous around us. Therefore, PEH can be an optimal solution through developments of compact and light-weight self-powered wireless sensor systems capable to convert strain energy into electrical energy, measure, record, and transmit useful data in a completely energy-autonomous manner.

For example, electrical energy can be freely generated by passing cars on bridges to detect their health status via piezoelectric inserts as shown in Figure 1-6.

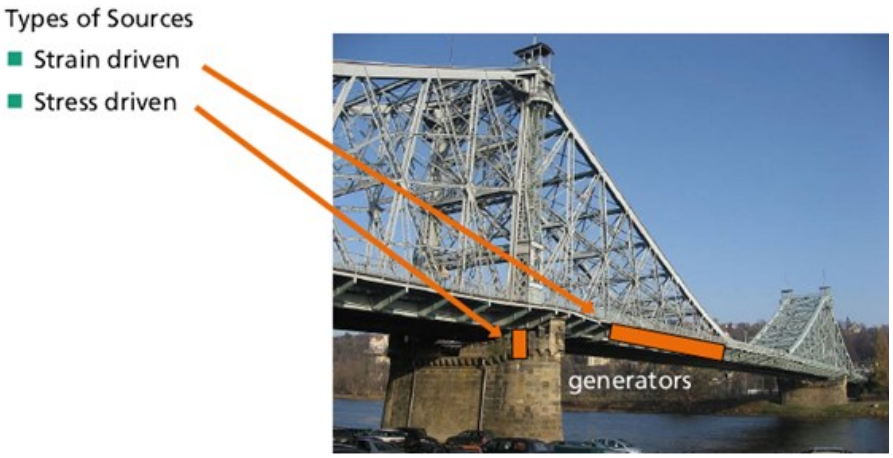

Figure 1-6 Bridge monitoring by mean of PEH powered wireless sensors (Figure courtesy of Fraunhofer-Gesellschaft Inc.)

Also buildings progressively accumulate damages during their operational lifetime due to seismic events, unforeseen foundation settlement, material aging, design error, etc. Harvesting pads can collect energy from the vibrations of trains passing through the railway by using piezoelectric architectures such as shown in Figure 1-7.

Figure 1-7 Pads for PEH from trains (Figure courtesy of Innowattech Ltd)

The pads can harvest mechanical energy and transduce it into electrical energy for counting the number, weight, diameter and position of wheels, or for detecting speed. PEH sensors can track damages on commercial and military vehicles including ships, aircrafts, and helicopters. Particularly, they can determine dynamic and static loads on rotating components without sleep rings and batteries by use of PEH powered wireless nodes as shown in Figure 1-8.

Figure 1-8 PEH powered wireless sensors aboard a helicopter (Figure courtesy of MicroStrain Inc.)

SHM military applications of PEH powered wireless sensor systems may also include perimeter defense such as oil pipeline protection. In collaboration with Intel, for example, BP has run a project for preventive maintenance on an oil tanker in the North Sea by use of sensor networks to support preventive maintenance onboard the ship. More in general, environmental/habitat monitoring offer plenty of case applications for energy-autonomous WSNs in relation to the integrity of the soil, water conditions, air regulations with regards to temperature and humidity. For instance, the FireBug wildfire instrumentation system developed by the University of California (Berkeley – CA) is a GPS-enabled wireless thermal sensor network based on TinyOS that self-organise itself for collecting real-time data in wild fire environments in order to allow predictive analysis of the evolving fire behavior [30]. In addition, energy-autonomous WSNs carry out the promise to improve streamline business practices by supplying real-time data. Even people's location tracking sensors and body area networks can be powered by limb movements during breathing, heart beating, normal walking, hand cranking or lifting. Medical applications for vital sign monitoring or accident recognition are thus attracting a lot of interest as a potential use of PEH powered wearable sensing nodes. The common denominator in the aforementioned scenarios are the sensor networks composed of low-cost, low-power miniaturised sensor nodes that communicate untethered across short distances to carry out their collective task. For these sensor networks to work, sophisticated architectures and efficient

communication protocols must be developed to allow large amounts of nodes to collect, process, and disseminate data. While wireless sensors have the advantage of eliminating wiring installation expense and weight, as well as connector reliability problems, they still require a considerable amount of power in order to operate. Indeed, if power outages occur, critical data may be lost.

1.2 Research motivation and challenges

One of the most important trends in the electronic equipment technology from its origins has been the reduction in size and the increase in functionality. The beginning of the nanotechnology era has brought about exceptional advances in the field of electronics and the reduction in size of electronic devices has been obviously followed by the reduction in their power consumption. At the current state of the development, battery-powered portable applications require a power supply in the mW range for sustaining most commonly used handheld/wearable devices and WSNs. Small-scale piezoelectric energy harvesters are compact, lightweight, and currently capable to achieve such power levels from ambient sources. However, supplying sufficient amounts of harvested energy on a real-time demand still represents a challenge due to either the discontinuous nature of the ambient sources or the low-efficient energy transfer from the harvester to the electrical load of the end-application. While it is not possible to change the environment, EH systems can be adapted to the environmental conditions in order to reduce the existing gap between energy harvested by small-scale piezoelectric transducers and the energy demanded by low-power electronic devices such as WSCNs. Most of the recent works carried out to enhance the performance of PEH systems have been focussing separately on three main research lines: mechanical configuration of the harvester, circuits for the interface with the harvester and the energy storage [31]. The works focussing on the mechanical unit of PEH systems typically consider a simple resistor as the electrical load thus overlooking the details of energy flow towards it as for the end-application. Those works focussing instead on the electrical units of PEH systems do not really consider the branches of energy flow which are not the harvesting ones [32-34].

Harvested and extracted energy have also been confused at times [35-36]. To date only few studies have been conducted at a system level and showed a successful energy-autonomous capability for real application case scenarios. Therefore, new research paradigms for conditioning and storing the electric charge generated by the piezoelectric harvester need to be investigated with a system approach or further improvement needs to be addressed for the existing ones. This is true, particularly, with regards to the commercially available integrated PEH architectures meant to be ready-to-use in connection with targeted low-power electronics. Such architectures either lack of efficiency for the purpose of being universal or are very “application-oriented” for the purpose of enhancing the energy-autonomous capability of the intended electrical load. The existing mismatch between harvested and demanded energy is even larger in the case of PEH powered wireless sensor for low-frequency applications as the energy that can be harvested is very low for low-frequency vibrations whilst the power consumption of wireless nodes is relatively high. Simply saying, the harvested energy is not high enough to power the sensor nodes for the case of low-frequency vibrations or the power consumption of the sensor nodes is higher than the harvested energy. Such an EH challenge prompts several research questions listed below for this research work:

1. Can wireless sensor systems be made completely self-powered, entirely using the energy harvested by small-scale piezoelectric transducers? If so, is it possible to use them in the case of low-frequency structural vibrations?
2. Is it possible to deal successfully with the mismatch between harvested and demanded energy in the case of PEH powered wireless sensor applications by better integrating off-the-shelf devices?
3. How can ultra-low power management units be achieved?
4. What are the already implemented power management modules for PEH applications and the limitations during their operation?
5. Can passive power management strategies be practically used to enhance the performance of PEH systems substituting active ones?

1.3 Scope of the research

The focus of this research is on PEH systems and, in particular, on the electronic circuitry therein. Given that a PEH system consists of three main basic blocks as depicted in the diagram of Figure 1-3, the scope of the presented work is to investigate a novel low power consumption PMM, which offers a high performance link between the harvester's output and the input of a connected electrical load for wireless sensor applications. Enhanced system integration with reduced power consumption is achieved through passive interfaces between the harvester and the PMM, for an improved extraction of the harvested energy, and through an energy-aware switching interface between the PMM and the electrical load, for a smart management of the energy flow. Among other energy harvesters, this work only considers piezoelectric transducers and disregards for the study of novel power generators rather relying on commercially available devices ready to be integrated into a vibrating host structure. Commercially available devices (i.e., wireless microcontroller and sensors) are also used for the implementation of a custom developed WSCN as the electrical load of the PEH system. Furthermore, this research does not intend to implement novel data acquisition or transmission protocols; on the contrary, it aims at reducing the power consumption of PEH systems and improving their performance by managing the flow of the harvested energy through a smarter use of selected low-power hardware components. In this framework, sensors are supposed to work statically and not dynamically as a proof of the achieved energy autonomous capability for the developed systems in the considered application scenarios. These scenarios are based on real case practice with focus on two case studies of resonant and non-resonant ambient vibrations featuring a narrow low-frequency range and selected levels of applied strain or acceleration. Within the scope of this research is the consideration of base-excited vibration EH only. "Direct force" or "impact" type EH systems are not taken into consideration in agreement with the input conditions of the examined case studies. The technology developed by this work might be used to address the challenges of self-powered wireless sensing for other SHM applications; however, the

identification of proper timing and methods for data acquisition and transmission in order to implement an effective SHM paradigm, in those cases or in the examined ones, is far from the targets of this work.

1.4 Research aim and objectives

The aim of this research is to enhance PEH powered wireless sensor nodes using novel passive interfaces and a novel low power management approach. The purpose of this thesis is then to deal with the mismatch between harvested and demanded energy by increasing the power harvested and decreasing the energy demanded at a system level. The target PEH systems are both under non-resonant and resonant low-frequency excitations.

In order to achieve the aim above, the following objectives (summarised in Figure 1-9) have been set:

1) Study of the state-of-the-art in PEH systems for wireless sensor applications through literature review in order to identify:
    - piezoelectric transducers for non-resonant and resonant low frequency applications along with low power consumption electronic devices for power conditioning and management, data sensing and wireless communicating;
    - ways of integration of PMMs from system-of-systems architectures with focus on energy-aware interfaces.
2) Development and characterisation of non-resonant and resonant piezoelectric energy harvesters.
3) Development and characterisation of novel passive interfaces for practically enhanced EH performance of the developed non-resonant piezoelectric harvesters.
4) Development and characterisation of novel passive interfaces for practically enhanced EH performance of the developed resonant piezoelectric harvester.

5) Development, characterisation, and comparative analysis with commercially available architectures of a novel low power consumption PMM for SHM applications along with a custom wireless sensor node.

6) Experimental validation of high performance integrated PEH powered wireless sensor systems for non-resonant and resonant applications, which use the developed energy harvesters, passive interfaces, low power consumption PMM and WSCN.

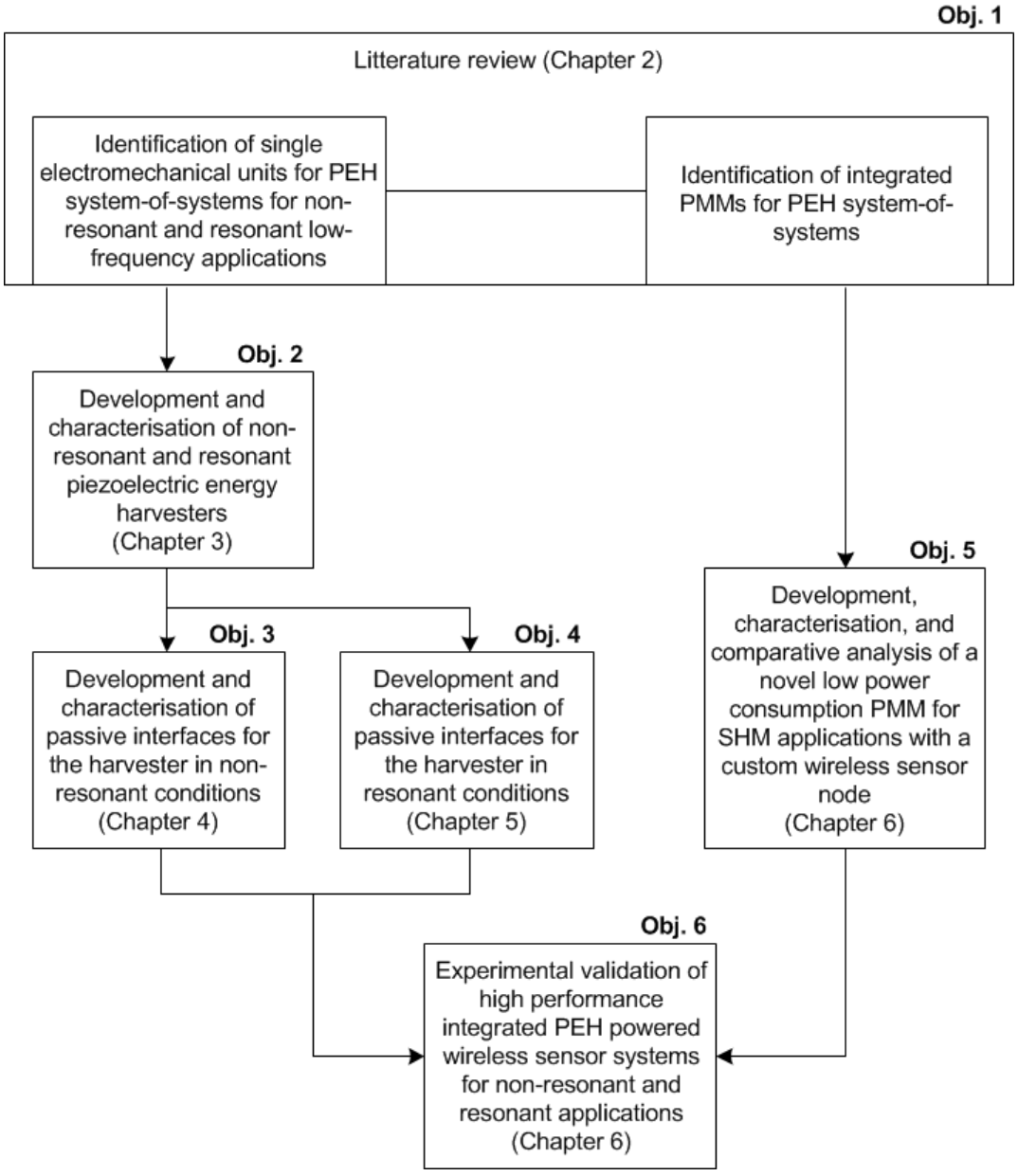

Figure 1-9 Summary of the objectives and the respective chapters of this thesis where they are addressed

1.5 Contribution and Novelties

The main contribution to knowledge of this thesis is the proposal of a novel EH circuitry, which is capable to practically enhance the performance of PEH powered wireless sensor nodes by using a whole-system approach rather than separately focussing on the single system's units shown as in the block diagram of Figure 1-3. This contribution lies in the recognition that: 1) there is an industrial need of a ready-to-use energy-autonomous solution for wireless sensor applications such as SHM; 2) the power output of small-scale piezoelectric energy harvesters is to date not enough to satisfy the power requirements of wireless sensor nodes, especially if power has to be supplied continuously in time. Techniques for increasing the resonance bandwidth of the vibration harvester [37], introducing enhancing mechanical non-linearities [38-41], amplifying the induced strain and tuning the harvester's frequency response [42] have been investigated in order to increase the energy input and the coupling term of the piezoelectric element. These techniques, however, may result cumbersome to be applied to PEH systems for applications in the low-frequency range of vibrations due to the low amount of ambient energy that is typically available in such a case.

In order to deal with the mismatch between harvested and demanded energy, this work has developed a novel EH circuitry for resonant and non-resonant PEH powered wireless sensor nodes and demonstrated:

1) a maximisation of the extraction of the energy harvested by the piezoelectric transducer;
2) a minimisation of the power consumption for conditioning the transduced signal;
3) an optimisation of the overall energy transfer from the piezoelectric harvester to the electrical load (i.e., the wireless sensor node).

For the accomplishment of 1), this work has developed a novel implementation of:

- A passive complex conjugate impedance matching (CCIM) interface that practically enhances the power output of piezoelectric energy harvesters in low-frequency applications.

State-of-the-art strategies, which adopt the impedance matching theory for PEH purposes in the low-frequency range, have implemented resistive or electrically active impedance matching configurations. However, a resistive circuit does not properly match the capacitive impedance of piezoelectric transducers in the low-frequency range [43-44] and active configurations require additional power. The proposed CCIM interface, on the contrary, is passive and based on a large inductive reactance but with a centimetre-scaled size for practically enhanced piezoelectric energy harvester performance at low frequency. In order to reach large inductances (i.e., kilo-Henries) in a small size (i.e., centimetre-scale) at low frequency, the interface is implemented as a toroidal PC permalloy core coil. Being a passive element, the implemented interface does not need an additional power source, partitions of the harvested energy-flow or switching conditions to be satisfied on the contrary of most of the state-of-art active impedance matching techniques for piezoelectric energy harvesters. Such an achievement has been successfully validated in a non-resonant PEH scenario for energy-autonomous aerospace SHM under real testing conditions.

- Passive non-linear interfaces that amplify the harvester's voltage output by reducing the time shift with its speed for low-frequency resonant excitations.

By enhancing the voltage onto which the piezoelectric current source drives its charge, the interfaces increase the power output of the harvester. The interfaces act passively in that no active circuits are used to trigger their operation but rather the displacement of the piezoelectric harvester (e.g., the swing oscillations of a cantilever beam). Based on that, novelties concern:

- the magnetic activation of a synchronised switching harvesting on inductor (SSHI) mechanism by use of permanent magnets and reed switches;
- the mechanical amplification of the force acting on the piezoelectric element by use of compression springs and conductive strips adopted as a fixed frame only;
- the mechanical activation of a SSHI mechanism by use of compression springs and conductive strips.

Validation has been successfully carried out in a resonant PEH scenario for energy-autonomous industrial SHM under real testing conditions.

For the accomplishment of 2), this work has developed a novel approach for conditioning the signal transduced by piezoelectric energy harvesters that is functional although it involves a minimum number of electronic components:

- The DC/DC voltage regulator, typical of PEH powered systems, has been replaced by a less power-hungry EAI.

The EAI has been connected to a custom WSCN and set in order to smartly adjust its duty cycle. By monitoring the available harvested energy through a voltage sensing device, the release of the stored energy is allowed to perform data acquisitions and wireless transmissions with minimum power consumption. Indeed, the WSCN is disconnected by the EAI until the stored energy is not high enough to power the end-application so as to limit the current drain during non-active phases.

- the AC/DC voltage rectifier, typical of piezoelectric EH powered systems, has been removed while powering the WSCN through the magnetically or mechanically activated SSHI interface and the EAI.

State-of-art voltage rectifiers involve certain power consumption (see Paragraph 2.2.1) as they involve the use of electronic diodes or switches driven through an active control. That is why voiding their use in PEH powered systems is a mean for performance enhancement. Indeed, physical diodes feature a voltage threshold below which the energy

generated by the piezoelectric transducer cannot be downstream transferred. Nevertheless, active controls for synchronous rectification require additional power to lower such a voltage threshold.

Through the introduction of the novel passive interfaces and the EAI in the PMM, this research work takes a whole-system approach to deal with the mismatch between the energy harvested from low-frequency vibrations and the energy demanded by wireless sensor nodes. This allows for the accomplishment of 3) and, as a result, it also brings about the capability to continuously power WSCNs in time intervals of a few seconds or fractions of a second rather than minutes. A significant improvement is therefore carried out in comparison with the majority of the cases reported in literature.

1.6 Research methodology

A review of the state-of-the-art in PEH systems for wireless sensor applications in non-resonant and resonant low-frequency ambient conditions is conducted through a study of the literature with a focus on the single units of the systems and their integration. Development of the piezoelectric harvesters, passive interfaces, PMM and custom WSCN are obtained by following the steps depicted in Figure 1-10 .

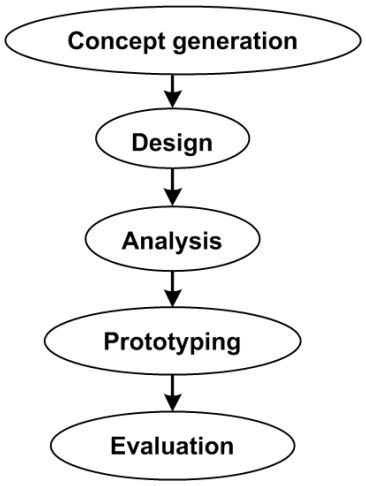

Figure 1-10 Flow chart of the steps carried out for the development of the piezoelectric harvesters, passive interfaces, PMM, and custom WSCN

For the synthesis of this thesis, only the final implemented designs are reported omitting the intermediate optimisation steps that have been carried out for the development. The experimental setup and testing conditions used for the characterisation of the developed systems are defined based on the two following case studies: 1) a non-resonant patch-like PEH system for wireless condition monitoring of commercial aircraft wings and 2) a resonant cantilever-based PEH system for wireless condition monitoring of large industrial machinery.

A 250 kN Instron tensile testing machine (Instron, High Wycombe – Bucks, UK) is used for 1) in order to apply to the substrate of the piezoelectric material a cyclic loading of the form:

$$F = F_{\text{pre}} + F_0 \sin(2\pi f t)\,. \tag{1-1}$$

The preload F_{pre} is chosen so that the substrates are always in tension during testing for simulation of the strain status of the lower skin of the aircraft wing in an active service [45]. Strain levels approximately between 440 and 1170 με peak-to-peak are used to reproduce the in-flight strain range, through harmonically varying the input force (F) from 0.5 to 51 kN. Excitation frequencies (f) of 2.5, 5.0, 7.5, and 10 Hz are used to reproduce the in-flight vibration frequency found in large transport commercial aircraft wings [46-47].

The electrical impedance of the piezoelectric materials and of the inductors used for implementation of the interfaces are measured by use of a N4L PSM1700 impedance meter under the applied AC voltages of 1, 5, and 10 V amplitude, and the swept frequency of up to 25 Hz. Different voltages are applied in order to observe the effects on the material's electrical response under the different mechanical strain levels induced by practical applications. Measurements are acquired at steps of 0.1 Hz and interpolated after denoising the acquired samples with median filtering.

For characterisation of the cantilever-based piezoelectric energy harvester under the resonant ambient conditions in 2), a V20 electro-dynamic shaker (Data Physics, San Jose – CA) is used with a frame made of nylon 6-6 as a

holding support. The nylon frame, featuring a height of about 16 cm from the top surface of the shaker, has also the function of voiding by distance any magnetic interaction between the harvester and the shaker. A rigid clamping is made so that, in proximity of the clamped end, the stress is maximum for the first flexural mode. As for the ambient conditions of 2), the first resonant mode of the vibration is set at the frequency of 11.5 Hz. Such a low-frequency motion produces little vibration in terms of acceleration, moderate vibration in terms of velocity, and relatively large displacement [48] as shown in Figure 1-11.

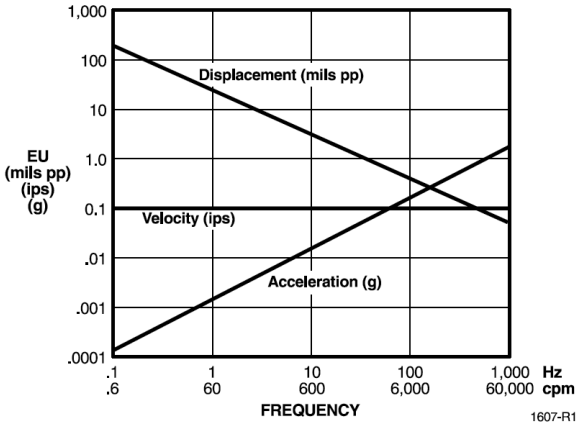

Figure 1-11 Relationship as a function of frequency between displacement and acceleration levels at constant velocity (Figure reprinted from [48])

The shaker is driven by a signal generator (HP 33120A) through a power amplifier (NF4505) in order to generate a sinusoidal continuous force and, in turn, drive the cantilever vibrations. A laser doppler vibrometer (LDV Polytec CLV-2534) is used to measure the velocity of the oscillation induced by the applied excitation both at the base of the cantilever beam (i.e., the top surface of the frame where the piezoelectric harvester is fixed into the vibrating host structure of the shaker) and at the tip (i.e., the free end of the beam straight before the proof mass). Known the amplitude and the frequency of the velocity (v) of the cantilever oscillations, the amplitude of the acceleration (a) of the applied excitation is calculated as:

$$|a| = \left|\int v dt\right| = |u|\omega^2 \tag{1-2}$$

where u is the beam displacement and ω the angular frequency of the induced oscillations. The driving signal of the shaker is set so as to measure the acceleration levels of 0.025 and 0.25 g at the base of the cantilever beam. As from different vibration surveys, such magnitude levels of the acceleration accurately represent the real ambient vibration conditions featured by large industrial machinery [49-50].

The power dissipated by a resistive load, directly connected to the harvesters' terminals, is used to characterise the correspondent EH capability. The harvested power and generated current are calculated based on the measured voltage developed across the connected resistive load. For the characterisation, a number of resistors up to 350 kΩ and to 700 kΩ are respectively used for 1) and 2). The instantaneous voltage across the connected resistors is measured by an Agilent 34401A and recorded at a rate of 1 kHz through a specifically developed LabVIEW interface. The internal resistance of the multimeter is kept into account to deduce the real electrical load connected to the harvesters. Similar experimental setup and testing conditions are used for the characterisation of the PEH systems in series connection to the novel developed interfaces. For comparison reasons, applied strain/acceleration levels and excitation frequencies are same as used for the characterisation of the harvesters without the interfaces. Same experimental setup and testing conditions are used to characterise the performance of the custom WSCN when powered by the implemented harvesters. The WSCN is connected in place of the resistive load through the PMM and the power supply capability for data acquisitions and wireless transmissions is measured based on: the time for cold start, t_c; and the time between consecutive wireless data transmissions from the WSCN to the base station. These time intervals are recorded while measuring the voltage across the capacitive energy storage of the PMM through a parallel connected Agilent 34401A under the excitations of the selected range of frequency and strain levels. The current drawn by the WSCN is also measured via series connecting an Agilent 34401A after the capacitive energy storage.

1.7 Thesis structure

The structure of this thesis is summarised below:

- Chapter 1 provides an introduction to the developed work, including: research background and applications of PEH powered wireless sensor nodes, research motivation and challenges, pursued aim and objectives, key findings and contributions to knowledge, along with the adopted methodology and scope.
- A literature review is conducted in Chapter 2, which covers:
    - the use of piezoelectric transducers for vibration EH focussing on the piezoelectric effect from the materials perspective and power generators implementation;
    - the state-of-the-art power conditioning and management of piezoelectric energy harvesters with regards to AC/DC rectifiers, DC/DC regulators, and energy storage devices;
    - the development of wireless sensor nodes and related power management techniques;
    - the existing strategies adopted to enhance the PEH capability of systems in use by mean of linear and non-linear electronic interfaces such as impedance matching and SSHI circuits;
    - the power management architecture of integrated vibration EH systems.
- Chapter 3 presents implementations, analyses, and characterisations of resonant and non-resonant piezoelectric energy harvesters based on two low-frequency vibration case studies;
- In Chapter 4 a passive impedance matching interface, based on a PC permalloy toroidal coil with large inductive reactance but with a centimetre-scaled size, is proposed and tested for practically enhanced performance of non-resonant piezoelectric energy harvesters at low frequency;
- In Chapter 5 passive interfaces, based on mechanically and magnetically activated SSHI implementations, are proposed and tested for practically

enhanced performance of resonant cantilever-based piezoelectric energy harvesters at low frequency;

- Chapter 6 introduces a novel low-power management design for PEH powered wireless sensor systems, which is shown capable of a higher performance in comparison with usual commercially available architectures from both the theoretical concept and the experimental results especially with the integration of the developed interfaces;
- The thesis concludes with Chapter 7, where the research is summarised and discussed based on the contribution to knowledge, limitations, and recommendations for future work.

2 LITERATURE REVIEW

This chapter presents an overview of piezoelectricity and piezoelectric materials, through which mechanical energy can be harvested from structural vibrations. First reason of this review of the literature in PEH systems and methods is to identify suitable piezoelectric transducers for non-resonant and resonant low frequency applications. Progress concerning the piezoelectric harvester as a single unit for power generation is indicated with a focus on patch-like and cantilever-based devices for real case application scenarios, whose aim is to overcome those issues related to the finite life-span of batteries. In addition, since piezoelectric energy transduction generates an alternating electrical output from alternating ambient vibrations, this chapter investigates the state-of-the-art PEH circuitry for signal rectification, filtering, storage, and regulation, so as to match electrical load compatibility. The single sub-systems of PEH architectures are investigated along with low power management techniques for designing integrated energy-autonomous wireless sensor nodes. Interfaces for the enhancement of the piezoelectric energy harvester performance and whole-system configuration approaches reported in the literature are also discussed so as to find out viable alternatives for an improved system-of-systems, which will be capable of dealing with the mismatch between the harvested energy and the energy demanded by wireless sensor nodes.

2.1 Piezoelectric transducers for vibration EH

2.1.1 Piezoelectricity

The piezoelectric effect has been used to convert mechanical energy into electricity for many years [51]. The concept idea behind it is actually more than two centuries old, although a conclusive relationship between stress and voltage was first demonstrated only in 1880 by the Curie brothers. Since then, it is clear that piezoelectric materials can become electrically polarised or undergo a change in polarisation when subjected to a stress. The applied stress, in fact, yields a proportional slight change in the dimension of a piezoelectric material

and results in the variation in bond lengths between cations and anions in its internal structure. Conversely, a piezoelectric material will have a change in dimension when it is exposed in an electric field. This inverse mechanism is called electrostriction. In order to observe macroscopic piezoelectricity in the material and use it to perform work, a “poling” process first has to be completed. This involves exposing the material to a strong DC electric field at an elevated temperature (usually below the Curie temperature of the material) that forces the alignment of the material’s dipoles and makes them active by leaving an overall internal polarisation. Those devices utilising the piezoelectric effect to convert mechanical strain into electricity are called transducers and are generally used in sensing applications (e.g., sensors, microphones, strain gages, etc.). Those devices utilising the inverse piezoelectric effect to generate a dimension change under an applied electric field are called actuators and used in actuation applications (e.g., positioning control devices, frequency selective device, etc.). The constitutive equations that define the behaviour of piezoelectric materials in the “strain-charge” form are shown by Equation (2-1) and Equation (2-2), which respectively describe the direct and converse piezoelectric effects as:

$$D = d\sigma + e^{\sigma}E \tag{2-1}$$

$$\varepsilon = s^{E}\sigma + d^{t}E \tag{2-2}$$

where: D is the polarisation (i.e., the electric displacement component, measured in C/m^2), d is the piezoelectric charge coefficient (measured in m/V or C/N), σ is the stress component (measured in N/m^2), e^{σ} is the absolute permittivity of the material under constant stress conditions (measured in F/m), E is the electric field (measured in V/m), ε is the strain component, and s^{E} the elastic compliance of the material under constant electric field conditions (measured m^2/N).

Figure 2-1 shows the orthogonal axes system typically used to describe the properties of piezoelectric materials.

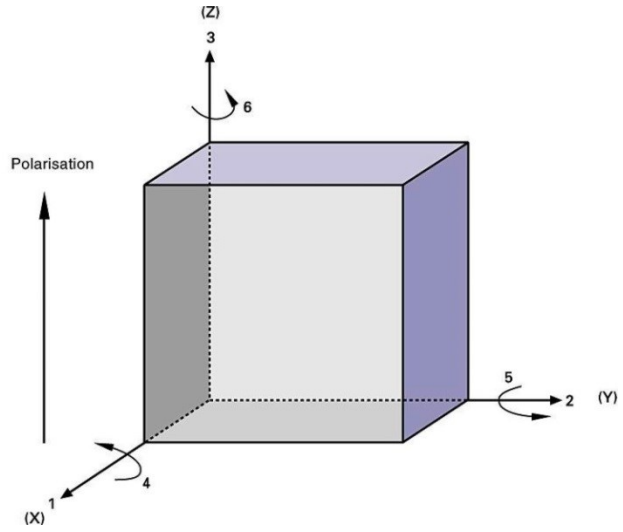

Figure 2-1 A Cartesian coordinate system describing the properties of a poled piezoelectric ceramic (Figure courtesy of PI Ceramic GmbH)

If the electrical condition is approximated to $E_1 = E_2 = 0$, like in the case of a piezoelectric transducer whose top and bottom surfaces are fully electrode, and considering mechanical stress only occurring along the 1-direction then the constitutive equations (2-1) and (2-2) become:

$$D_3 = d_{31}\sigma_1 + e_{33}^{\sigma}E_3 \tag{2-3}$$

$$\varepsilon_1 = s_{11}^{E}\sigma_1 + d_{31}E_3 \tag{2-4}$$

where: D_3 and E_3 are the polarisation and electric field developed in the 3-direction (i.e., the thickness direction of the piezoelectric transducer), respectively; and ε_1 and σ_1 are the induced strain and the stress applied in the 1-direction (i.e., the length direction of the piezoelectric material), respectively. It can be observed that if the electric field E_3 is negligible or there is no piezoelectric coupling term d_{31}, then Equation (2-3) becomes the Hook's law; similarly, if there is no stress σ_1 or no term s_{11}^{E}, Equation (2-4) becomes the Gauss' law for electricity or dielectric equation.

In order to evaluate the effectiveness with which a piezoelectric material converts mechanical energy into electrical energy or electrical energy into

mechanical energy, the coupling coefficient defined in Equation (2-5) can be taken into account:

$$k = \sqrt{\frac{\text{Mechanical energy stored}}{\text{Electrical energy applied}}} \text{ or } \sqrt{\frac{\text{Electrical energy applied}}{\text{Mechanical energy stored}}} \tag{2-5}$$

For this research work the piezoelectric material will only be used to convert mechanical energy into electricity; in other words, the direct piezoelectric effect will be used.

2.1.2 Piezoelectric materials

Different types of piezoelectric materials are nowadays available such like single crystals (e.g., quartz SiO_2 and Rochelle salt), ceramics (e.g., lead zirconate titanate [Pb(ZrxTi1-x)O3] – PZT – and $BaTiO_3$ – BTO), thin films (e.g., ZnO and PZT), thick films (e.g., PZT), and polymers (e.g., polyvinylidene fluoride – PVDF). Table 2-1 lists the properties of some of these popular piezoelectric materials.

Table 2-1 Properties of typical piezoelectric materials for harvesters

Material and form	$\lvert d_{31} \rvert$ (pm/V)	$\varepsilon_{33}/\varepsilon_0$ [a]	k_{31}	Tc (ºC)b
Quartz (single crystal) [52]	2.3	4.4	-	-
BTO (polycrystalline) [53]	79	1900	0.21	120
PZT (polycrystalline) [54]	190~320	1800~3800	0.32~0.44	230~350
PVDF (film) [55]	23	12~13	0.12	80~100
PZT (sol-gel thin film) [56]	190-250	800-1100	-	-
PZT (sputtered thin film) [57]	100	-	-	-
ZnO (sputtered thin film) [56]	10.5-11.5	10.8-11	-	-
AlN (thin film) [58-59]	-	8.6	-	-

[a] *$\varepsilon_0 = 8.854 \times 10^{-12}$ F/m, permittivity of vacuum*

[b] *Curie or maximum temperature*

Despite quartz and ferroelectric crystals, such as tourmaline and Rochelle salt, are good examples of piezoelectric materials, the superior properties of ceramic PZT justify why this is the most widely-used piezoelectric material for EH applications. From Table 2-1, it can be observed that PZT has a higher

electromechanical coupling factor and higher Curie temperature, which means that PZT piezoelectric material remains active operating at higher temperatures. PZT material is not only more resistant to high temperatures but to atmospheric pressures too. In addition, PZT is resilient, chemically inert, easily poled, and has a wide range of dielectric constant, which are all key benefits considering the greatest opportunity for PEH in industrial applications. A further key advantage of PZT material is that it can be optimised to suit specific applications being easily manufactured in any shape or size. The perovskite unit structure of PZT, which determines the described piezoelectric properties of this material, is shown in Figure 2-2.

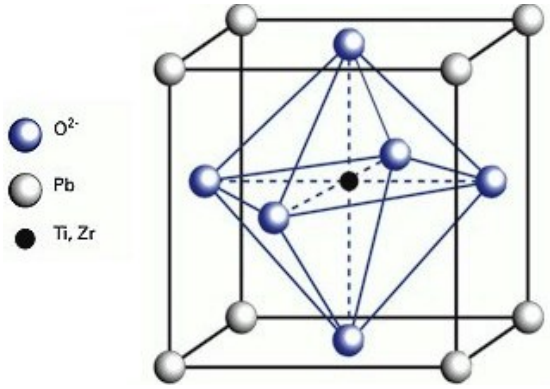

Figure 2-2 Cubic perovskite lattice of PZT (Figure courtesy of PI Ceramic GmbH)

Under a strong electric field, the Ti^{4+} or Zr^{4+} deviates from the neutral position at the centre of the unit cell thus forming a dipole. As a consequence, by reversing the internal dipoles through an applied electric field, the PZT material results deformed. Similarly, a deformed PZT material can produce electric charge on its surface electrodes due to the deviation of its internal dipoles. Commercial PZT ceramic was doped with either acceptor dopants, which create oxygen (anion) vacancies and generate hard PZT, or donor dopants, which create metal (cation) vacancies and generate soft PZT. The cation vacancies facilitate the domain wall motion, so soft PZT has a higher piezoelectric constant but larger loss due to internal friction. The hard PZT has lower piezoelectric constant and also lower losses because the domain wall motion is pinned by the impurities.

2.1.3 Piezoelectric power generators

Piezoelectric materials are used as energy harvesters in different modes. When mechanical stress is applied to a piezoelectric material in the longitudinal direction (parallel to polarization), strain is generated in the longitudinal direction or in the thickness of the piezoelectric material; thereby, a voltage is generated, in order to return the material to its original thickness as shown in Figure 2-3(a). This is known as the "33" mode of operation of piezoelectric materials as from the Cartesian diagram depicted in Figure 2-1. When stress is applied to a piezoelectric material in a transverse direction (perpendicular to polarization), strain is generated in the transverse direction or in the length of the piezoelectric material; thereby, a voltage is generated in order to return the material to its original length and width as shown in Figure 2-3(b). This mode of operation of piezoelectric materials is known as the "31" mode.

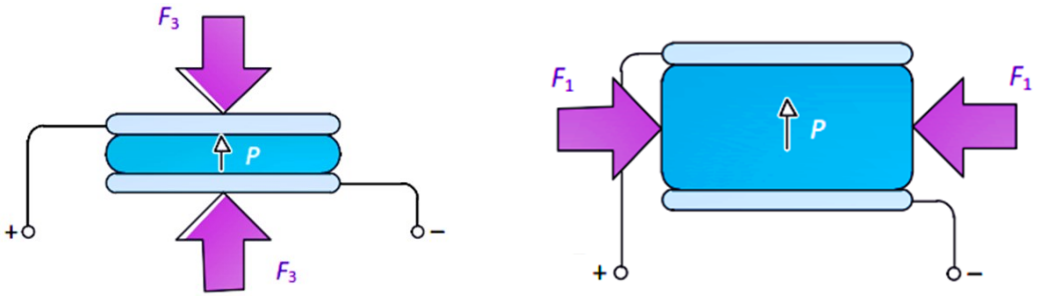

(a) (b)

Figure 2-3 (a) 33 and (b) 31 working modes of piezoelectric harvesters

Although not widely used for PEH applications another mode of operation is the "15", which linearly couples shear mechanical stress, hence strain, with the generated electric charge. The "33" mode has typically higher converting coefficient than the "31" mode; for example, in the case of PZT-5H, k_{31} and k_{33} are respectively equal to 0.44 and 0.75. Depending on the intended PEH application, the operating mode and configuration that generates the largest strain when having the same force input is obviously favourable for the purpose of generating more power.

Different piezoelectric harvester configurations have been proposed for the purpose of harvesting energy from vibrations. Examples are: cymbal structures, which are capable to produce a large in-plane strain under a transverse external

force as presented by Kim *et al.* [60] and Li *et al.* [61]; multi-stacking structures, which feature a large capacitance but are more likely weak under mechanical shocks as presented by Adhikari *et al.* [62] and Lefeuvre *et al.* [63]; shell structures, which can generate larger strain than flat plate thus improving PEH efficiency as presented by Yoon *et al.* [64-65] and Chen *et al.* [66]; and cantilever structures, which can produce a large deformation under vibrations, especially in resonant condition and with an end mass, as presented by Elvin *et al.* [67], Roundy *et al.* [68], Leland *et al.* [69], Shen *et al.* [70], Liu *et al.* [71], Choi *et al.* [72], etc. The cantilever structure, in particular, has been widely used as it results in one of the least stiff structures for a given volume. This means that the cantilever offers both a low resonant frequency and a high average strain in its materials for a given volume. Such characteristics are an advantage to PEH systems as allow for a high power output in the low frequency range where ambient vibrations typically occur. Under steady-state vibration conditions, the tip (free end) of the cantilever moves up and down repeatedly with respect to the fixed end that is attached to a host structure in the vibrating environment. As the tip moves upwards (downwards), the piezoelectric layer is put under tension (compression) which, for a positive polarisation in the 3-direction, means that the charge generated on the surface electrode is positive (negative) with respect to the charge generated on the substrate layer electrode. This, in turn, results in an electrical output through the electrodes of the device in the 3-direction as a consequence of the piezoelectric direct effect. Such an effect for a cantilever-based piezoelectric harvester is typically modeled as the electromagnetically coupled spring-mass-damper system shown in Figure 2-4, where: u represents the displacement; F the applied force; V and I the piezoelectric output voltage and current, respectively; M the dynamic mass; C the structural damping coefficient; and K_E the open-circuit stiffness.

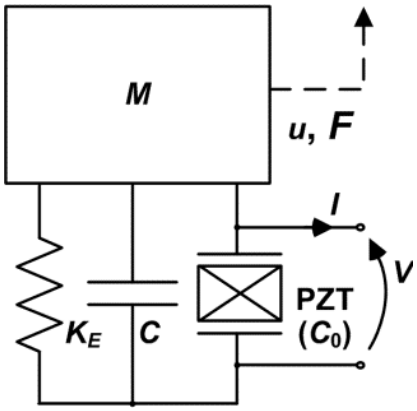

Figure 2-4 An analytical model of a cantilever-based piezoelectric harvester

Different shapes for the cantilever structure have also been proposed, being the triangular shape the most favourable one as the maximum tolerable excitation amplitude can be much higher. In this case, in fact, all of the piezoelectric material can be homogenously stressed to a value just below the yield stress. Cantilever-based piezoelectric harvesters can be arranged either as a unimorph, bimorph, or multi-layer bimorph, as shown in Figure 2-5.

In bimorph and multilayer bimorph arrangements the device can be physically wired so that the piezoelectric layers are connected either in parallel or in series. For the same device's size, the power output remains the same regardless of whether the device is poled for parallel or series. However, the ratio of current to voltage changes: for a device poled for series the output voltage is double that of a device poled for parallel; and for a device poled for parallel the output current is double that of a device poled for series [74]. This is because in the parallel case, the surface area of the electrodes is double that for the series case, and in the series case the floating voltage outputs of each piezoelectric layer are connected in series.

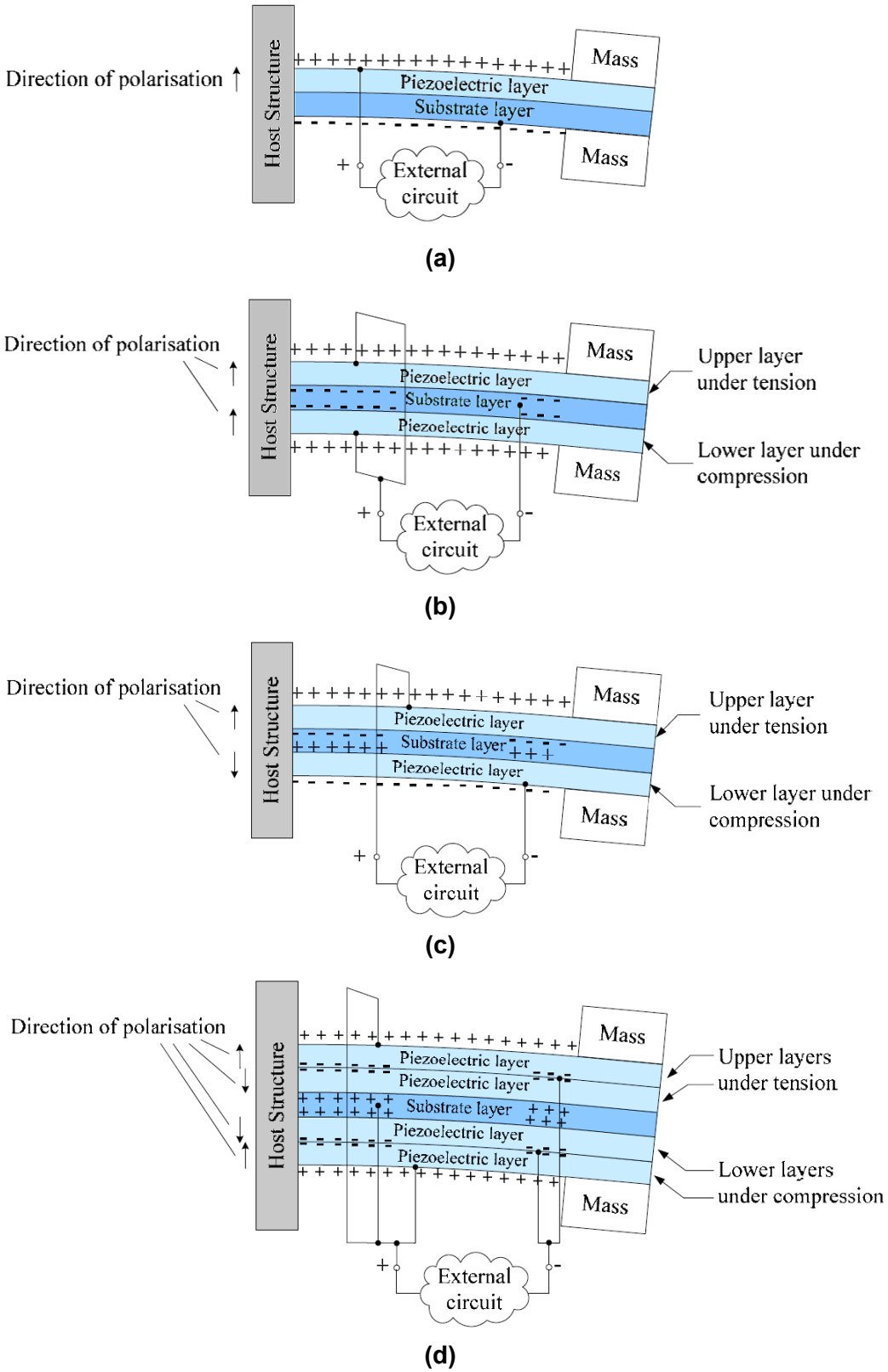

Figure 2-5 Cantilever-based piezoelectric harvester configurations: (a) unimorph, (b) bimorph poled for parallel, (c) bimorph poled for series, and (d) multilayer bimorph poled for parallel (Figure reprinted from [73])

Monolithic PZT materials are of affirmed use as both sensors and actuators especially because of their compactness. Certain restrictions, however, arise in relation to real-world applications because of their brittle nature [75-76], which requires additional attention during handling and bonding procedures. Moreover, PZT materials show very poor conformability to curved surfaces. In order to overcome these limitations, Tien and Goo [77] analysed a piezoelectric composite composed of layers of carbon/epoxy, PZT ceramic and glass/epoxy for vibration EH purposes. A number of active composites have been also commercialised such as the MFC [78] and THUNDER [79], which can provide the durability and flexibility required by practical PEH applications. The MFC, in particular, is a new piezoelectric composite patented by NASA. The MFC device consists of rectangular piezo-ceramic rods embedded in a resin matrix along with electrodes and polyimide film, finally enclosed in kapton film as shown in Figure 2-6(a). The commercially available MFC product is shown in Figure 2-6(b).

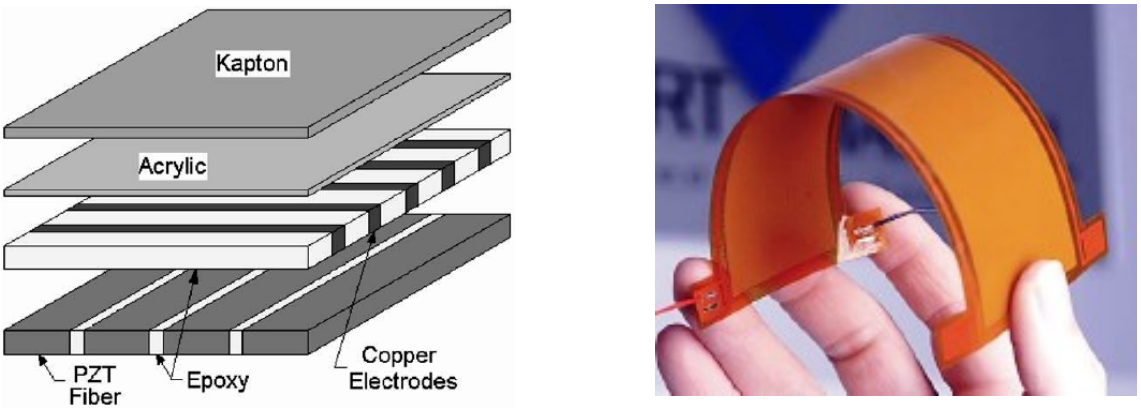

(a) (b)

Figure 2-6 MFC material: (a) a schematic showing the cross-sectional layout [80] and (b) the commercially available product (Figure courtesy of Smart Material Corp.)

Since the MFC is based on piezoelectric fibres, the overall strength of the material is higher than that of the base material as well as its flexibility due to a thickness of only 0.3 mm. From a study of the literature, it has been found that the MFC material has been mainly used as an actuator [81] whilst its sensing capabilities have not been fully developed or tested. Sodano et al [82] compared the efficiencies of three different piezoelectric systems: the traditional

PZT, a quick pack actuator, and the MFC. From that work, it was concluded that the MFC material is less efficient than conventional piezoelectric materials but how to improve its PEH efficiency was not indicated. If the MFC's efficiency can be improved, this is expected to be applicable for a wider range of real applications in comparison with PZT due to its attractive flexibility property.

2.2 Power conditioning and management of piezoelectric energy harvesters

The output of a piezoelectric energy harvester is not directly suitable as power supply of electronic devices due to the fact that its voltage and current vary depending on the ambient conditions. Therefore, there is the need to interconnect a power conditioning and management circuit, which is capable to adapt the input from the piezoelectric harvester to the requirements of the electrical load connected at its output.

2.2.1 AC/DC signal conditioning and filtering

Piezoelectric energy harvesters and, more in general, vibration energy harvesters generate an alternating output signal as ambient vibrations are alternating in nature. The harvested signal is then fed into an AC/DC rectifier, whose key task is to execute the conversion while achieving high efficiency starting from low input powers and voltages. Even though output voltages of piezoelectric harvesters are generally higher than similarly sized magnetic harvesters, energy is usually discontinuous.

The vibration spectrum of typical PEH applications is characterised by high spikes shortly damped to levels from which it is very difficult to obtain useful energy. Depending on the generated voltage, start-up systems may be required and become non-trivial. For example, the 4-diode bridge configuration shown in Figure 2-7 is typically used to perform the AC/DC full-wave voltage regulation of PEH systems.

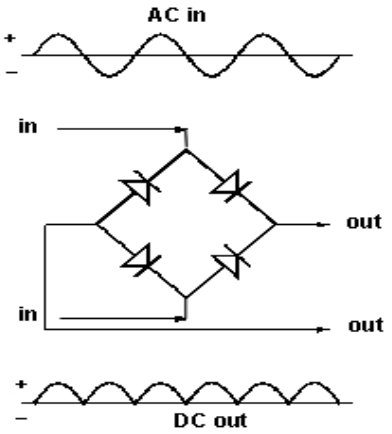

Figure 2-7 A 4-diode bridge rectifier circuit (Figure reprinted from [83])

Nevertheless, conventional full-wave rectifiers suffer a voltage drop of about 1.4 V, which means that the rectifiers will not start-up until the input signal overcomes such a voltage threshold. As a general rule, passive junction-based semiconductor rectifiers are generally not suitable for input voltages under 0.5 V due to the forward-bias voltage drop associated with the diodes. For the purpose of making the system work from low input voltages and reducing the waste energy before the diode threshold has been reached, the use of Schottky diodes has been investigated [83]. Despite the fact that the voltage drop of Schottky diodes is lower, Schottky technology typically features higher reverse currents thus not making it worthwhile over regular diodes. The use of half-bridge diode rectifiers has also been examined [84] for reducing the drop of the generated voltages although the inconvenience that, in such cases, energy will be harvested only for half the duration of the input cycles. Rectifiers for PEH circuits based on a voltage-doubler configuration, hence using only two diodes as shown in Figure 2-8, have been taken into consideration [83].

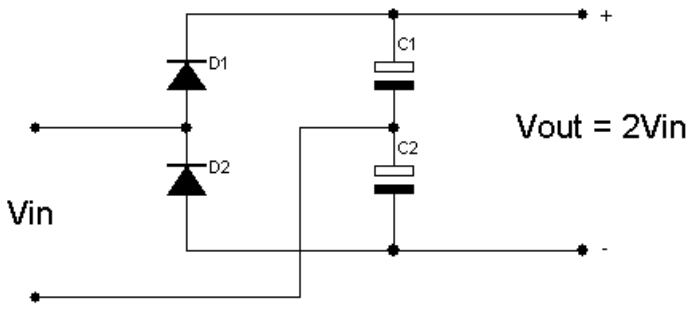

Figure 2-8 A voltage doubler circuit

The result is a maximum power extraction comparable to the bridge rectifier case but, since this occurs at a lower current, the dissipated power is much lower. In order to avoid the losses related to the use of diodes, rectification based on switches has been proposed [85]. For example, conventional full wave rectifiers implemented in MOSFET technology have been implemented by using four MOSFETs connected as diodes, as depicted in Figure 2-9.

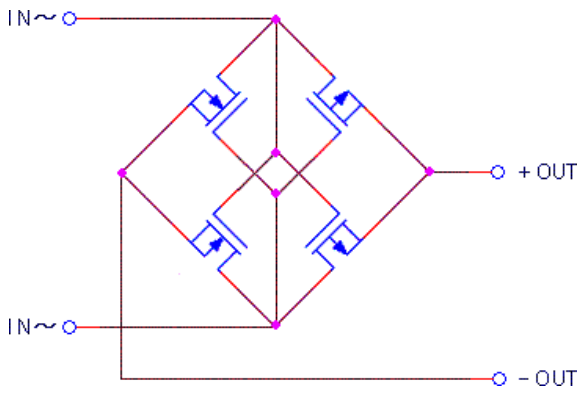

Figure 2-9 A 4-MOSFET bridge rectifier circuit (Figure reprinted from [83])

Since transistors substitute diodes, the drop of the generated voltage is a function of the transistors' drain-to-source resistance ($R_{DS\text{-}on}$) but, although lower in such a case, it is still present. An alternative technique consisting of diode-connected MOS-transistors with an added capacitor between the gate and the source of the switching transistor has been proposed in [86] for RF EH as shown in Figure 2-10.

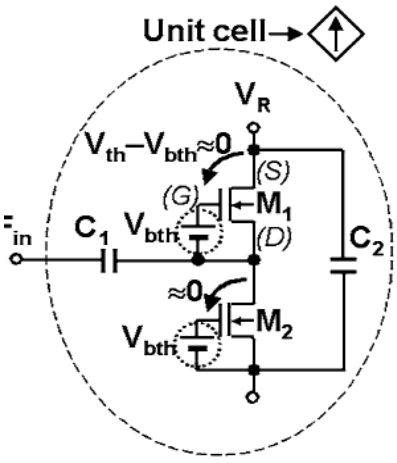

Figure 2-10 A modified rectifier circuit with reduced turn-on voltage (Figure reprinted from [86])

From the circuit in Figure 2-10, it can be observed how the transistors of the rectifier can conduct as soon as the input voltage starts to increase. A smart improvement has been presented in [87], which replaces two diode-connected transistors with two cross-coupled transistors; therefore, the voltage drop of one diode is abolished. Aiming at reducing the voltage drop of common diodes, the use of active diodes has been proposed especially in power transmission and medical applications [88-89]. An active diode is basically a MOS-transistor switching circuit controlled by a comparator, whose input is connected to the MOSFET source and drain terminals whilst its output to the MOSFET gate terminal as shown in Figure 2-11:

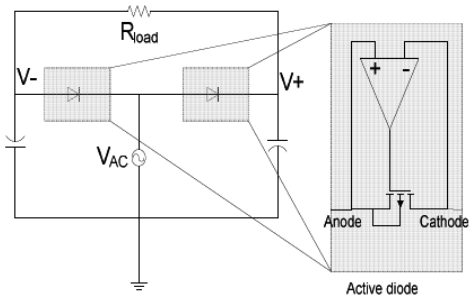

Figure 2-11 A bridge voltage doubler with active diodes (Figure reprinted from [90])

The behaviour of such a diode can approach an ideal behaviour as in the case of a smart switch, which is active or not for any voltage at the anode higher than the voltage at the cathode. The main drawback of this circuit configuration is that it requires a comparator, thus costing a few microwatts of power. The power supply generation for the comparator can represent an additional issue that needs to be taken into account in an EH system design. Alternatively, active MOS-based synchronised rectification is possible and can be implemented by controlling the MOSFET conduction with a clock signal that is in phase with the input signal [91]. Since such an approach makes use of voltage control signal higher than the threshold voltage of the MOSFET, it also requires the use of further driving circuits such as a microprocessor and A/D converters with external active feedback sensors. They obviously increase the circuit's dissipations and reduce the efficiency of the energy harvester especially at low power. More recently, the use of a synchronised rectifier with

an active diode has been proposed for PEH systems [92] but the minimum rectifiable input voltage was reported to be around 1.25 V, which shows how this approach does not overcome fully the voltage threshold limitations of other self-driven synchronised rectifiers.

Integrated circuits (ICs) for AC/DC rectification have also been presented aiming at achieving higher efficiency for low power consumption PEH systems. For example, a pulsed-resonant rectifier and integrated controller have been reported in [93] for use with resonant piezoelectric transducers with output frequency in the 10 Hz to 1 kHz range. As shown in Figure 2-12, this circuit uses two rectifiers connected in parallel and optimised to work for input voltages above and below 0 V, respectively.

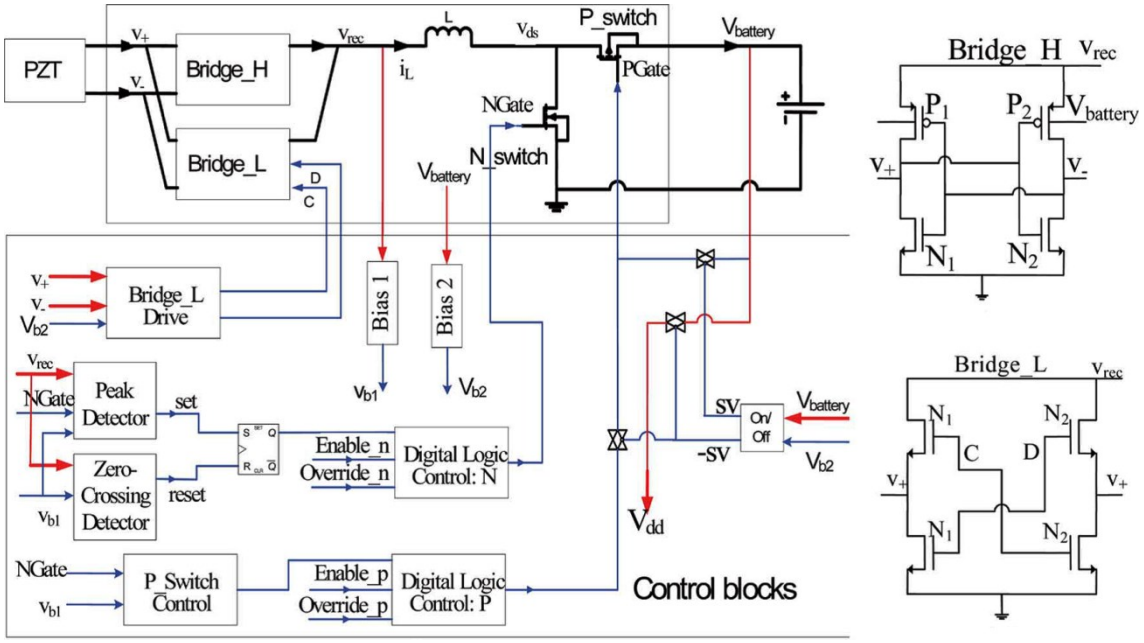

Figure 2-12 A pulsed-resonant rectifier circuit with an integrated controller where the high and low synchronous bridge rectifiers are respectively shown (Figure adapted from [93]

The output of this circuit is first charged by the parasitic body diode of the switches and then, when the input voltage amplitude reaches 1.2 V, the control circuit fully operates with an overall power consumption as low as 0.6 µW and an efficiency up to 70%. In [94], Le developed a modified synchronous rectifier through a PMOS transistor to generate two-phase clocking for a voltage

doubler, thus reaching an AC/DC conversion as efficient as around 90%. Such an integrated rectifier is depicted in Figure 2-13.

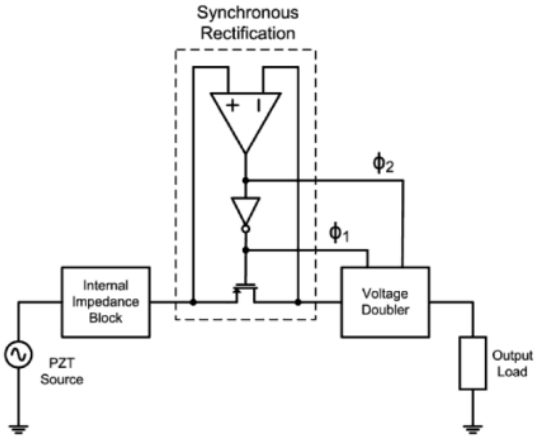

Figure 2-13 A modified synchronous rectifier circuit (Figure reprinted from [94])

With the aim to develop a high-efficient full wave AC/DC converter for multi-phase piezoelectric energy harvesters, N.J. Guilar *et al.* have also designed an IC consisting of two CMOS-controlled rectifiers connected in parallel [95], as shown in Figure 2-14.

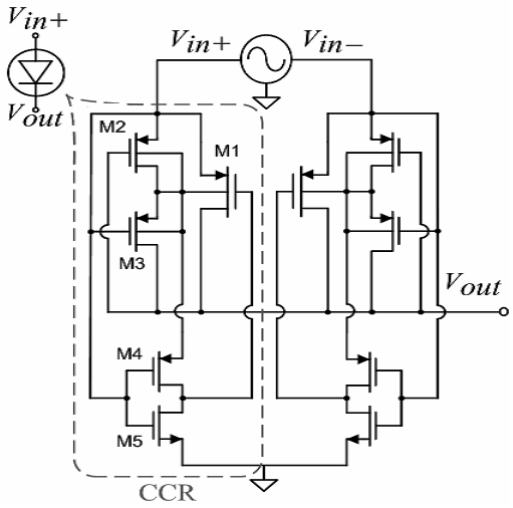

Figure 2-14 A full-wave rectifier circuit for multiphase piezoelectric energy harvesters (Figure reprinted from [95])

In this circuit, the body bias transistors M2 and M3 ensure that the pn-junction associated with the n-well of the large PMOS transistor M1 does not become forward biased; at the same time, they work as a peak detector. The CMOS

inverter made by the transistor M4 and M5, instead, functions as a low-power comparator, whose output is based upon the held peak-detector voltage and the input voltage. The inverter can be set so that M1 turns on when the input voltage gets higher than half of the peak held voltage and permits an efficiency up to 98%.

In addition, a small capacitor is typically connected to the output of the rectifier in order to smooth any ripple. In certain cases, the small capacitor may be replaced by a large capacitor so as to perform simultaneously the function of energy storage or simply to allow more stability over a discontinuous energy input for supplying power to a DC/DC converter downstream connected.

2.2.2 DC/DC signal conditioning

DC/DC converters with a variable conversion factor have been typically used to provide the electrical load of the PEH powered system with the right electrical input for the targeted application.

The most appropriate DC/DC design is chosen depending on the system parameters and ambient energy source. The following voltage regulation topologies are typically found in the literature:

- Buck conversion (step-down);
- Boost conversion (step-up);
- Buck-boost conversion (flyback);
- Charge pump.

Buck conversion is a natural choice for those applications where the piezoelectric voltage can be very high on average compared to the desired electrical output. A simplified control scheme allows also achieving a condition of maximum power flow, which is implemented via adjusting the converter's duty cycle [96]. The boost and charge pump converter principles are also reported in the literature as a way to deal with low-voltage input EH applications where small scale piezoelectric transducers are used. The boost converter exhibits a high flexible conversion factor and efficiency, where the efficiency is the fraction of the input power that is available at the output. Although in theory

a lossless implementation is possible, the series resistance of the inductor and the switches cause losses in practice. In Figure 2-15 is shown a schematic of a boost converter connected to a capacitive storage and a resistive load.

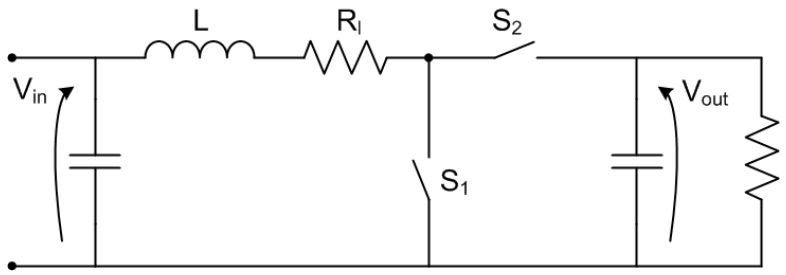

Figure 2-15 A schematic of a boost converter connected to a capacitive storage and a resistive load

In Figure 2-15, R_l is the series resistance of the inductor and of the switches that, if neglected, allows calculating the power P_L transferred to the load as:

$$P_L = \frac{2R_L V_{in}^{\ 2}}{3}\sqrt{\frac{2T_s\left(V_{out}-V_{in}\right)}{LR_l 3V_{out}}} \tag{2-6}$$

where T_s is the closing time of the switch S_1, and V_{in} and V_{out} are respectively the input and output voltage of the circuit depicted in Figure 2-15. From Equation (2-6), it can be seen that the power transfer can be enhanced by choosing a larger L, a smaller T_s, and a smaller R_l so as to reduce the losses in the circuit. In order to achieve a high efficiency rate, DC/DC converters often make use of an external inductor. When an integrated solution is required for the PMM, IC inductors with or without magnetic core should be considered. However, integrated boost converters have lower efficiency than converters based on discrete components due to the fact that IC inductors typically feature small inductance and large R_l values. Alternatively, in order to obtain an efficient DC/DC regulation with small power and volumes, charge pumps with switched capacitors have been implemented. Examples are: the voltage doubler [97-98], the Dickson charge pump [99], the ring converter [100], and the Fibonacci converter [101]. The charge pump conversion factor is not as flexible as in the case of boost converters with inductors. The Dickson charge pump with n

stages is shown in Figure 2-16 in connection with a capacitive storage and a resistive load, where the input voltage V_{in} is equal to the clock amplitude.

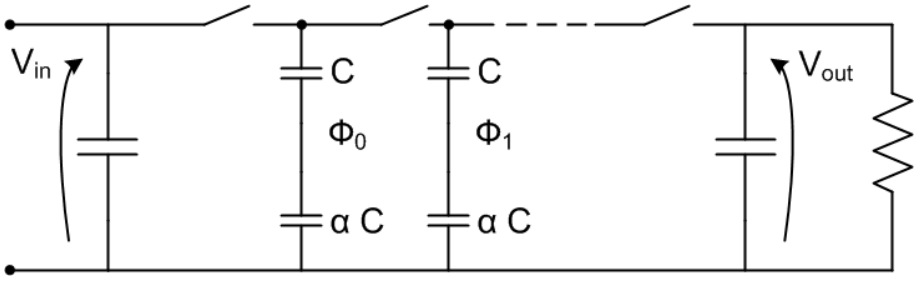

Figure 2-16 A schematic of the Dickson charge pump DC/DC converter, with *n* switching capacitor stages, connected to a capacitive storage and a resistive load

From [103], the efficiency of the circuit in Figure 2-16 can be derived as in Equation (2-7):

$$\eta = \frac{V_{\text{in}} I_{\text{out}}(n+1) - \frac{n I_{\text{out}}^{\ 2}}{Cf}}{V_{\text{in}} I_{\text{out}}(n+1) + \alpha C f V_{\text{in}}^{\ 2}} \tag{2-7}$$

where f is the clock frequency, C the value of the capacitors; αC the parasitic capacitance of the bottom plate, I_{out} the output current, and V_{in} the input voltage of the converter. The efficiency can be optimised by reducing α. But, even for α=0, the efficiency will be below 1 as soon as the circuit delivers power to its output ($I_{\text{out}} \neq 0$). The losses can be limited by optimising n, C and f. More flexibility in the design of circuits that require voltage regulation is given by buck-boost converters, which can work whether the converter input voltage is higher or lower than its output voltage (e.g., the storage voltage), thus enabling optimisation of PEH systems with energy storage cells having various voltages. Main advantages are also encountered for the power optimisation of the piezoelectric generator itself as, fixed the duty cycle and the switching frequency, a discontinuous current mode (DCM) buck-boost converter exhibits a constant input average resistance [104]. It is worthwhile to mention that a further controller needs to be integrated into a PEH system if the regulated

voltage is first supplied to a rechargeable battery functioning as the system's energy storage device. Indeed, it is essential to ensure the battery safe operating conditions when this is charged at the output.

2.2.3 Energy storage devices

Energy storage devices are a key part of EH powered wireless sensor systems and, particularly, of piezoelectric systems as ambient vibrations are often discontinuous and may not be present at all for a prolonged time. By storing energy it is possible to sustain the requirements of the electrical load for an intended application as the stored energy will be released all at once at a convenient time under higher peaks of power. The characteristics of the implemented energy storage devices have a significant impact on the overall EH system's performance.

A first group of characteristics is associated to the long-term lifetime of the EH system, which includes energy density (and its ageing effects) and limitations such as the maximum number of rechargeable cycles. In addition to these parameters, a second group of characteristics determine the efficiency of the energy storage device and, in turn, the short-term lifetime of the EH system; literally, how long the electrical load will remain active by only utilising the stored energy. Such parameters are, for example, the leakage current and the equivalent series resistance (ESR) of the energy storage device, which lead to power losses during charging and discharging.

Typical energy storage devices are capacitors/supercapacitors or rechargeable batteries. They provide different energy performance in a number of footprints and configurations. Batteries, in particular, advance on two fronts: 1) increased *specific energy* for longer time intervals (i.e., the battery capacity in Wh/kg); and 2) improved *specific power* for good power delivery on demand (i.e., the battery's powering capability in W/kg). Figure 2-17 illustrates the energy and power densities of lead acid, nickel-cadmium (Ni-Cd), nickel-metal-hydride (Ni-M-H), and Lithium-ion (Li-ion) batteries.

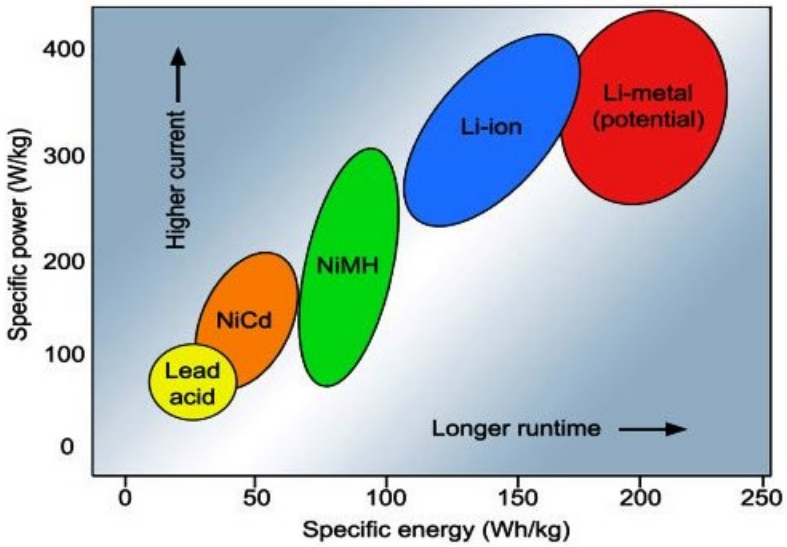

Figure 2-17 Specific energy and specific power of rechargeable batteries (Figure reprinted from [105])

Taking into account the small sizes aimed by integrated PEH systems, both high specify energy and specify power are an important factor. Up to date, Li-ion technology is then the most promising battery choice for energy-autonomous devices. A more detailed performance comparison of various rechargeable batteries is given in Table 2-2, where batteries of the Li-ion family are distinguished in *liquid* and *polymer* depending on their implementation.

Table 2-2 Comparison of performance for various rechargeable batteries based on their average values [106]

Parameters	Lead acid	Ni-Cd	Ni-M-H	Liquid Li-Ion	Polymer Li-ion
Voltage (V)	2	1.2	1.2	3.6	3.6
Weight energy density (Wh/Kg)	35	50	80	125	170
Volume energy density (Wh/l)	80	150	200	320	400
Cycle life (times)	300	500	500	800	1000
Self-discharge (%/month)	0	25-30	30-35	6-9	2-5
Electrolyte state	Liquid	Liquid	Liquid	Liquid	Polymer Gel
Min. thickness	>10mm	>3mm	>3mm	>3mm	<1mm
Memory effect	No	Yes	No	No	No
Pollution	Yes	Yes	No	No	No
Production Cost	Lowest	Low	Middle	High	Middle
Advantages	High drain current and low cost	Middle drain current and low cost, smaller volume	Middle drain current and cost, higher capacity	Higher capacity and lighter weight	Highest capacity, lighter weight and flexible shape
Disadvantages	Too heavy	Environmentally not friendly	Higher self-discharge and weight	Low drain current and higher cost	Low drain current and very high cost
Applications	Car and lighting	Power tool, cordless phone and emergency lighting, etc.	Toy, PDA, MP3 and digital camera, etc.	Cellular phone and laptop computer	Laptop computers

More specifically, the Li-ion family can be divided into three major battery types named upon their cathode oxides, which are: cobalt, manganese, and phosphate. The characteristics of these Li-ion systems are summarised in Table 2-3.

Table 2-3 Characteristics of the most commonly used lithium-ion batteries [107]

Specifications	Li-cobalt LiCoO2 (LCO)	Li-manganese LiMn2O4 (LMO)	Li phosphate LiFePO4 (LFP)
Voltage (V)	3.6	3.8	3.3
Charge limit (V)	4.2	4.2	3.6
Cycle life	500-1,000	500-1,000	1,000-2,000
Operating temperature	Average	Average	Good
Specific energy (Wh/kg)	150-190	100-135	90-120
Specific power (C)	1	10, 40 (pulse)	35 (continuous)
Safety	Average; requires protection circuit and cell balancing of multi-cell pack. Requirements for small formats with 1 or 2 cells can be relaxed		Very safe; needs cell balancing and voltage protection
Thermal runaway (°C)	150	250	270
Cost	High for raw materials	Average	High
In use since	1994	1996	1999
Researchers, Manufacturers	Sony, Sanyo, GS Yuasa, LG Chem, Samsung, Hitachi, Toshiba	Hitachi, Samsung, Sanyo, GS Yuasa, LG Chem, Toshiba, Moli Energy, NEC	A123, Valence, GS Yuasa, BYD, JCI/Saft, Lishen
Notes	Very high specific energy; limited power; cell phones and laptops	High power, good to high specific energy, power tools, medical, EVs	High power, average specific energy, elevated self-discharge

There are many other lithium-ion based batteries. For instance, lithium-ion-polymer (Li-polymer) and lithium-metal (Li-metal), which may be the future of EH technology. Lithium titanate (Li4Ti5O12), for instance, is a promising alternative material for the negative electrode, which delivers better cycle stability than conventional mixed graphite anodes. A breakthrough of the recent years is represented by the Thinergy® MEC (Infinite Power Solutions, Inc. – Littleton, Colorado) thin film batteries. Such a battery technology adopts a solid state electrolyte called lithium-phosphorus-oxynitride (LiPON), where the extremely low electron conductivity results in ultra-low self-discharge (1% annual charge loss) and superior power performance (30-60 mA peak discharge current) [108]. Thin film li-ion batteries are similar to regular li-ion

batteries, but they are made of thin materials in the nanometre or micrometre scale so that the overall thickness of the battery is of a few millimetres in total. Like other Li-on rechargeable batteries, however, there is also a low-limit voltage threshold that has to be taken into account for the design of a whole EH system-of-systems. For example, the aforementioned Thinergy® MEC battery has an operating voltage range between 2.1 V and 4.1 V. Compelling works involving the use of rechargeable batteries in the EH research community are those carried out by Ottman *et al.* [96] and Sodano *et al.* [109]. The use of capacitive energy storage, however, appears in the literature more often; especially with regard to the research community rather than commercially available architectures. The reason could be that off-the-shelf discrete components, such as capacitors, can more easily allow to show the EH capabilities of a new developed system. Energy is stored by capacitors through static charge (*Q*) rather than an electro-mechanical reaction: applying a voltage differential (*V*) on the positive and negative plates charges the capacitor as depicted in Figure 2-18.

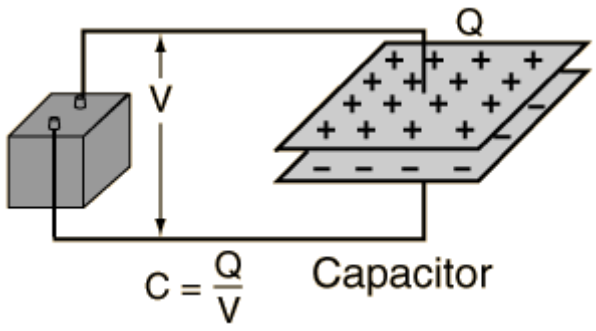

Figure 2-18 Energy storage on a capacitor

Capacitors are better suited to deliver very high power peaks and several voltage ratings. They can be grouped into three main family types:

- electrostatic capacitors, which use a dry separator and have a very low capacitance, from a few pico-Farad to low microfarad;
- electrolytic capacitors, which use a moist separator and are typically rated in microfarads;

- supercapacitors, whose capacitance is rated in farads, are ideal for energy storage that undergoes frequent charge and discharge cycles at high current and short duration.

Supercapacitors are also known as ultracapacitors, because of their high capacitance density properties, or as electrochemical capacitors (EC). As shown in Figure 2-19, supercapacitors store charge in an electric double layer set up by ions at the interface between a high-surface area carbon electrode and a liquid electrolyte [110-111].

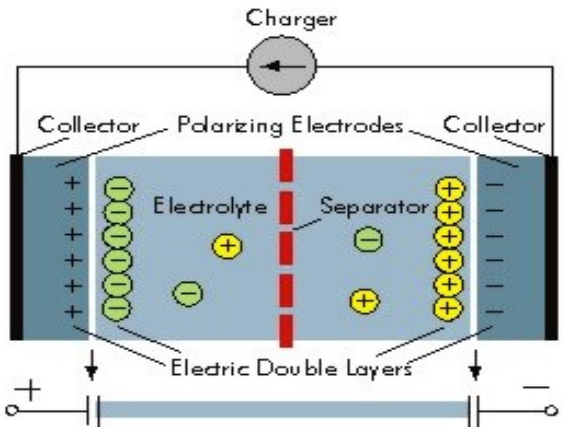

Figure 2-19 Internal structure of a supercapacitor [112]

Because of their internal structure, however, the operating voltage of supercapacitors is limited by the specific potential at which the electrolyte undergoes chemical reactions (e.g., 1 to 3 V per cell). For high-voltage applications, supercapacitors' cells like batteries can be series-connected but voltage balancing techniques may be required to prevent any cell from going into over-voltage. Specific energy of supercapacitors is relatively low and ranges from 1 to 30 Wh/kg. Although high compared to a regular capacitor, 30 Wh/kg is one-fifth that of a consumer Li-ion battery. In addition, whereas electrochemical batteries deliver a steady voltage in the usable power band, the voltage of supercapacitors decreases on a linear scale from full to zero voltage as shown in Figure 2-20.

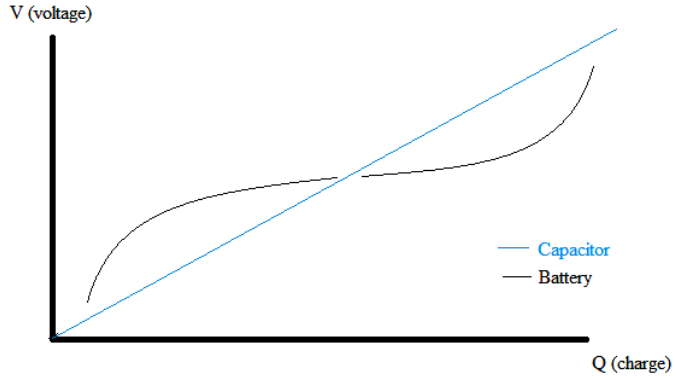

Figure 2-20 Voltage vs charge for battery and capacitor technology; same behaviour can be consider for discharging [113]

Nevertheless, the highly reversible electrostatic charge storage in supercapacitors does not produce the changes in volume that usually accompany the redox reactions of the active masses in batteries, thus causing a limited cycle life of batteries in the range of several hundred to a few thousand cycles versus the millions full charge-discharge cycles of supercapacitors. It is also worthwhile to mention that the energy density of a battery decreases with the decrease of the battery size. Novel lithium battery manufacturing process have been developed to mitigate such an issue, for example: using secondary thin-film deposition [114], downsizing laser welded metal casings and glass feed [115], 3d assembly [116], improving conductivity through nano-sized silicon columns [117], adopting Li intercalation [118], integrating substrate of short length and high surface area [119]. Despite the battery capacity can be increased upon using the above methods, the timing cost of the manufacturing process increases. More recently portable fuel cell system have also been investigated, although scaling down the components used by current fuel cell technology is not simple such as for the water management systems.

Hybrid Energy Storage solutions also represent a valid solution for energy-autonomous WSN applications. The combination of super-capacitors and thin film solid state batteries has been proposed to practically achieve an enhanced performance of EH applications [120]. This is mainly due to the long-term lifetime characteristics of both super-capacitors and thin film batteries, which have demonstrated more than 20 years of operation and over one million

rechargeable cycles [121] and more than 10 years and over 10 thousands rechargeable cycles [122], respectively. However, in terms of efficiency, both technologies present some issues. Super-capacitors with 1-10 F capacitance have a typical leakage current of 0.01-0.1 mA. For example, for the Maxwell PC10 2F supercapacitor, the average leakage current is measured at 40 μA [123] in the first 12 hours of discharge. For applications with charge/discharge of 0.1-10 A current, e.g. camera ash light, such a level of leakage current is negligible. However, for EH powered wireless sensor systems, the charge/discharge current is several orders of magnitude lower at 0.1 mA level. For example, at 3.3 V node's operation, 132 μW of power would be dissipated by the Maxwell PC10 2F supercapacitor. Similarly, thin film batteries typically have a leakage current less than 1 μA but the ESR is 50-75 Ω. When active mode currents of wireless sensor nodes of around 15-17 mA are drained from the battery, then 11-22 mW of conduction loss can be attributed to the internal resistance.

2.3 Wireless sensor nodes and related low power management

A wireless sensor network consists of three main components for gathering, processing, and communicating data: nodes, gateways, and software. Tens or hundreds of nodes can be integrated into the same network together with other control systems. Nodes interface with sensors to monitor assets or their environment as shown in Figure 2-21.

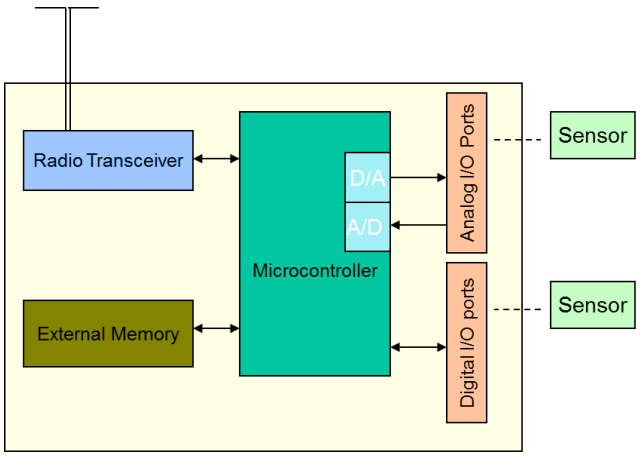

Figure 2-21 A typical wireless sensor node internal block

The acquired data are wirelessly transmitted to the gateway so as to establish a communication with neighboring nodes or the outside world over the different and non-overlapping channels of the available ISM radio bands, which are: 433 MHz, 916 MHz, and 2.4 GHz. The gateway acts as the network coordinator in charge of node authentication and message buffering. It can operate independently or connect to a host system where data can be collected, processed, analysed, or simply viewed through dedicated software.

One way to minimise the overall power consumption of a PEH powered wireless sensor system is to reduce the power consumption of the sensing nodes at hardware level. Therefore, from the wireless sensor node structure in Figure 2-21, it follows that the first key step lies in the microcontroller selection. CPUs with 4-, 8-, 16-, and 32-bit data bus width are typically used for the implementation of wireless sensor nodes. 4-bit CPUs are mainly intended for acquiring on/off signals such as light detection, temperature, and movement. Wireless sensor nodes realised with 8-bit CPU have on average a power consumption that varies from 3 mW up to 30 mW in active mode of operation and is about 10 μW in power down mode. Wireless sensor nodes with 16/32-bit CPU are intended for multimedia data acquisition such as voice and image. Their power consumption is therefore higher; for example, a 32-bit CPU in active mode can consume more than 100 mW. Popular choices for the 8-bit and 16-bit microcontroller are the ATmega128L (Atmel Corporation, San Jose – CA) and the MSP430 (Texas Instrument, Dallas – TX), respectively. An internal memory is provided for both these devices, thus reducing further the power consumption of the wireless node, although specific memory requirements may be different depending on the targeted end-application. More details of ATmega128L and MSP430 devices can be found in [124] and [125], respectively, whilst in Table 2-4 is presented a more exhaustive list of commercially available microcontrollers and their power consumption.

Table 2-4 Often used microcontrollers and their power consumption

CPU	CPU bit	Voltage supply (V)	Power active (mW)	Power down (µW)	Sensor Node
EM6603	4	1.2 – 3.6	0.0054	0.3	
EM6605	4	1.8 – 5.5	0.012	0.9	
ATtiny 261V / 461V / 861V	8	1.8 – 5.5	*0.38 mA @ 1.8V, 1MHz	*0.1	
PIC16F877	8	2 - 5.5	1.8	3	CIT
MC68HC05PV8A	8	3.3 - 5	4.4	485	
AT90LS8535	8	4 - 6	15	45	WeC Rene
ATmega163L	8	2.7 – 5.5	15	3	Rene2 Dot
ATmega103L	8	2.7 – 3.6	15.5	60	Mica IBadge
C8051F311	8	2.7 – 3.6	21	0.3	Parasitic
ATmega128L	8	2.7 – 5.5	26.7	83.15	Mica, Mica2Dot, Mica2, BTnode
PIC18F452	8	2 – 5.5	40.2	24	EnOcean TCM
80C51RD+	8	2.7 – 5.5	48	150	RFRAIN
MSP430 F149	16	1.8 - 6	3	15	Eyes, BSN
MSP430F1611	16	1.8 – 3.6	3, 1.5	15, 6	Telos, SNoW[5]
MC68EZ326	16	3.3	60	60	SpotON
AtmelAT91 ARM Thumb	32	2.7 – 3.6	114	480	
Intel PXA271	32	2.6 – 3.8	193	1800	iMote2
Intel StrongArm SA1100	32	3 – 3.6	230	25	WINS, µAMPS

In addition to the microcontroller, the radio module of the wireless sensor node is the other main source of power consumption depending on factors such as: modulation scheme, data transfer rate, communication protocol, and operational

duty cycle. Examples of commercially available radio modules and their power consumption are presented in Table 2-5.

Table 2-5 Often used radio modules and their power consumption

Type	Clock (MHz)	Rx power (mA)	Tx power (mA/dBm)	Power down (µA)
MPR300CB	916	1.8	12	1
SX1211	868-960	3	25/10	
TR1000	916	3.8	12/1.5	0.7
CC1000	315-915	9.6	16.5/10	1
mRF401	433 - 434	12	26/0	
CC2500	2400	12.8	21.6	
XE1205	433 - 915	14	33/5	0.2
CC1101	300 - 928	14.7	15	0.2
CC1010	315 - 915	16	34/0	0.2
CC2520	2400	18.5	17.4/0	<1
CC2420	2400	19.7	17.4/0	1
CC1020	402 - 915	19.9	19.9	0.2
CC2430	2400	19.9	19.9	
PH2401	2400	20	20	
nRF2401	2400	22	10/0	0.4
CC2400	2400	24	19/0	1.5
CC2530F32	2400	24	29/1	
RC1180	868	24	37/0	
LMX3162	2450	27	50	
STD302N-R	869	28	46/0	
MC13191/92	2400	37	34/0	1
ZV4002	2400	65	65/0	140

It is worthwhile to mention that integrated solutions, which include microcontroller and wireless transceiver together on the same chip, are also available and could represent a better alternative to reduce internal power dissipations despite their lower flexibility. An example is the 2.4 GHz IEEE 802.15.4 compliant JN5148 (NXP Semiconductors – Manchester, UK) with 32-bit RISC CPU and integrated 4 Mbit serial flash memory, 128 kB ROM memory, and 128 kB RAM for program code and data storing [127].

From the communication point of view, power consumption of a wireless sensor node should be considered based on the status of its physical layers:

- Off, when the only node's power consumption is leakage current but time of the order of milliseconds may be required to wake it up;
- Sleep/Standby, when the node consumes as little as 100-300 μW and can wake-up quickly unless the main crystal oscillator of the microcontroller is turned off;
- Listen, when the node is listening for a packet to arrive, so most of the radio receiver is on with a power consumption ranging from 9 mW up to 40 mW;
- Active Rx, which is similar to the Listen state but with power consumption up to 50 mW because of the transceiver and additional circuitry requirements;
- Active Tx, when the node is in the transmit state and active components involved include the RF power amplifier for an average power consumption of around 40 mW with 0 dBm of transmission power.

Table 2-6 shows, as an example, the power consumption of a Tyndall wireless sensor node at 3.3 V and with a sleep mode of 300 s interval between two consecutive measurements of temperature and light intensity.

Table 2-6 Power consumption of a Tyndall node at 3.3 V [121]

Mode	Symbol	Power (mW)	Current (mA)	Time (ms)	Energy (mJ)
Active Mode	P_{Act}	57.1	17.1	87	4.97
Sleep Mode	P_{Slp}	0.033	0.01	300,000	9.9
Average	P_{Avg}	0.050	0.016	300,087	14.87

Based on the aforementioned example, two main polices are typically carried out to save power: 1) the radio transceiver is powered down when unused; and 2) the CPU is switched to a low power mode when no computation is required.

More specifically, in order to achieve efficient energy reduction in the operation of a wireless sensor node, it is necessary to:

- reduce to an absolute minimum the energy needed for data transmission;
- optimise for speed and duration all processes running in the wireless sensor node;
- switch off all the components not needed to support the process running at any point;
- reduce the energy consumption of those processes that have to run continuously.

At hardware level these approaches can be implemented by mean of:

- threshold detectors, to monitor whether spontaneous sensor information is available;
- a timer, to control periodical processes;
- control logic, to control the available energy sources (i.e., signals for switching on/off clock/power or adjusting voltage/clock frequency).

Different techniques are then used to reduce the energy consumed by a wireless sensor node, which are:

- duty cycling, namely waking-up the wireless sensor node only for the time needed to acquire a new set of samples and then powering it off immediately [128-131];
- adaptive-sensing strategy, capable to dynamically change the node's activity based on the real dynamics of the occurring operation process [132].

Examples of the aforementioned approaches found in the literature are the following techniques:

- clock gating, which simply shuts off the clock to portions of the wireless sensor node that are inactive (Figure 2-22(a));
- voltage islands, which run the slower blocks at lower frequency and turn down the supply voltage for a pre-determined time interval (Figure 2-22(b));

- power gating, which implies turning off the voltage supply to a certain block so as to stop static and dynamic-power consumption along (Figure 2-22(c));
- dynamic voltage frequency scaling, which adjusts the voltage and clock frequency of each block so as to perform on time the pre-selected task (Figure 2-22(d));
- dynamic threshold voltage control, which dynamically controls the threshold of individual sets of transistors (Figure 2-22(e)).

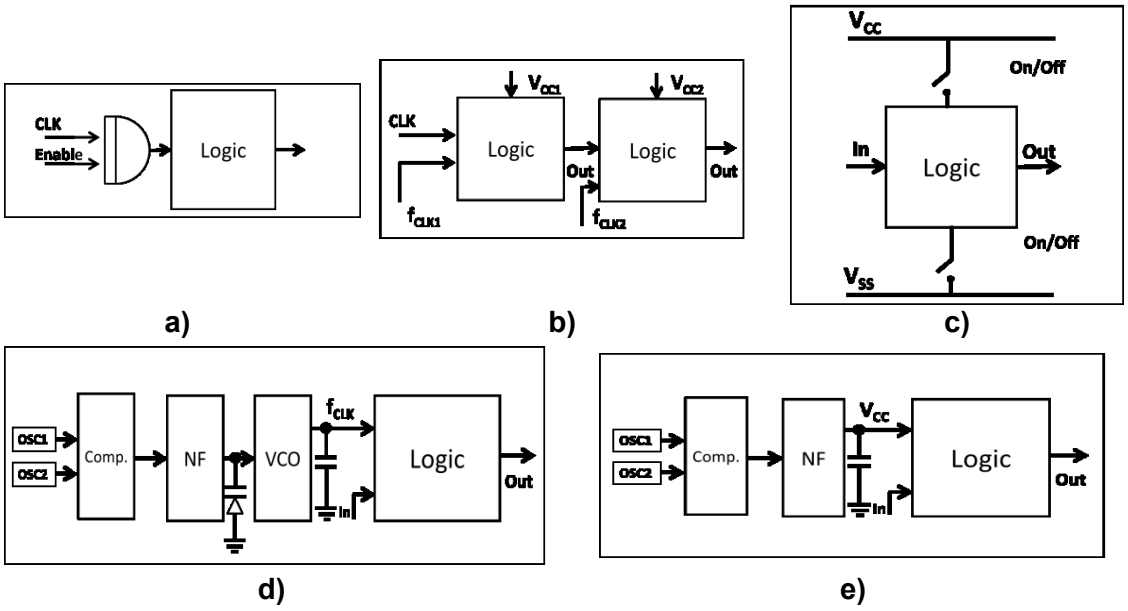

Figure 2-22 Power management techniques for wireless sensor nodes: (a) clock gating, (b) voltage islands, (c) power gating, (d) dynamic voltage frequency scaling, and (e) dynamic threshold voltage control

At software level the implemented protocol layers also influence the power consumption of the sensor node as well as the quality of the wireless communication. The standards developed by the IETF typically run on radio chips that comply with the IEEE802.15.4 standard. IEEE802.15.4 provides a healthy trade-off between data rate (250 kbps), range (10 s to 100 s of metres), power consumption (5 mA to 20 mA when transmitting or receiving) and packet size (up to 127 bytes) [133]. This trade-off makes IEEE802.15.4 a good fit for WSNs although component-based architectures working on dedicated systems, such as TinyOS, have also been developed aiming to achieve low complexity and power consumption through use of sleeping phases of longer duration

[134]. Other narrowband (FSK) or spread spectrum communications, such as DS-SS (e.g., ZigBee) and FH-SS (e.g., Bluetooth) are also currently used to establish correct data communication through wireless sensor nodes [135]. In addition, although typical commercially-available devices transmit data at a power of around 0 dBm and feature sensitivity as low as -110 dBm, some energy-aware data communication strategies can be implemented so as to adapt the instantaneous performance to meet the timing and error rate constraints while minimising energy/bit. Over the conventional methods, which involve direct communication with the base station, or multi-hop schemes, which use for example other intermediate nodes for data transmission, novel developed data-dissemination schemes are for example:

- Low Energy Adaptive Clustering Hierarchy (LEACH), which has been designed for sensor networks where an end-user wants to remotely monitor the environment [136].
- Maximum Energy Cluster Head (MECH), which has self-configuration and hierarchical tree routing properties [137]. It constructs clusters based on radio range and the number of cluster members, thus distributing more equally the cluster topology in the network.
- Media Access Control (MAC) scheme, which has been implemented in different topologies [138] of two main categories: 1) contention-based schemes, designed for minimum delay and maximum throughput with transceivers monitoring the channel at all times; and 2) reservation-based or schedule-based schemes, where the neighboring radios are detected before allocating collision-free channel to a link. In particular, an example of 1) is represented by Sensor-MAC (SMAC), in which a node periodically sleeps during the transmission period of other nodes; whilst an example of 2) is represented by Time Division Multiple Access (TDMA)-based solutions and Power Aware Clustered TDMA (PACT).
- Address-free architecture (AFA), in which a randomly selected unique identifier is assigned for each transaction [139].

Security and authenticity should be also guaranteed as wireless data communication is typically unreliable, mainly because of external interference and multipath fading. The use of channel and path diversity can be the key to build reliable wireless systems without sacrificing low power operation. Such techniques, for example, were implemented in the SmartMesh® system (Dust Networks, Inc. – Hayward*, CA*) through time-synchronised, channel-hopping mesh networking. The power efficiency of the sensors is also crucial and several factors need to be considered such as: volume, assembly compatibility with other system components, packaging needs, duty cycling suitability, signal sampling and conversion, signal conditioning, and A/D conversion. Especially this last factor has to be considered in terms of power consumption and quality of the output signal for the choice of analogue or digital devices. It is also worthwhile to mention that the costs of sensors and the circuitry involved must be taken into consideration. In fact, especially in the case of large networks required for example by WSNs for SHM, the implemented wireless solution must be economically viable.

2.4 Interfaces for integrated PEH systems

Modelling of simple PEH systems (e.g., harvester connected to a resistive load [140-141]) and more complex systems (e.g., harvester connected to an electrical load through a specific PMM [142-143]) have showed that the circuit connected to the piezoelectric harvester influences its vibration response and, in turn, its power output. In order to enhance the energy extraction from the transducer and reduce the gap between the energy scavenged by small-scale piezoelectric harvesters and the energy demanded by wireless sensor nodes, different electronic interface circuits have been proposed. Two main research lines have been followed by respectively focussing on the development of:

- interfaces for matching the impedance of the piezoelectric transducer;
- interfaces for a non-linear treatment of the transduced signal.

2.4.1 Impedance matching interface circuits

In electronics, the maximum power transfer theorem [144] applied to AC circuits states that, in order to obtain maximum external power from a source, the load impedance must equal the complex conjugate of the source impedance as viewed from its output terminals. If Z_S is the impedance of the piezoelectric harvester and Z_L the impedance of the connected electrical load, this means in formulas that the maximum power transfer from the piezoelectric harvester is obtained when:

$$Z_S = Z_L^* . \tag{2-8}$$

Because of the dielectric behaviour of the piezoelectric transducer, for operational frequencies below its resonance, an inductive load needs to be added in order to implement the complex conjugate match of the transducer's impedance and increase the efficiency of the energy harvester based on the conditions of the maximum power transfer theorem. In [145], Renno *et al.* demonstrated that adding an inductor to a piezoelectric EH circuit can substantially enhance the harvested power and allow tuning the piezoelectric device for achieving a broader range of operational frequencies. In [146], Brufau-Penella and Puig-Vidal experimentally validated this concept on a commercial piezoelectric transducer (i.e., QP40w from Mide Technology) by showing 20% increment of the generated power when an inductive element was directly connected between the transducer and a resistive load. However, this implementation was suitable for a high operational frequency only (i.e., at 935 Hz, the fourth resonant mode of the piezoelectric harvester) but not practical for low frequencies because of the very-large value of inductive reactance needed to make the complex conjugate impedance match work. Since for low frequencies the size and weight of the inductors become exceedingly large and very poor becomes their quality factor, an approach to overcome the challenge in the literature is the implementation of the gyrator theory. A gyrator device, in fact, realises an inductance in the form of an

integrated circuit, inverting the current-voltage characteristic of a capacitive circuit [147] as shown in Figure 2-23.

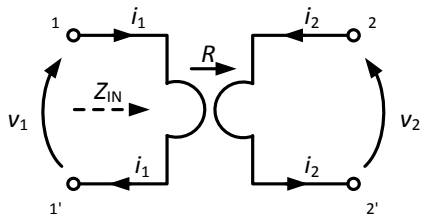

Figure 2-23 Gyrator schematic

Being R the gyration resistance, the Z matrix representation of the gyrator is symbolically given by:

$$Z = \begin{bmatrix} 0 & -R \\ R & 0 \end{bmatrix}. \tag{2-9}$$

Therefore, the gyrator transmits a signal unchanged in the forward direction but generates a 180º phase-shift of the backward travelling signal [148]. Now, if port 2 - 2' is terminated into a capacitor C, the input impedance seen at port 1 - 1' is equal to: $Z_{\text{in}}(\text{i}\omega) = \text{i}\omega k^2 C$, which corresponds to an inductor of $k^2 C$ Henries. So, an inductor has been realised by mean of the gyrator terminated into a capacitor.

There have been distinct techniques of inductance simulation by the inversion of a capacitive driving-point function, using both op-amps [149-157] or transistors [158-160] as active devices. Multi op-amp configurations with gyrators or positive impedance converters (PICs) are used in applications requiring high *Q* with low sensitivity. Beside those, active devices like positive-gain voltage-controlled voltage source (VCVS) [161], negative immittance converters (NICs) [162], voltage to current converters or vice versa [163] have been presented. Many attempts have also been shown in realising appropriate feedback networks to increase the *Q*-factor [164] such as negative resistance circuits in conjunction with the simulated inductors. However, for simulation of low *Q* inductances, single amplifiers inductances are preferable due to the additional advantages of lower cost and power consumption, being the number

of passive components involved as low as two resistors and one capacitor. For the same reason, synthetic inductors with op-amps have been found more suitable for EH applications given also the high gain, high input impedance and very low output impedance of such configurations. Examples of single op-amp synthetic inductor configurations as proposed by Ford and Girling [149], by Prescott [150], and by Berndt and Dutta Roy [151], respectively, are depicted in Figure 2-24:

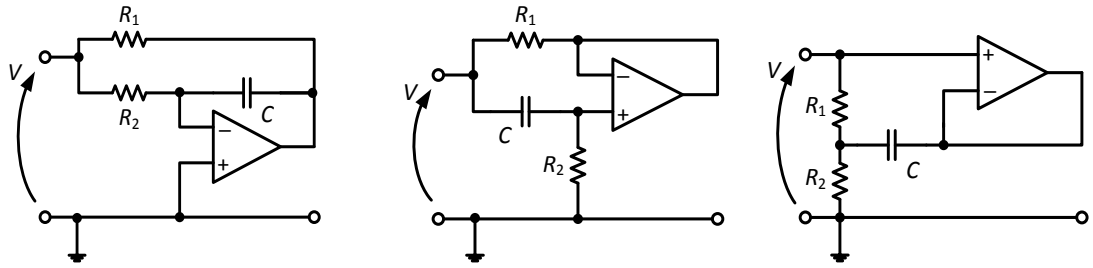

Figure 2-24 Single op-amp synthetic inductor configurations: (a) Ford and Girling circuit [150]; (b) Prescott circuit [151]; and (c) Berndt and Dutta Roy circuit [152]

The electrical scheme in Figure 2-24(a) shows an op-amp connected as an integrator; in the other two circuits, respectively in Figure 2-24(b) and Figure 2-24(c), the op-amp is connected as a voltage follower. All the configurations in Figure 2-24 simulate a grounded inductance. However, in order to realise an interface for matching the impedance of the piezoelectric transducer, the implementation of a series inductance is required. A simple way to obtain a floating inductance with no need of additional op-amp stages has been proved via connecting two gyrators back-to-back. An example of a floating inductor, obtained from the original Prescott design, is depicted in Figure 2-25:

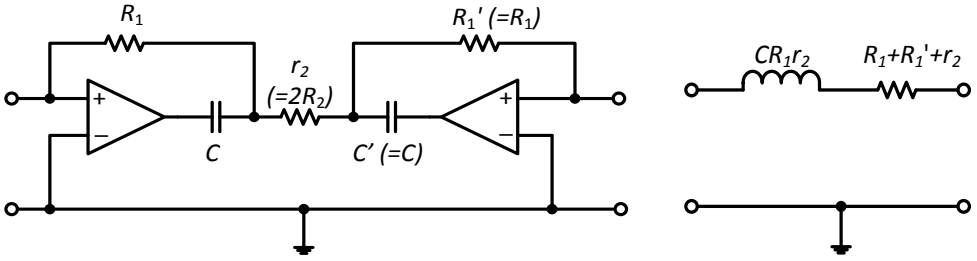

Figure 2-25 A synthetic floating inductor: (a) electrical scheme and (b) equivalent circuit

The impedance of the floating inductor in Figure 2-25 is equal to:

$$Z(\mathrm{i}\omega) = R + \mathrm{i}\omega L \tag{2-10}$$

where,

$$R = 2(R_1 + R_2) \tag{2-11}$$

and

$$L = 2CR_1R_2\,. \tag{2-12}$$

It is worthwhile to mention that the two gyrator configurations used for achieving the floating inductance can be different as the only condition that must be satisfied is:

$$CR_1 = C'R_1\,. \tag{2-13}$$

From Equation (2-13), the resulting impedance in the generalised case is equal to:

$$Z(\mathrm{i}\omega) = R_1 + R_1' + r_2 + \mathrm{i}\omega C\mathrm{R}_1\mathrm{r}_2' \tag{2-14}$$

where

$$r_2 = R_2 + R_2'\,. \tag{2-15}$$

Synthetic impedance circuits as described above have been successfully used in piezoelectric shunt circuits for vibration damping so as to simulate large inductance values up to thousands of Henries. Such inductor implementations, however, are generally a poor representation of ideal inductors as they are difficult to tune, very sensitive to component variations, and require an external power supply. Although modern op-amp technology requires a very low supply, the described configurations involve very big series resistances. The gyrator theory, in fact, makes use of resistance multipliers to invert the capacitive load into an inductive one. Since, in the low-frequency range, the inductance required for the CCIM reaches up to thousands of Henries, it follows that resistors of the order of kilohm may be required as from Equation (2-12). Furthermore, these resistances are added in series to the energy harvester,

which means that the harvested energy can hardly flow towards the end-user load. Therefore, synthetic impedance circuits are not really suitable for practical implementations of small-scaled PEH systems.

Another approach found in the literature with regards to the implementation of impedance matching interface circuits for PEH systems is based on the use of a DC/DC converter, which permits to achieve an adaptive control similar to the one used for maximising the power output from solar cells. Basically, the optimal power point is tracked by controlling the converter so that its input average current is proportional to its input voltage with an average voltage/current ratio equal to the matching load resistance. In [165], for example, a bidirectional DC/DC converter tuned by a two-dimensional Maximum Power Point Tracker (MPPT) via a microcontroller was used to obtain an equivalent resistive-reactive load and achieve the maximum power output from a piezoelectric harvester. In [166], Ottman *et al.* achieved automated power optimisation by using an adaptive DC/DC converter right after the AC/DC converter of standard EH system configurations so that the DC output of the rectifier could be regulated to maximise the power transfer to the storage device. As shown in Figure 2-26, the piezoelectric power output is rectified and temporary stored by the capacitor C_o, whose voltage level is kept at the optimal rectifier voltage. The input power is then transferred through the DC/DC converter to a battery at the voltage level V_{esd} with a 400% increase of energy flow in comparison with standard configurations.

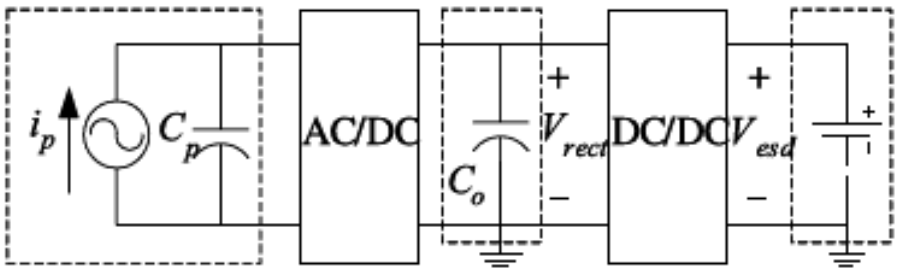

Figure 2-26 Generalised two-stage PEH circuit. From left to right, inside the dashed boxes: piezoelectric element; temporary storage; energy storage device

In another work [167], assuming that the piezoelectric material can generate a higher voltage than the voltage level of the battery, Ottman *et al.* introduced a method to regulate the power flow from the piezoelectric element to the connected electrical load by defining the optimal duty cycle for a step-down converter operating in discontinuous conduction mode (DCM). Similarly, Lefeuvre *et al.* [168] proposed the use of a sensor-less buck-boost converter running in DCM to track the optimal working points of a piezoelectric generator. Lallart and Inman [169] reported an architecture capable of enhancing vibration EH when the piezoelectric voltage reaches the optimal voltage based on sensing zero-crossing detections of the harvester's displacement. In order to reduce the power consumption of the control circuit, a simple control technique based on the use of a buck-boost (flyback) converter was proposed in [170]. In [171], a power conditioning circuit consisting of an AC/DC converter followed by a DC/DC converter with adaptive duty cycle was implemented by Kong *et al.* for the resistive matching of a given piezoelectric harvester's impedance. Also in [172], the non-linear interface circuit presented by Kim *et al.* was taken as an equivalent resistance in order to increase the electrical power transfer from a multi-layered piezoelectric transducer. Although more power can be extracted upon implementing those methods, they may become impractical due to their power consumption levels that are not always suitable for the low-power piezoelectric transducers at the current state of the EH technology development. Moreover, significant loss of the harvested power arises when the impedance of the EH circuit matches the equivalent impedance modulus of the piezoelectric generator rather than its real and reactive parts separately [171].

2.4.2 Non-linear electronic interface circuits

In a PEH system, the rectified voltage level of the transduced signal usually depends on the vibration amplitude. If a simple AC/DC converter is directly connected to the harvester output, it is not possible to achieve the optimal rectified voltage for all vibration levels; rather, if the generated electric charge does not build-up a voltage across the inherent capacitance of the piezoelectric element higher than the voltage across the smoothing capacitor after the

AC/DC rectifier, then the harvested energy will not flow further as it cannot be stored. Non-linear electronic techniques have been implemented in small scale for enhancing the output voltage of typical piezoelectric harvesters and achieving gain up to 20 in terms of energy conversion and 10 in terms of harvested energy [173]. The process operated by such interfaces consists of reversing the piezoelectric voltage when it reaches its extrema (maximum and minimum values) and permits reducing the time shift with its speed so as to allow a non-linear conversion. The voltage continuity of the signal transduced by the piezoelectric harvester also insures a cumulative process that increases the voltage amplitude and further permits increasing the effective bandwidth of the generator [174]. By taking advantage of the dielectric nature of the piezoelectric element, the inversion process has been commonly performed by briefly connecting the piezoelectric element to an inductive element, among other elements (e.g., a capacitor [175]); thus being identified as SSHI process. In such a way, the inherent capacitance of the piezoelectric harvester and the added inductive element shape a resonant electrical network. An example of the SSHI circuit implementation is shown in Figure 2-27(a), which depicts a connection of the added inductor in series (series SSHI) with the piezoelectric energy harvester operated through an in-line digital switch. In the interface circuit configuration of Figure 2-27(b), the inductive element is also connected through a switch to the piezoelectric harvester but in parallel (parallel SSHI) so that the voltage inversion occurs after an energy extraction process [176]; on the contrary, inversion and energy extraction occur at the same time for the series SSHI [177-178].

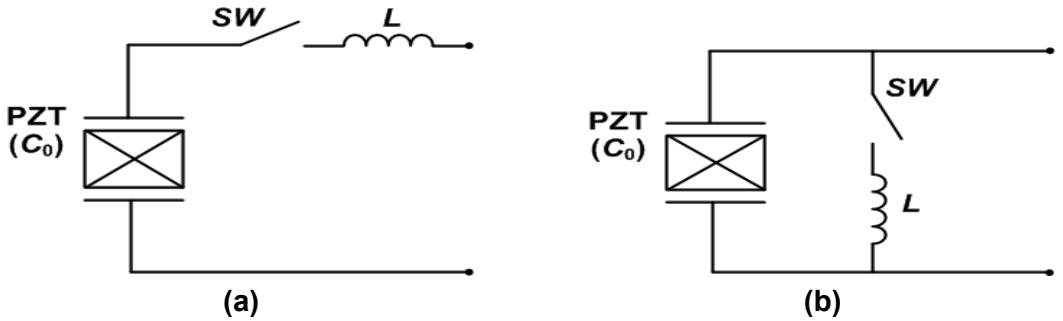

Figure 2-27 SSHI circuit implementations in the (a) series and (b) parallel configurations

The digital switch is closed for half a period of the electrical oscillation (whose period is much smaller than the vibration period), thus leading to an almost instantaneous inversion of the voltage. Particularly, this is the case of PEH systems operating under a low-frequency excitation. The voltage inversion, however, is not perfect because of the losses in the switching device (especially resistive losses in the inductor).

From the series SSHI and parallel SSHI configurations other approaches have arisen such as: the synchronised switching and discharging to a storage capacitor through an inductor (SSDCI) [179], where the switching process is commanded through a diode bridge rectifier for transferring the charge cumulated in the piezoelectric element to a storage capacitor through an inductance; the synchronous electric charge extraction (SECE) [180], where the energy available on the piezoelectric element is transferred to an inductance, used as energy storage, and further transferred to a capacitor once the piezoelectric element has been disconnected from the circuit; and the double synchronised switch harvesting (DSSH) [181], where the energy on the piezoelectric element is transferred first to an intermediate capacitor and used for the inversion process, then from the intermediate capacitor to the inductance, and finally to the storage stage. Architectures where the inversion process is enhanced by an initial voltage on an intermediate capacitor, like the enhanced synchronised switch harvesting (ESSH) [182], by featuring energy injection through a feedback loop [183], or by an inverter for an active EH scheme [184-185] have also been presented. In this last case, by assisting the voltage inversion via pulse-width modulation (PWM), for example, is possible to achieve an almost perfect inversion. Figure 2-28 shows the normalised harvested powers under constant vibration magnitude for different EH configurations.

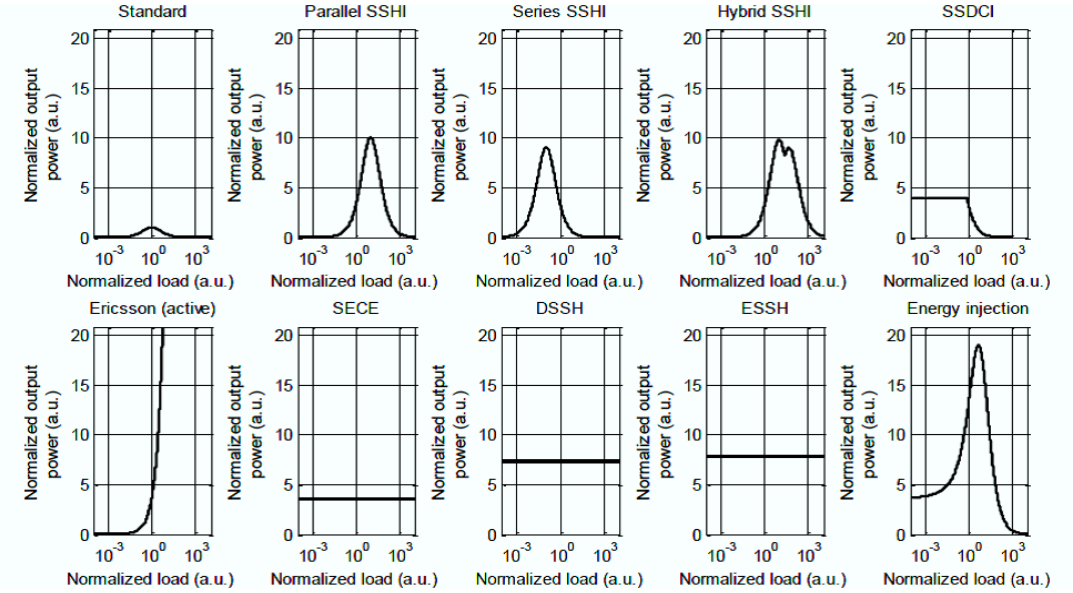

Figure 2-28 Normalised harvested powers under constant vibration magnitude for different EH configurations (Figure adapted from [186])

From Figure 2-28, it can be seen the ability of non-linear electronic interfaces to enhance the power output of piezoelectric harvesters. Although more power can be extracted upon implementing the methods described above, they may become impractical due to their power consumption levels that are not always suitable for the low-power piezoelectric transducers at the current state of the EH technology development. Indeed, whilst the process of the piezoelectric voltage inversion can be simply implemented by briefly switching the connection of the piezoelectric element output onto an inductor, a realistic implementation of that switching control can be costly in terms of energy supply and determine a negative balance between harvested energy and required energy. In order to avoid the use of an externally powered microcontroller as in most of the studies regarding the implementation of such non-linear treatments, several architectures have been proposed to make the switch control autonomous [187-193] despite the drawback of the high power consumption for the use of active elements. Two main approaches have been followed to date for the extrema detection of the SSHI implementation: 1) computing the derivative of the piezoelectric voltage (which gives the extremum position when it cancels); 2) comparing the piezoelectric voltage with its delayed version. Nevertheless, 1) is not really stable and is sensitive to noise as a feature of the derivative operator;

and 2) suffers from the limitations of the dissipative components involved and the switching delay phase. The limitations of 2) also arise from the self-powered synchronised switch system proposed in [194] by Lallart *et al.*, where an envelope detector with energy storage, a comparator, and a digital switch are realised by use of only common off-the-shelf-components. In addition, such a self-powered switch design may result quite complex for the techniques of the SECE, DSSH, ESSH, and energy injection although some implementations have been presented [195]. With respect to the implementation of the control system, difficulties also occur in the particular case of small-scale systems and microsystems (e.g., MEMS devices) [196]. The main limitations in these cases are due to the electronic command and, especially, to the threshold values (e.g., voltage gaps) featured by discrete components such as diodes and transistors [193]. In order to reduce the minimum voltage requirements for the rectification of the piezoelectric harvester's signal, the use of a transformer has also been proposed in the synchronised switch harvesting on inductor using magnetic rectifier (SSHI-MR) technique [197] and hybrid SSHI technique [198], where the voltage gap seen by the piezoelectric element is divided by the transformation ratio. However, the aforementioned techniques suffer the limitation of the transformer's miniaturisation for possible MEMS implementations. Diodeless implementation of the rectification stage by mean of reed switches has also been presented in [199] and only conceptually introduced for the series SSHI in [186]. Nevertheless, the former design appears of hard tuning in correspondence to low-magnitude acceleration inputs whilst the latter involves switching mechanisms which, in turn, involve the foreseen control issues for the detection of maxima and minima of the piezoelectric voltage.

2.5 Integrated PMM for vibration EH systems

An effectively integrated EH powered wireless sensor system must be capable to guarantee a match between harvested and consumed energy. Otherwise, if energy consumption exceeds energy generation, the system will stop working sooner or later due to either empty energy storage or not sufficiently available

ambient sources. Kansal *et al.* presented an energy-neutral operation theory in order to quantify such an energy matching condition [200]. This theoretical work considered non-ideal energy storage devices and same mathematical model for both the system's energy sources $P_s(t)$ and consumers $P_c(t)$. In addition, an efficiency η lesser than one was considered for the energy storage device along with the power leakage $P_{leak}(t)$. Therefore, the energy-neutral operation was stated upon satisfying the condition:

$$B_0 + \eta \int_0^T \left[P_s(t) - P_c(t)\right]^+ dt - \int_0^T \left[P_c(t) - P_s(t)\right]^+ dt - \int_0^T P_{leak}(t) dt \le B \qquad \forall T \in [0, \infty) \quad (2\text{-}16)$$

where B and B_0 are the storage capacity and the initial stored energy, respectively, whilst $^+$ is the Heaviside function of the quantity that is applied to multiplied by itself.

The harvested energy has to reach a minimum threshold in order to activate the end-application. Although such activation has been often based on a pre-fixed time demand, different technologies have been developed for monitoring the amount of the harvested energy so as to supply power to the electrical load on an event basis and optimise the overall energy transfer from the piezoelectric transducer. In general, any kind of sensing can be used to find out when energy is enough for supplying the end-user load. In [201], for example, a hydrogen sensor was used for waking up the microcontroller which commands energy-autonomous RF transmissions. However, especially in regard of PEH systems, voltage detection across the energy storage device has been usually implemented in the literature. Some examples of vibration EH powered wireless sensor systems that integrate such a power management approach are following described. At the MIT Media Laboratories, Paradiso and Feldmeier developed a compact piezoelectric pushbutton, which is totally energy–autonomous and capable to wirelessly transmit a digital 12-bit ID code to the surrounding region within 50-100 foot radius [202]. As from Figure 2-29, a 4 μF tank capacitor collects the charge transferred from a button strike and powers a MAX666 low-dropout linear regulator for the power supply of a 418 MHz

wireless transmitter. At roughly 10 ms after the strike, the regulator becomes active thus providing power to the transmitter and the encoder circuitry for at least 30 ms. The required time for successful completion of a transmission is 20 ms that, for a consumption of power approximately equal to 7.5 mW, leads to a total of 150 J. Nevertheless, the piezoelectric transformer is capable of delivering 2 mJ of energy per push, hence 0.5 mJ at 3 V after the linear regulator.

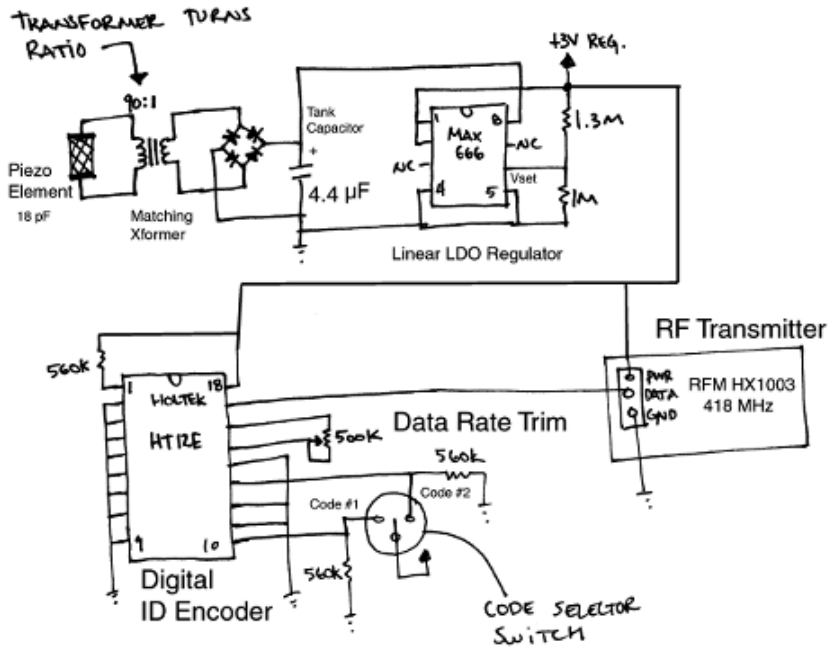

Figure 2-29 Schematic diagram of a self-powered pushbutton (Figure reprinted from [202])

Similarly to the case above, the piezoelectric transmitter module PTM 100 (EnOcean Gmbh – Oberhaching, Germany) was developed for the implementation of a self-powered 868 MHz wireless remote control. In this module, a common piezoelectric transducer is actuated by a bow through an appropriate push-button or switch rocker. Electrical energy is generated every time the bow is pushed down and, as a consequence, an RF telegram is transmitted including a 32-bit module ID. A different telegram data is generated when the bow is released and transmitted, as for the bow activation, along with the operating status of the contact nipples used as in the configuration of Figure 2-30.

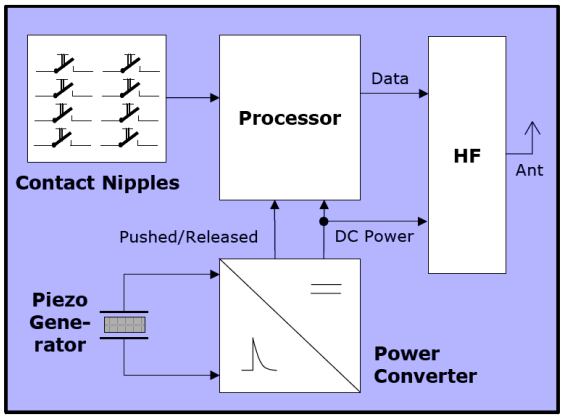

Figure 2-30 Block diagram of the piezoelectric transmitter module PTM100 (Figure courtesy of EnOcean Gmbh)

A micro power generator, which can generate up to 120 μW with a maximum output voltage of 2.4 V, was developed by Yuen [203]. The harvested energy is stored in a 1 mF capacitor. Then, as from Figure 2-31, a start-up module is used to activate a DC/DC switching regulator in order to power a long-term temperature monitoring system. Data are measured in a time of about 1.4 s and transmitted via radio frequency to a host computer with an overall energy consumption of around 212 μJ. Under an excitation of 4.63 m/s^2 of acceleration and 80 Hz of frequency, an interval of 32 s is needed before the first activation of the wireless RF thermometer whilst 18 s are enough for later measurements.

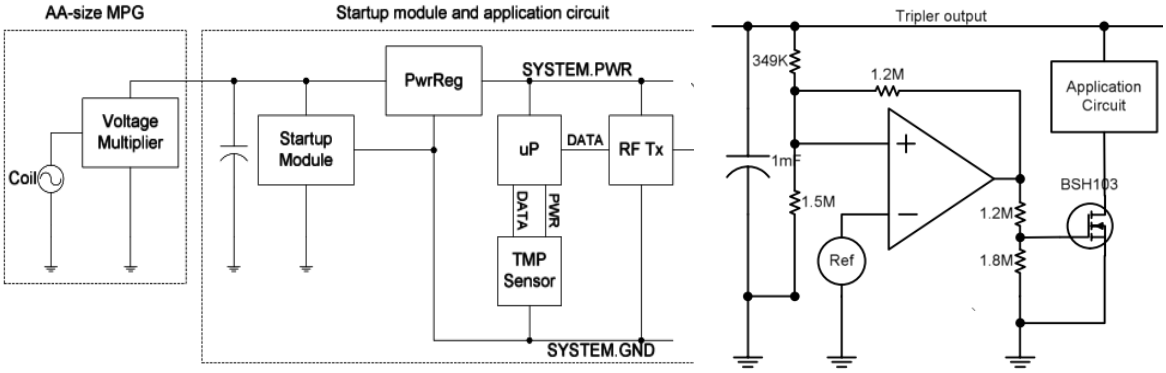

(a) **(b)**

Figure 2-31 A micro power generator: (a) system block diagram and (b) schematic of the start-up module (Figure adapted from [203])

As in the aforementioned work carried out by Yuen, other affirmed cases of vibration EH powered wireless sensor systems using electromagnetic

transducers have been reported in literature such as the industrial monitoring technology developed by Perpetuum Ltd (Southampton, UK) with harvesters mechanically tuned to an optimised resonant frequency typically in the band around 50-60 Hz [204]. Examples of PEH powered wireless sensor systems for SHM have also been reported in literature such as the works on self-powered damage detection wireless sensors carried out in [205] and [206]. In [207], Churchill *et al.* developed a wireless sensor node powered by 17 cm^2 piezo-harvester on a composite beam test specimen to demonstrate the capability of powering an embedded WSN without batteries. Under a harmonic excitation from 75 to 300 με peak and frequency between 60 and 180 Hz, the piezo-harvester implemented by Churchill *et al.* generated up to almost 0.8 mW. The harvested energy was then used to power a wireless sensor node (StrainLink, MicroStrain, Inc., Williston – Vermont, USA) at intervals as short as 15 s under the peak strain of 300 με at 180 Hz. Such a technology was also used by Microstrain in 2007 for the first successful flight test of an EH powered wireless strain sensor capable to directly monitor the load of a helicopter rotating pitch link [208]. Four piezoelectric elements were installed on the pitch link of a Bell Model 412 experimental rotorcraft so that, running entirely from the harvested strain energy, load data were continually logged at acquisition rates up to 128 samples/second and wirelessly transmitted on board and up to an external distance of 50 feet from the rotorcraft. With regard to aerospace applications, several cases have been reported on vibration-powered systems capable of detecting the defects of operating elements on helicopter structures. The mechanical energy that can be harvested from vibrations in helicopters originates from sources such as the main rotor, the tail rotor, the engine and other rotating systems (e.g., hydraulic pumps and air forces acting on the fuselage) [209]. A compelling work, which focusses on harvesting the in-flight vibrations of a helicopter, was carried out in a laboratory by Zhu *et al.* [210]. In that work, Zhu *et al.* developed a credit card sized self-powered smart sensor node, which generates a maximum output power of 240 μW under an excitation of 67 Hz and a peak acceleration of 0.4 g, and transmits data of acceleration, temperature, and pressure at intervals of around 800 s. Particularly, a voltage

supervisor was used for monitoring the energy harvested from the ambient vibrations and collected in a 0.55 F supercapacitor before it was delivered to a TPS61097 DC/DC converter (Texas Instruments Inc. – Dallas, TX) that stepped up to 3.3 V voltages starting from 0.9 V for the intended application. Flight testing of a Radio Controlled (RC) aircraft was also performed by Anton *et al.* as a proof of concept study on PEH in Unmanned Aerial Vehicles (UAV) applications [211] whilst, with focus on a Royal Australian Air Force (RAAF) F/A-18 aircraft, Galea *et al.* have implemented a self-powered SHM system on a composite bonded patch attached to an aileron hinge [212]. From flight loads data and design data of the hinge, an excitation of between 8 Hz to 42 Hz in frequency and operational peak strains of the order of 1500 με were assumed by the work of Galea *et al.* A combination of two stacks of three 28 μm thick, 155 mm long by 20 mm wide PVDF elements, located on both sides of the strut, and two 0.66 mm thick, 32 mm long by 12.5 mm wide PZT bimorph elements, located on the lower side of the hinge strut, were used as electric charge generators. In order to reduce that system's power consumption, sensor data acquisition was performed only when the structure was experiencing significant strain and the information was kept into a Ferroelectric Random-Access Memory (FRAM) to be further downloaded via an external hand-held interrogator.

From the examples shown above it can be seen that, in general, PEH from low frequencies is a relatively new topic and has not been the focal point of the research community. On the other hand, the low-frequency range of structural vibrations covers a lot of practical applications in different fields, such as aerospace, automotive, and industrial monitoring. Because of the low mechanical energy levels that are available under low-frequency conditions, harvesting energy from low-frequency vibrations is still a challenge that needs to be addressed for the development of energy-autonomous wireless sensor systems along with minimising their overall power consumption.

2.6 Key findings

Given that the energy harvested from low-frequency vibrations by use of small-scale piezoelectric energy harvesters is not high enough to continuously supply power to WSCNs, possible ways to address the challenge have been searched through an attentive review of the state-of-the-art in PEH systems. From a review of the literature, it has been found that:

- The d_{33} mode of operation for a piezoelectric material, when both the electric field and mechanical strain act in the 3-direction (i.e., in-line with the polarisation of the material - through the electrodes) has usually larger coefficient values than the d_{31} mode (i.e., d_{33} and k_{33} are usually larger than d_{31} and k_{31}). However, the use of the d_{31} mode enables the benefits brought about by the low stiffness of the harvester configuration, thus making it more effective.
- Among other piezoelectric materials and power generator configurations at the current state of the development, embedded MFC and cantilever-based PZT better suit non-resonant and resonant PEH applications, respectively. Indeed, MFC features more flexibility than PZT, but the latter allows for higher power density levels.
- In order to link a piezoelectric energy harvester to an electrical load, such as a WSCN, there is the need of a PMM that performs power conditioning and storage tasks. The energy consumed by this module to make usable the generated signal must be smaller than the harvested energy. With regards to the power conditioning performed by the PMM, challenges mainly arise from the voltage drop of the rectifiers implemented for the signal AC/DC conversion, the size of the components required to build a DC/DC regulator, and the efficiency rates of the regulator (typically, the smaller the difference between the input and output voltages the higher the efficiency). With regards to energy storage devices, low form factor capacitors/supercapacitors and rechargeable lithium batteries are the most promising technologies for PEH systems, being the former preferred for short term power need with higher current bursts.

- WSCNs perform data acquisitions from sensors and wireless transmissions for the intended application. Such operations are typically driven via a microcontroller. Therefore, there are at least three level through which is possible to reduce the overall node's power consumption: hardware, software, and data transmission. Different strategies have been developed in order to reduce the power consumption of WSCNs, being duty-cycling data acquisitions and transmissions the most adopted technique for its simplicity and flexibility.
- Integrated PEH system solutions consider the use of interface circuits with the piezoelectric transducer and aim to increase the overall EH capability through either impedance matching or non-linear treatments of the transduced signal. However, the use of active circuits for an effective realisation of such interfaces has been found in the literature in case of low-frequency excitation and this diminishes their correspondent efficiency for typical small-scale implementations of PEH systems.
- PMMs with specifically developed interfaces with the WSCN that make use of voltage sensing devices across the system's energy storage have also been developed. Their implementation, however, typically involves the use of a microcontroller to manage the flow of the stored energy thus consuming high levels of power. This reduces the system capability to perform fast consecutive data acquisitions and transmissions as time intervals of the duration of minutes are typically required by the WSCN to receive enough power to be in an active state.
- In the case of low-frequency structural vibrations, only few works have been reported that deal at a system level with the mismatch between energy harvested by small-scale piezoelectric transducers and energy demanded by wireless sensor nodes. For those works, an interval gap of the order of minutes has been typically recorded between two consecutive wireless data transmissions due to the lack in energy supply for the node activation.

Considering that in the case of real-life low-frequency application scenarios only few works have been applying a whole-system approach, from the development

of the piezoelectric energy harvester to the WSCN, this research addresses the drawbacks found in the literature in order to achieve a PEH powered system that approaches the capability to continuously power a WSCN running entirely from harvested vibration energy.

3 IMPLEMENTATIONS, ANALYSES, AND CHARACTERISATIONS OF PIEZOELECTRIC ENERGY HARVESTERS

The literature review in Chapter 2 has shown that one common method to harvest energy from ambient vibrations is to utilise the direct effect of piezoelectric transducers. In particular, two mechanical approaches have been identified for such a PEH process: 1) a typically non-resonant approach, where mechanical strain is transferred from a vibrating structure to a piezoelectric transducer integrated into it; and 2) a typically resonant approach, where a mass-spring-damper system is formed by a piezoelectric transducer onto an oscillating supporting structure.

Based on 1) and 2), this chapter describes two low-frequency vibration PEH case studies and focusses on implementations, analyses, and characterisations of resonant and non-resonant piezoelectric energy harvesters, which will be further considered in this thesis to fulfil the targeted aim. Respectively, these are: 1) a MFC patch-like piezoelectric transducer bonded as strain-energy harvester to aluminium and composite substrates, singularly or in multiple combinations, for wireless condition monitoring of large transport commercial aircraft wings; and 2) a ceramic cantilever beam with a proof mass clamped on a Nylon 6-6 support frame for wireless condition monitoring of large industrial machinery. MFC transducers are capable of large deformation with little brittle risk and, along with their flexibility, feature a long lifespan in comparison with traditional piezoelectric ceramic materials such as PZT. For the same active area of the piezoelectric transducer, however, ceramic materials are capable to generate higher currents than MFCs; hence higher power densities, especially in resonant conditions.

3.1 Two low-frequency case studies for SHM applications

Built-in sensors can continuously monitor different variables in different locations and automatically report on early warning signs of structural failure. Therefore, sensed data can be collected to track the historical condition of a structure and

support on-condition maintenance by assessing the health status of a sub-system [213]. Despite corrective maintenance, carried out in response to a fault, and fixed-scheduled maintenance, carried out periodically based on the typical life-span of a component, on-condition maintenance permits intervention before a fault is developed as many modes of failure show early warnings signs. The use of sensors thus aims to produce real-time and continual health assessment by detecting, for instance, structural fatigue status and onset of cracks.

3.1.1 Case study 1: a non-resonant patch-like PEH system for wireless condition monitoring of commercial aircraft wings

In the last decades, aviation safety and cost-effective maintenance have generated significant interests on WSNs for aircraft SHM to facilitate predictive maintenance of critical components [214-215] by providing on-line indications of structural integrity. The adoption of wireless sensor nodes, capable of collecting data and transmitting them wirelessly to a central hub on the aircraft would solve the problem represented by the additional weight and complexity introduced by the wires required for supplying power and transporting information. However, since power has to be supplied locally to the wireless sensor nodes, a maintenance-free alternative to replaceable or rechargeable batteries is to harvest energy from the aircraft vibrations. Numerous reasons can be the cause of airplane vibrations, including landing gear extension and retraction, extension of speed brakes, engine operation at some spool speeds, free play in movable surfaces, and systems malfunctions. Aerodynamics and external factors such as atmospheric turbulence can also cause abnormal airplane vibrations; examples are buffets, caused by aerodynamic excitation and associated with separated airflow, and flutters. In normal flight-conditions aircraft wings experience vibrations as a consequence of mass distribution and structural stiffness. When external forces act on the aircraft, such as normal airflow over the surfaces, low-level vibrations occur although they are barely noticeable. More noticeable but normal is also the airplane reaction to turbulent air in which the magnitude of the vibrations may be larger and thus appear clearly visible. Figure 3-1(a) shows a typical stress spectrum for flight-by-flight simulation where each load block simulates 4200 flights and is related to the

lower wing cover of a passenger aircraft. Maximum stress condition equals ~130 MPa whilst mean flight stress is ~80-85 MPa [46-47]. Mean strain derived from such stress level equals ~1200 $\mu\varepsilon_{p\text{-}p}$ for ~3.5 mm tick skin layer characterised by a Young's modulus ~70 GPa such as in the case of aluminium alloy or composite materials currently used by aircraft manufacturers. Nevertheless, strain amplitude up to 4000 $\mu\varepsilon_{p\text{-}p}$ has been recorded on-board during atmospheric turbulences of aircraft in active service (i.e., up to 60,000 feet of altitude). Non-resonant vibrations up to 10 Hz of frequency are typical during normal in-flight conditions on the wings of large transport commercial aircraft [46-47].

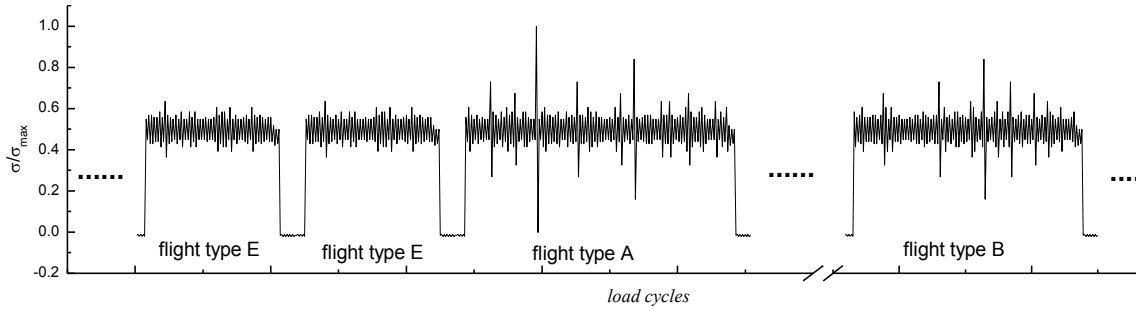

(a)

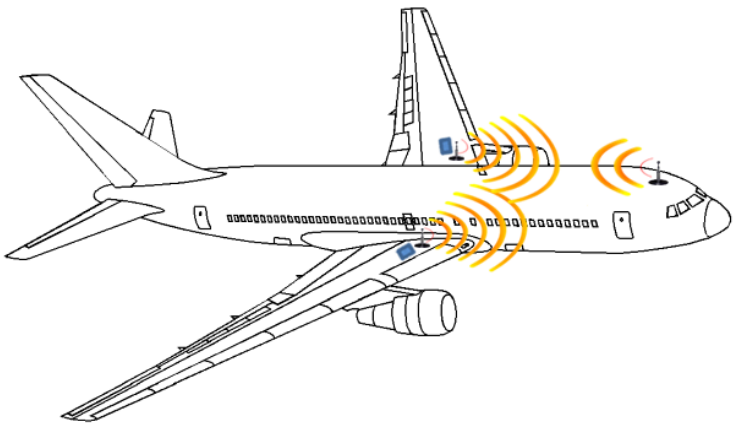

(b)

Figure 3-1 (a) A typical stress spectrum for flight-by-flight simulation of the lower wing cover of a passenger aircraft (Figure adapted from [47]) and (b) a potential deployment of a PEH powered wireless sensor system

Figure 3-1(b) shows a potential deployment of a PEH powered wireless sensor system for aircraft SHM of aircraft wings. The system is designed to harvest energy from wing vibration of aircraft in active service and then convert the

harvested energy into usable electrical energy to provide electrical power for sensors and a wireless communication unit. The system must be self-sufficient in energy supply so as to power the WSCN entirely from the harvested energy for on-line monitoring of structural health conditions such as aircraft wing fatigue and in-flight loading. In order to meet the requirements of the aeronautic industry and offer a valid design solution to supply power to wireless sensor nodes on board of aircraft, the piezoelectric harvester has to be easily embeddable, crack tolerant, compact, lightweight, and durable. MFC transducers perfectly match such requirements and carry the promise of being retrofittable to existing aircraft. Indeed, featuring an overall thickness around 0.3 mm and a large flexibility, MFC transducers can be attached as patches onto aircraft wing skins. As the wings deflect during flight, due to the aerodynamic loading that generates the vibrations, the MFC patches will be strained and thus create energy to supply to a WSCN. Since strain energy obtains its higher value in the region surrounding the wing root rather than on the wing tip [216], on the contrary of kinetic energy, the piezoelectric energy harvester is integrated into the inner side of the lower skin of the aircraft wings. A central hub on top of the aircraft will collect the data wirelessly transmitted by the WSCN in order to maintain flight safety, prevent excessive wear or airframe damage, and facilitate troubleshooting and maintenance activities.

3.1.2 Case study 2: a resonant cantilever-based PEH system for wireless condition monitoring of large industrial machinery

Industrial applications have some of the harshest operating environments and large industrial machinery, in particular, have the most stringent demand for data integrity often associated to their cost value. When data integrity is assured, efficiency, productivity and safety of industrial plants can be significantly improved. Because traditional wired industrial sensors are expensive to install, only a small fraction of potential measurement points in a plant are traditionally instrumented. This creates significant demand for wireless condition monitoring systems in industrial applications and, in turn, of battery-alternative solutions to provide free energy to wireless sensor systems with no additional costs or burdens to maintenance. Low-frequency vibration monitoring

is an integral part of the overall predictive maintenance program of industrial machines such as paper machines, cooling towers, excavators, stone crushing equipment, and slow speed agitators or pumps [217–219]. Cooling towers, for example, are used throughout power generation processes of various industries. As shown in Figure 3-2, cooling towers feature a motor driven shaft coupled to a reduction gear driven fan; the fan is located on top of a tower through which water is passed and cooled.

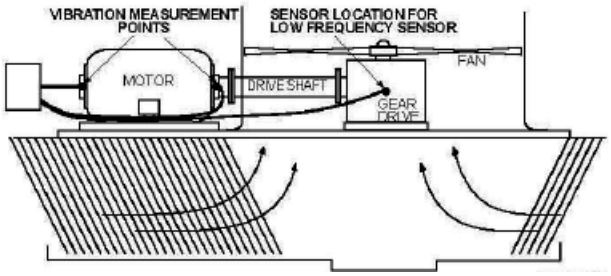

Figure 3-2 Critical sensor points in a cooling tower (Figure adapted from [48])

Disastrous failure can be caused by damaged gears and blades, which in turn determine lost production and high costs. Traditional monitoring systems for cooling towers consist of vibration switches or accelerometers coupled to the driving motors. However, vibration switches are typically unreliable in shutting down a damaged machine and accelerometers measuring only at certain time intervals do not really provide an overall view of the conditions of the gear box and fan, for example. On the contrary, a proactive cooling tower monitoring system requires permanent low-frequency sensors mounted on the gear box [48]. Fan speeds may range from 1.5 to 15 Hz, although turning speeds of typical roller element bearings may be as low as 12 Hz. Low-speed machines feature very low resultant vibrations on their bearing housing as the magnitude of the dynamic forces generating such vibrations decreases with the decrease of the rotational speed; additionally, low-speed machines are also typically massive in size. As a consequence of that, the resultant vibrations are typically very low and vary within the range from 10^{-3} to 10 m/s^2. As an example, Table 3-1 shows the acceleration a_1, a_2, a_3 respectively measured along the axis x, y, and z of HVAC (heating, ventilation, and air conditioning) and water systems in the machine room of a large building [220].

Table 3-1 Three-axis acceleration of HVAC and water systems in the machine room of a large building with harvesters mounted on different vibration sources

Source	a_1 (g·Hz$^{-1/2}$)	a_2 (g·Hz$^{-1/2}$)	a_3 (g·Hz$^{-1/2}$)
^{V}Fan belt cage 1	0.332	0.241	0.118
^{V}Fan belt cage 2	0.120	0.096	0.094
^{V}Fan belt cage 3	0.236	0.216	0.163
^{V}Fan belt cage 4	0.376	0.070	0.210
^{S}Fan belt cage 1	0.159	0.150	0.144
^{S}Fan belt cage 2	0.178	0.173	0.164
^{S}Fan belt cage 3	0.223	0.206	0.199
^{H}HVAC duct 1	0.020	0.020	0.014
^{H}HVAC duct 2	0.174	0.157	0.156
^{H}HVAC duct 3	0.042	0.042	0.037
^{V}HVAC duct 4	0.055	0.054	0.050
^{V}HVAC duct 5	0.042	0.041	0.037
^{V}HVAC duct 6	0.054	0.050	0.047
^{S}HVAC duct 7	0.058	0.057	0.056
^{S}Compressor	0.113	0.110	0.099
^{H}Compressor base	0.074	0.064	0.035
^{V}Controller	0.408	0.384	0.311
^{H}Pipe	0.064	0.041	0.037
^{S}Water pump	0.669	0.669	0.539
^{H}Belt drive motor	0.090	0.056	0.055
^{H}Floor by fan	0.020	0.017	0.017
^{V}Fan housing	0.049	0.048	0.044
^{H}Transformer	0.035	0.025	0.010

^{V} Vertical, ^{H} horizontal, or ^{S} slanted surface

Gear boxes, compressors and other higher speed machinery may also exhibit faults in the low frequency region, which can result in permanent machine damage, lost production, and worker safety hazards [221]. Figure 3-3(a-c) are the result of a pump measurement, where an accelerometer output is respectively displayed in terms of displacement, acceleration, and velocity as a function of frequency (being 1CPM=(1/60) Hz).

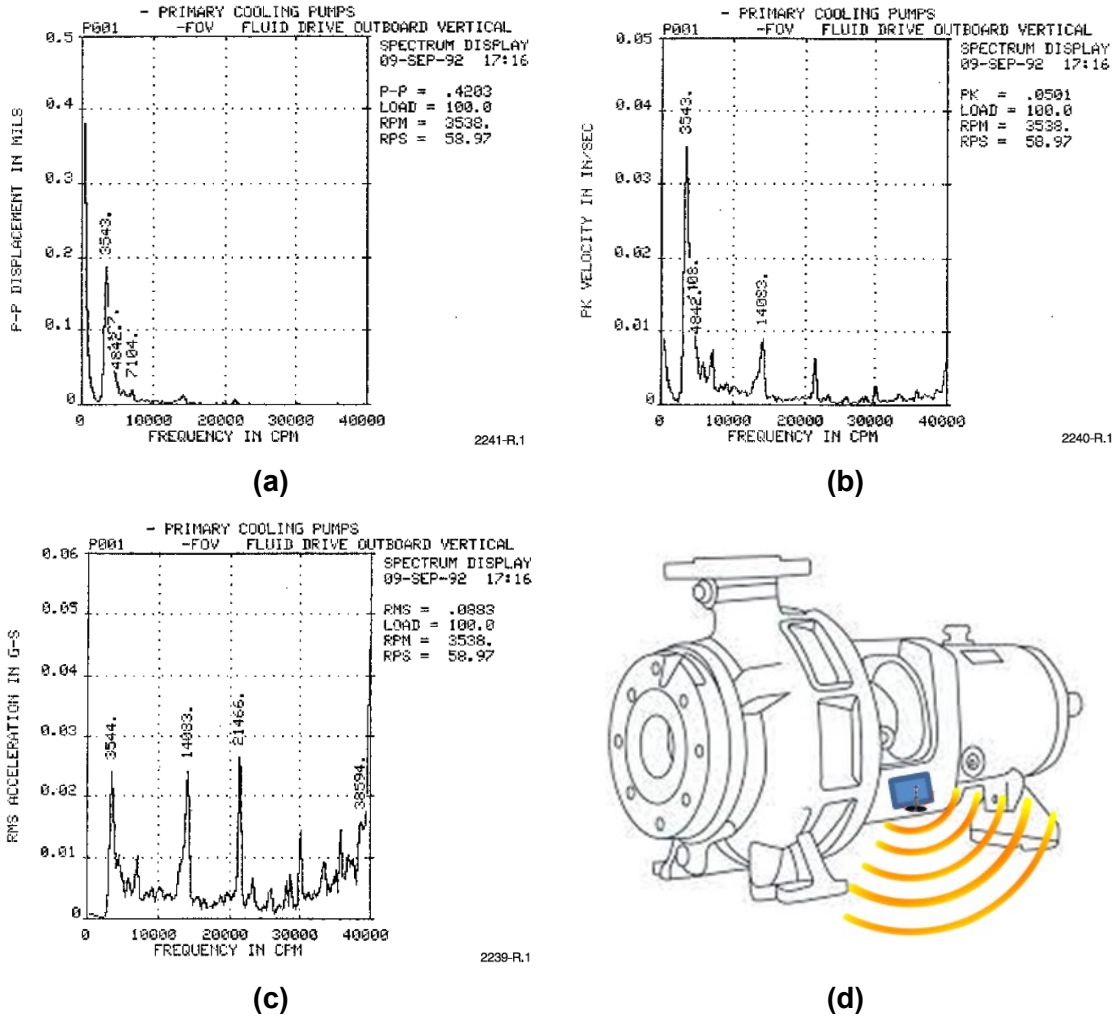

Figure 3-3 A measurement from a large industrial pump, where an accelerometer output is respectively displayed in terms of (a) displacement, (b) velocity, and (c) acceleration as a function of frequency, and (d) a potential deployment of a PEH powered wireless sensor system onto its housing (Figure adapted from [48])

By embedding a cantilever-based piezoelectric material into the housing of a pump machine, as shown in Figure 3-3(d), energy will be harvested when the machine moves rigidly in the vertical direction. Considering a mass on the tip of the piezoelectric cantilever beam, this will start oscillating due to effects of inertia when the housing moves up and down. The oscillations will cause strain in the beam and thus generate energy. The electrical signal generated by the piezoelectric material under excitation will be further rectified, stored, and regulated so as to power a WSCN for acquiring and transmitting data related to health status of the pump machine.

3.2 Implementations of the piezoelectric energy harvesters

3.2.1 Single MFC material on aluminium and composite substrates for case study 1

Aluminium alloys are traditional materials for aircraft wings and structural components. Modern aircraft, on the contrary, are being developed with composites made of carbon laminates as a prime structural material with the aim to lower the weight of the overall aircraft body; therefore, to lower fuel consumption and carbon emissions. Carbon fibre/epoxy resin composite (e.g., Umeco LTM®26EL with woven carbon plies) is currently adopted by aircraft industries for manufacturing fuselage and wing skin. In order to realise the piezoelectric energy harvester of the wireless sensor system described by case study 1 and convert in-flight airframe vibrations into electric charges, a MFC active element was respectively bonded to an aluminium and a composite substrate simulating a portion of an aircraft wing skin. Particularly, the implemented energy harvesters were based on the MFC M8528-P2 piezoelectric element (Smart Material GmbH – Dresden, Germany), which was respectively bonded to the surface of a standard aircraft industrial material, made of aluminium alloy Al 2024, and of a carbon- fibre/epoxy resin composite material, made of 16 HexPly M21 carbon plies having layout $[45/-45]_n$.

The MFC M8528-P2 operates in the d_{31} mode and has an active area of 85×28 mm^2. The orientation of the PZT fibres, with respect to the interdigitated electrodes, is depicted in Figure 3-4.

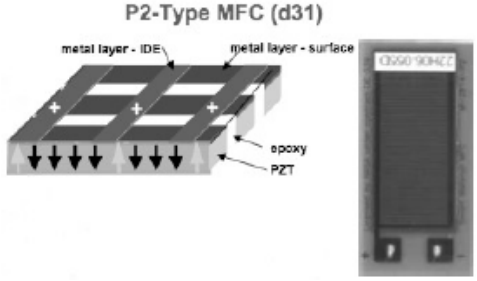

Figure 3-4 Structure of a MFC device in d_{31} mode of operation (Figure adapted from [222])

More details of the geometric and material parameters of the MFC M8528-P2 piezoelectric element used for the implementation of the non-resonant energy harvesters are listed in Table 3-2 as stated from the manufacturer [223].

Table 3-2 Geometric and material parameters of the MFC element used for the implementation of the piezoelectric harvesters

Parameter	Value
Overall length	105 mm
Overall width	34 mm
Active length	85 mm
Active width	28 mm
Active area density	5.44 g/cm^3
Thickness	0.3 mm
Capacitance (C_s)	172 nF
PZT material type	Navy Type II
Max operational tensile strain	4500 με
Piezoelectric coefficient (d_{31})	-170 pC/N
Dielectric permittivity (e_{33}^{σ})	1558.6×ε_0 F/m
Young's modulus (Y)	30.336 GPa

The thicknesses of the aluminium and composite substrate are respectively 3 mm and 4 mm. Both substrates are 210 mm wide and 300 mm long, with aluminium plates at the top and the bottom of the composite substrate as reinforcement for the grip areas. In order to ensure effective mechanical strain transfer from the substrate to the piezoelectric element, the thickness of the adhesive layer has to be as thin as possible. Therefore, the following procedure for bonding was followed: 1) sand the substrate surface with a fine emery paper to ensure a smooth surface; 2) wipe the substrate surface with isopropyl alcohol to make sure of a clean surface; 3) mark the place where the MFC is going to be bonded and define the boundary by using thin adhesive tape (~30 μm); 4) spread 3M's DP460 epoxy adhesive on the marked area; 5) lay the MFC over the epoxy adhesive; 6) apply a compressive pressure of about 400 kPa and maintain for approximately 20 hours; and 7) cure for 2 hours at 65 C^o to ensure

full adhesion. The described procedure was used for bonding the MFC transducers to both the aluminium and composite substrates. In order to apply the required compressive pressure for completion of the bonding procedure, the harvester specimens were horizontally placed one at a time between the pistons of a 250 kN tensile testing machine (Instron, High Wycombe – Bucks, UK). Additionally, to quantify the applied strain levels, a strain gauge type FLA-10-11 (Tokyo Sokki Kenkyujo Co. Ltd, Shinagawa-Ku – Tokyo, Japan) was bonded to the front surface of the composite substrate and to the back surface of the aluminium substrate in correspondence of the MFC element. A sample of the finalised version of the MFC energy harvester on composite substrate is shown in Figure 3-5.

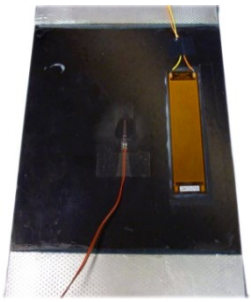

Figure 3-5 A photograph of a finalised MFC energy harvester on composite substrate

3.2.2 Multiple MFC materials on composite substrate for case study 1

Following the bonding procedure reported in Paragraph 3.2.1, three M8528-P2 MFC elements were bonded one at a time to the surface of a 4 mm tick carbon-fibre composite laminate made with 16-ply HexPly® M21. The carbon fibres in each layer are also in this case perpendicular to the adjacent layers and oriented at 45 deg to the longitudinal direction of the sample. After curing time, the MFCs were electrically connected in parallel so as to achieve a higher current rather than voltage output (i.e., the result of a series connection). Figure 3-6 shows a photograph of the composite specimen with the three MFC transducers bonded to it when the specimen was clamped between the pistons of a tensile testing machine.

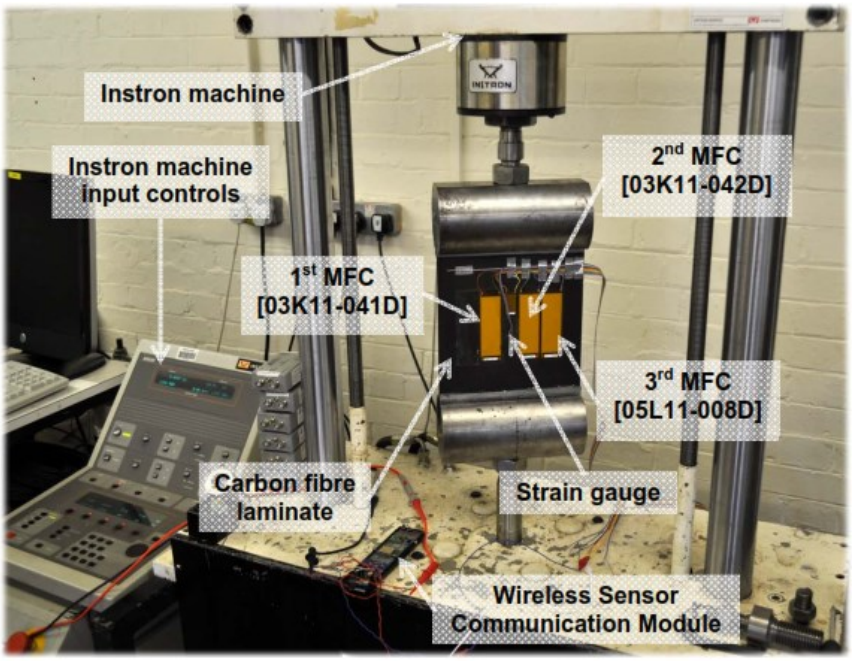

Figure 3-6 A photograph of a composite specimen with three MFC transducers bonded on while clamped between the pistons of a tensile testing machine

From Figure 3-6 it can be noticed that, in addition to the three M8528-P2 MFC elements, a strain gauge (type FLA-10-11) and a smaller MFC element (type M2814P2) were bonded to the composite substrate for further sensing applications. However, since these applications are far from the scope of this research work, they are not going to be considered by this thesis.

3.2.3 Ceramic material on brass substrate for case study 2

Figure 3-7 shows a 2D representation of the cantilever-beam configuration used for resonant PEH applications as described by case study 2 in Paragraph 3.1.2.

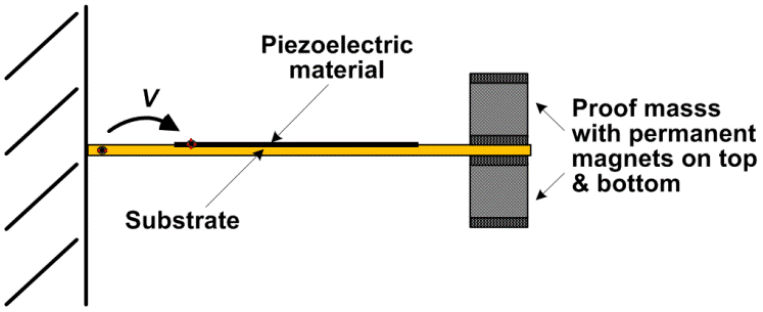

Figure 3-7 A 2D representation of the cantilever-beam configuration used for resonant PEH study

The harvester is made of a monolithic piezoelectric transducer integrated onto a substrate, which acts as a cantilever beam, with a proof mass on both the top and bottom side of the beam's tip. At the ends of each proof mass there is also a permanent magnet.

The design parameters of the piezoelectric harvester are presented in Figure 3-8(a). The piezoelectric element is a simple ceramic-disc "buzzer" transducer (part number FT-20T-6A1) manufactured by Bell Piezo Ceramics Inc. (New Taipei City, Taiwan), which was selected rather for its direct and cheap availability at Maplin Electronics (Rotherham, UK) than for its electromagnetic properties as a monolithic transducer. The surface area of the active element is approximately equal to 177 mm^2 and has a thickness of only 0.16 mm. The substrate where the piezoelectric material is attached to is a brass disc of area and thickness respectively equal to 314 mm^2 and 0.22 mm, which has been cut on one side in order to be easily fitted for use as a cantilever beam in resonant PEH applications. Higher stress is applied to the piezoelectric material by shortening the length of the substrate material; therefore, higher power output is expected to be generated by the harvester for the same excitation input. Additionally, the length of the cantilever beam influences the resonant frequency of the piezoelectric harvester as much as the position and weight force of the added proof masses. By reducing either the length of the cantilever beam or the weight force of the added masses the resonant frequency increases. The masses are made of a central aluminium cylinder of 0.75 mm radius and 12 mm height, plus a top and a bottom neodymium cylinder having the same radius but a shorter height of 1.5 mm each. The overall weight on top and bottom of the harvester's tip is equal to 21 g, being the weight of the aluminium and the magnetic rods each equal to 15.8 and 2.6 g, respectively. A photograph of the implemented cantilever-based harvester for resonant PEH applications is shown in Figure 3-8(b), where a thin protective layer was put at the interface between the brass substrate and the magnet of the proof masses.

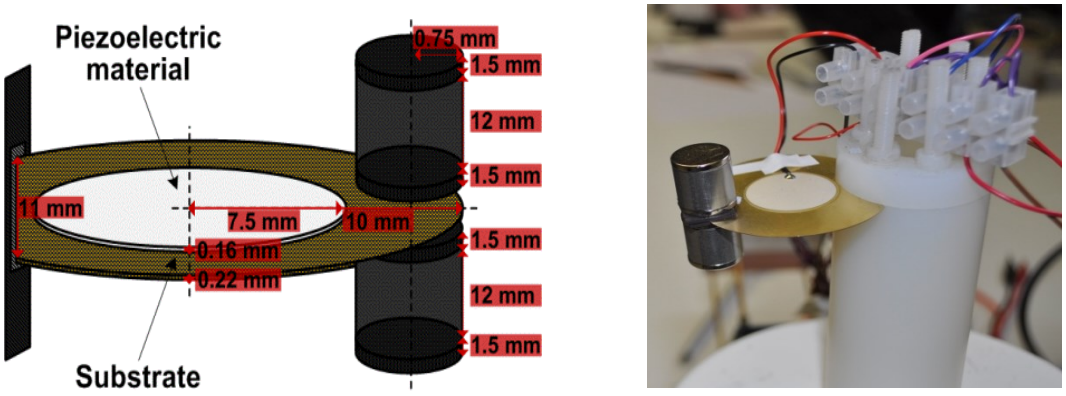

Figure 3-8 The implemented cantilever-based harvester for resonant PEH: (a) design parameters and (b) a device photograph

The implemented cantilever-based piezoelectric harvester can be potentially useful for energy-autonomous applications where the size/weight of the implemented structure is not a significant constraint such as on the housing of heavy machines.

3.3 Theoretical analyses

In order to analyse the harvested power under an applied excitation, an equivalent circuit representation of a piezoelectric element is shown in Figure 3-9, where the element is represented by the voltage source V_{oc} and the internal impedance made by the series of the capacitor C_s and the resistor R_s. It is worthwhile to mention that such a circuit representation is valid for the low-frequency range of vibrations considered by this work.

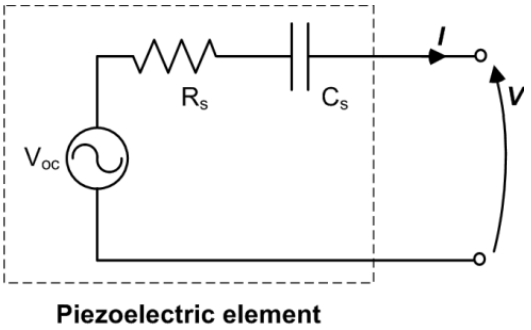

Figure 3-9 Equivalent circuit representation of a piezoelectric element

Considering mechanical stress only occurring along the 1-direction (i.e., the axis through the vertical centre of the harvester), the charge density D_3 on the electrodes of the piezoelectric element can be calculated from the linear constitutive equation of piezoelectricity [224] as:

$$D_3 = e_{33}^{\sigma} E_3 + d_{31}\sigma_1 \tag{3-1}$$

where e_{33}^{σ} is the dielectric permittivity of the piezoelectric material under a constant stress (σ_1) condition, E_3 is the electric field developed in the 3-direction, d_{31} is the piezoelectric charge coefficient, and σ_1 is the stress generated in the 1-direction. By applying the condition D_3=0, the voltage source V_{OC} is defined as:

$$V_{\mathrm{OC}} = -\frac{d_{31} t Y}{e_{33}^{\sigma}} \varepsilon_1 \tag{3-2}$$

where t is the thickness of the piezoelectric element, Y its Young's modulus, and ε_1 the strain induced on it by the mechanical stress σ_1.

In order to consider the behaviour of the harvester in typical applications a circuit has to be taken into account. The effects of the backward coupling, for which converting mechanical energy and extracting electrical energy leads to a modification of the properties of the global structure, will not be taken here into account. In Figure 3-10, an electrical resistive load (R_{L}) is connected to the piezoelectric harvester. The resistive load dissipates the generated electric charge and is typically used for the purpose of analysing and comparing the EH capability of piezoelectric harvesters in terms of their voltage, hence their power output.

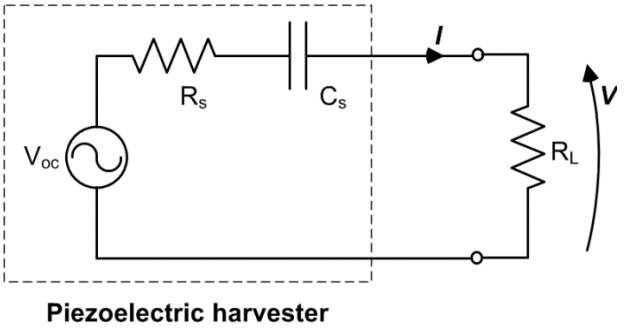

Figure 3-10 Equivalent circuit representation of a piezoelectric element with a connected electrical resistive load

Assuming that the piezoelectric material undergoes a sinusoidal steady-state stress due to the applied excitation and the resistive load R_{L} is connected to it, the amount of AC current I flowing through the series made by the harvester's impedance and R_{L} can be calculated as:

$$|I| = \frac{d_{31} t Y}{e_{33}^{\sigma}} \frac{|\varepsilon_1|}{\sqrt{\left(R_{\mathrm{L}} + R_{\mathrm{p}}\right)^2 + 1/\left(\omega \mathrm{C_s}\right)^2}}. \tag{3-3}$$

The amount of the voltage V and power P developed across the load, hence across the energy harvester, respectively follow from Equation (3-3) as:

$$|V| = \frac{d_{31} t Y}{e_{33}^{\sigma}} \frac{R_{\mathrm{load}} |\varepsilon_1|}{\sqrt{\left(R_{\mathrm{L}} + R_{\mathrm{s}}\right)^2 + 1/\left(\omega \mathrm{C_s}\right)^2}} \tag{3-4}$$

and

$$P = \frac{|V|^2}{2R_{\mathrm{L}}}. \tag{3-5}$$

In case the piezoelectric element is bonded onto a substrate, which is clamped at one end and oscillates under an impinging force perpendicular to the neutral axis of this system so as to form a cantilever-based energy harvester, the strain ε_1 can be related for small deflections of the cantilever beam (i.e., when $\sin(\alpha) \approx \alpha$) to the displacement u in the x direction as:

$$\varepsilon_1 = \frac{\partial u}{\partial x}. \tag{3-6}$$

The relative displacement u of the mass moving out of the plane with the host structure results in a curvature of the cantilever beam, as shown in Figure 3-11, and is related to the variable acceleration a of the applied excitation:

$$u = \iint a dt. \tag{3-7}$$

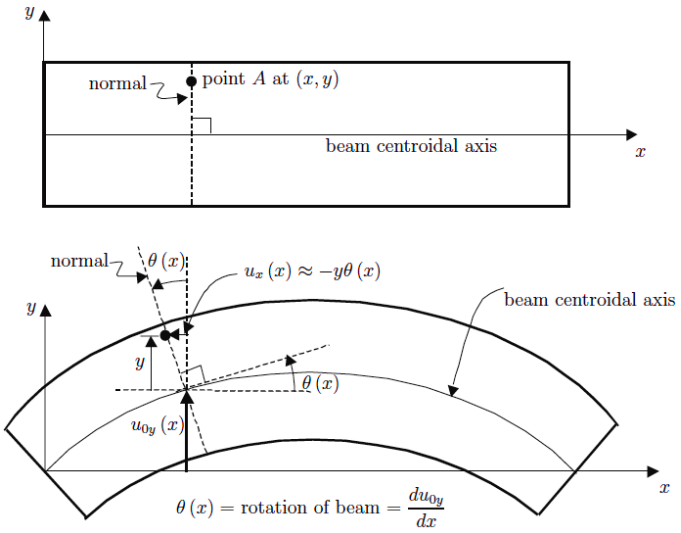

Figure 3-11 Deformation of linear elastic beam in bending (Figure reprinted from [225])

3.4 Experimental characterisation based on case study 1

3.4.1 Impedance of the MFC material

Figure 3-12 shows the measured electrical impedance characteristics of the MFC material used for the implementation of the energy harvesters; particularly, Figure 3-12(a), Figure 3-12(b), and Figure 3-12(c) respectively show the measured MFC's impedance amplitude, impedance phase, and capacitance. It can be observed that there is a dominant capacitive behaviour of the piezoelectric harvester under low-frequency (below resonance) excitations as the amplitude varies with an inverse relationship on the applied frequency and the phase is approximately constant and near -90 deg. This means that the resistive part of the MFC's impedance is much smaller than its capacitive part within the tested low-frequency range. The measured capacitance of the MFC is

around 175 nF under tested applied voltages and frequencies, which is very close to the value of 172 nF provided by the manufacturer [223].

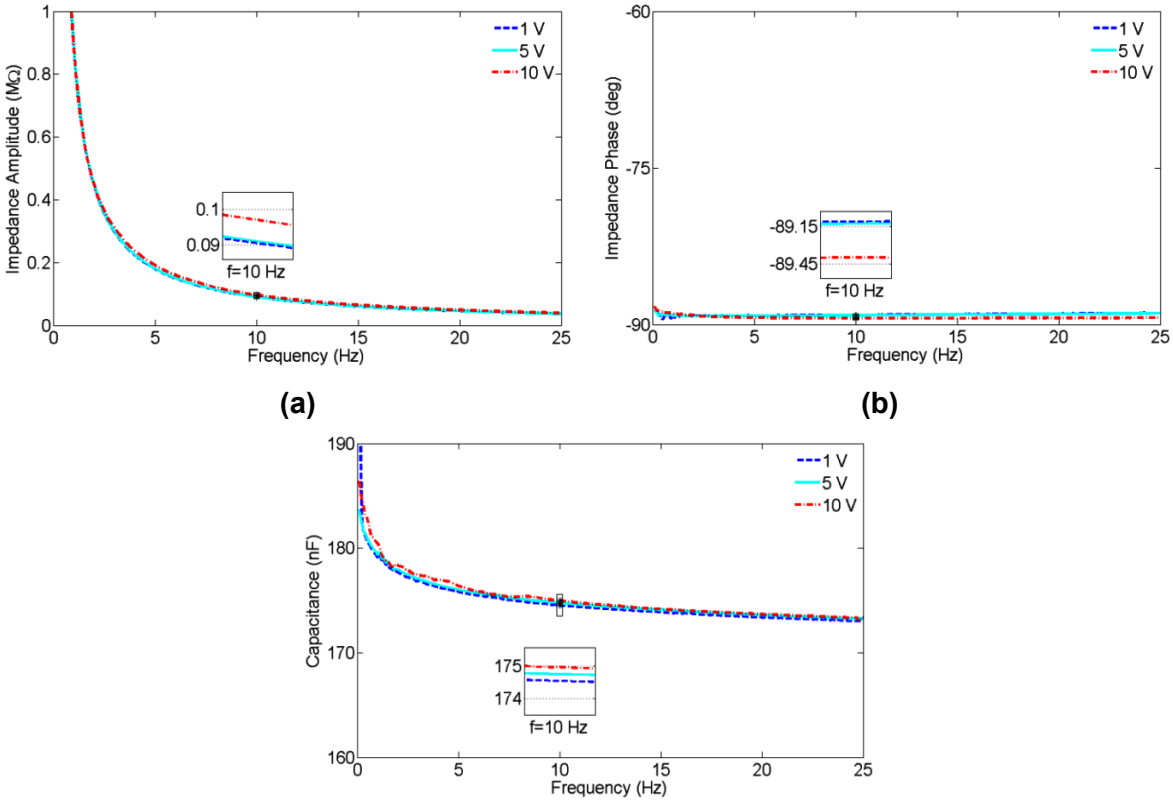

Figure 3-12 Measured (a) impedance amplitude, (b) impedance phase, and (c) capacitance of the MFC material as a function of frequency for the applied AC voltage of 1, 5, and 10 V, respectively

3.4.2 Characterisation of the single MFC material on aluminium substrate

Figure 3-13 shows the circuit configuration of the single MFC energy harvester used for testing based on the conditions of case study 1.

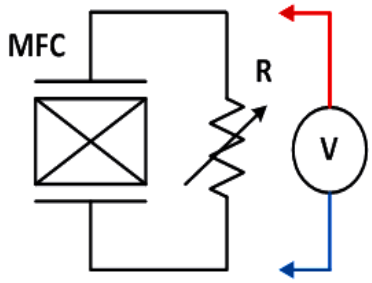

Figure 3-13 Testing configuration of the single MFC energy harvester

Figure 3-14 to Figure 3-16 show the root-mean-square voltages, currents, and the average powers generated by the MFC energy harvester on aluminium substrate as a function of the resistive load for different excitation frequencies and strain levels with comparison to the theoretical results, where the solid lines depict the experimental trend, fitted from the measured results of the scattered points, and the dotted lines the theoretical results, calculated from Equation (3-3) to (3-5), respectively. It should be mentioned that the measured value R_s =5 kΩ was used for calculations of the theoretical results.

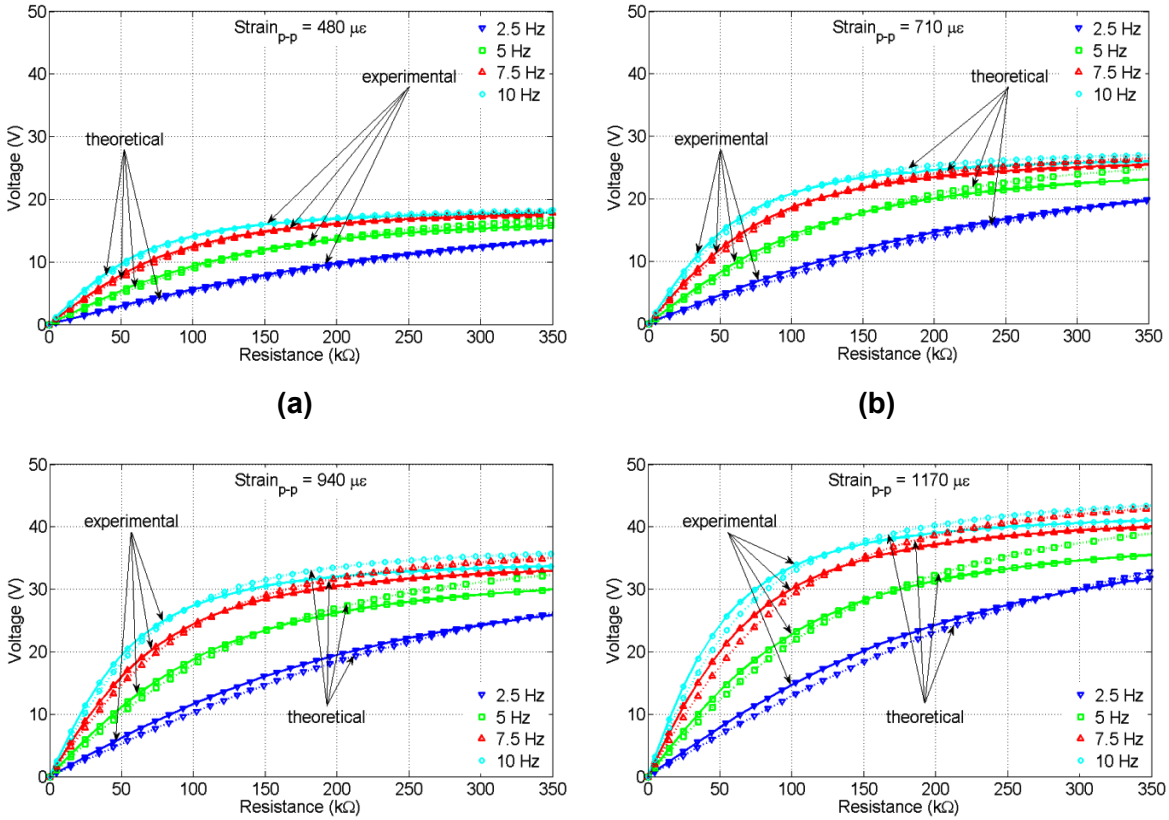

Figure 3-14 Theoretical and experimental root-mean-square voltage generated by the MFC energy harvester on aluminium substrate as a function of the resistive load for different excitation frequencies and different applied strain: (a) for 480 με, (b) for 710 με, (c) for 940 με, and (d) for 1170 με

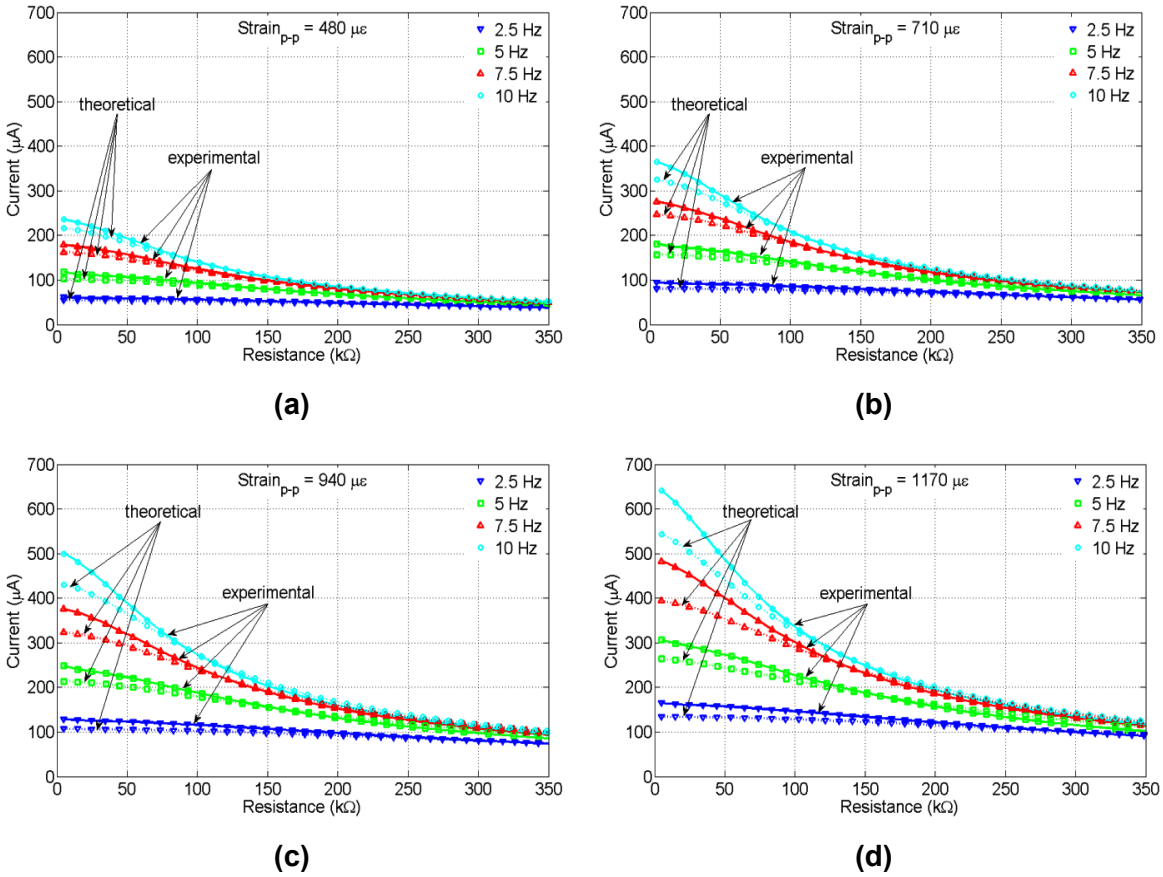

Figure 3-15 Theoretical and experimental root-mean-square current generated by the MFC energy harvester on aluminium substrate as a function of the resistive load for different excitation frequencies and different applied strain: (a) for 480 με, (b) for 710 με, (c) for 940 με, and (d) for 1170 με

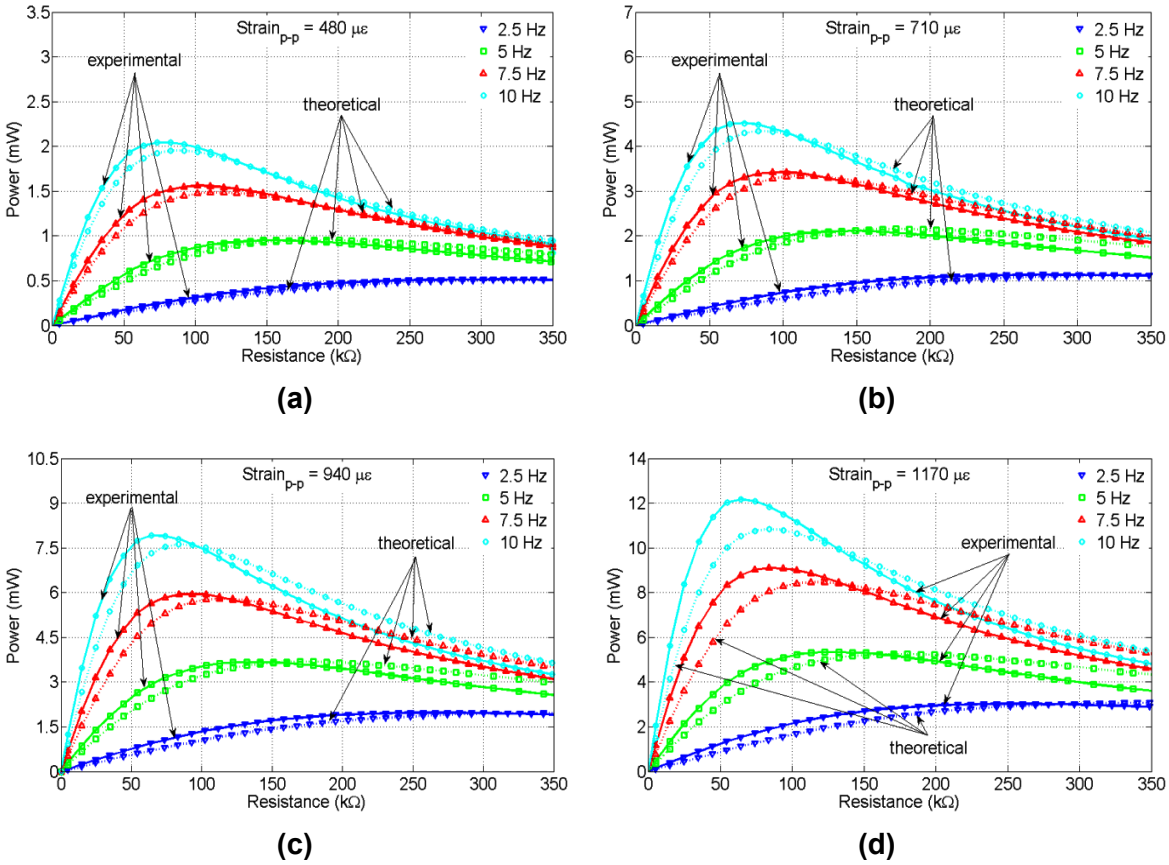

Figure 3-16 Theoretical and experimental average power harvested by the MFC energy harvester on aluminium substrate as a function of the resistive load for different excitation frequencies and different applied strain: (a) for 480 με, (b) for 710 με, (c) for 940 με, and (d) for 1170 με

From Figure 3-14 to Figure 3-16, it can be observed that: 1) the voltage vs. electrical load curves exhibit a monotonic growth towards an asymptotic value (the open circuit voltage), namely up to 18 V for the applied strain of 480 με and 42 V for the applied strain of 1170 με; 2) the current vs. electrical load curves start at a high value (the short circuit current) and then decrease monotonically, but staying above the value of 40 μA for the applied strain of 480 με or above 100 μA for the applied strain of 1170 με; 3) there is a Maximum Power Point (MPP), corresponding to the connected optimal resistive load in the power curves; 4) the maximum harvested power was measured around 12.16 mW across a resistive load of 66 kΩ under an excitation of 1170 με peak-to-peak at 10 Hz; and 5) there is a good agreement between theoretical and experimental results with slight differences, which can be explained based on the effects that the applied strain and frequency have on the internal impedance of the MFC

harvester (e.g., the increasing measured values of C_s for frequencies below 10 Hz). The voltage at the MPP (V_{MPP}) and the corresponding optimal resistive load (R_{MPP}) for the measured cases are listed in Table 3-3.

Table 3-3 Root-mean-square voltage generated by the MFC energy harvester on aluminium substrate at the MPPs

$Strain_{p-p}$ (με)	R_{MPP} (kΩ)				V_{MPP} (V)			
	f = 2.5 Hz	*f* = 5 Hz	*f* = 7.5 Hz	*f* = 10 Hz	*f* = 2.5 Hz	*f* = 5 Hz	*f* = 7.5 Hz	*f* = 10 Hz
480	304	155	105	79	12.5	12.1	12.8	12.7
710	284	144	98	74	17.9	17.4	18.3	18.3
940	268	136	93	70	23.0	22.4	23.5	23.5
1170	253	128	86	66	27.7	26.1	28.1	28.2

In order to analyse the effects of vibrational strain and frequency on the performance of the system, Figure 3-17 shows the voltage (V_{MPP}), power (P_{MPP}) and optimal resistive load at the MPP (R_{MPP}).

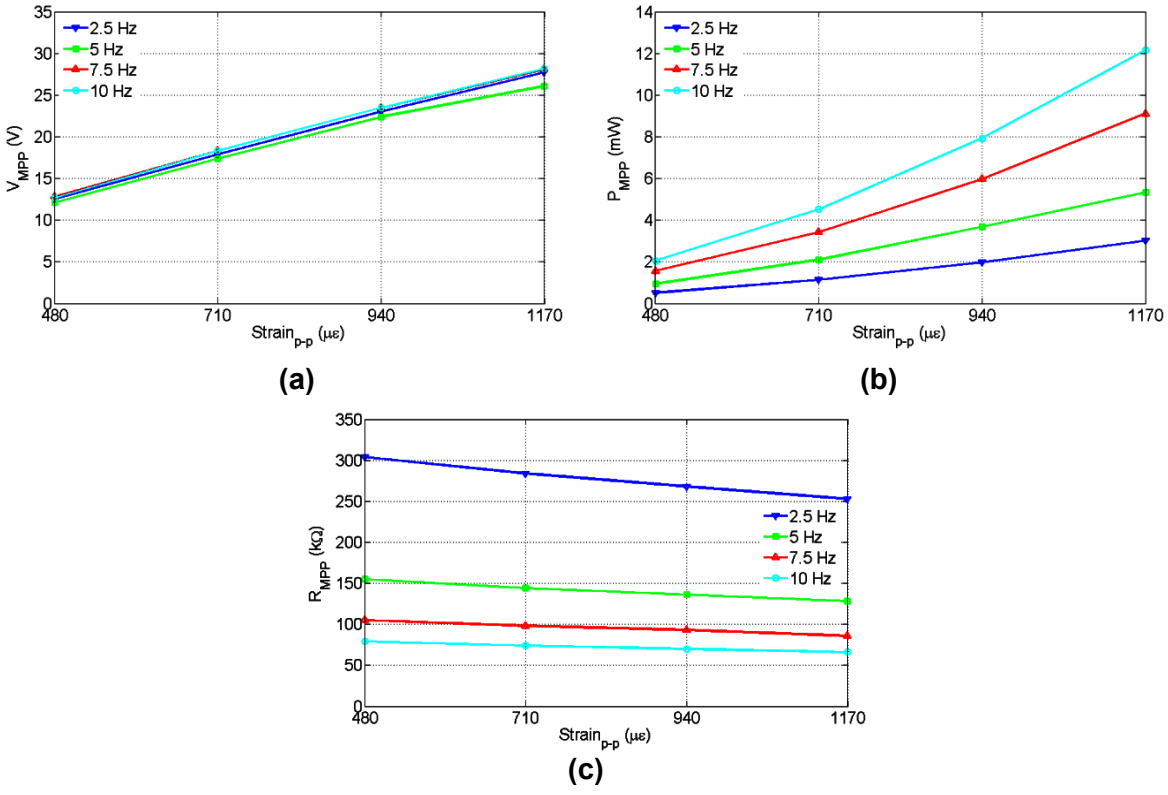

Figure 3-17 Measured performance at the MPPs of the MFC energy harvester on aluminium substrate as a function of tested strain levels for different excitation frequencies: (a) voltage V_{MPP}, (b) power P_{MPP}, and (c) optimal resistive load R_{MPP}

From Figure 3-17, it can be observed that the voltage V_{MPP} is around 12 V for the applied strain of 480 με and 28 V for the applied strain of 1170 με for all tested frequencies. This means that the applied frequency does not contribute significantly to the voltage at the MPP. It can be also observed that the voltage V_{MPP} is approximately linear with the applied strain whilst the power P_{MPP} is more or less proportional to the square of the applied strain. Furthermore, there is a major dependence of the resistive loads at the MPPs on the frequency and a minor dependence on the strain level. It can be deduced that this dependence between the optimal load R_{MPP} and the frequency is a consequence of the impedance matching theory; thereby, there is an inverse relationship between them due to the dielectric behaviour of the piezoelectric harvester. The weak dependence between R_{MPP} and the strain could be due to the fact that the bonding layer affects the piezoelectric internal resistance or to the non-linear material response of the MFC harvester observed in Paragraph 3.4.1.

3.4.3 Characterisation of the single MFC material on composite substrate

Results similar to the case of the MFC on aluminium substrate were obtained for the power harvested by the MFC on the composite substrate. Also for this case, the solid lines depict the experimental trend of the collected data, with the scattered points as the measured results, whilst the dotted lines depict the theoretical trend of the results obtained by applying equation (3-5) in correspondence to the same scattered points and with the foreseen MFC's material parameters. A good match between theoretical and experimental results can be observed, although a value for C_{s} higher than the standard value of 172 nF used to reproduce this fit would reduce the differences between the two trends of data.

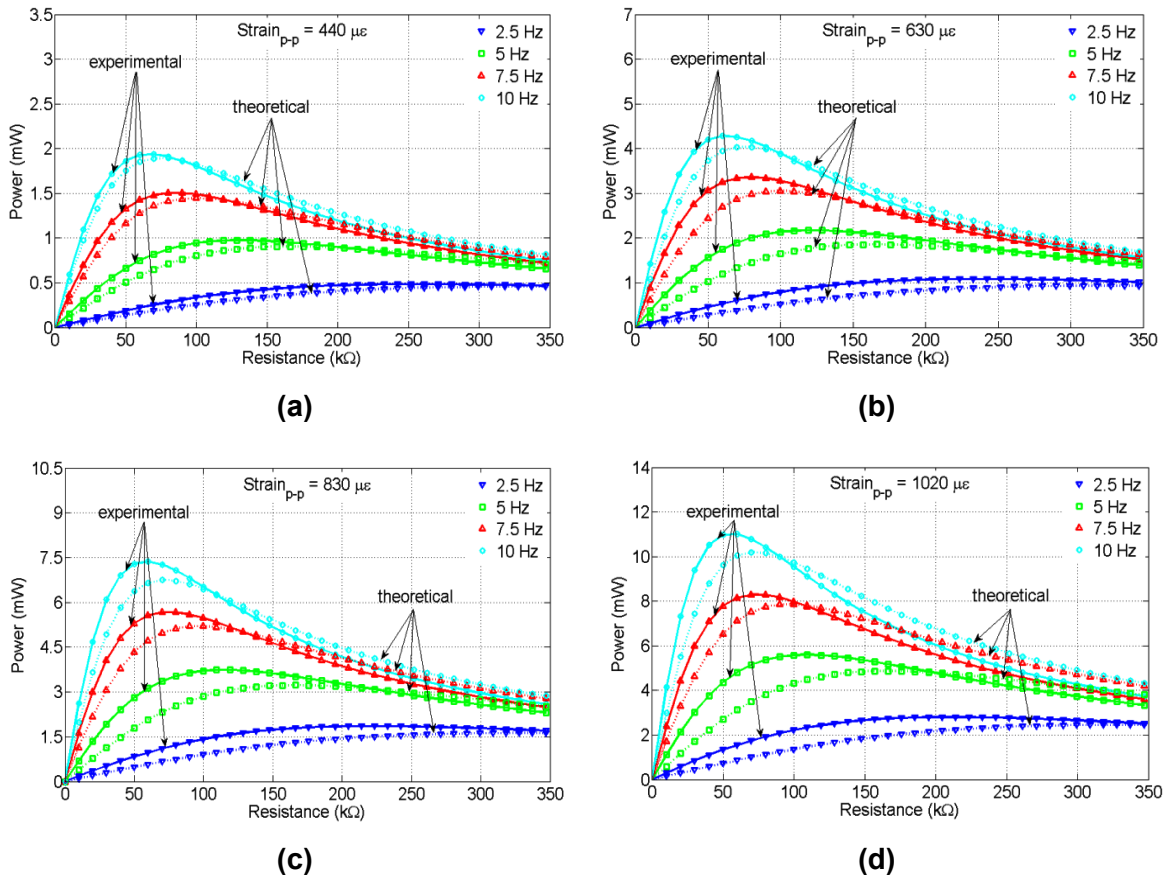

Figure 3-18 Theoretical and experimental average power harvested by the MFC energy harvester on composite substrate as a function of the resistive load for different excitation frequencies and different applied strain: (a) for 440 με, (b) for 630 με, (c) for 830 με, and (d) for 1020 με

From Figure 3-18, it is easy to visualise that there is a weak dependence of the resistive load at the MPPs (R_{MPP}) on strain, although there is a slight decrease of R_{MPP} with the increase of the applied strain level at the lowest frequency. Table 3-4 reports the measured root-mean-square voltage generated by the MFC energy harvester on composite substrate at the MPP, corresponding to the connected optimal resistive load, for tested excitation frequencies and applied strain levels.

Table 3-4 Root-mean-square voltage generated by the MFC energy harvester on composite substrate at the MPPs

$\text{Strain}_{\text{p-p}}$ (με)	R_{MPP} (kΩ)				V_{MPP} (V)			
	f = 2.5 Hz	*f* = 5 Hz	*f* = 7.5 Hz	*f* = 10 Hz	*f* = 2.5 Hz	*f* = 5 Hz	*f* = 7.5 Hz	*f* = 10 Hz
440	257	131	89	66	11.2	11.3	11.4	11.3
630	237	122	82	63	16.1	16.3	16.3	16.4
830	224	115	77	59	20.4	20.7	20.7	20.9
1020	211	108	73	56	24.3	24.6	24.7	24.9

For a comparison reason, Table 3-5 lists the powers harvested by the MFC on aluminium (Al) substrate and on composite (Comp) substrate at the MPP for the measured cases, where the data are based on the fitted curves.

Table 3-5 Comparison of the power harvested by the MFC energy harvesters on aluminium (Al) substrate and on composite (Comp) substrate at the MPPs

$\text{Strain}_{\text{p-p}}$ (με)	P_{MPP} (mW)							
	f = 2.5 Hz		*f* = 5 Hz		*f* = 7.5 Hz		*f* = 10 Hz	
	Al	Comp	Al	Comp	Al	Comp	Al	Comp
440	0.43	0.49	0.80	0.98	1.31	1.45	1.72	1.93
480	0.51	0.58	0.95	1.16	1.56	1.72	2.05	2.44
630	0.95	1.09	1.77	2.18	2.88	3.24	3.80	4.29
710	1.13	1.38	2.11	2.77	3.43	4.12	4.52	5.45
830	1.65	1.86	3.09	3.73	5.01	5.56	6.65	7.39
940	1.97	2.38	3.68	4.77	5.96	7.12	7.92	9.46
1020	2.54	2.80	4.49	5.59	7.65	8.32	10.22	11.06
1170	3.02	3.70	5.35	7.38	9.11	10.98	12.16	14.60

Maximum harvested power of around 11.06 mW was obtained across a resistive load of 56 kΩ when the MFC on composite substrate was tested under an excitation of 1020 με peak-to-peak at 10 Hz. From Table 3-5, it can be seen that slight more power was harvested by the MFC on composite. Based on the theoretical analyses from Equation (3-3) to Equation (3-5), the generated current, voltage, and power are related to the MFC's material properties and the mechanical excitation input. If the material and the applied vibration frequency and strain are the same, theoretically, they should generate the same electrical output. The reason for the slight different electrical outputs for the two energy harvesters is that their interfaces between the substrates and the MFC element are different. It is possible that, because of the different directionality of the

surface layer, the MFC's adhesion on the composite substrate performs slightly better for bonding and so gives a slightly better mechanical strain transfer to the piezoelectric element.

3.4.4 Characterisation of the multiple MFC materials on composite substrate

The composite substrate with the three MFCs bonded on it was tested under an applied peak-to-peak strain level of 1020 με at 2.5 and 5 Hz by using the circuit configuration shown in Figure 3-19.

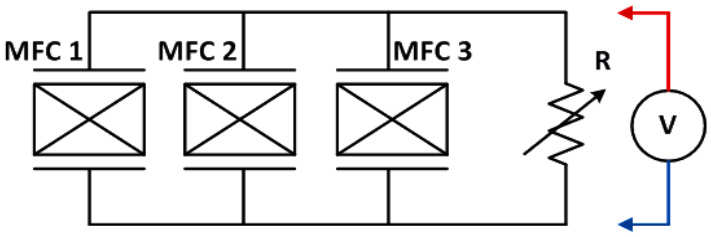

Figure 3-19 Testing configuration of the multiple MFC energy harvester

The experimental results are respectively shown in Figure 3-20 and Figure 3-21, where the root-mean-square voltages and power outputs of the three MFCs are plotted singularly and in parallel connection as a function of the connected resistive loads. In Figure 3-20 and Figure 3-21, the scattered points are the result of the measurements.

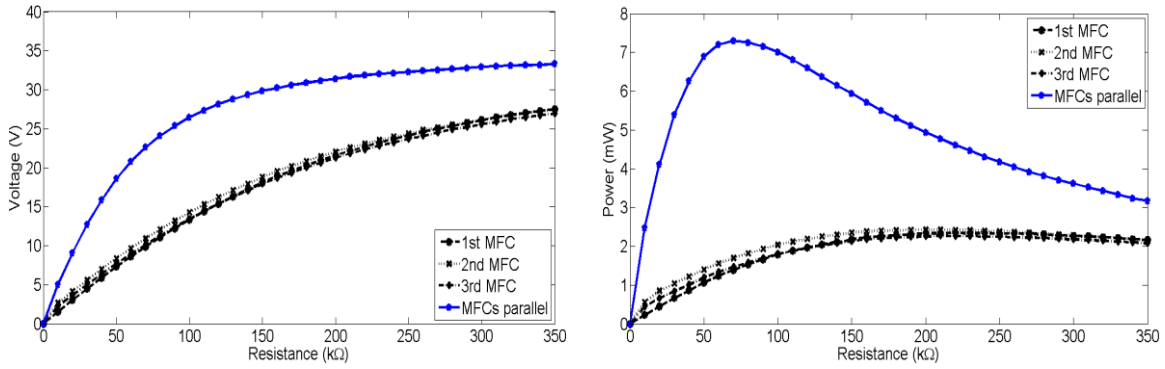

(a) **(b)**

Figure 3-20 Experimental results for single and three MFC(s) in parallel connection on composite substrate, where the excitation is 1020 με at 2.5 Hz: (a) root-mean-square voltage and (b) power output

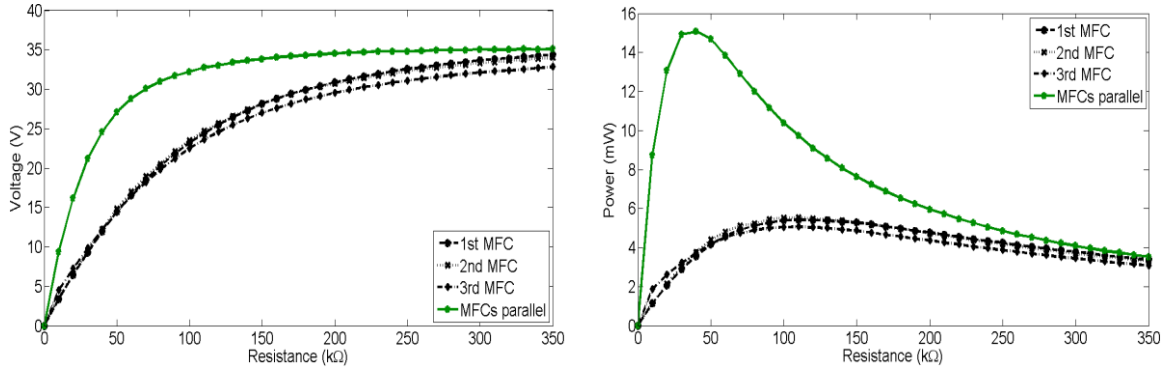

(a) (b)

Figure 3-21 Experimental results for single and three MFC(s) in parallel connection on composite substrate, where the excitation is 1020 με at 5 Hz: (a) root-mean-square voltage and (b) power output

The values of the resistance, voltage, current, and power in correspondence to the MPPs are reported in Table 3-6.

Table 3-6 Experimental results of MFC performances at MPPs, when bonded to the composite substrate singularly and in parallel connection, under 1020 με excitation at 2.5 and 5 Hz

	1st MFC		2st MFC		3st MFC		MFCs parallel	
f (Hz)	2.5	5	2.5	5	2.5	5	2.5	5
R_{MPP} (kΩ)	220	110	200	110	210	110	70	40
V_{MPP} (V)	22.68	24.39	22.03	24.67	21.82	23.60	22.60	24.55
I_{MPP} (μA)	103.17	222.22	110.30	224.16	104.03	214.40	323.01	613.85
P_{MPP} (mW)	2.34	5.42	2.43	5.53	2.27	5.06	7.30	15.07

From Table 3-6, it can be observed that the measured voltage outputs at the MPPs are approximately in the range between 22 V and 24 V whilst correspondent current outputs were calculated between 100 μA and 600 μA. The harvested power reaches up to 2.3 mW and 5.5 mW respectively at 2.5 and 5 Hz. These results are comparable with the results presented in Paragraph 3.4.3 for the single MFC energy harvester on composite substrate. As for the case of the single MFC circuit configuration, it can be seen that there is a linear relationship between the excitation frequency and the power harvested for the same strain level of excitation. This means that the higher the excitation frequency the higher the harvested power. Additionally, it can also be seen that

the harvested power is higher for higher levels of the applied strain. In particular, P_{MPP} is proportional to the square of the applied strain as the voltage at MPPs is linear to it. The 3rd MFC patch (i.e., MFC_5L11-008D in Figure 3-6) shows a slightly worse performance compared to the other two, which is more evident when the composite substrate undergoes the excitation applied at 5 Hz of frequency. This can be explained as the effect of a lower quality harvester's implementation possibly because, since the 3rd MFC was the last glued, the distribution of the pressure applied for bonding was not as uniform as for the other two MFCs. From Table 3-6, it can be also observed that the optimal resistive load R_{MPP} decreases with the increase of frequency as a consequence of the impedance matching theory and is only marginally dependent on strain. The parallel connection of the three MFCs, in particular, makes three times larger the inherent capacitance of the energy harvester; hence, three times smaller its internal impedance that is capacitive at low frequencies (i.e., $\left|Z_{\mathrm{MFCs\ \ parallel}}\right| = \left|1/\left(3\mathrm{i}\omega C_{\mathrm{s}}\right)\right| < \left|Z_{\mathrm{MFC}}\right| = \left|1/\left(\mathrm{i}\omega C_{\mathrm{s}}\right)\right|$). Therefore, the optimal resistive load R_{MPP} is also three times smaller (i.e., from approximately 120 kΩ to 40 kΩ). Correspondently, the maximum power output harvested by using the implemented multiple MFC configuration is three times higher in comparison with the single MFC configuration as the result of the superposition of the electrical effects.

3.5 Experimental characterisation based on case study 2

3.5.1 Resonant frequency and impedance properties of the harvester

The amplitude of the displacement of the piezoelectric cantilever beam is dependent on its material properties, on the physical parameters of the harvester's design, and on the characteristics of the impact vibration. With regard to the impact vibration, the amplitude of the displacement increases sharply in a narrow frequency band around the mechanical resonance of the piezoelectric harvester, being otherwise approximately constant for an input acceleration with little variations. In correspondence to its mechanical resonance, the transducer is considerably deformed even with low levels of

vibration thus generating a considerable amount of electrical energy. For the implemented resonant cantilever-based piezoelectric energy harvester, proof masses were adapted in order to get a resonance frequency for the first flexural mode close to 11.5 Hz and mechanically amplify the deformation of the piezoelectric element so as to achieve a higher power output. Figure 3-22 shows the result of a frequency sweep up to 20 Hz, performed at steps of 0.5 Hz, for the open circuit voltage of the implemented cantilever-based piezoelectric harvester under an excitation of 0.5 g of acceleration measured at the base of the cantilever beam.

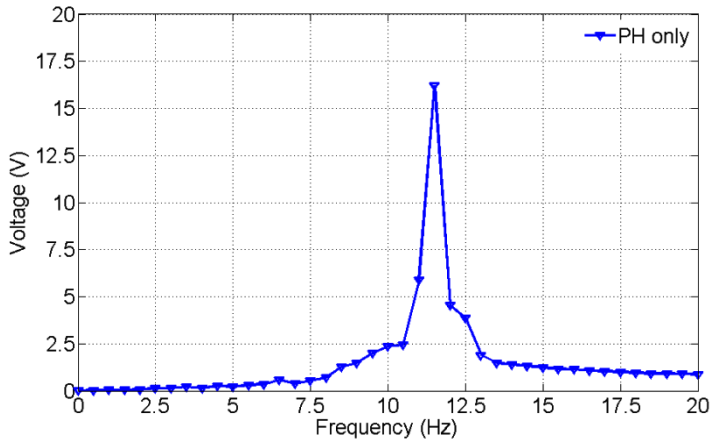

Figure 3-22 A frequency sweep for the open circuit voltage of the implemented cantilever-based piezoelectric harvester under an excitation of 0.5 g of acceleration

It is worthwhile to mention that, due to the inertia of the beam, to an acceleration of 0.5 g measured at the base of the cantilever beam, as shown in Figure 3-23(a), corresponded a measured acceleration level of about 0.56 g at the tip of the cantilever beam, as shown in Figure 3-23(b), with an increase around 12%.

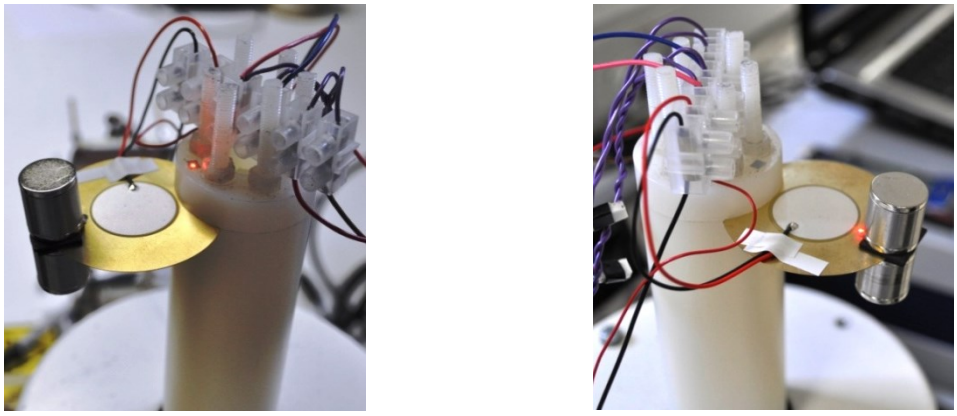

(a) (b)

Figure 3-23 Focal points of the laser doppler vibrometer used to measure the velocity of the oscillation induced by the applied excitation (a) "at the base" and (b) "at the tip" of the cantilever beam

Given the piezoelectric energy harvester model in Figure 3-9, the inherent capacitance and resistance of the implemented resonant cantilever-beam structure were measured approximately equal to 50 nF and 8 kΩ, respectively, under the applied voltage of 1 V amplitude and 11.5 Hz frequency.

3.5.2 Characterisation of the harvester in resonant conditions

Figure 3-24 shows the circuit configuration used to characterise the EH capability of the implemented resonant cantilever beam based on the conditions of case study 2.

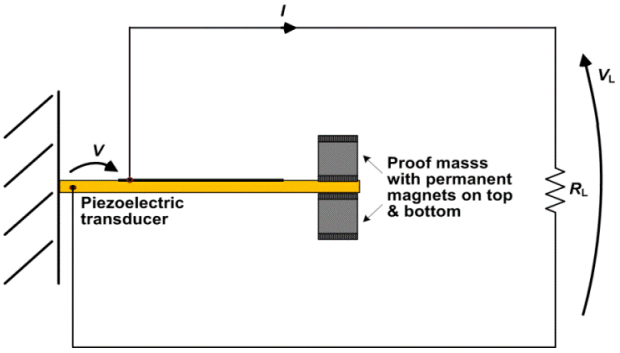

Figure 3-24 Circuit configuration used for testing the implemented cantilever-based piezoelectric harvester

Figure 3-25 shows the root-mean-square voltages, currents, and the average powers generated by the implemented cantilever-based piezoelectric energy

harvester as a function of the connected resistive load for the resonant frequency of 11.5 Hz and the acceleration levels of 0.025 and 0.25 g.

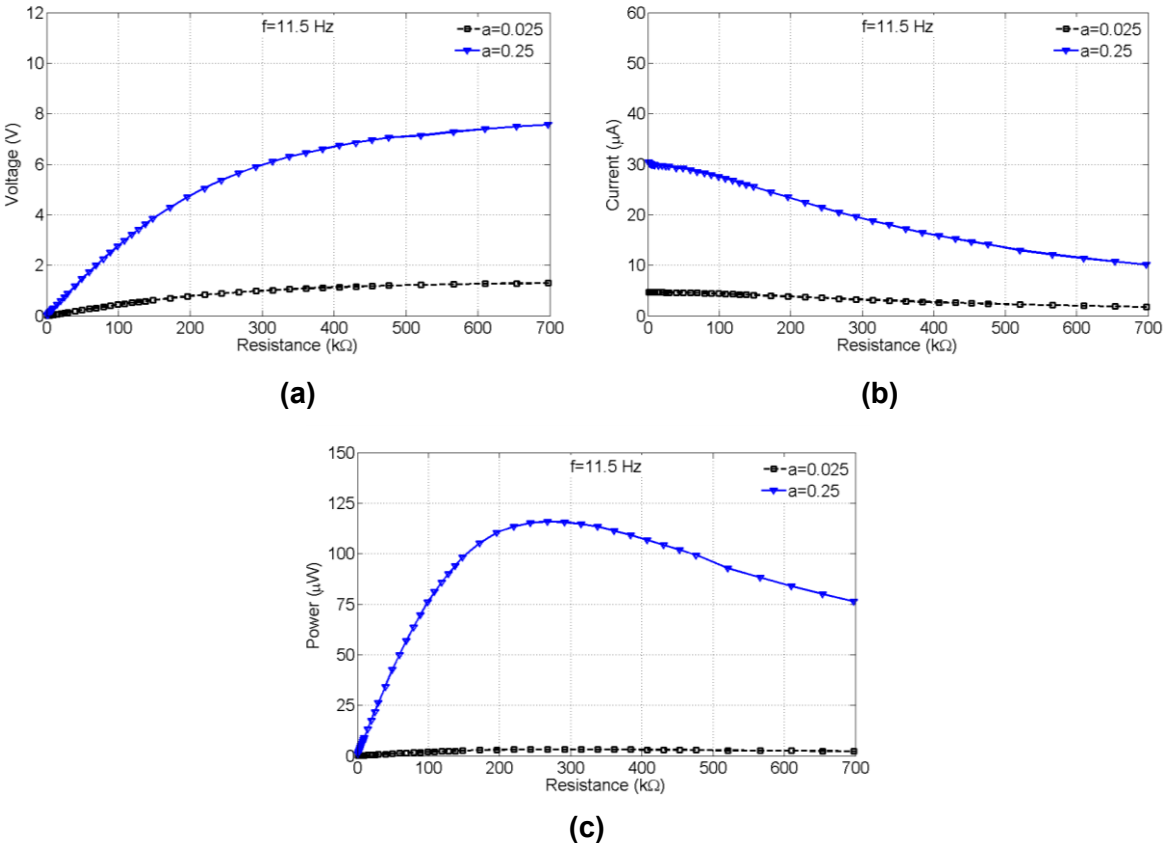

Figure 3-25 Experimental results for the implemented cantilever-based piezoelectric energy harvester as a function of the connected resistive load under a resonant excitation of 11.5 Hz of frequency and acceleration levels of 0.025 and 0.25 g: (a) root-mean-square voltage, (b) root-mean-square current, and (c) average power

From Figure 3-25, it can be observed that the plots of voltage, current, and power present the same features of the MFC characterisation seen in Paragraph 3.4, with the voltage rising towards the open circuit value, the current decreasing progressively from the short circuit value, and the power rising rather quickly up to the MPP and then slowly decreasing as the electrical load is further increased. As expected from the theoretical analyses in Paragraph 3.3, the higher the acceleration of the applied excitation the higher the harvester's output. In particular, a list of the results achieved in correspondence to the MPPs is presented in Table 3-7.

Table 3-7 Performance of the cantilever-based piezoelectric energy harvester at the MPPs for the resonant frequency of 11.5 Hz and different acceleration levels

a (g)	R_{MPP} (kΩ)	V_{MPP} (V)	I_{MPP} (μA)	P_{MPP} (μW)
0.025	298	1.0	3.2	3.2
0.25	277	5.7	20.5	116.8

From Table 3-7, it can be observed that the power harvested at resonance reaches a peak (P_{MPP}) of 3.2 μW and 116.8 μW for the acceleration levels of 0.025 and 0.25 g, respectively. The correspondent optimal resistive loads (R_{MPP}) are respectively equal to 298 KΩ and 277 kΩ, which do not differ too much from each other as R_{MPP} is mainly dependent on the applied frequency according to the considerations explained in Paragraph 3.3. The voltage output at the MPP (V_{MPP}) is directly usable when 0.25 g of acceleration is applied to the cantilever-based piezoelectric energy harvester but needs to be boosted-up in the case of the lower acceleration of 0.025 g. The current levels achieved at the MPP result pretty low in both tested cases thus yielding the need of an energy storage device and further technical strategies to reach higher power levels that suit practical applications.

3.6 Summary

Starting from the description of two low-frequency case studies of vibration powered wireless sensor systems for SHM, this chapter has presented implementations, analyses, and characterisations of non-resonant and resonant piezoelectric energy harvesters. In particular, non-resonant patch-like PEH systems for wireless condition monitoring of commercial aircraft wings have been described, based on the use of novel MFC material as the energy harvester, whilst a resonant cantilever-based PZT harvester has been described aiming at wireless condition monitoring of large industrial machinery. Ultra-thin MFC materials were bonded to aeronautical grade aluminium alloy and carbon fibre composite substrates in both single and multiple configurations, and tested under applied excitations with a range of frequencies

and strain levels that are typical of in-flight vibrations of transport aircraft wings in an active service. Up to 12 mW of power was generated from the single MFC configuration across a range of resistive loads (up to 350 kΩ), with manageable output voltages in the range of 12-28 V at the MPP. It has been shown that a multiple configuration of parallel connected piezoelectric transducers, integrated onto a host substrate, may lead to higher power output levels as a result of the larger inherent capacitance of the harvester. This is also an advantage for power extraction purposes as it lowers the overall harvester's impedance. It was observed that higher PEH capability is obtained for ambient conditions featuring higher applied strain levels and vibration frequency up to resonance. In order to tune the mechanical resonance of the implemented PZT cantilever-based energy harvester in the low-frequency range and so to achieve a higher power output, proof masses were added on the tip of the cantilever beam. Under the resonant excitation of 0.25 g of acceleration at 11.5 Hz the harvested power was measured approximately equal to 117 μW. However, testing at a lower acceleration level has shown that cheap off-the-shelf piezoelectric materials with small active area require further improvement to meet the energy requirements of practical applications. In order to add reliability for truly performing the SHM applications described by the two case studies in an energy-autonomous manner, the development of passive interfaces for non-resonant and resonant piezoelectric energy harvesters operating at low frequency will be further investigated in Chapter 4 and 5, respectively.

4 A PASSIVE IMPEDANCE MATCHING INTERFACE FOR NON-RESONANT PIEZOELECTRIC ENERGY HARVESTERS

The characterisation of the MFC energy harvesters presented in Chapter 3 has shown the capability to achieve power levels in the millwatt range under vibrations typically found on aircraft wings. In order to increase such power levels, hence to approach a continuous power supply to wireless sensor nodes at the current state of the development, this chapter focusses on the development of a passive impedance matching interface. The aim is to fulfil the conditions for the maximum power transfer so as to maximise the energy extracted from the piezoelectric harvester. It is well known that low-frequency vibrations lead the impedance of piezoelectric harvesters to a large capacitive reactance value. To achieve the maximum power transfer conditions, it is impractical to match such impedance by use of conventional inductors as their volume would easily reach a few cubic metres. This chapter addresses the challenge adopting PC permalloy material to implement a passive interface that consists of a single toroidal coil of just a few centimetres and practically performs the complex conjugate load match of the MFC energy harvester on aluminium substrate, implemented as in Paragraph 3.2.1, at the frequency of 10 Hz. The effects of the developed interface on the voltage, current, and power transferred to a resistive load are examined through comparisons with the results that have been achieved from the standard MFC characterisation (without the interface) for the applied strain levels and frequencies in the range between 480–1170 με peak-to-peak and 2.5–10 Hz, respectively, as from case study 1.

4.1 Description of the interface

Figure 4-1 shows the circuital configuration of the developed passive impedance matching interface, where an added inductive element of inductance L_{add} is used to enhance the performance of a piezoelectric harvester connected to a resistive load R_{L}.

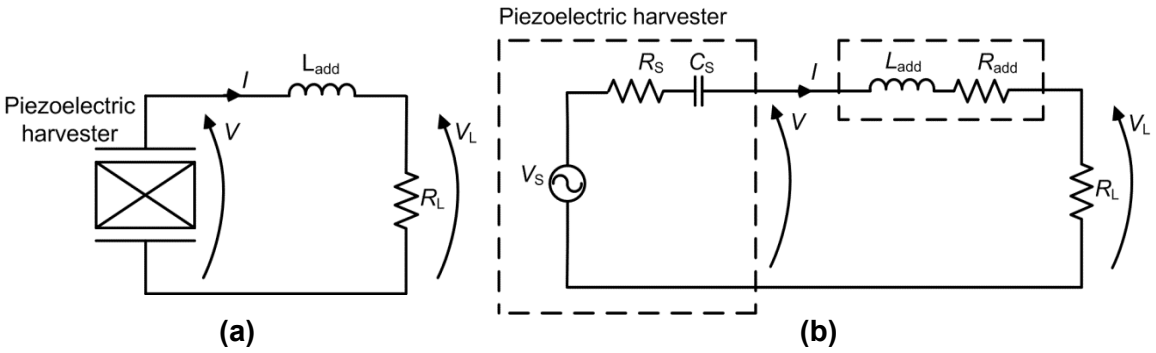

Figure 4-1 Circuital configuration of the passive impedance matching interface with an added inductive element to enhance the EH performance of a piezoelectric harvester connected to a resistive load: (a) a schematic of the circuit and (b) an analytical circuit model

When the frequency f of the input vibration is low and the angular frequency $\omega = 2\pi f$ along with it, the impedance of piezoelectric harvesters features a large capacitive reactance $X_s = -1/(\omega C_s)$, which is not practical to be matched by use of conventional inductors in order to satisfy the condition in Equation (4-1) for the maximum power transfer:

$$L_{add} = \frac{1}{\omega^2 C_s} \tag{4-1}$$

being C_s the inherent harvester's capacitance.

Indeed, a few metres in diameter would be the physical size of standard manufactured ferrite or powdered-iron solenoid inductors required to achieve the right L_{add} value (in the kilo-Henry range) for the complex conjugate impedance match of typical piezoelectric harvesters working at low frequency. Thereby, toroidal shape was considered to be used for this experimental study and PC permalloy material was first introduced here to implement a small-sized coil as passive CCIM interface that is practical at low-frequencies for the enhancement of a piezoelectric harvester performance. Indeed, the high initial magnetic permeability property of the PC permalloy material permits to reach at low frequency the condition in Equation (4-1) with a centimetre-scaled inductor.

4.2 Theoretical analyses

In order to understand how the added inductive element of inductance L_{add} enhances the power output from a piezoelectric harvester, theoretical analyses are given in this section.

Figure 4-1(b) shows the analytical electrical model of the piezoelectric harvester in Figure 4-1(a), where L_{add} is the added inductive element, R_{add} a resistance to take into account the internal losses of the inductive element, and R_{L} the resistive load. This model is similar to the one reported in Figure 3-9, where the piezoelectric harvester is assumed to be the voltage source V_{OC} in series with the inherent capacitance C_{s} and resistance R_{s}. As shown in Paragraph 3.4.1, the dielectric behaviour of the piezoelectric harvester leads to a predominantly capacitive impedance at low frequencies. This affects the total electric charge generated by the piezoelectric transducer under an externally applied stress and can be explained by the following analyses. Assuming that stress only occurs along the 1-direction and the piezoelectric harvester undergoes a sinusoidal steady-state stress due to the external vibration, then the voltage source V_{OC} of the electrical model in Figure 4-1(b) is still as in Equation (3-2). Therefore, given the applied strain level ε_1, the amount of AC current I flowing through the circuit of Figure 4-1 can be calculated as:

$$|I| = \frac{|d_{31}|tY|\varepsilon_1|}{\varepsilon_{33}^{\sigma}\sqrt{\left(R_{\text{s}} + R_{\text{add}} + R_{\text{L}}\right)^2 + \left(\omega L_{\text{add}} - \frac{1}{\omega C_{\text{s}}}\right)^2}}. \tag{4-2}$$

From Equation (4-2), it can be deduced that the inductive element L_{add} can yield an increment of the maximum current I generated by the piezoelectric harvester and, in turn, of the maximum power P_{L} dissipated by the load R_{L}, being P_{L} equal to:

$$P_{\mathrm{L}}=\left[\frac{\left|d_{31}\right|tY\left|\varepsilon_1\right|}{\varepsilon_{33}^{\sigma}\sqrt{\left(R_{\mathrm{s}}+R_{\mathrm{add}}+R_{\mathrm{L}}\right)^2+\left(\omega L_{\mathrm{add}}-\frac{1}{\omega C_{\mathrm{s}}}\right)^2}}\right]^2\frac{R_{\mathrm{L}}}{2}. \tag{4-3}$$

By taking into account the condition in Equation (4-1), it can be derived from Equations (4-2) and (4-3) that the enhancement of the piezoelectric energy harvester performance is more significant in those applications that involve large values of the harvester's reactance. From Equation (4-2) and (4-3), the amplitude of the voltage V and V_{L}, respectively across the piezoelectric harvester and the resistive load R_{load}, can be also calculated as:

$$\left|V\right|=\left[\frac{\left|d_{31}\right|tY\left|\varepsilon_1\right|}{\varepsilon_{33}^{\sigma}}\right]\frac{\left(R_{\mathrm{add}}+R_{\mathrm{L}}\right)^2+\omega^2{L_{\mathrm{add}}}^2}{\sqrt{\left[\frac{L_{\mathrm{add}}}{C_{\mathrm{s}}}-\omega^2{L_{\mathrm{add}}}^2-\left(1+R_{\mathrm{s}}\right)\left(R_{\mathrm{add}}+R_{\mathrm{L}}\right)^2\right]^2+\left(\frac{R_{\mathrm{add}}+R_{\mathrm{L}}}{\omega C_{\mathrm{s}}}+\omega R_{\mathrm{s}}L_{\mathrm{add}}\right)^2}} \tag{4-4}$$

and

$$\left|V_{\mathrm{L}}\right|=\frac{R_{\mathrm{L}}\left|d_{31}\right|tY\left|\varepsilon_1\right|}{\varepsilon_{33}^{\sigma}\sqrt{\left(R_{\mathrm{s}}+R_{\mathrm{add}}+R_{\mathrm{L}}\right)^2+\left(\omega L_{\mathrm{add}}-\frac{1}{\omega C_{\mathrm{s}}}\right)^2}}. \tag{4-5}$$

4.3 Design considerations

In order to implement within real-case EH systems for low-frequency applications the passive impedance matching interface analysed in Paragraph 4.2, design considerations are presented below to achieve a small-sized physical inductor.

Assuming toroidal shape for the coil used to implement the added inductance L_{add} of the circuit in Figure 4-1, the magnetic field B is constant along the radius r of the torus, due to its geometric symmetry, and the magnetomotive force Λ_B can be calculated as:

$$\Lambda_B = B2\pi r\,. \tag{4-6}$$

If N turns of wire are wrapped around the toroidal core of the interface inductive element, from the Ampère' s law, the magnetic field B inside the toroid is equal to:

$$B = \frac{\mu_0 \mu_r NI}{2\pi r} \tag{4-7}$$

where I is the current that flows through the N turns, and μ_0 and μ_r are respectively the magnetic permeability of the free space and of the core's material. From Equation (4-7), the magnetic field flux φ_B through each loop of the coil can be calculated as:

$$\varphi_B = \int_a^b Bh\mathrm{d}r = \frac{\mu_0 \mu_r NIh}{2\pi}\int_a^b \frac{\mathrm{d}r}{r} = \frac{\mu_0 \mu_r NIh}{2\pi}\ln\frac{b}{a} \tag{4-8}$$

where a, b, and h are the inner diameter, the outer diameter, and the height of the coil, respectively.

Therefore, the added inductance L_{add} of the circuit in Figure 4-1 is:

$$L_{\mathrm{add}} = \frac{N\Lambda_B}{I} = \frac{\mu_0 \mu_r N^2 h}{2\pi}\ln\frac{b}{a}\,. \tag{4-9}$$

From Equation (4-9) it can be observed how geometric parameters and material properties of the coil determine L_{add}; hence, the following four basic design guidelines can be obtained:

1) the higher the number of turns (N) of wire in the coil the higher the inductance L_{add} as the generated magnetomotive force Λ_B will be higher for a given amount of coil current I;
2) the wider the cross-sectional area ($b >> a$) of the coil the higher the inductance L_{add} as the reluctance of the coil will be lower for a given amount of force Λ_B;

3) the longer the coil's height (h) the higher the inductance L_{add} as the magnetic field flux φ_B will be higher for a given amount of field strength;
4) the higher the magnetic permeability of the coil's core (μ_r) the higher the inductance L_{add} as the magnetic field flux φ_B will be higher for a given amount of field strength.

4.4 Implementation using a PC permalloy coil

Figure 4-2 shows the physical coil sourced from Shin Core Techology (HK) Ltd and used to implement the inductance L_{add} of the passive impedance matching interface.

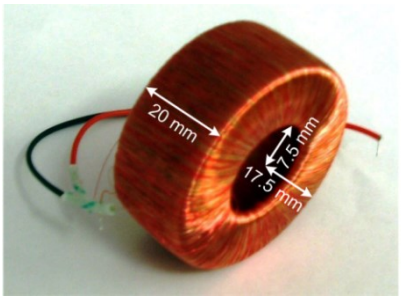

Figure 4-2 Toroidal coil used to implement the passive impedance matching interface

The coil has toroidal shape and is made of 1J85 PC permalloy (~78–80% Ni-Fe, 4.2–5.2% Mo) core. The PC permalloy material has a high magnetic permeability property, from 6×10^4 H/m ($\mu_{r\_init.}$) to a maximum of around 45×10^4 H/m ($\mu_{r\_max.}$). This permits to achieve the large inductance values required in the low-frequency range in order to satisfy the CCIM condition in Equation (4-1). Furthermore, it follows from Equation (4-9) that, given the same number N of coil turns, the inductor coil made of PC permalloy core has a small physical size of only a few centimetres in diameter rather than the metre-size required for the implementation of standard manufactured ferrite or powdered-iron solenoid inductors. The toroidal geometry of the coil also contributes to obtain higher levels of inductance in a smaller size. Another advantage is that, since the magnetic field is confined to the inside core, the toroidal coil can be placed near other electronic components without concern about unwanted

inductive interactions. As from Equation (4-9), a number of turns of copper wire N = 2800 was arranged to perform the impedance match with the connected piezoelectric harvester and achieve the inductance L_{add} ≈1.6 kH at 10 Hz (under the applied AC voltage of 1 V amplitude). Having a radius ($r = \frac{b+a}{2}$) equal to 25 mm, the total volume and weight of the toroidal coil were respectively measured around ~15 cm^3 and ~75 g. Details of the physical parameters and electromagnetic material properties of the toroidal coil used to implement this passive impedance matching interface are listed in Table 4-1.

Table 4-1 Physical parameters and electromagnetic material properties of the toroidal coil used to implement the passive impedance matching interface

Parameter	Value
Core material	1J85 PC permalloy
Core's case material	Nylon 66
Wire material	Copper (Cu)
Inner diameter (a)	15 mm
Outer diameter (b)	35 mm
Height (h)	20 mm
Wire diameter	0.14 mm
No. of turns (N)	2800
Occupation coefficient	90%
Core weight	44.74 g
Coil weight	75.06 g
Initial magnetic permeability ($\mu_{r\_init.}$)	6×10^4 (H/m)
Maximum magnetic permeability ($\mu_{r\_max.}$)	45×10^4 (H/m)
Saturation magnetostrictive coefficient	$< 2\times10^{-6}$
Coercive force	< 2.3 (A/m)
Saturation flux density	0.75 (T)
Quality factor (Q) [for 1 V applied at 10 Hz]	59.5

4.5 Results and discussions

4.5.1 Impedance characteristics of the implemented interface

Figure 4-3 shows the measured electrical impedance characteristics of the toroidal coil used to implement the passive impedance matching interface for the enhancement of the performance of the connected MFC energy harvester.

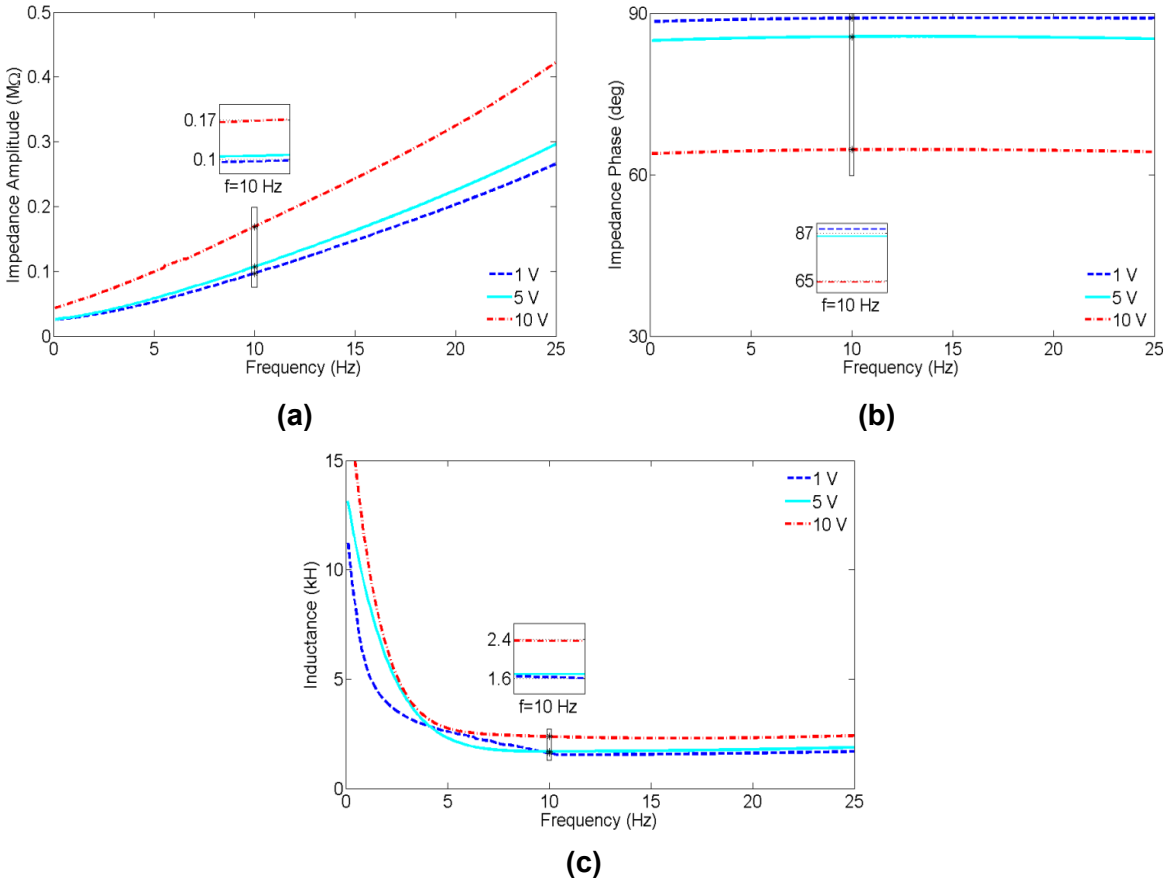

Figure 4-3 Measured (a) impedance amplitude, (b) impedance phase, and (c) inductance of the implemented impedance matching interface as a function of frequency, where the applied AC voltage is 1, 5, and 10 V, respectively

From Figure 4-3, it can be observed that: 1) the measured coil's impedance amplitude is linearly dependent on the applied frequency, which is typical of an inductor; 2) the higher the amplitude of the applied voltage the higher the amplitude of the coil's impedance; 3) there is a strong inverse dependence of the impedance phase on the applied voltage, which means an increase of the coil's resistance and a decrease of its quality factor Q with the increase of the amplitude of the applied voltage, where the measured Q values are 59.5, 13.0,

and 1.9 at 10 Hz for the applied voltages of 1, 5, and 10 V amplitude, respectively; 4) the measured Q values are approximately constant for different excitation frequencies within the measured frequency range up to 25 Hz as the phase curves are almost flat lines; however, it should be expected an increment of the parasitic resistance at frequencies higher than the tested range due to the skin effect in the winding wires and the losses in the core material, which cause a decrement of Q; 5) the measured inductance of the coil was around 1.6 kH and 2.4 kH when 1 V and 10 V amplitudes of voltage were respectively applied to the coil at 10 Hz of frequency; and 6) higher values of inductance were obtained at lower frequencies.

4.5.2 Effects of the interface on the harvester's performance

Figure 4-4 shows the actual experimental setup used for the characterisation on the enhancement of the EH performance achieved by connecting the implemented passive impedance matching interface in series between the piezoelectric energy harvester and its resistive load.

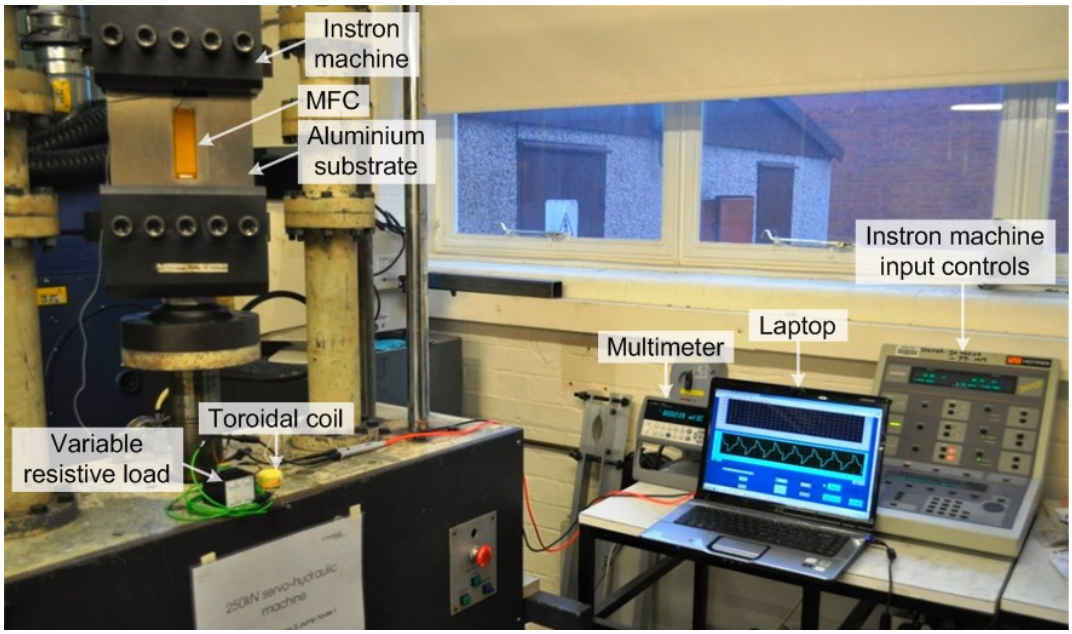

Figure 4-4 A photograph of the experimental setup used for the characterisation of the implemented passive impedance matching interface

Figure 4-5 and Figure 4-6 respectively show comparisons of the root-mean-square current (I_{rms}) and the average power (P_{L}) transferred to the connected resistive load (R_{L}) between the configurations with and without the interface (with L and stnd) for different applied peak-to-peak strain levels of 480, 710, 940, and 1170 με and excitation frequencies, where the scattered points represent the measured data and the depicted curves their fit.

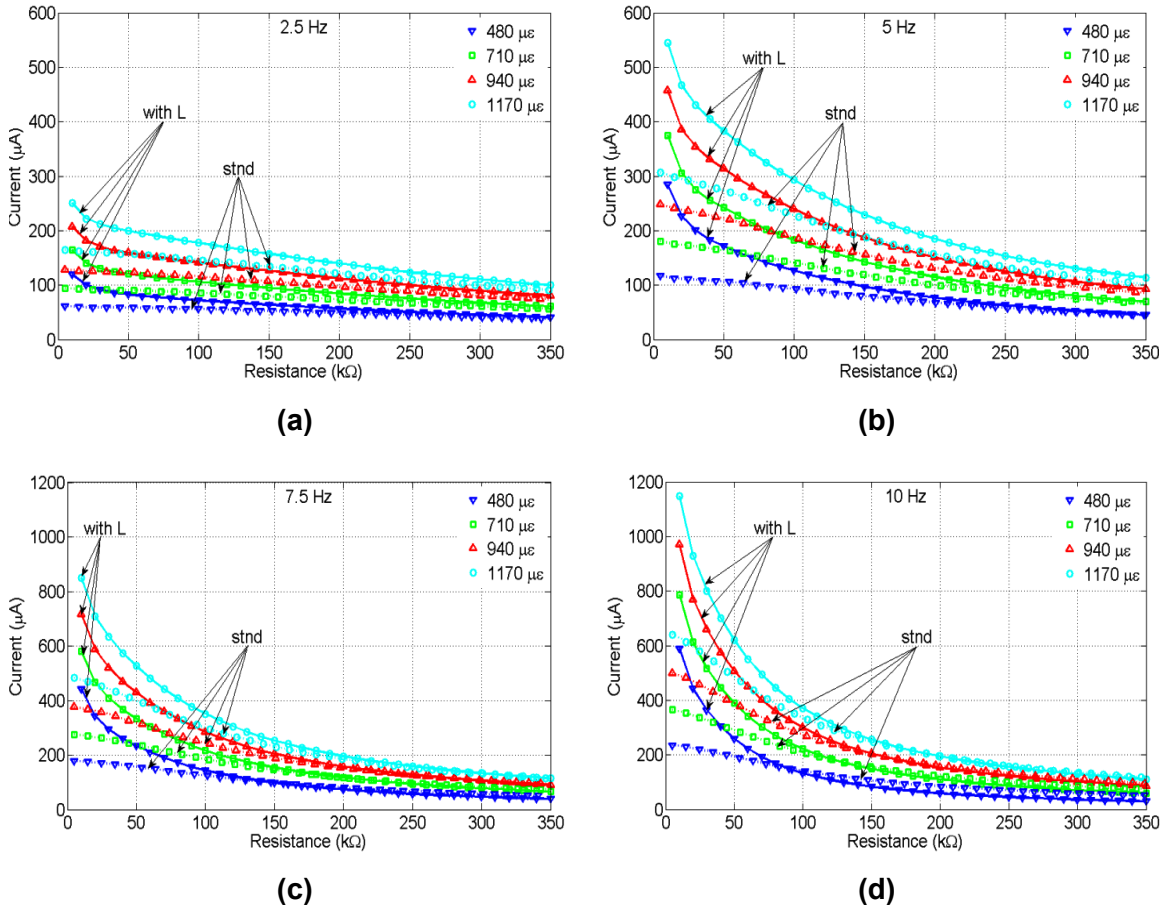

Figure 4-5 Comparisons of the root-mean-square current between the configurations with and without the interface (with L and stnd) for different applied peak-to-peak strain levels of 480, 710, 940, and 1170 με and excitation frequencies: (a) for 2.5 Hz, (b) for 5 Hz, (c) for 7.5 Hz, and (d) for 10 Hz

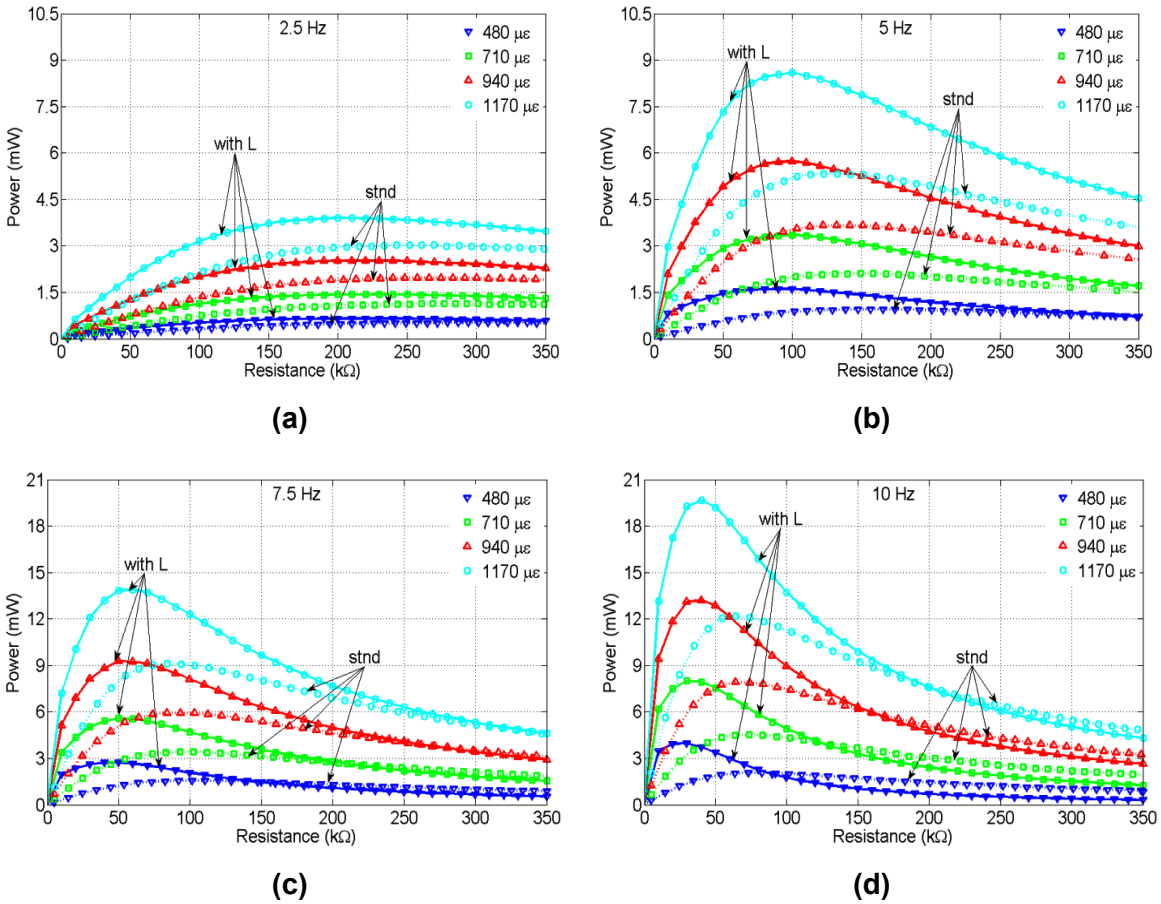

Figure 4-6 Comparisons of the average power transferred to the resistive load between the configurations with and without the interface (with L and stnd) for different applied peak-to-peak strain levels of 480, 710, 940, and 1170 με and excitation frequencies: (a) for 2.5 Hz, (b) for 5 Hz, (c) for 7.5 Hz, and (d) for 10 Hz

From Figure 4-5 and Figure 4-6, it can be observed that for an applied strain of 1170 με peak-to-peak at 10 Hz, around 20 mW of power was transferred to a 40 kΩ resistive load in the circuit with the interface whilst 12.16 mW was the highest average power developed across 66 kΩ in the circuit without the interface; the corresponding root-mean-square currents are 702 μA and 430 μA, respectively. I_{rms} and P_{L} increase with the increase of the applied strain and frequency; however, under the same excitation frequency and applied strain level, for the circuit with the interface there is a clear increment of I_{rms} and P_{L} associated with the lower values of R_{L}. This is due to the fact that the inductive reactance of the interface diminishes the internal impedance of the energy

harvester by matching, wholly or in part, its capacitive reactance. Such a reactance cancellation causes upward and leftward shifts of the current vs. load curves and power vs. load curves for the circuit configuration with the added interface. It can be also observed that there is a decrease of the optimal resistive loads ($R_{\mathrm{L\_MPP}}$) at the MPPs. Ideally, when the electrical resonance is perfectly achieved by mean of the added inductance, $R_{\mathrm{L\_MPP}}$ is equal to the real part (R_{s}) of the harvester's impedance.

In order to compare the effects of the implemented interface on the EH performance, Table 4-2 lists the results obtained at the MPPs under tested strain levels and frequencies of the root-mean-square voltage $V_{\mathrm{L\_MPP}}$ and current I_{MPP}, the optimal average power $P_{\mathrm{L\_MPP}}$, and the corresponding resistive load $R_{\mathrm{L\_MPP}}$ for the configurations with and without the interface (with L and stnd). It further confirms the lower values of $R_{\mathrm{L\_MPP}}$ and higher values of I_{MPP} and $P_{\mathrm{L\_MPP}}$ when the developed interface is added into the circuit.

The theoretical values of $V_{\mathrm{L\_MPP}}$, I_{MPP}, and $P_{\mathrm{L\_MPP}}$, respectively calculated based on Equations (4-5), (4-2), and (4-3) for the circuit with the interface, have also been listed in Table 4-2. For the calculation of the theoretical values, the medium value of 5 kΩ was used for R_{s} and R_{add} regardless of the strain and frequency effects on the harvester's impedance reported in Figure 3-12. The medium values of 4.7 kH, 2.5 kH, 2.05 kH, and 2.0 kH were used for L_{add} to take into account the frequency effect on the coil's impedance reported in Figure 4-3.

Table 4-2 Comparisons of the optimal resistive load, average power, root-mean-square voltage and current across the load at the MPPs between the configurations with and without interface (with L and stnd) for different peak-to-peak strain levels and excitation frequencies

ε_1 (με)	f(Hz)	R_{L_MPP} (kΩ)		V_{L_MPP} (V)			I_{MPP} (μA)			P_{L_MPP} (mW)		
		stnd	with L	stnd	with L		stnd	with L		stnd	with L	
					exp.	theor.		exp.	theor.		exp.	theor.
480	2.5	304	216	12.5	11.9	11.0	41	55	51	0.51	0.65	0.56
	5	155	88	12.1	11.9	11.6	78	135	131	0.95	1.61	1.52
	7.5	105	47	12.8	11.4	10.9	122	241	233	1.56	2.75	2.54
	10	79	23	12.7	09.6	9.4	161	416	408	2.05	3.99	3.82
710	2.5	284	226	17.9	18.0	16.8	63	80	74	1.13	1.44	1.25
	5	144	98	17.4	18.1	19.0	121	185	193	2.11	3.35	3.67
	7.5	98	52	18.3	17.0	17.1	187	328	330	3.43	5.58	5.65
	10	74	35	18.3	16.7	17.7	247	479	504	4.52	8.00	8.91
940	2.5	268	219	23.0	23.5	21.8	86	108	99	1.97	2.54	2.17
	5	136	97	22.4	23.6	23.9	164	245	247	3.68	5.78	5.91
	7.5	93	56	23.5	22.8	23.6	253	407	422	5.96	9.28	9.97
	10	70	39	23.5	22.8	24.6	336	584	631	7.92	13.31	15.52
1170	2.5	253	207	27.7	28.4	26.1	109	137	126	3.02	3.89	3.30
	5	128	96	26.1	28.5	29.6	205	294	309	5.35	8.38	9.14
	7.5	86	57	28.1	28.2	29.7	325	494	521	9.11	13.93	15.45
	10	66	40	28.2	28.1	31.0	430	702	774	12.16	19.73	23.98

From Table 4-2, it can be observed that: 1) the experimental results for the circuit with the interface reasonably agree with the theoretical results; 2) there is a higher enhancement of the energy harvester performance under the excitation frequency of 10 Hz for all the tested strain levels; 3) there is a major dependence of the resistive loads at the MPPs on the excitation frequency and a minor dependence on the applied strain level. The major dependence between R_{L_MPP} and the frequency is a direct consequence of the impedance matching theory. There is an inverse relationship between them as the harvester has predominantly capacitive impedance at the low frequencies investigated herein. The minor dependence between R_{L_MPP} and the strain is due to the fact that the optimal resistive load matches the impedance of the

whole EH system. In theory, $R_{\mathrm{L\_MPP}}$ should maintain the same value for all the applied strain levels for a linear system. However, for the implemented system it is possible that there are non-linearities in the impedance characteristics of the MFC energy harvester and of the interface especially.

The effects on the energy harvester performance obtained by adding the developed impedance matching interface are also listed in Table 4-3 in terms of the increased or decreased percentage of $V_{\mathrm{L\_MPP}}$, I_{MPP}, $P_{\mathrm{L\_MPP}}$, and $R_{\mathrm{L\_MPP}}$.

Table 4-3 Effects in percentage (%) of the interface on the optimal resistive load, average power, root-mean-square voltage and current across the load at the MPPs for different applied peak-to-peak strain levels and excitation frequencies based on the experimental results

ε_1 (με)	*f* (Hz)	Effect (%)			
		$R_{\mathrm{L\_MPP}}$	$V_{\mathrm{L\_MPP}}$	I_{MPP}	$P_{\mathrm{L\_MPP}}$
480	2.5	-28.9	-4.8	+34.1	+27.5
	5	-43.2	-1.7	+73.1	+69.5
	7.5	-55.2	-10.9	+97.5	+76.3
	10	-70.9	-24.4	+158.4	+94.6
710	2.5	-20.4	+0.6	+27.0	+27.4
	5	-31.9	+4.0	+52.9	+58.8
	7.5	-46.9	-7.1	+75.4	+62.7
	10	-52.7	-8.7	+93.9	+77.0
940	2.5	-18.3	+2.2	+25.6	+28.9
	5	-28.7	+5.4	+49.4	+57.1
	7.5	-39.8	-3.0	+60.9	+55.7
	10	-44.3	-3.0	+73.8	+68.1
1170	2.5	-18.2	+2.5	+25.7	+28.8
	5	-25.0	+9.2	+43.4	+56.6
	7.5	-33.7	+0.4	+52.0	+52.9
	10	-39.4	-0.4	+63.3	+62.3

In Table 4-3, the “+” sign represents the increased percentage and the “-” sign represents the decreased percentage. It can be seen that, when the excitation frequency approaches the matched value of 10 Hz, there is more enhancement of the energy harvester performance for a lower applied strain level. This is

caused by the higher Q values discussed in the previous section and by the fact that the inductive reactance of the interface coil more closely matches the capacitive reactance of the MFC energy harvester at lower applied strain levels. Based on the experimental data, the maximum percentage variations of I_{MPP} and $P_{\mathrm{L\_MPP}}$ were calculated in correspondence to the excitation of 480 με peak-to-peak at 10 Hz and are equal to an increment of 158.4% and 94.6%, respectively.

4.6 Summary

This chapter has presented a passive impedance matching interface that practically enhances the performance of a piezoelectric energy harvester at low frequency. The interface was based on a large inductive reactance but with a centimetre-scaled size so as to be able to match the capacitive reactance of a given piezoelectric harvester when the frequency of the input vibration is as low as a few hertz and thus satisfy the conditions for the maximum power transfer. More specifically, the interface used for this experimental study consisted of a single passive PC permalloy toroidal coil with a high initial magnetic permeability of 6×10^4 H/m, which permitted to achieve a large inductance of around 1.6 kH at 10 Hz (under the applied AC voltage of 1 V amplitude) with a small volume of around 15 cm^3. The coil was easily interconnected in series with the MFC harvester on aluminium substrate, implemented as in Chapter 3, and can be retrofittable to existing EH systems. Furthermore, being a passive element, such an implemented interface does not need an additional power source, partitions of the harvested energy-flow or switching conditions to be satisfied, on the contrary of most of the active controls required by the state-of-art impedance matching techniques for piezoelectric energy harvesters. A comparison with the results from standard MFC characterisation showed that by adding the developed interface there is a significant increment in the levels of current and power transferred to a connected resistive load, and a decrement of the MPP corresponding to the optimal resistive load. It was found that the improvement of the EH performance achieved by adding the interface decreases with the decrease of the excitation frequency from 10 Hz

downwards, being 10 Hz the frequency input matched by the implemented design. However, there is an increment of the EH performance with the decrease of the applied strain due to a non-linear intrinsic material response of the implemented coil. The highest current and power improvement obtained by adding the developed interface into the testing circuit were respectively calculated equal to 96.4% and 158.4%, when the lowest tested strain of 480 με peak-to-peak was applied at 10 Hz to the MFC energy harvester.

The interface presented in this chapter has been specifically implemented to satisfy the conditions of the maximum power transfer theorem at the frequency of 10 Hz from the M8528-P2 MFC element to a resistive load. Nevertheless, the proposed method can be applied to cantilever-based piezoelectric energy harvesters and, more generally, can be potentially useful for the enhancement of PEH performances where neither the size/weight required by the interface's coil nor the coil's parasitic resistance would represent a significant constraint for the design of the EH system (e.g., for energy-autonomous wireless monitoring applications of heavy machines). In Chapter 6, the effects of the developed interface within a PEH powered wireless sensor system will be further investigated.

5 PASSIVE INTERFACES FOR RESONANT CANTILEVER-BASED PIEZOELECTRIC ENERGY HARVESTERS

This chapter introduces passive interfaces, which exploit the deflection of the harvester's beam to enhance the voltage onto which the generated current drives its charge in order to enhance the harvester's output power. It has been shown in Paragraph 2.4.2 how available electronic interfaces and the SSHI technique, in particular, permit to achieve a significant power gain based on a non-linear process of the output voltage of the piezoelectric material. Typical implementations of those, however, involve significant power consumption due to the active switching circuits used for the non-linear conditioning of the piezoelectric generated signal. On the contrary, this chapter presents passive (either magnetic or mechanical) switch interfaces to control the non-linear SSHI and practically enhance the harvester's performance. A further mechanical enhancement developed via compression springs for a passive amplification of the force acting on the harvester's beam is also described. The presented interfaces are easy in implementation and do not need additional power sources or partitions of the harvested energy-flow, with a consequent reduced power-consumption in comparison with the state-of-the-art designs. The implementation of the interfaces is described along with the experimental setup in connection with the cantilever-based piezoelectric energy harvester developed as in Paragraph 3.2.3. In order to reproduce the real working conditions featured by case study 2, tests were performed under excitations of around 0.025 and 0.25 g of acceleration at the low resonant frequency of 11.5 Hz.

5.1 SSHI concept and theoretical analyses

Active SSHI techniques have been effectively demonstrated capable of increasing the power output of piezoelectric transducers by shaping at intervals (i.e., every half cycle of the vibration period) a resonant electrical network between the inherent piezoelectric capacitance (C_s) and an added inductive

element (L_{add}) for the inversion of the generated voltage (V). Figure 5-1(a) shows a schematic of the electrical circuit used to implement the series SSHI technique in connection with a piezoelectric harvester and a resistive load (R_L).

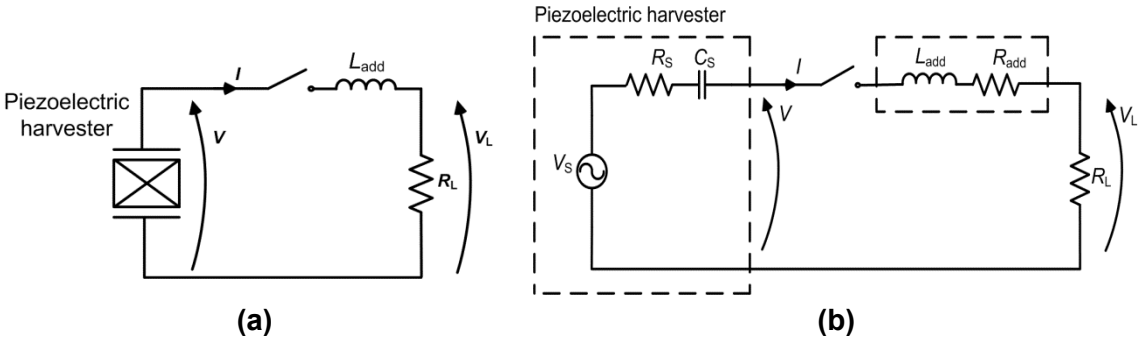

Figure 5-1 Circuital configuration of the series SSHI interface with an added inductive element: (a) a schematic of the circuit and (b) an analytical circuit model of the piezoelectric harvester and the interface

The connection between the piezoelectric harvester and the resistive load R_L is through the switching inductor L_{add}. As in the model of the circuit showed by Figure 5-1(b), the effects of a further non-negligible resistance in series to the inductor L_{add} can be taken into account to consider the losses introduced by L_{add}. The SSHI interface is said passive if the switching inductor L_{add} does not require any additional electrical control, hence power, in order to be connected or disconnected at the right time from the rest of the circuit.

The principle of operation of the series SSHI involves two different steps in the PEH process: 1) open circuit phase (i.e., the harvester under excitation is disconnected from the rest of the circuit and electric charge accumulates in the inherent capacitance C_s); 2) harvesting and inversion phase (i.e., the electric charge accumulated in the capacitor is transferred to L_{add}, the voltage V is inverted, then the electric charge is transferred to R_L where power is dissipated for the purposes of the intended application). Each time V reaches a maximum or minimum value, the inductance L_{add} is connected to the piezoelectric transducer. Such a connection causes an oscillation of V around 0 as the initial electric charge accumulated in C_s starts moving to the inductance L_{add}. After half

a period of this electrical oscillation, V is inverted and the inductance is again disconnected from the piezoelectric harvester. Especially under a low-frequency excitation, the inversion process is assumed to be quasi-instantaneous as the inversion time is chosen to be much smaller than the period of the mechanical vibration $\Delta t \approx \pi\sqrt{L_{\text{add}}C_{\text{s}}} \prec T$, where $T = \frac{2\pi}{\omega}$. Being the capacitive value C_{s} of the piezoelectric harvester typically in the range of nano-Farads, a few milli-Henries inductor connected in series to C_{s} generates an oscillation period from 4 to 2 orders of magnitude smaller than the period of usual ambient vibrations and the voltage V changes with the inversion factor: $\gamma = e^{\pi/(2Q)}$, with Q the electrical quality factor of the circuit. If R_{s} and R_{add} are the internal resistance of the piezoelectric harvester and of the inductor, respectively, and thus $R_{\text{loss}} = R_{\text{s}} + R_{\text{add}}$ takes into account the internal losses of the overall complex made by the piezo-transducer plus the switching mechanism, then the quality factor of the circuit terminated by the resistive load R_{L} can be calculated as:

$$Q = \frac{1}{R_{\text{loss}} + R_{\text{L}}}\sqrt{\frac{L_{\text{add}}}{C_{\text{s}}}}. \tag{5-1}$$

At the extrema of the tip displacement the electric charge polarities are reversed almost instantaneously through the SSHI interface. As the tip of the harvester's cantilever beam remains at its maximum (minimum) displacements, then the piezoelectric layer becomes negative (positive) with respect to the substrate layer. As the tip then moves downwards (upwards), the piezoelectric layer moves from a state of tension (compression) to compression (tension), which means that a new positive (negative) electric charge is generated with respect to the substrate layer. As a result of the SSHI process, however, the piezoelectric layer is already positively (negatively) charged with respect to the substrate; therefore, this newly generated positive (negative) electric charge is added onto the existing electric charges of the piezoelectric layer. Thus the SSHI technique takes advantage of the mechanical displacement of the harvester in order to maximise its power output. Because of the inversion

process operated by L_{add}, the voltage V_L across R_L at the moment when the switch is closed can be calculated as:

$$V_L = 2V_{OC}\sqrt{\left(\frac{1+\gamma}{1-\gamma}\right)} \approx 4\sqrt{\frac{Q}{\pi}}V_{OC}. \quad (5\text{-}2)$$

Since R_L conducts the same current as the resistors R_s and R_{add}, then the energy dissipated by the load per half cycle will be divided in proportion to the resistors' magnitude as:

$$W = \frac{1}{2}\left(\frac{R_L}{R_L + R_{loss}}\right)C_s{V_L}^2 \approx \left(\frac{R_L}{R_L + R_{add}}\right)\left(\frac{8Q}{\pi}\right)C_s{V_{OC}}^2. \quad (5\text{-}3)$$

From Equation (5-3) it can be observed that W is maximised when $R_L = R_{loss}$, for which:

$$Q = \frac{1}{2R_{loss}}\sqrt{\frac{L_{add}}{C_s}}. \quad (5\text{-}4)$$

This, in turn, corresponds to a maximum load power equal to:

$$P_{max} = \frac{\omega}{\pi}W \approx \left(\frac{2Q}{\pi^2}\right)\frac{{V_{OC}}^2}{{R_s}^2\omega C_s}. \quad (5\text{-}5)$$

Magnetically and mechanically activated interfaces are here proposed to passively achieve the SSHI and so to enhance the performance of resonant cantilever-based piezoelectric energy harvesters.

5.2 Description of the interfaces

5.2.1 Magnetically activated SSHI

Figure 5-2 depicts the design of a novel developed passive interface with magnetically activated SSHI for resonant cantilever-based piezoelectric energy harvesters at low frequency.

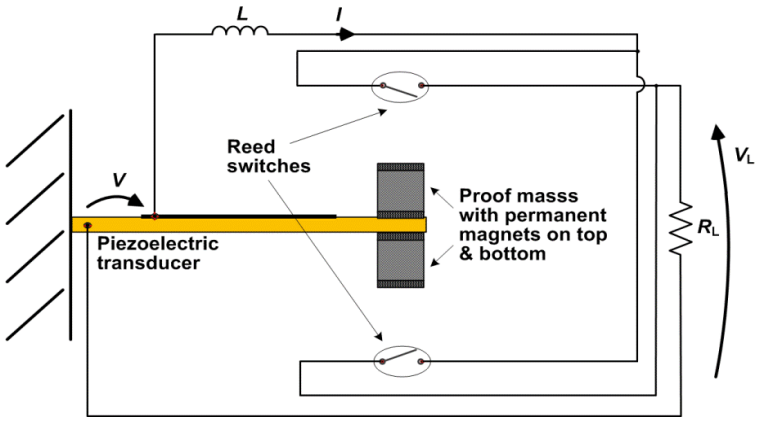

Figure 5-2 A schematic of the passive interface circuit with two reed switches for magnetically activated SSHI

This circuit configuration is like the one seen in Figure 3-7 for the implemented cantilever-based piezoelectric energy harvester but, in this case, the inductor L_{add} is added in series to the piezoelectric harvester and the connected resistive load R_{L}; in addition, two reed switches determine the flow of the generated current into the circuit. The reed switch is an electrical switch made of two contacts on ferrous metal reeds, which are magnetisable, flexible, and hermetically sealed at the opposite ends of a glass envelope. In the circuit configuration of Figure 5-2 the contacts are separated by a small gap as the reed switches are in a normal open condition, thus drawing zero power, but can be operated (i.e., closed contacts) by an applied magnetic field of the right intensity. The reed switches, in fact, are characterised by a specific pull-in distance, which is defined as the distance from the permanent magnet used for its activation. Such a distance depends both on the switch's design and the intensity of the generated magnetic field. The harvester's permanent magnets on the top and bottom of the proof masses are essential for the correct working order of such a passive interface design. Due to the displacement of the beam under vibrations, the magnetic tip mass gets closer to the respective reed switches. As a general rule, a 50% overlap region ensures 100% activation of the switch. The majority of the manufacturers also specify 20% hold region and 80% close region [226]. Therefore, the switch has to deflect on either side for a certain amount in order to ensure that the switches will be activated. In

particular, known the tip displacement of the piezoelectric beam at resonance and within the acceleration region of interest, the position of the reed switches can be set so as to be closed when the beam deflection has reached an extremum. The same behavior is desired for both the top and the bottom set of the switches. By reaching the desired deflection, the piezoelectric element is not in an open circuit anymore but connected to the inductor L_{add}, which causes the inversion of the piezoelectric voltage v, for an enhanced power transfer to the resistive load R_{L}. The resistive load is then connected when v is maximal in either polarity (i.e., at the zero crossing of the current source), which coincides with the extremum displacements of the cantilever beam. As the beam tip bends back away from the switches and the magnets move along, the switches return to their normally open state. Such an operation repeats at every half cycle of the sinusoidal input but could be adopted for any kind of input whose waveform reaches the same peak levels in terms of amplitude rather than time. Being hermetically sealed, hence protected from the outside environment, the contacts of the reed switches are not susceptible to wear and can typically perform billions of reliable operations.

5.2.2 Compression springs for force amplification through fixed strips

Figure 5-3 depicts the piezoelectric harvester implemented as in Paragraph 3.2.3 with, in addition, two compression springs on the free end of the proof masses.

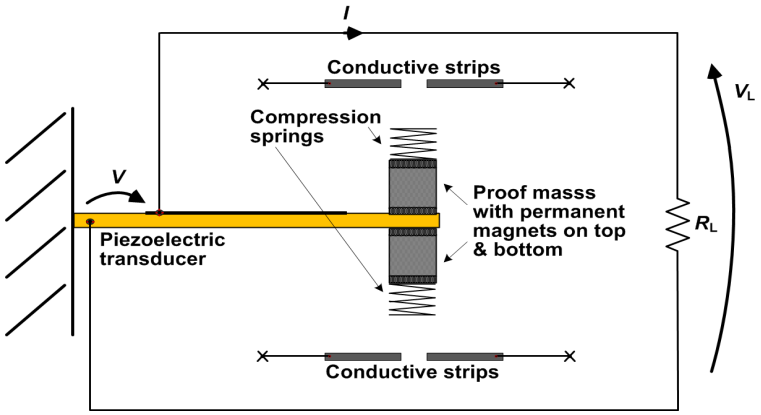

Figure 5-3 A schematic of the passive interface circuit with two compression springs on the free end of the proof masses and two strips for the amplification of the applied force

On both sides of the harvester's cantilever beam, close to the compression springs, there are also two conductive strips that are spatially fixed. The strips are on each side separated by an air gap and not connected to the rest of the circuit so that, from an electrical point of view, they represent an open circuit and do not contribute to the overall working functioning of the circuit. From a mechanical point of view, however, the strips form a fixed frame that counteracts the deflection of the piezoelectric beam tip under vibration. The presence of the compression springs generates an enhancement of the mechanical force acting on the tip of the piezoelectric beam depending on the design of the harvester and on the characteristics of the input vibration (i.e., the magnitude of the acceleration in the case of resonant applications). The diameter of the springs is bigger than the air gap between the strips and they are reciprocally aligned in a way that, at each deflection of the beam tip, the ends of the springs impact against the strips leaving their air gap in between. As the springs offer resistance to the compressing force, they push back the beam tip trying to restore their original length. Because of the compression springs, such an interface is more flexible to small variations of the vibration input, especially in the case of resonant applications or applications where the frequency of the excitation is always within a narrow bandwidth. The distance of the strips from the springs can be set in a way that the deflection of the piezoelectric cantilever beam is not damped but magnified as the constrained swing of the beam, between the two frames, generates a mechanical resonance through the reciprocal compression of the springs. The compression of the springs required to trigger the mechanical enhancement on the acting force is tiny for low resonant frequency applications under small acceleration magnitudes. This increases the service life of the springs as contact stress is reduced; additionally, side deflections or loading problems related to the maximum speed of shifts of the moving end of the spring are also reduced.

5.2.3 Mechanically activated SSHI

Figure 5-4 is based on the circuit configuration of Figure 5-3 but introduces the inductive element L_{add} as for the implementation of the SSHI technique, whose

activation is here operated by the mechanical contact between the compression springs and the conductive strips.

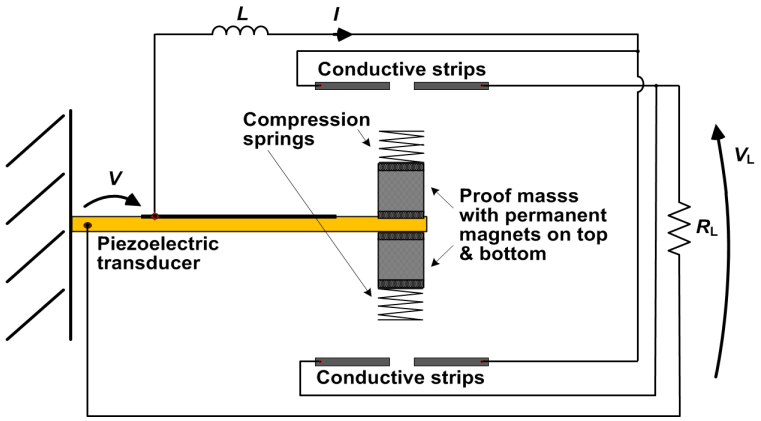

Figure 5-4 A schematic of the passive interface circuit with compression springs and conductive strips for mechanically activated SSHI

One end of both the conductive strips at the top side and bottom side of the piezoelectric cantilever beam is connected to the series made by the harvester and the inductor L_{add} whilst the opposite ends are connected across the resistive load R_{L} in a reciprocal way. The electrical circuit is left open in correspondence of the air gap between the two ends of the conductive strips and closed by the contact onto the compression springs at every positive or negative beam deflection that reaches the pre-tuned distance between the springs and the strips. Thus the flow of the current from the harvester to the resistive load can be ensured through the inductance L_{add} at every half cycle of the input excitation. Known the displacement of the cantilever beam in correspondence to a certain excitation frequency (e.g., resonance) and acceleration magnitude, the position of the strips can be experimentally determined to achieve the synchronisation of the switching process at every extremum displacement of the piezoelectric cantilever beam. In such a way, the SSHI technique is passively enabled in a mechanical way. The inversion process, started from the contact between the compression springs and the conductive strips, is naturally blocked with the release of that contact in correspondence to a change of direction in the beam's displacement. Figure 5-5(a) illustrates the trend of the voltage developed across the piezoelectric cantilever-beam as a consequence of the

switching process, whose main steps are show in Figure 5-5(b) for the duration of a whole cycle of the beam's oscillation.

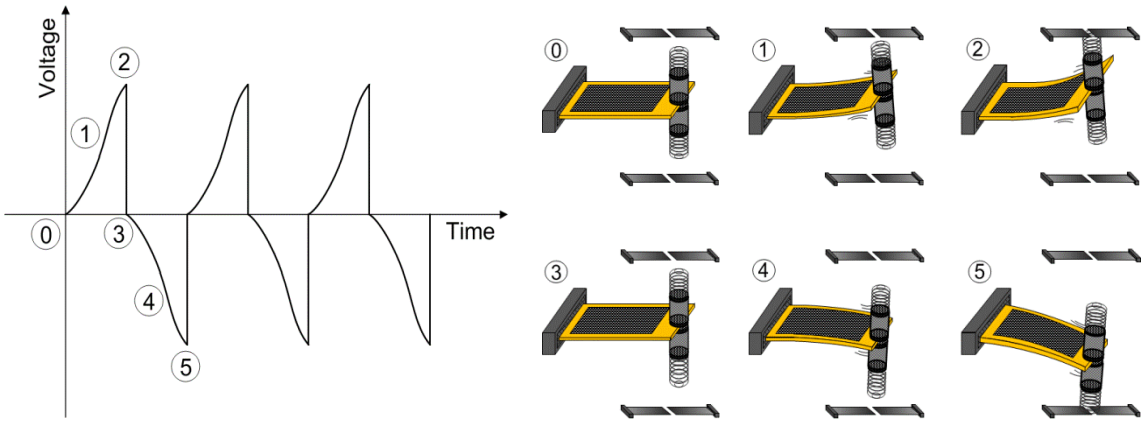

Figure 5-5 An illustration of the mechanically activated SSHI process: (a) a trend of the voltage developed across the piezoelectric cantilever-beam and (b) the correspondent beam's oscillation for the duration of a whole cycle

It has to be noticed that the compression springs act like a mechanical energy storage under the acting force of the piezoelectric cantilever beam. The energy stored by the contact between the compression springs and the conductive strips is released immediately after that contact, thus yielding an increase of the inversion quality towards a more effective PEH process where the voltage onto which the piezoelectric current source drives its charge is further augmented.

5.3 Implementations

Given the implementation of the resonant cantilever-based piezoelectric harvester in Paragraph 3.2.3, the described interfaces that will be connected to it have been implemented as following. It is worthwhile to mention that the described interfaces, because of the wearing parts featured by their mechanical structure, are better suited for PEH applications featuring a low excitation frequency as in the scope of this research work.

5.3.1 Magnetically activated SSHI

Figure 5-6 shows the implemented interface used in connection to the developed resonant cantilever-beam piezoelectric harvester in order to obtain a magnetically activated SSHI process.

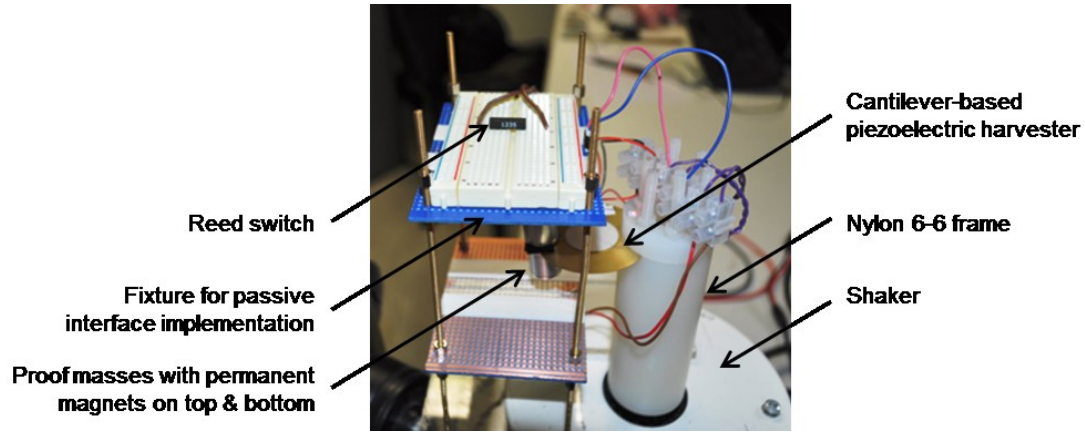

Figure 5-6 A photograph of the implemented interface used in connection to the developed resonant cantilever-beam piezoelectric harvester in order to obtain a magnetically activated SSHI process

Two electronic breadboard circuits were fixed above and below the implemented cantilever beam through a non-magnetic metallic frame. Two 59600-495 SPST reed switches (Hamlin Electronics Ltd, Norwich – UK) were connected into the breadboard circuits so as to make the generated current flow to the electrical resistive load every time the cantilever beam approaches its extremum positions. The switches are 15 mm long and 3.2 mm wide including the celanex body covering the ferromagnetic reeds, hermetically sealed in a glass envelope. Details of the physical parameters and electromagnetic properties of the reed switches can be found in [227]; particularly, the maximum initial contact resistance is approximately equal to 100 mΩ and distances larger than 2 mm and smaller than 14 mm are respectively stated by the manufacturer to operate and release the switches. Reliability and degradability of the switches have also been considered as critical factors among the parameters chosen for implementing such a circuit configuration. The magnetic coupling of the magnet to the reed switch is important as the ferromagnetic reeds of the switch will need to close as soon the right magnetic field intensity is brought nearby. The frame of the implemented interface structure permits to vary the height of the breadboard circuits so as to move the position of the reed switches mounted on them. They were fixed at the point where the magnetic field carried by the permanent magnets at the tip of the cantilever beam exactly equals the switches' pull-in distance in correspondence to the maximum and minimum

displacements of the harvester for an excitation of the selected amplitude and resonant frequency. For the low and high acceleration testing conditions used at resonance as following described, the base of the breadboard circuits was respectively fixed at a distance of 1.9 and 2.1 cm from the horizontal axis of the cantilever beam. In addition, for the purpose of the SSHI, a 13R105C 1 mH inductor (Murata Power Solutions, Milton Keynes – UK) was connected in series to the harvester's electrical output. The value of the inductor was chosen such that the energy accumulated by the inherent capacitance of the piezoelectric harvester can be all transferred at every half cycle of the applied excitation and, therefore, such that the oscillation frequency of the LC_s resonator is much higher than the applied excitation frequency.

5.3.2 Compression springs for force amplification through fixed strips

In the experimental setup of Figure 5-6 two thick conductive strips were symmetrically obtained onto the surface of both the breadboard circuits above and below the contact point of the piezoelectric cantilever-beam by use of SCP03B silver conductive paint (Electrolube Ltd, Ashby de la Zouch – UK). The strips are close to each other, separated by a small gap to avoid undesired short circuits and allow the mechanical amplification of the acting force on the cantilever beam as described in Paragraph 5.2.2. For that, small compression springs (i.e., 10 mm of height and 15 mm of diameter) were positioned on top of the tip masses at the free-end of the cantilever beam. The compression springs maintained their position due to the magnetic force carried out by the permanent magnets on the proof masses of the cantilever beam although they could be glued if high acceleration magnitudes are featured by the applied excitation. Soft compression springs were preferred in order to avoid high damping of the impact force and crack of the ceramic piezoelectric material. For the low and high acceleration levels used for testing, the base of the breadboard circuits was respectively fixed at a distance of 1.7 and 1.9 cm from the horizontal axis of the cantilever beam with a slight angle to ensure full contact between the compression springs and the conductive strips.

5.3.3 Mechanically activated SSHI

The same experimental setup described in Paragraph **Error! Reference source not found.** was used to implement the passive interface for the mechanically activated SSHI of the developed cantilever-based piezoelectric harvester but adding a 13R105C 1 mH inductor (Murata Power Solutions, Milton Keynes – UK) in series to the harvester's electrical output. The position of the breadboard circuits on the supportive frame was fixed so that the springs, electrically conductive, could close by contact the circuit from the harvester to the connected electrical resistive load at every maximum and minimum deflection of the cantilever beam.

5.4 Results and discussions

Figure 5-7 shows the voltage developed across the piezoelectric harvester when this is connected to a resistive load of 70 kΩ under a resonant excitation of 11.5 Hz and 0.025 g of acceleration in the configurations without (PH only) and with the implemented interfaces, respectively the interface for magnetically activated SSHI (PH + magn SSHI), the added compression springs (PH + springs) for the force amplification through conductive strips, and the springs together with the interface for the mechanically activated SSHI (PH + springs + mech SSHI).

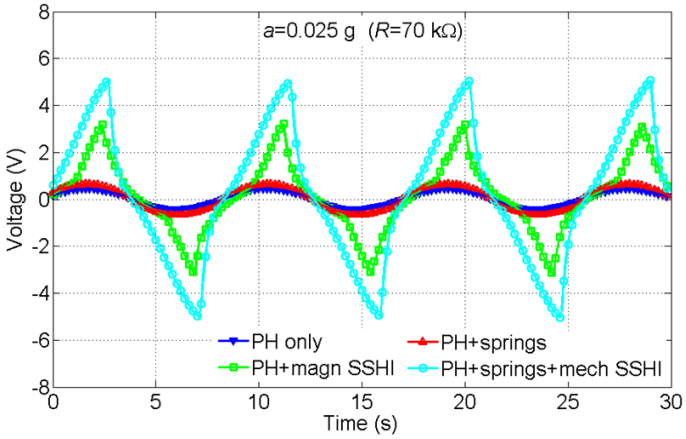

Figure 5-7 Voltage developed across the piezoelectric harvester when this is connected to a resistive load of 70 kΩ under a resonant excitation of 11.5 Hz and 0.025 g of acceleration for different implemented configurations

The piezoelectric voltage of a resonant cantilever-based harvester is typically proportional to the harvester's displacement. From Figure 5-7, it can be observed that, when the implemented passive interfaces are connected to the piezoelectric harvester, the voltage is amplified. Particularly, when springs only are added to the harvester configuration for the force amplification through the conductive strips, the piezoelectric voltage maintains the same trend whilst it appears slightly distorted and shifted in time for the configurations that implement the SSHI. The amplification of the piezoelectric voltage is much higher when the SSHI is performed as from the analyses reported in Paragraph 5.1. Indeed, when the harvester is shunted through the added inductor L_{add}, the voltage on the piezoelectric inherent capacitance C_{s} is reversed and, as the process continues, a steady regime is obtained as illustrated in Figure 5-7. The continuity of the voltage under continuous vibrations ensured by the dielectric behavior of the piezoelectric element leads to a cumulative effect that allows a significant increase of the voltage itself. From Figure 5-7 , it can be observed that the voltage of the piezoelectric harvester, when this is connected to a resistive load of 70 kΩ, is higher for the interface configuration featuring compression springs and mechanically activated SSHI rather than magnetically activated SSHI only. This can be explained from the superposition of the SSHI effect and the mechanical amplification of the force acting on the harvester's cantilever beam as a result of the added compression springs. It can also be observed from Figure 5-7 that, when the SSHI process is performed either magnetically or mechanically, the voltage reversal is not perfect. This is due to the parasitic resistance of the inductor and the mechanical limitations of the performed interfaces' implementation, which naturally lead to damped oscillations. An improved experimental setup could lead to a greater overall voltage amplitude and PEH capability along with it.

Direct comparisons of the measured voltage developed across connected resistive loads and the correspondent transmitted current and power between the resonant cantilever-based piezoelectric harvester without and with the implemented interfaces are shown in Figure 5-8 to Figure 5-10, respectively.

Since the current experienced by the load resistor is alternating, similar comparisons are reported in the literature as “AC comparisons” when the SSHI performance has been evaluated for different harvester configurations.

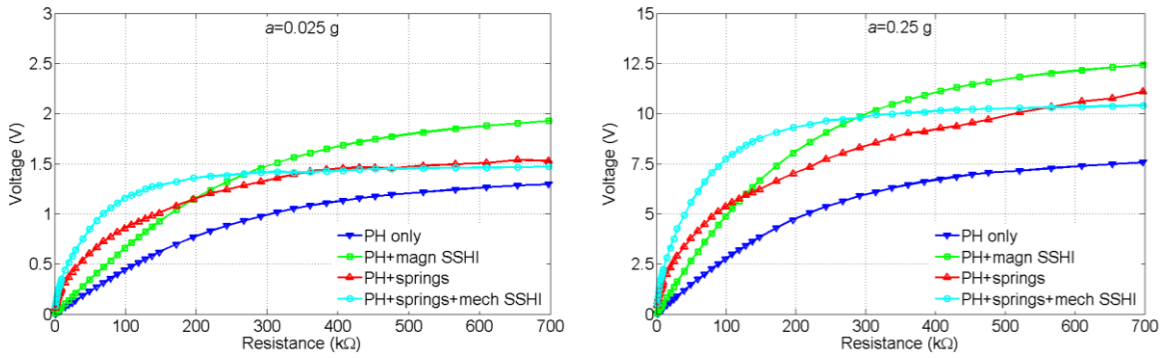

(a) **(b)**

Figure 5-8 Comparisons of the root-mean-square voltage between the implemented configurations without and with the implemented interfaces for the resonant frequency of 11.5 Hz and different acceleration levels of: (a) 0.025 g and (b) 0.25 g

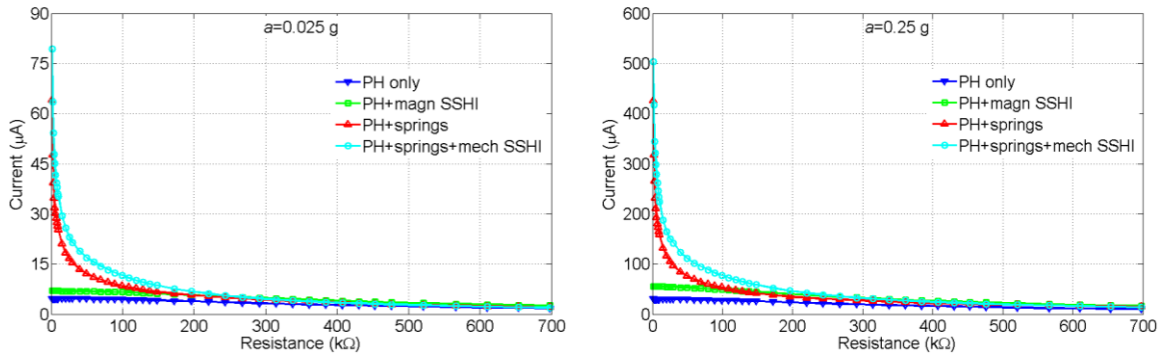

(a) **(b)**

Figure 5-9 Comparisons of the root-mean-square current between the implemented configurations without and with the implemented interfaces for the resonant frequency of 11.5 Hz and different acceleration levels of: (a) 0.025 g and (b) 0.25 g

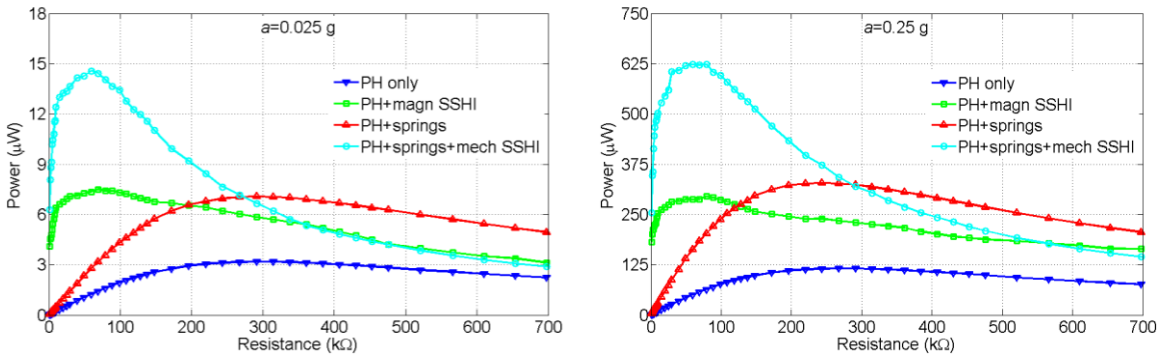

(a) **(b)**

Figure 5-10 Comparisons of the average power between the implemented configurations without and with the implemented interfaces for the resonant frequency of 11.5 Hz and different acceleration levels of: (a) 0.025 g and (b) 0.25 g

From Figure 5-8 to Figure 5-10, it can be observed that: 1) the voltage vs. electrical load curves exhibit a monotonic growth towards the asymptotic value represented by the open circuit voltage, which is higher for the case when the interface configuration featuring the mechanically activated SSHI with added compression springs was connected to the piezoelectric harvester and respectively decreases for the cases with the added springs only, the magnetically activated SSHI interface, and the piezoelectric harvester without any connected interface; 2) in correspondence to a resistive load of 700 kΩ, the measured voltage reaches up to around 2 V and 12.5 V for the applied resonant excitations of 0.025 and 0.25 g of acceleration, respectively; 3) the current vs. electrical load curves start from the high value represented by the short circuit current and then monotonically decrease within the tested interval down to a few tens of μA; 4) the power vs. electrical load curves rise rather quickly up to the MPP, corresponding to the connected optimal resistive load ($R_{\text{L\_MPP}}$), and then slowly decrease as the electrical load is further increased; 4) $R_{\text{L\_MPP}}$ is lower for the interface configurations featuring the SSHI process. In addition, $R_{\text{L\_MPP}}$ is further lowered by adding the compression springs in the interface circuit as a consequence of the fact that the reactive force generated by the impact with the conductive strips slightly increases the frequency of the beam's

oscillations. Since $R_{\mathrm{L\_MPP}}$ is proportional to the quantity $1/(\mathrm{i}\omega C)$, then if f increases $R_{\mathrm{L\_MPP}}$ decreases. Such an effect is obviously more significant when the acceleration level of the applied excitation is higher as the impact force is higher. A complete experimental evaluation of the EH capability of the resonant cantilever-based piezoelectric energy harvester without and with the implemented interfaces at the MPPs under tested ambient conditions featured by case study 2 is presented in Table 5-1.

Table 5-1 Comparisons of the optimal resistive load, root-mean-square voltage and current, and average power transferred to the load at the MPPs between the implemented configurations with and without interfaces for resonant excitation with different acceleration levels

	PH only		PH + magn SSHI		PH +springs		PH +springs + mech SSHI	
a (g)	0.025	0.25	0.025	0.25	0.025	0.25	0.025	0.25
$R_{\mathrm{L\_MPP}}$ (kΩ)	298	277	74	69	290	252	66	61
$V_{\mathrm{L\_MPP}}$ (V)	1.0	5.7	0.7	4.5	1.4	9.1	1.0	6.3
I_{MPP} (μA)	3.2	20.5	10.9	65.7	5.1	36.1	14.7	102.2
$P_{\mathrm{L\_MPP}}$ (μW)	3.2	116.6	7.6	295.7	7.1	328.5	14.7	643.8

Table 5-1 lists the results of the optimal resistive load, the measured voltage, and the current and power transferred to load at the MPPs, showing a practically enhanced PEH performance when the implemented interfaces are added into the EH circuitry. Compared with the circuit configuration where the piezoelectric harvester is directly connected to the electrical resistive load, the generated voltage, current, and power are higher in correspondence to a lower optimal resistive load. The circuit configuration which mechanically implements the SSHI and uses compression springs yield the highest PEH performance as it combines the SSHI effects with the passive mechanical amplification of the force applied to the cantilever beam. In such a case, the power enhancement was calculated equal to 359% at 0.025 g and 452% at 0.25 g. Taking into account the passive implementation of the presented interfaces, despite state-

of-art non-linear PEH interfaces, such results are significantly promising. For instance, Guyomar et al. who first introduced the SSHI technique in 2005 [228] experimentally demonstrated a power increase around 380% for the AC case. The enhancement is higher for a higher acceleration level of the applied excitation as the SSHI effect is both dependent on the coupling factor and the voltage output of the piezoelectric harvester [229], which are indeed higher as from the theoretical analyses in Paragraph 5.1. In addition, the probability to correctly operate the switching process via the implemented interface configuration is higher for higher acceleration levels due to the stronger mechanical impact between the featured compression springs and conductive strips. The mechanical response of the impinging force operated by the compression springs is also higher in such a case thus leading to a higher amplification of the force acting on the cantilever beam. This is confirmed by the higher power enhancement achieved by only adding compression springs to the piezoelectric harvester, which is equal to 122% and 182% at 0.025 and 0.25 g of acceleration, respectively.

5.5 Summary

Non-linear electronic interfaces, such as the SSHI technique, have been comprehensively studied to increase the transduction capability of a piezoelectric harvester. Although non-linear treatments of the harvester's output signal can significantly increase the harvested energy, the control command required for their implementation is typically active thus being costly in terms of energy consumption. Yet, the autonomous versions of those implementations suffer the limitations from dissipative losses of the involved components and switching delay phase.

In order to address the challenges, this chapter has presented novel passive interfaces that are suitable for resonant cantilever-based piezoelectric energy harvesters operating at low frequency. Since low-frequency motion produces little vibration in terms of acceleration, moderate vibration in terms of velocity, and relatively large displacement, the interface circuits described in this chapter exploit the deflection of the piezoelectric beam in order to practically enhance

the PEH performance in a passive way. Passive implementations of the SSHI technique, using either a magnetic or mechanical activation, have been described. Further mechanical enhancement by use of compression springs for a passive amplification of the force acting on the piezoelectric beam has also been described. Design and implementation of the developed passive interfaces have been presented in series connection with the cantilever-based piezoelectric energy harvester developed as in Paragraph 3.2.3. Testing and performance comparisons were performed at the low resonant frequency of 11.5 Hz and under excitations of 0.025 g and 0.25 g of acceleration. An enhanced PEH performance was shown in terms of voltage, current, and power transferred to a connected resistive load. In particular, power enhancements up to 359% and 452% were achieved at resonance for the acceleration levels of 0.025 g and 0.25 g, respectively.

Being passive, the developed interfaces do not require additional power sources, partitions of the harvested energy-flow, or specific software or algorithms to accurately control the process of the energy extraction from the piezoelectric harvester. The presented interfaces are easy to be implemented and allow enhancing the EH performance of low-frequency resonant cantilever-based piezoelectric harvesters under excitations with magnitude levels featuring a small range of variation. Despite the state-of-the-art in non-linear electronic interfaces, the power consumption level of the developed interfaces has been reduced and carries out the promise of successfully applying such a technology to autonomously power standalone systems or extend the lifespan of battery–powered systems such as WSNs. For that purpose, the effects of the developed interfaces within a PEH powered wireless sensor system will be further investigated in Chapter 6.

6 A NOVEL ENERGY AWARE ARCHITECTURE FOR POWERING WIRELESS SENSOR NODES

This chapter reports design and development of a novel energy-aware architecture for the power management of PEH powered wireless sensor nodes, which intend to minimise the power consumption for conditioning the transduced signal and optimise the overall energy transfer from the piezoelectric harvester to the electrical load (i.e., the wireless sensor node). Chapter 4 and 5 have showed how to maximise the extraction of the energy harvested by piezoelectric transducers; however, decreasing the demand of energy is as important as increasing its availability in order to achieve energy-autonomous systems running entirely from ambient harvested-energy.

Typical modes of operation of commercially available PMMs are described and analysed through experimental testing. A novel approach to reduce the power consumption of an integrated PEH powered system is then presented. The novel design integrates a capacitive charge-accumulator and reduces the number of active stages adopted by standard power management modules for EH applications. In particular, the DC/DC regulation stage for conditioning the piezoelectric-transduced signal is replaced by an EAI connected to the capacitive energy storage. Core of the EAI is a voltage monitoring system capable of adjusting the duty cycle for the activation of the end-application depending on the available stored energy. The performance of the novel circuit design is tested in connection with the energy harvesters earlier developed and with a custom WSCN so as to reproduce in laboratory the case studies reported in Paragraph 3.1. The number of data acquisitions and transmissions performed within a certain time interval, running entirely from vibration-harvested energy, is measured in order to evaluate the performance of the developed architecture. Performance optimisation is also presented by using the passive interfaces earlier described in addition to the piezoelectric energy harvesters. It is shown that shorter pauses are needed to deal with the mismatch between the harvested energy and the energy demanded by the WSCN when the passive interfaces are connected into the EH circuitry; therefore, the developed PEH

systems approach the capability to continuously supply power to the connected end-user load.

6.1 Design considerations based on off-the-shelf products

The EH source has a direct impact on the strategy implemented by the hardware circuitry that, connected to the energy harvester, aims to condition the generated electrical signal and make it usable for the end-user load. Indeed, while some ambient sources can be very constant and predictable, others can behave in a stochastic way. In both cases, however, two main features are typical of PEH systems: 1) an AC/DC rectifier and 2) an energy storage device. The presence of an AC/DC rectifier within PEH systems is related to the nature of the external excitation as ambient vibrations are alternating in nature whilst a DC signal is required by electrical loads such as WSCNs. The presence of an energy storage device is a common characteristic of EH systems as the energy requirements of the electrical load are typically higher than the real-time capability of small-scale energy harvesters. Therefore, by use of an energy reservoir it is possible to implement power management techniques such as duty cycling the activation of the electrical load to make this work only during certain intervals under higher peaks of power. Depending on 2), whether the energy storage device is implemented as a capacitor or a rechargeable battery, a first difference can be identified in the hardware circuitry of an EH system. In order to explain such a difference, Figure 6-1 and Figure 6-2 show two commercially available architectures for the conditioning and management of energy harvested from ambient sources, which are: a LTC3588-1 (Linear Technology, Inc. – Milpitas, California) device and a D-PPMU-00B (Infinite Power Solutions, Inc. – Littleton, Colorado) device, respectively. In particular, Figure 6-1(a) and Figure 6-2(a) represent a simplified block diagram of the two devices whilst Figure 6-1(b) and Figure 6-2(b) are real photographs of those in the specific configurations under consideration. The D-PPMU-00B device is connected to a Thinergy® MEC101-10PES rechargeable battery with performance grade features of 40 mA maximum continuous discharge current and 1.0 mAh minimum energy capacity. The LTC3588-1 device is connected to

the inductor L_1 = 10 µH, the capacitors C_1 = 1.0 µF and C_2 = 4.7 µF, the input capacitor C_{IN} = 4.7 µF, and the output supercapacitor C_{OUT} = 120 mF. It is worthwhile to mention that further power switching and routing circuits integrated into the two commercially available architectures in Figure 6-1 and Figure 6-2 have not been taken into account in order to focuss on their logic functioning.

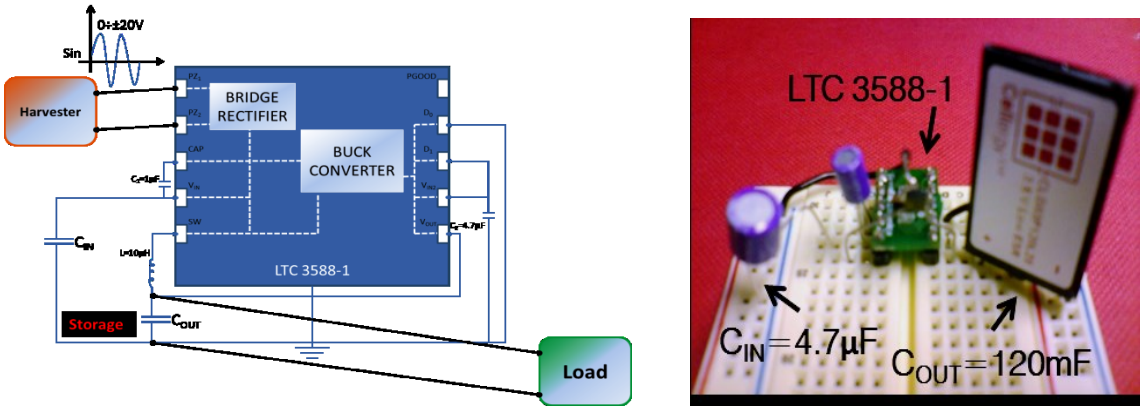

(a) (b)

Figure 6-1 LTC3588-1 device: (a) a simplified block diagram and (b) a photograph in a specific configuration that includes a 120 mF supercapacitor as energy storage

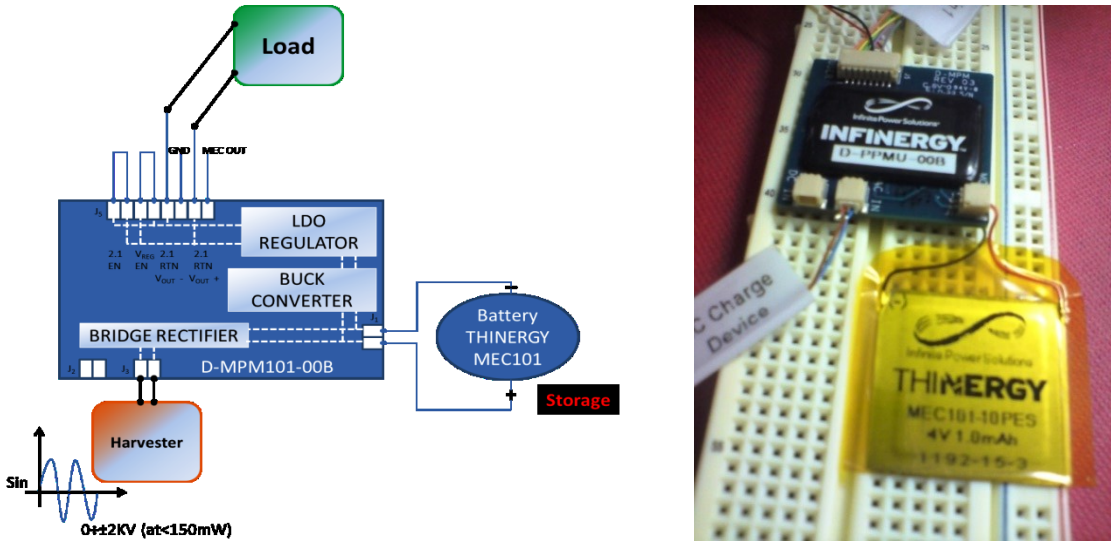

(a) (b)

Figure 6-2 D-PPMU-00B device: (a) a simplified block diagram and (b) a photograph in a specific configuration that includes a Thinergy® MEC101-10PES rechargeable battery as energy storage

From Figure 6-1(a) and Figure 6-2(a) it can be noticed that the D-PPMU-00B device contains at least one more block within its internal structure, which is a low drop-out (LDO) regulator. The reason is that the D-PPMU-00B device is designed to adopt a rechargeable battery as storage for the harvested energy, specifically one of the thin film LiPON electrolyte batteries from the Thinergy® MEC family, whilst the LTC3588-1 device is designed to use capacitors externally from the integrated circuit. Despite the advantages/disadvantages of batteries over capacitors, which have been described in Paragraph 2.2.3, one main drawback of using a rechargeable battery within EH systems is represented by the fact that an additional unit for voltage comparisons needs to be included in the hardware circuitry to protect the battery itself. This means that another small dedicated circuit has to be considered to stop charging or discharging the battery in circumstances such as over-charge, over-discharge, short-circuit, and overheating in some cases. Capacitive energy storage suffers less these circumstances if it is taken into account that capacitors allow higher voltage ratings in a single unit and that, both capacitors and supercapacitors, do not present a low-voltage limit of operation. With regard to the Thinergy® MEC101-10PES battery in Figure 6-2, for example, a safe operational voltage between 2.1 V and 4 V is indicated by the manufacturer. In order to protect the battery, a LDO voltage regulator was then included in the hardware circuitry of the D-PPMU-00B device as this permits operations with a very small input-output differential thus being more suitable for low-voltage applications of EH systems. LDO regulators work in the same way as all linear voltage regulators; however, the main difference between non-LDO and LDO regulators is in that the former utilise an emitter follower transistor topology whilst the latter utilise an open collector or open drain topology. Open collector and open drain configurations enable transistor saturation, which limits the voltage drop to only the saturation voltage. Power FETs are preferable rather than bipolar transistors as in this last case significant additional power is lost to control it (especially for high voltages under very low in-out difference). However, the use of FET transistors significantly increases price and arise problems when the regulator is

supposed to work for low input voltage as FETs usually require 5 to 10 V to open completely.

An input capacitor is used in both the circuital configurations represented in Figure 6-1 for filtering the signal generated by the energy harvester, immediately after this has been rectified by a 4-diode bridge. It is worthwhile to mention that both devices are suitable for energy harvesters of different kind, including photovoltaic cells and thermoelectric generators; thereby, in both the LTC3588-1 and the D-PPMU-00B circuits there are direct DC input connections from an external pin to the input capacitor. In the case of the LTC3588-1 device, the harvested energy flows from the input capacitor C_{IN} to the output capacitor C_{OUT} while it powers a buck converter for the conditioning of the DC input voltage in a regulated DC output voltage. In the case of the D-PPMU-00B device, instead, energy is first transferred to the rechargeable MEC battery and used to drive the LDO voltage regulator before powering the DC/DC converter that regulates the output voltage. For the circuital configurations shown in Figure 6-1 and Figure 6-2, a stable 3.3 V output will be available for the power supply of a connected electrical load as soon as enough energy has been stored in C_{OUT} or in the MEC battery, respectively. It is worthwhile to mention that, differently from the D-PPMU-00B device, the LTC3588-1 design allows also three other pre-fixed output voltages through a properly addressed connection of its external pins.

At the current state of the development five different Thinergy® MEC-200 series batteries are offered by the manufacturer for use with the D-PPMU-00B device, with capacity options from 0.13 mAh up to 2.5 mAh. From this point of view, the LTC3588-1 device appears more flexible in that it allows choosing the input and output capacitors for a better fit with the targeted end-application. C_{IN} and C_{OUT} can be differently selected in order to achieve either faster activation of the DC/DC converter, hence faster transfer of the harvested energy to the electrical load, or longer discharging time of the output storage. The following design guidelines can be taken into account:

- the smaller C_{IN} → the faster its charging/discharging process → more quickly the regulated output voltage will be reached/lost;
- the bigger C_{IN} → the slower its charging/discharging process → more slowly the regulated output voltage will be reached/lost;
- the smaller C_{OUT} → the faster its charging/discharging process → more quickly the regulated output voltage will be reached/lost;
- the bigger C_{OUT} → the slower its charging/discharging process → more slowly the regulated output voltage will be reached/lost.

It is clear to understand how the best configuration depends on the nature of the EH source, as stated the beginning of this paragraph, and on the targeted end-application. As a general guide, however, it is possible to point out that adding functional units within an EH system leads an increment of its power consumption for both the execution of additional tasks and the power dissipation of the involved hardware. Therefore, the use of capacitors or supercapacitors is suggested in those applications where batteries are not otherwise strictly required, for example, where very-high energy capacities are not necessary. Additionally, the use of a capacitive energy storage may be of benefit for applications such as the one described by the case study 1, where the EH system undergoes harsh external conditions (e.g., hot/cold temperature). It should be also mentioned that using a compact on-chip system design is preferable as it limits the power dissipated between the connections of the electric components in the circuit. With regard to PEH, in particular, it is worthwhile to mention that the piezoelectric energy harvester is subjected to an intermitted mechanical input in a real scenario with discontinuous ambient vibrations. As a direct consequence, in a circuital configuration such as the LTC3588-1 one, the output voltage can be easily lost due to the low amount of electric charge into the input capacitor C_{IN}, which is supposed to start-up the DC/DC converter. In order to achieve the desired 3.3 V output, for instance, the LTC3588-1 device in Figure 6-1 needs to reach ~ 5.5 V across C_{IN}. The use of a higher voltage threshold DC/DC converter for the conditioning of piezoelectric harvested energy can thus be a benefit. Following such a consideration, the E-821 device (PI Ceramic GmbH – Lederhose, Germany) depicted in Figure 6-3

has been also identified by this author among the promising off-the-shelf market solutions for the conditioning and management of piezoelectric harvested energy.

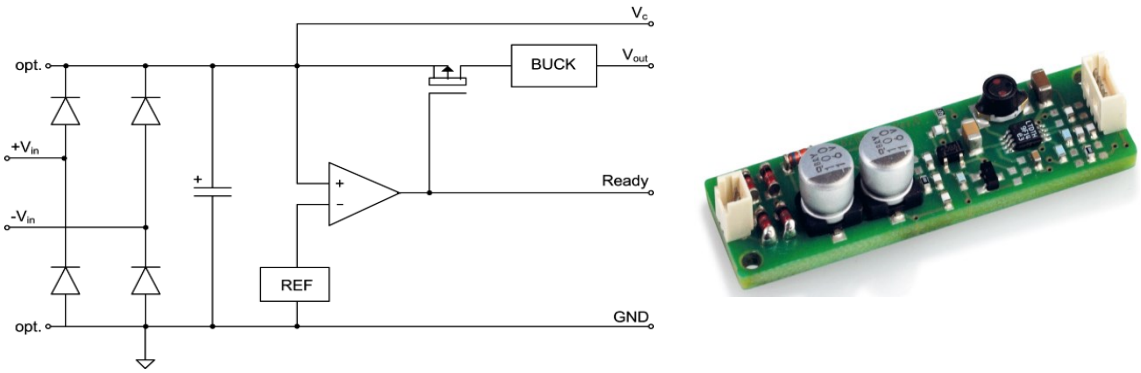

(a) (b)

Figure 6-3 E-821 device: (a) a simplified circuit diagram and (b) a photograph (reprinted from [230])

Strengths of PI's design as a ready-to-use alternative are: the simple electronic configuration, due to the presence of a capacitive energy storage of 220 μF; the compact on-chip design; and the 12.9 V threshold of the DC/DC converter.

Nevertheless, especially in those applications where long pauses can be predicted between successive mechanical vibration inputs to the piezo-harvester's host structure, the use of rechargeable batteries may still result more convenient due to their lower self-discharging property. A hybrid structure would also benefit the advantages of both technologies, being batteries used for long-term energy storage, although higher power consumption is required for safely addressing the harvested energy, and capacitors used as low-maintenance memory backup to bridge short power interruptions.

6.2 A novel energy-aware concept

In order to deal with the mismatch between energy harvested by small-scale piezoelectric transducers and energy demanded by wireless sensor nodes, the power management technique most commonly reported in literature is the duty cycling one. If the entire EH system is considered as a whole and, therefore, it is taken into account the use of energy storage devices as well as the fact that

wireless sensor nodes typically support sleeping modes, then duty cycling appears as a direct approach for practically exploiting PEH. The basic idea is to store the harvested energy while the end-user load is disconnected or in a sleeping status and, only after a certain amount of time, to release it from the storage device under higher peaks of power for an indefinite number of repeated cycles. Most of the times, however, this technique has been implemented in literature in a static way by setting a fixed duty cycle so that the average energy consumption matches the average energy production. It means that the system sends out information to a remote base station based on a time-demand; hence, it provides output current bursts for the activation of the electrical load whether or not vibrations have occurred during the pre-scheduled time interval between two consecutive data transmissions. Such a time-based approach is depicted in Figure 6-4 from where it can be observed how the electrical load is always ON (active state) and thereby energy is consumed even during those intervals when energy has not been generated. Energy is consumed to power sensors and transmitter unit, by use of large energy storage devices, even when there is no power input from vibrations.

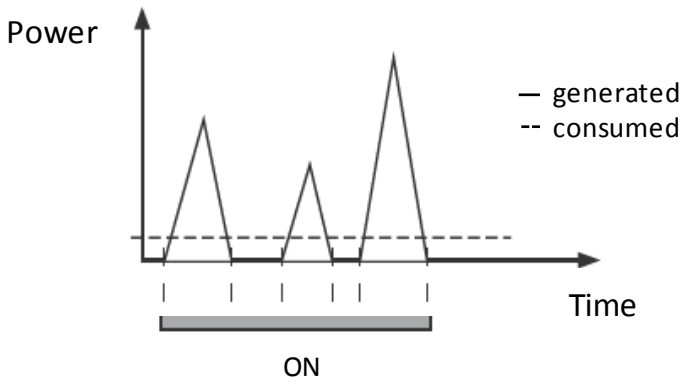

Figure 6-4 A time scheduled approach for PEH powered SHM applications

In Figure 6-5, for example, the average power requirements of a SHM wireless node, which senses temperature and acceleration for rail transport applications, are plotted as a function of time.

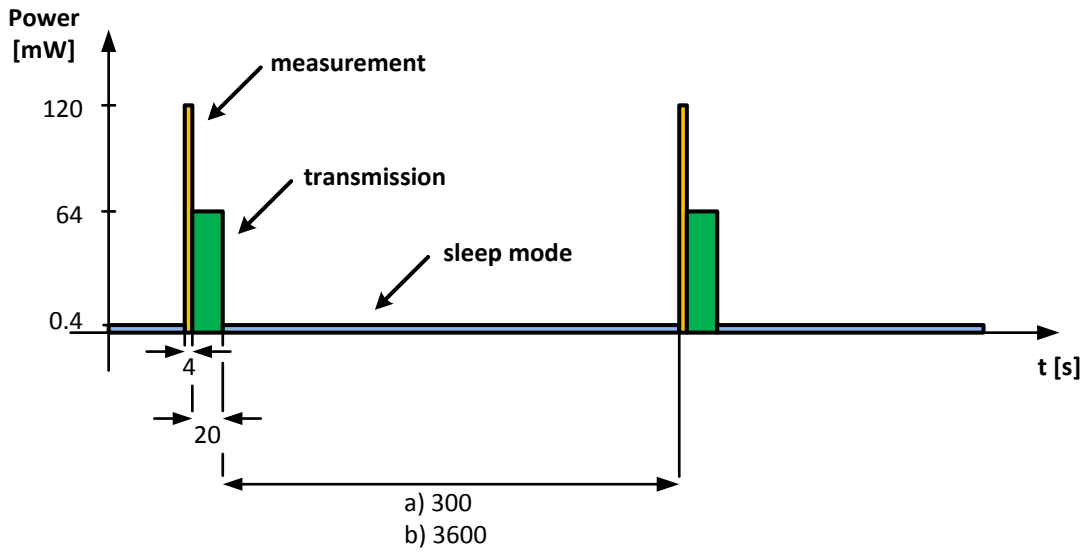

Figure 6-5 Typical power requirements of a SHM wireless node used in the rail industry for sensing: a) temperature and b) acceleration [Figure courtesy of Alstom UK Ltd]

From Figure 6-5, it is possible to distinguish an alternation of sleeping phases, when the system keeps its internal consumption as low as possible for energy storing, and active phases, when the system utilises the collected energy to make the end-application work. By looking at the power consumption levels in the active mode, when data acquisition or transmission is occurring, and comparing it with the standard energy harvested by small-scale piezoelectric transducers, it is easier to figure out the benefits of duty cycling the working status of a connected wireless sensor node and the need of an energy storage device. The fixed time-based approach, however, suffers the two following scenarios: 1) if the piezoelectric harvester is providing more energy than the system consumes, then it will waste excess energy once the storage has reached a full charge; 2) when energy production is less than energy consumption, the system will eventually deplete the storage reserves and stop working. Due to the discontinuous nature of ambient vibrations in lots of real-case application scenarios, 2) is very likely to happen if the strategy depicted in Figure 6-4 is adopted. In order to address the challenges, a dynamic approach implemented through an EAI is here proposed. Figure 6-6 shows an unscheduled wireless sensing alternative to the time-based approach, which

can be implemented for achieving the capability to continuously power wireless sensor nodes from piezoelectric harvested energy.

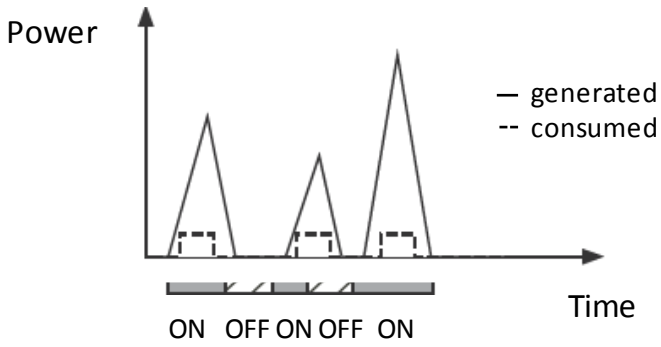

Figure 6-6 An unscheduled approach based on energy-aware management for PEH powered SHM applications

From the illustration in Figure 6-6, it can be noticed that, differently from the usual approach, energy is now consumed only during the same intervals that it is generated. This means that the wireless sensor node is powered on to acquire and transmit data only depending on the energy availability rather than on a time demand. Then higher efficiency levels can be achieved and small energy storage devices used to supply power to sensors and transmitting unit. With regard to PEH systems this means that, if vibrations occur then there is need for acquiring and transmitting data from the sensors whilst if vibrations do not occur there is no need for the wireless sensor node to be active. Sensors will start their measurements, and these data will be transmitted to a remote base station, only when external vibrations are as intense as to enable the activation of the wireless sensor node. To make such an approach successful for applications such as energy-autonomous SHM, the time interval during which energy is consumed should start as fast as possible with the starting of the energy generation interval and last as long as possible to cover its whole duration. Therefore, minimising the whole system's power consumption needs to be taken into consideration to reduce the mismatch between harvested energy and demanded energy towards a continuous operation of the wireless sensor node. Implementing the approach in Figure 6-6 allows two main differences at hardware level, which can be used to reduce the system's power consumption: 1) the time counting can be replaced by voltage supervision; 2)

the use of the DC/DC converter can be omitted if proper capacitive energy storage is selected depending on the targeted application. In order to implement 1) and 2), an EAI has been introduced in the novel low power management design of PEH powered wireless sensor systems and used in connection to a large enough capacitive energy storage. This will manage to provide a DC output voltage high enough to perform a whole cycle of data acquisitions and transmissions, without use of usual DC/DC converters. In addition, the EAI contains low power consumption voltage sensing device and switching circuit, which act as a circuit breaker to connect/disconnect the wireless sensor node. The EAI will be capable to activate the wireless sensor node by releasing the stored energy every time the voltage across the capacitor reaches a certain threshold.

Figure 6-7 illustrates the working principle of the system when it is subjected to a continuous excitation.

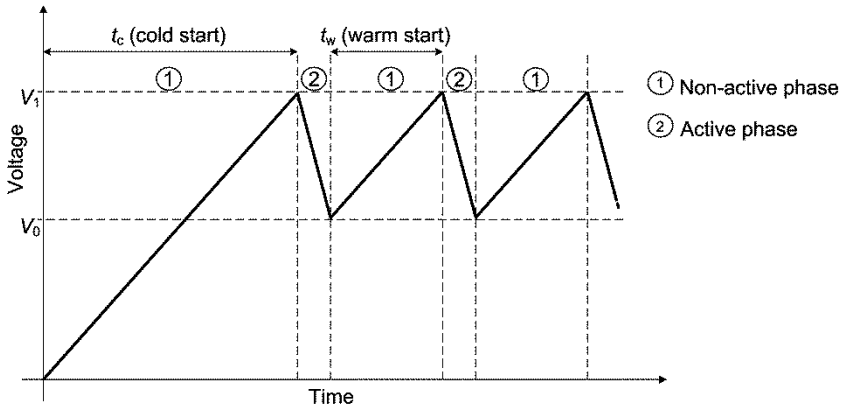

Figure 6-7 Illustration of the trend of the voltage developed across the capacitive energy storage as a function of time

When the voltage accumulated in the capacitive energy storage is not high enough for powering the WSCN on, the system is in a non-active phase. As soon as a pre-set voltage threshold, for example V_1, is reached, the energy flow is delivered to the WSCN and the system is in an active-phase. At this time, in fact, the energy flow between source and load has been managed and the incoming energy, stored in the capacitor bank, activates the WSCN for a complete execution of a data acquisition and data transmission cycle. Because

the WSCN in active phase uses the stored energy to perform sensing and transmitting operations, the voltage accumulated in the capacitive energy storage drops down from the pre-set voltage threshold for the WSCN activation, for example to the value V_0. An immediate consequence is that the WSCN switches off and the system enters in a new non-active phase until enough energy is restored. It should be noted that: the time t_c, shown in Figure 6-7, is defined as the time for cold start, which is the time needed by the capacitive energy storage to reach the first pre-set activation voltage that is capable to power the WSCN on; and the time t_w, shown in Figure 6-7, is defined as the time for warm start, which is the time needed for compensating the voltage drop across the capacitive energy storage, after any active phase of the WSCN, in order to restart a new cycle. It should be additionally mentioned that t_w is shorter than t_c as the drop of energy (hence voltage) in the capacitive energy storage, after an active phase, is only partial. Based on the storage capacity, the threshold voltage will be pre-set so as to make available an amount of energy high enough to run a whole active cycle of the wireless sensor node.

It is worthwhile to notice that, since the described dynamic approach is not based on a time-demand for the activation of the wireless sensor node, there is no need for counting the time flow. Differently from the described case, typical EH powered wireless sensor systems presented in literature make use of an internal microcontroller for the purpose of counting the time flow. This increases the system's energy consumption as the power needed to keep awake the microcontroller and allow running its quartz is on average higher than in cases when the microcontroller is in deep sleep mode or is disconnected from the circuit together with the electrical load. Voltage sensing devices, on the contrary, can operate with just a few micro-Ampere of current, which is around three orders of magnitude lower than the standard power requirement of an 8-bit microcontroller or a higher computationally performant one. A further advantage upon the implementation of the EAI could be achieved by using a low-power electronic voltage supervisor with integrated timer delay as voltage sensing device. This adds reliability to PEH systems whose operation has to be guaranteed under discontinuous ambient vibrations. Indeed, when the threshold

level is detected across the capacitive storage, energy will not flow directly to the wireless sensor node but will keep accumulating over threshold based on a longer or shorter time delay. A more constant voltage regulation can then be guaranteed. Compared to prior state-of-art designs, any drop of the voltage will affect much less the operation of the system. The time delay can be adjusted according to the specifications of the end-application and the parameters of the energy storage. It is possible to pre-set the delay driver either at a hardware level or at a software level, according to the EH scenario. Programmable delay drivers can be used for a more flexible functioning of the EH system although a trade-off with their power requirements has to be taken into consideration. It is also worthwhile to mention that a fixed scheduled approach, if required by the end-application, could be easily achieved by keeping the same electrical configuration but adding an external low-power consumption timer capable of running independently from microcontrollers. So far, when the threshold level will be detected across the capacitive storage, energy will enable the timer by mean of an additional switching circuit and further stored to supply power to a backup element in case of critical operations. For instance, additional sensors can be autonomously powered or a reservoir battery can be charged in order to avoid power outages during data transmission.

6.3 A PEH powered wireless sensor system with an EAI

6.3.1 Description of the system

Figure 6-8 shows the block diagram of the developed PEH powered wireless sensor system.

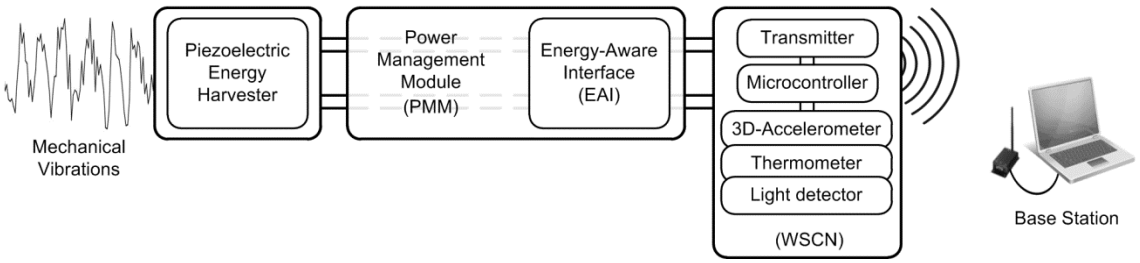

Figure 6-8 Block diagram of the developed PEH powered wireless sensor system

The system consists of: a piezoelectric energy harvester to harvest strain

energy from structural vibrations and convert it into electrical energy; a PMM to convert the harvested electrical energy into usable electrical energy and store it for the end-user application; and a custom developed WSCN as the end-user, which senses and wirelessly transmits data to a base station. The novelty of the implemented system is that an EAI block is integrated within the PMM to manage the flow of the harvested energy so as to store it with minimum power consumption, during the non-active phases of the system, and then release it to perform data acquisitions and wireless transmissions. The system is specifically implemented as a whole to approach the capability to continuously power the WSCN entirely from the harvested energy for on-line SHM applications. After energy transduction, the mechanical strain on the substrate that transfers to the piezoelectric transducer appears as an alternating electrical input to the PMM. The PMM rectifies this electrical signal and stores its energy into an internal capacitor bank, which is used to power the WSCN during each active cycle for data acquisitions and wireless transmissions. In the developed system, capacitive energy storage was preferred to rechargeable batteries as capacitors can achieve faster charging intervals, longer lifetime and better performance in harsh conditions (i.e., at very hot/cold temperature). It is worthwhile to mention that the stored energy flows to the WSCN through the EAI, which regulates the voltage supply downstream of it. Indeed, the EAI consists of a voltage sensing device and switching circuitry for monitoring the amount of the stored energy while electric charges are generated by the harvester and accumulate in the capacitor bank for later use as from the concept illustration in Figure 6-7. The custom developed WSCN consists of three units: 1) sensors, to acquire required information from surrounding conditions; 2) microcontroller, to process data from sensors and coordinate data transmissions; and 3) wireless transmitter, to transmit collected and processed data to a base station. When enough energy has been stored, the WSCN is powered through the EAI and a proper length of time slots is allocated to its operation via the microcontroller, for activating the sensors and the transmitter so as to establish a data wireless communication with the base station.

6.3.2 Implementation of the system

Figure 6-9 shows the circuit diagram of the implemented system, including the PMM, the EAI, and the WSCN, which used ultra-low power consumption hardware to minimise the overall power consumption of the system.

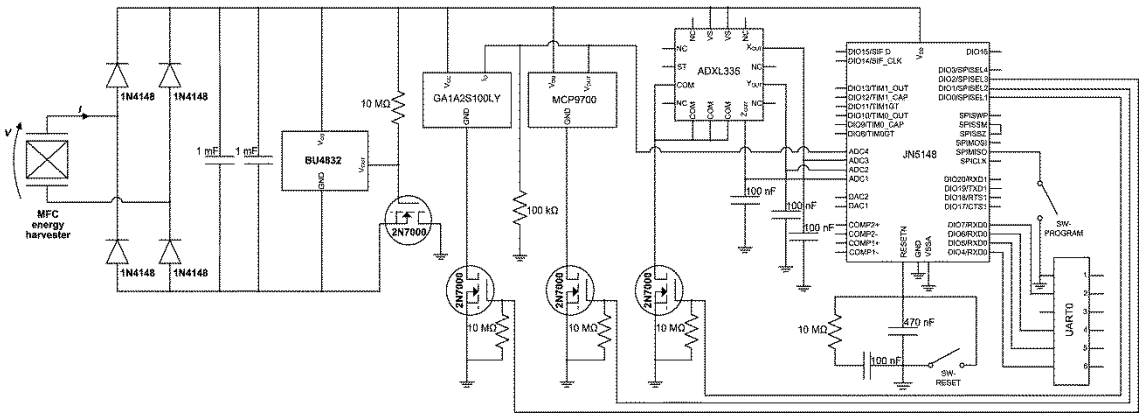

Figure 6-9 Circuit diagram of the implemented system

A standard 4-diode bridge configuration was used to implement the AC/DC rectifier of the PMM. Fast switching 1N4148 diodes were arranged to achieve full-wave rectification of the electrical signal generated by the piezoelectric energy harvester. For the energy storage of the PMM, two aluminium electrolytic capacitors of 1 mF capacitance were connected in parallel to the diode bridge output. Voltage across these capacitors was constantly monitored by the EAI through a low current consumption BU4832 voltage detector (ROHM Semiconductor GmbH, Willich-Munchheide – Germany), which was connected from ground to the wireless microcontroller of the WSCN through a 2N7000 N-MOS transistor. The transistor acted as a switch to enable the alternation of the non-active phase and the active phase of the WSCN. When the voltage across the capacitive energy storage reaches the threshold voltage of 3.2 V, the EAI output enables the activation of the wireless microcontroller via restoring its ground connection. Data are acquired and wirelessly transmitted; hence, the stored energy is consumed by the WSCN. The EAI detects if the monitored voltage is under the threshold voltage and, if so, it brings the transistor into a high-impedance state. As this cuts the power supply to the JN5148 wireless microcontroller, a new non-active phase of the cycle is then performed. The

2.4 GHz IEEE 802.15.4 compliant JN5148 (NXP Semiconductors, Cheshire – Manchester, UK), with features such as 128 kb Random Access Memory (RAM) and 4 Mbit serial flash memory, was selected as the wireless microcontroller of the WSCN due to the low power consumed in active mode for data transmitting. Furthermore, the JN5148 wireless microcontroller offers the possibility to set the clock speed of the Central Processing Unit (CPU) up to 32 MHz, which is the configuration implemented in the developed system. For the purpose of SHM, a ADXL335 3-axis accelerometer (Analog Devices International, Limerick, Ireland, UK), a MCP9700 temperature sensor (Microchip Technology, Inc., Chandler - Arizona, USA), and a GA1A2S100 light detector (Sharp Electronics, Ltd, London, UK) were integrated into the prototype board. Connection from ground through 2N7000 N-MOS transistors was also implemented for each of this system's sensors so as to enable them one at a time and only for the duration of that data acquisition cycle, thus consuming less energy. The selected sensors all have very short initialisation time (≤ 1 ms) so as to have low power consumption for data acquisition. Reduction of power consumption was also considered at software and data transmission levels by implementing TDMA (Time Division Multiple Access) protocol on IEEE 802.15.4 star configuration, as it has been described in [231]. 100 bytes of information were serially acquired from the different sensors; then, wirelessly transmitted at +2.5 dBm over three channels of the 16 available in the 2.4 GHz standard frequency range. Data byte collisions and interference issues are better managed as the result of such a multi-channel transmission. Wireless communication was established with the base station at a distance of approximately 12 m from the WSCN, where collected data were received with no indication of data loss.

6.4 Performance of the implemented wireless sensor system

6.4.1 Results and discussions based on case study 1

Figure 6-10 shows the actual experimental setup used for the characterisation of the implemented low power consumption wireless sensor system where, based on case study 1, a 250 kN tensile testing machine (Instron, High Wycombe – Bucks, UK) was used to reproduce desired strain levels and

frequencies on the aluminium substrate of the MFC energy harvester presented in Paragraph 3.2.1.

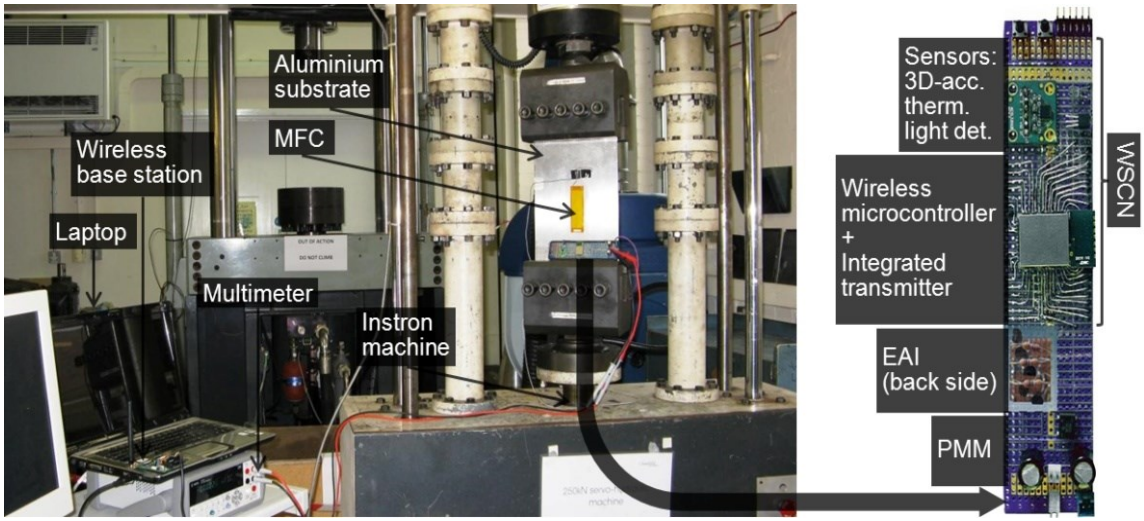

Figure 6-10 A photograph of the experimental setup where the energy harvester based on the MFC bonded on aluminium substrate is shown

Table 6-1 lists the experimental results of the time for cold start and the time between consecutive transmissions when power was harvested by the MFC energy harvester on aluminium substrate under peak-to-peak strain levels of 480, 710, 940, and 1170 με at 2.5, 5, 7.5, and 10 Hz.

Table 6-1 Measured time for cold start and time between two consecutive transmissions of the custom developed WSCN powered by the MFC energy harvester on aluminium substrate

$Strain_{p-p}$ (με)	Time for cold start (s)				Time between consecutive transmissions (s)			
	f = 2.5 Hz	f = 5 Hz	f = 7.5 Hz	f = 10 Hz	f = 2.5 Hz	f = 5 Hz	f = 7.5 Hz	f = 10 Hz
480	141.6	71.1	58.3	38.1	4.9	2.4	1.7	1.4
710	87.3	44.0	30.3	22.7	2.7	1.5	1.1	0.7
940	61.7	31.7	21.9	17.1	2.0	1.0	0.7	0.6
1170	47.7	24.5	17.0	13.4	1.5	0.8	0.6	0.4

The effects of the applied strain and frequency on the capability to power the WSCN, hence on the time for the cold start of the WSCN and the time between consecutive transmissions, are shown in Figure 6-11.

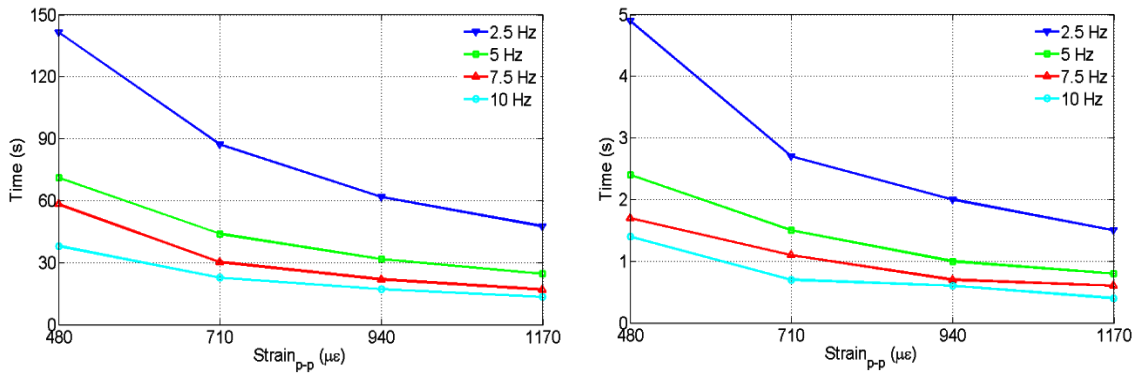

(a) **(b)**

Figure 6-11 (a) Measured time for cold start and (b) time between two consecutive transmissions of the custom developed WSCN powered by the MFC energy harvester on aluminium substrate as a function of tested strain levels for different excitation frequencies

From Figure 6-11, it can be observed that the time needed for the cold start of the WSCN and the time between consecutive transmissions decrease with the increase of the excitation frequency and strain. This means that the WSCN activation voltage threshold is reached more frequently and, therefore, that the WSCN is powered more frequently. This also means that more power is harvested by the system. Similar results for the capability to power the WSCN were obtained when the MFC energy harvester on the composite substrate was tested.

In order to understand the time response of the developed system when the WSCN is powered on or off by the harvested energy, Figure 6-12 shows one of the experimental results when a cyclic excitation of 1170 με was applied at 10 Hz to the MFC energy harvester on the aluminium substrate, where: (a) is the plot of the electrical voltage across the capacitive energy storage of the PMM; and (b) is the plot of the electrical current drawn by the WSCN through the EAI.

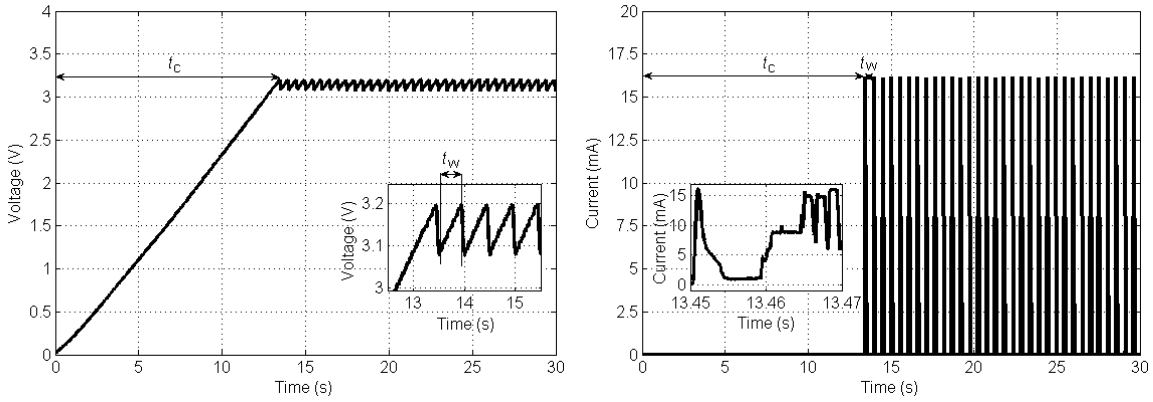

Figure 6-12 Performance of the custom developed WSCN, powered by the MFC energy harvester on aluminium substrate, when a cyclic excitation of 1170 με was applied at 10 Hz: (a) electrical voltage across the capacitive energy storage of the PMM and (b) electrical current drawn by the WSCN through the EAI

From Figure 6-12(a), it can be observed that the electrical voltage generated by the MFC energy harvester rises until the pre-set voltage of 3.2 V is reached and, only at this time, the WSCN is powered on by the EAI. An immediate consequence of this is that the voltage across the capacitive energy storage drops down of around 120 mV, at which point the power to the WSCN is cut off again and the system enters in a new non-active phase. Simultaneously, the current drawn by the WSCN rises from 1.19 μA, measured in the non-active phase [231], to approximately 16 mA during the active phase. From Figure 6-12(b), it can be observed that the current reaches the first peak when the WSCN is waken up and there are three more peaks before the successive non-active phase takes place. The last three peaks of the current drawn by the WSCN are the result of the multi-channel 2.4 GHz data transmission described above. For the case illustrated in Figure 6-12, when an input excitation of 1170 με was applied at 10 Hz, the time for the cold start of the WSCN was measured around 13 s. After the first data acquisition and data transmission, around 0.4 s of time were needed to restore the voltage dropped in the capacitive energy storage before performing the active phase of the next working cycle. The intervals of 13 s for cold start and 0.4 s for two consecutive wireless data transmissions show that the developed system has the capability

to continuously power the WSCN with no need to pause for minutes as in other cases reported in literature.

6.4.2 Comparison with a commercially available architecture

In order to proof the benefit of the implemented PMM design over commercially available architectures in a practical application scenario, a comparison of the time between consecutive transmissions achieved by the WSCN is given in Table 6-1. The commercially available PMM used for the performance comparison is the PI module described in Paragraph 6.1, which has been shown to be the most promising off-the-shelf device among considered power management architectures. The input of the PI module was connected to the MFC energy harvester on aluminium substrate whilst its output to the custom developed WSCN. Voltage was measured as for the previous experimental setting across the 2 mF capacitive energy storage of the novel implemented PMM design and at the output of the PI module, respectively, in order to figure out the alternation of non-active and active phases under the excitations of the selected range of frequency and strain levels. A comparison of the experimental results is given in Table 6-2.

Table 6-2 Comparison of the WSCN time between two consecutive transmissions for a commercially available PMM (from PI Ceramic GmbH) and the novel implemented PMM design connected to the MFC energy harvester on aluminium substrate (experimental results)

$Strain_{p-p}$ (με)	Time between two consecutive transmissions (s)			
	Comm. available PMM		Novel implemented PMM	
	f=5 Hz	*f*=10 Hz	*f*=5 Hz	*f*=10 Hz
480	11.7	5.5	2.4	1.4
710	6.2	3.4	1.5	0.7
940	4.2	2.2	1.0	0.6
1170	3.1	1.6	0.8	0.4

From Table 6-2 it can be observed that when the PI module is used there is a significant longer gap between consecutive transmissions, although this time gap decreases with the increase of the excitation frequency and strain as well as in the case of the novel implemented PMM design. The shorter time between consecutive transmissions needed by use of the novel implemented PMM is

clearly shown in Figure 6-13, which depicts the trend of the voltages measured at the input of the custom developed WSCN under the excitation of 1170 με peak-to-peak at 10 Hz. In Figure 6-13 the green solid line and black dashed line respectively represent the voltage trends when the PI module and the novel implemented PMM design were connected to the MFC energy harvester on aluminium substrate.

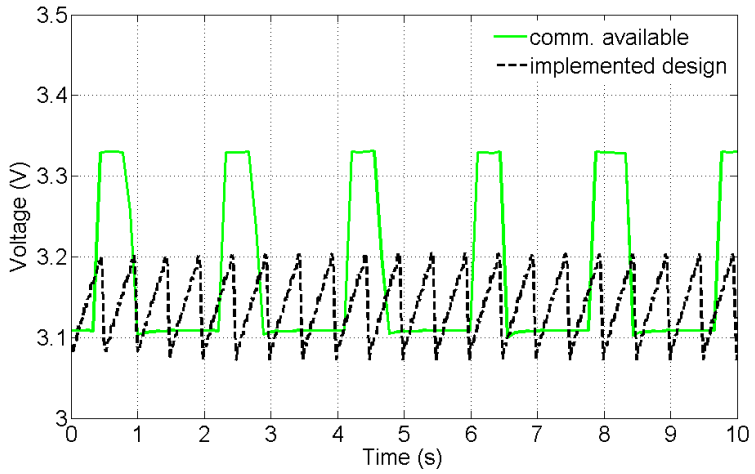

Figure 6-13 Trend of the voltages measured at the input of the custom developed WSCN for a commercially available PMM (from PI Ceramic GmbH) and the novel implemented PMM design powered by the MFC energy harvester on aluminium substrate under a cyclic excitation of 1170 με at 10 Hz

The microcontroller integrated within the WSCN of the developed system has an operating voltage between 1.8 and 3.6 V. From Figure 6-13 it can be observed that the PI module reaches an output of 3.3 V for the activation of the microcontroller whilst the implemented PMM design delivers the stored energy at a voltage of ~3.2 V. Data are acquired by the WSCN and transmitted in correspondence of every voltage peak. From Figure 6-13, it can also be observed that, under a continuous excitation of 1170 με at 10 Hz, the novel implemented PMM design allows the execution of 4 data transmissions whilst only 2 occur during the same time interval when the PI module is used. In fact, the PI module as well as other commercially available architectures, regulates the output voltage that feeds the microcontroller of the WSCN through a DC/DC converter. By using a DC/DC converter to condition the signal generated by the

piezoelectric transducer there is an increase in the power consumption of the system. In addition, since the DC/DC converter keeps its regulated voltage output until energy stored by an input capacitive reservoir does not drop down significantly, then the microcontroller keeps drawing power until the DC/DC is active. Although the microcontroller is powered on, however, the power supply is not enough to execute a second active cycle of data acquisition and transmission; hence, the stored energy is consumed with no benefit.

On the contrary, the EAI of the novel implemented PMM design disconnects the microcontroller straight after it performs an active cycle of data acquisition and transmission. In such a way, less energy is drawn from the capacitive energy storage that keeps collecting electric charge for the successive WSCN activation, which does occur at an earlier time when compared to the system using commercially available power management architectures. In the specific case shown in Figure 6-13, for instance, data transmissions are performed by the WSCN at every 0.4 s by use of the implemented PMM design whilst 1.6 s were needed with the PI module connected into the system. Therefore, the implemented PMM design permits to reduce the power consumption of the system and increase the capability to approach continuous power supplying to wireless sensor nodes from the strain energy of a vibrating structure.

6.4.3 Results and discussions based on case study 2

Figure 6-14 shows the actual experimental setup used for the characterisation of the implemented low power consumption wireless sensor system based on case study 2, when energy is harvested by the resonant cantilever-based piezoelectric transducer presented in Paragraph 3.2.3.

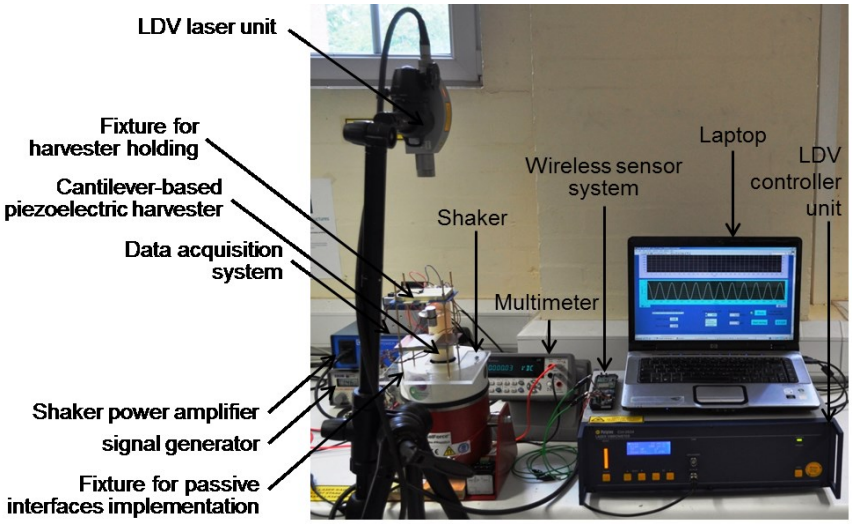

Figure 6-14 A photograph of the experimental setup for testing the implemented resonant cantilever-based PEH powered wireless sensor system

It is worthwhile to mention that, for this characterisation, the deflection of the piezoelectric cantilever-beam does not reach the fixture used for the interfaces implementation. In order to understand the time response of the developed system based on case study 2, when the WSCN is powered on or off by the energy harvested via the implemented cantilever-based piezoelectric harvester, Figure 6-15 shows the voltage measured across the 2 mF capacitive energy storage of the PMM for the continuous applied excitations of 0.025 g and 0.25 g of acceleration at the resonant frequency of 11.5 Hz.

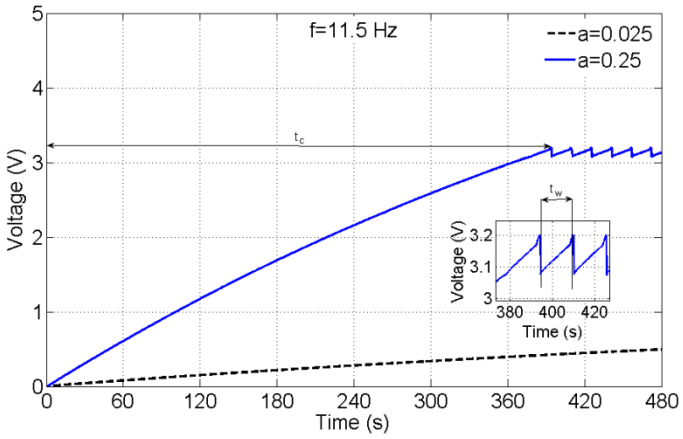

Figure 6-15 Performance of the custom developed WSCN, powered by the cantilever–based piezoelectric harvester, for the excitations of 0.025 g and 0.25 g of acceleration at the resonant frequency of 11.5 Hz

From Figure 6-15 it can be observed that, within the measured time interval of 480 s, the implemented resonant harvester is not capable to activate the WSCN under an applied excitation of 0.025 g of acceleration. In such a case, in fact, the voltage measured across the capacitive energy storage of the PMM does not reach the threshold voltage that permits the EAI to let the stored energy flow towards the WSCN. On the contrary, under an applied excitation of 0.25 g of acceleration the implemented resonant harvester generates enough electric charge to power the WSCN on. In particular, a cold start interval (t_c) of 394 s is required to reach the threshold voltage of 3.2 V for the first activation of the WSCN whilst a warm start interval (t_w) of only 15.8 s is required by the system to restore the voltage dropped in the capacitive energy storage before performing a new active cycle, hence successive data transmissions. The working principle of the system is as described in Paragraph 6.3.1: the electrical voltage across the capacitive energy storage of the PMM rises until the pre-set voltage fixed by the EAI; at this point the WSCN is powered on and performs data acquisition and transmission; the voltage across the capacitive energy storage drops down of around 120 mV; then, the power to the WSCN is cut off again and the system enters in a new non-active phase. The current drawn by the WSCN varies as it has been shown in Figure 6-12(b) but following the time intervals of 394 and 15.8 s for cold and warm start, respectively. As well as it has been shown for the case study 1, when the time response of the developed system powered by the MFC energy harvester decreased with the increase of the applied strain, similarly the time needed for the cold and warm start of the WSCN decrease with the increase of the acceleration at which the cantilever tip of the implemented resonant piezoelectric harvester is deflected as more power is harvested. As a direct consequence, a bigger amount of energy is stored in a shorter amount of time and is available to supply the power requirements for the end-user application.

6.5 Enhanced wireless sensor systems using the proposed interfaces

6.5.1 Results, discussions and a parametric study based on case study 1

In order to experimentally evaluate how the passive impedance matching interface presented in Chapter 4 optimise the performance of the implemented non-resonant PEH powered wireless sensor system, a comparison between the trend of the voltages measured across the capacitive energy storage of the novel implemented PMM is shown in Figure 6-16 for both the configurations without and with the interface. For the characterisation, a peak-to-peak strain level of 480 με was applied at 10 Hz to the MFC harvester on aluminium substrate implemented as described in Paragraph 3.2.1. Such strain level and frequency were chosen because the effectiveness of the proposed method has been shown to be more convincing under the tested excitation of 480 με peak-to-peak at 10 Hz of frequency and because at lower strain there is more need to further improve the performance of the non-resonant PEH powered wireless sensor system.

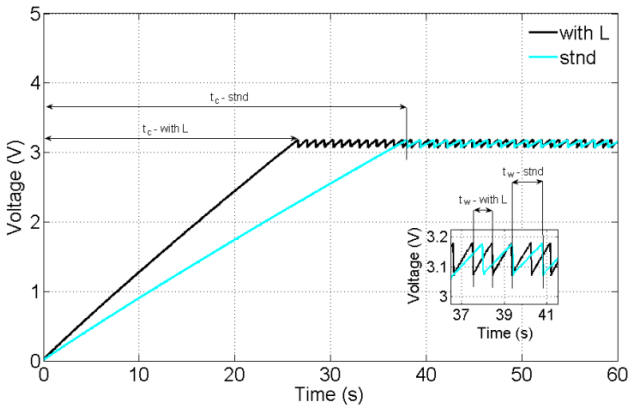

Figure 6-16 Comparison of the voltages measured across the capacitive energy storage of the implemented wireless sensor system powered by the MFC energy harvester between the configurations without and with impedance matching interface (stnd and with L) for the applied peak-to-peak strain level of 480 με at 10 Hz of frequency

From Figure 6-16, it can be observed that the performance of the developed system is enhanced when the impedance matching interface is connected in

series to the MFC harvester as both the time for the WSCN cold start (t_c) and warm start (t_w) are shorter in comparison to the standard case without interface. In particular, for an applied strain of 480 με peak-to-peak at 10 Hz, around 26.6 s rather than 38 s were needed for the WSCN cold start so as to reach from 0 V the threshold voltage of 3.2 V and around 0.9 s rather than 1.4 s were needed for the WSCN warm start after any active cycle for data acquisition and transmission. This means a performance improvement equal to 30% and 36% for the cold start and warm start of the system, respectively. The 2 mF energy storage capacitance is higher than the inherent capacitance (C_s) of the implemented energy harvester and, during the charging time of this energy storage, the load is disconnected from the rest of the circuit (i.e., kept in a high-impedance state so as to draw as less current as possible). Therefore, by connecting in series to the harvester an additional inductive element, the EH circuit works in a way similar to the circuit connected to the resistive load R_L seen in Chapter 4 in order to improve the performance of the system. The added inductive element L_{add} performs at every half a cycle of the piezoelectric-generated signal the impedance match with the total series capacitance ($C_{tot} = \frac{C_s \cdot C_{storage}}{C_s + C_{storage}} \approx C_s$) in the path where current is flowing through the forward-biased couple of diodes of the AC/DC bridge rectifier. The increment of this current, due to the reactance cancellation in the considered electrical path, occurs as in the circuit connected to the resistive load but leads to a higher amount of energy accumulating into the capacitive storage until the electrical load does not draw significant current; hence, for the whole duration of the non-active phases of the system. Therefore, by adding the impedance matching interface, the charging time of the capacitive energy storage is shorter than for the same circuital configuration without interface.

In order to proof the effectiveness of the implemented method in different application scenarios and independently from the capacitance of the energy storage, which is supposed to be anyway larger than the piezo-harvester capacitance, a parametric study was carried out by simulating the electrical

response of the circuit schematics shown in Figure 6-17(a) and Figure 6-17(b) without and with the added interface, respectively.

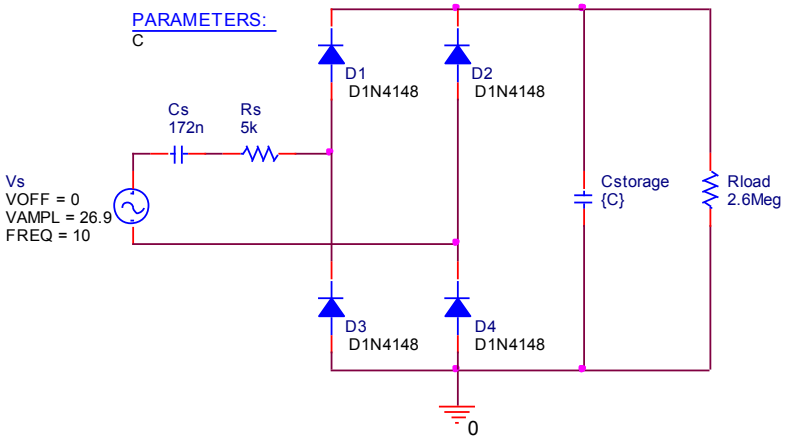

(a)

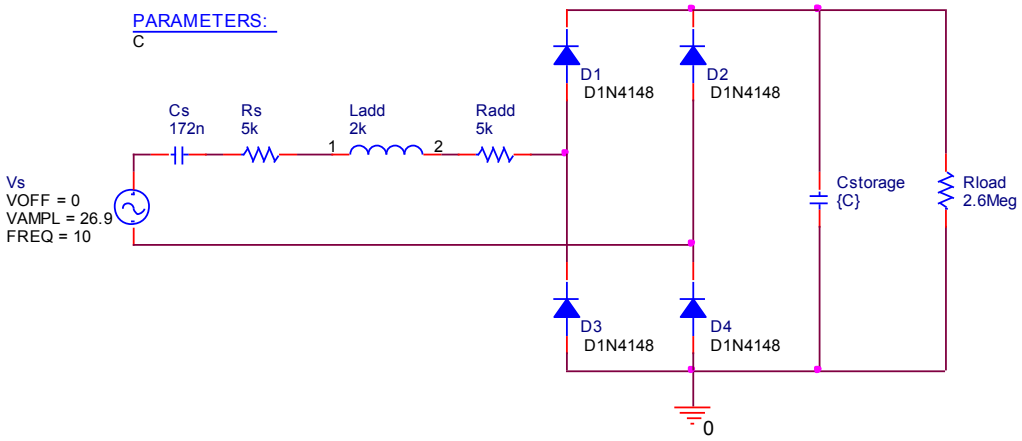

(b)

Figure 6-17 Schematic of the circuit of the developed wireless sensor system powered by the MFC harvester during a non-active phase for the configurations without (a) and with (b) the implemented impedance matching interface, where the circuit parameters is related to the input strain of 480 με at 10 Hz of frequency

In both circuit schematics the energy source is reproduced as the MFC harvester model depicted in Figure 3-9, where the voltage value V_{OC} =26.9 V has been calculated from Equation (3-2) in order to simulate the piezoelectric response under the excitation of 480 με at 10 Hz of frequency. Such a piezoelectric energy source is then connected to the resistive load R_{load} through

a 1N4148 4-diode bridge rectifier and a capacitive energy storage in parallel to it as from the design of the PMM for the implemented system. The capacitance of the energy storage has been set as the target parameter and varied from 2 to 50 mF as shown in the graphs of Figure 6-18(a) and Figure 6-18(b). The value R_{load}, on the contrary, has been fixed to the WSCN high impedance state during a non-active phase of the system. This was calculated equal to 2.6 MΩ based on the current consumed by the WSCN (I) and to its voltage mean value (V) during a warm start interval between two consecutive active cycles, which are 1.19 μA and 3.14 V as from the considerations reported above. Since during such time intervals there are no other active units enabled, the resistance $R_{\text{load}} = V / I$ can be accurately associated to the WSCN to model the system behaviour in a non-active mode. Such a simulative approach used to predict the time response of the developed system is effective as the system is in a non-active mode of operation for most of its time. The parametric study on C_{storage} permits to understand how the system would perform in similar applications that require larger energy storage to supply power to different sensors or for accomplishing tasks that feature a higher energy demand. In order to evaluate the effects of the implemented passive impedance matching interface on the overall system's performance, the inductive element L_{add} and its parasitic resistance have also been introduced in series to the model of the MFC harvester. The values of L_{add} and R_{add} have been set as the average values used for the theoretical calculation reported above, respectively equal to 2.0 kH and 5 kΩ. Transient analyses in the time domain of the voltage across the capacitive energy storage and the current through it were simulated by use of the commercial software OrCAD PSpice® 9.2 Student Version and the results are shown in Figure 6-19(a) and Figure 6-19(b), respectively.

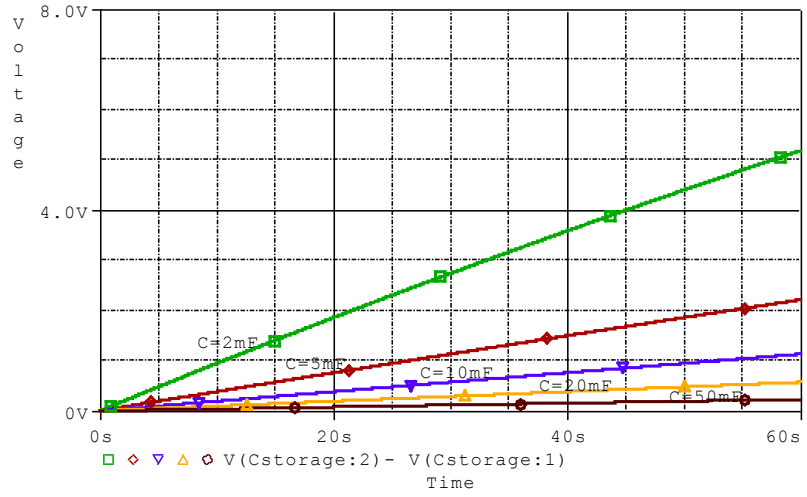

(a)

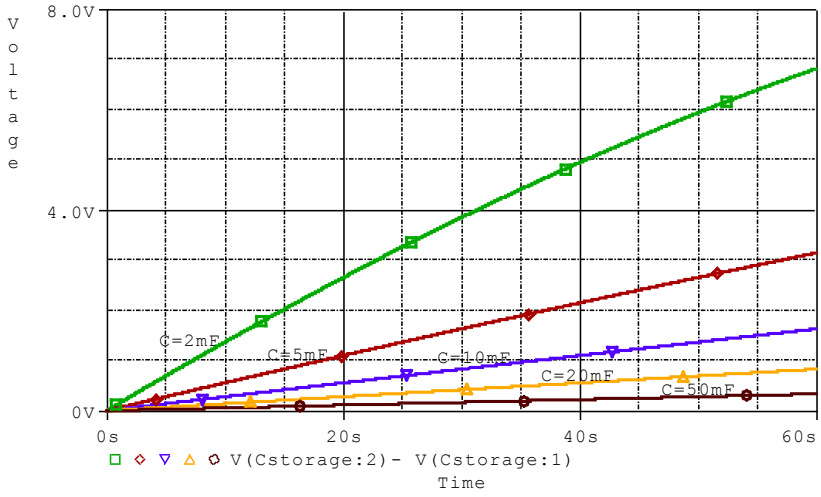

(b)

Figure 6-18 Simulated voltage across the capacitive energy storage in the circuit configurations (a) without and (b) with the developed impedance matching interface for different capacitance values and under an excitation of 480 με peak-to-peak at 10 Hz

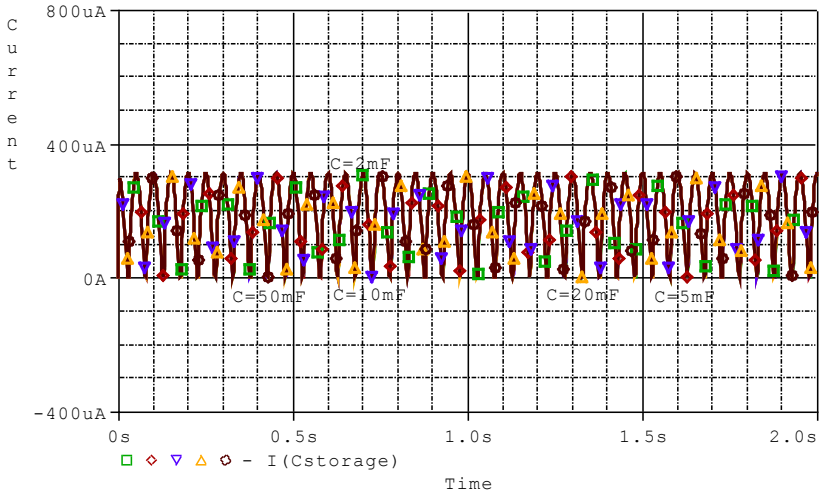

(a)

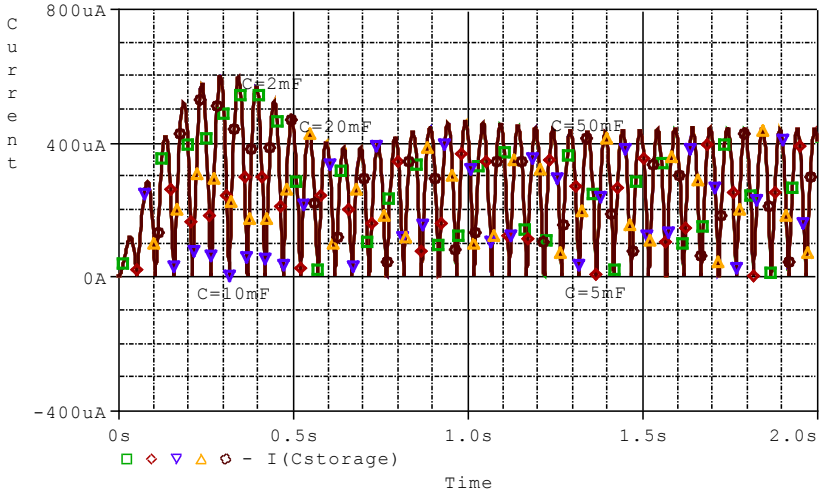

(b)

Figure 6-19 Simulated current through the capacitive energy storage in the circuit configurations (a) without and (b) with the developed impedance matching interface for different capacitance values and under an excitation of 480 μstrain peak-to-peak at 10 Hz

From a direct comparison between the voltages vs time curves in Figure 6-18(a) and Figure 6-18(b), it can be observed that for the circuit configuration with the added interface the time needed to reach a certain voltage level is shorter than for the circuit configuration without interface. Such a performance optimisation is more evident for smaller values of the capacitance C_{storage} as more electric charge is obviously accumulated during the tested time interval of 60 s. For instance, in order to reach the 3.2 V threshold required for the activation of the

WSCN, the simulated cold start time when C_{storage}=2 mF as for the implemented system configuration is shown to be equal to around 38 s, which well agrees with the experimental result in Paragraph 6.4.1. Similarly, from a comparison between the current vs time curves in Figure 6-19(a) and Figure 6-19(b), it can be observed that for the circuit configuration with the added interface the average current is higher than for the circuit configuration without interface as a direct consequence of the cancellation of the harvester's reactance. Particularly, the current reaches a maximum root-mean-square value of around 600 μA and is approximately equal to 450 μA in steady state whilst a current of only 300 μA was measured in the system configuration without the interface. Furthermore, the current trends are in both cases independent from the capacitance of the energy storage thus indicating that the proposed passive impedance matching method is effective in practical PEH powered applications, such as energy-autonomous wireless sensing, and can be potentially useful to enhance the performance of the connected piezoelectric energy harvester.

6.5.2 Results and discussions based on case study 2

Full-wave 4-diode bridge rectifiers and voltage doublers are the conventional circuits used as the AC/DC converters of piezoelectric harvesters. Typical implementation of these rectifier circuits is respectively shown in Figure 6-20(a) and Figure 6-20(b), where the output capacitor C holds the rectified voltage essentially constant on a cycle-to-cycle basis for the power supply of a connected electrical load such as a wireless sensor system.

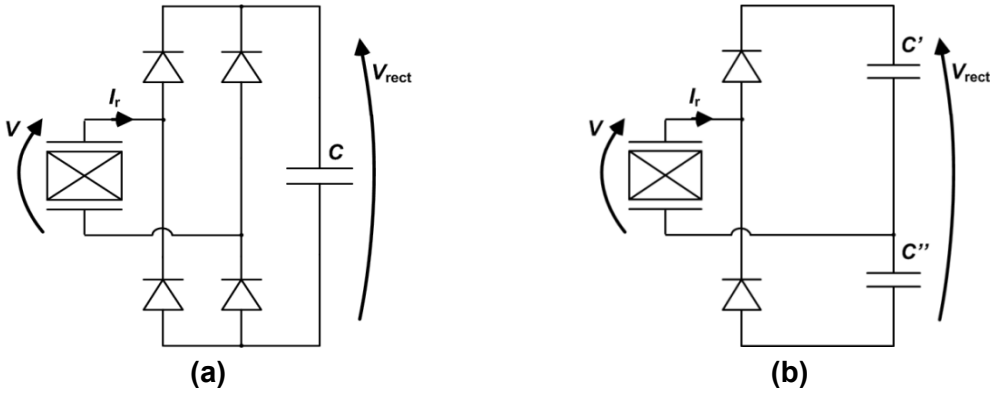

Figure 6-20 Conventional circuits used as the AC/DC converters of piezoelectric harvesters: (a) a 4-diode bridge rectifier and (b) a voltage doubler

Assuming the input excitation to be sinusoidal in nature and the diodes in the rectifier configurations above to be ideal, the electrical power that can be extracted from the full-bridge circuit in (a) is equal to:

$$P_{\text{rect}} = \frac{2V_{\text{rect}}}{\pi}(I_{\text{r}} - V_{rect}\omega C_0) \tag{6-1}$$

where V_{rect} is the rectified voltage developed across the capacitor C whilst C_0 is the inherent capacitance of the piezoelectric harvester. The extracted power varies with the output voltage and reaches the maximum value:

$$P_{\text{rect,max}} = \frac{{I_{\text{r}}}^2}{2\pi\omega C_0} \tag{6-2}$$

when

$$V_{\text{rect,max}} = \frac{I_{\text{r}}}{2\omega C_0}\,. \tag{6-3}$$

For the voltage doubler case, while the maximum power that can be extracted from the harvester is same as for the full-bridge configuration, the voltage output V_{rect} at which this is achieved is twice the value. The main limitation of the full-bridge rectifier is that, most of the current available from the harvester does not reach high voltages at the output. This is because the generated current first has to accumulate into the capacitor C_0 until the voltage V_{rect} is reached. This happens every time current changes direction from positive to negative and vice-versa as the voltage across C_0 has to change from $+V_{\text{rect}}$ to $-V_{\text{rect}}$ or from $-V_{\text{rect}}$ to $+V_{\text{rect}}$. This loss in charge, due to charging and discharging of C_0, limits the maximum power that can be extracted using the full-bridge rectifier. Further power losses are obviously related to the use of discrete components.

The advantage of the developed interface for the mechanically activated series SSHI of a cantilever-based piezoelectric harvester is that the rectification of the

harvester's output can be passively performed with no use of diodes via implementing the circuit configuration shown in Figure 6-21.

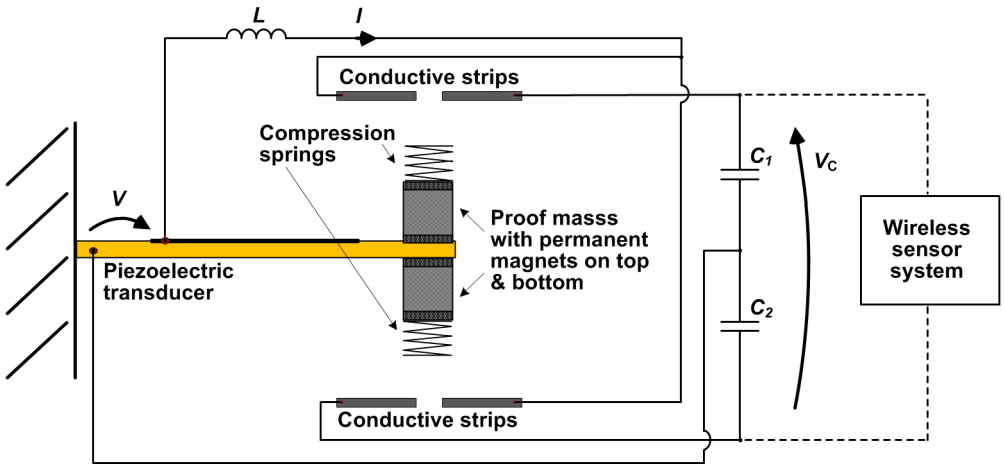

Figure 6-21 A schematic of the circuit of the novel mechanically activated AC/DC rectifier for cantilever-based piezoelectric harvesters

During every deflection of the beam under an applied excitation, the compression springs of the developed passive interface build up a closed path between the piezoelectric energy harvester and the capacitive energy storage. The added springs in such a circuit configuration permits that small variations of the beam displacement do not affect the rectification functioning as electric charge keeps being passively transferred to the capacitors C_1 and C_2. The springs, indeed, deform accordingly with the beam oscillation even after that contact with the conductive strips has been established. However, applications where the piezoelectric cantilever is bent at a fixed frequency, or within a small frequency range of variation, receive more benefit from the adoption of such an interface. During positive and negative cycles of the input vibration, electric charge accumulates in the inherent capacitor C_0 of the piezoelectric harvester. Then, the voltage V across C_0 is inverted and augmented by the series inductor L for a quasi-instantaneous energy transfer to the capacitor C_1 or C_2, respectively in correspondence to every maximum or minimum deflection of the cantilever beam. In such a circuit configuration, energy is stored throughout the whole cycle of the input vibration by the capacitors C_1 and C_2 for a self-

powered functioning of a custom-developed wireless sensor system. The wireless sensor system in Figure 6-21 was implemented as the complex made of the EAI and WSCN presented in Paragraph 6.3. A threshold voltage is set for the sensing device of the EAI, which monitors the voltage developed across the series C_1-C_2 and permits the stored energy to be transferred to the microcontroller of the wireless sensor system to perform data acquisitions and transmissions to a base station. Therefore, the EAI permits to: 1) avoid that the electric charge stored in C_1 (C_2) flows back to the inherent capacitance C_0 of the piezoelectric harvester when this reaches a positive (negative) extremum deflection; 2) guarantee a level of energy able to sustain the requirements of the WSCN of the wireless sensor system. By enhancing the performance of the piezoelectric harvester, the described mechanically activated SSHI circuit with no discrete components such as diodes and with compression springs for the amplification of the force acting on the cantilever beam reduce the time needed for both the cold and warm start of the WSCN. This represents a step forward in order to deliver a continuously energy-autonomous SHM approach. A comparison between the trends of the voltage measured across the capacitive energy storage of the novel implemented PMM design is shown in Figure 6-22 for the circuit configurations with the cantilever-based piezoelectric harvester only and with the added springs and mechanical SSHI interface described in Paragraph 5.2.3. Particularly, Figure 6-22(a) and Figure 6-22(b) respectively show the measured voltage across the 2 mF capacitive energy storage as a function of time for the applied excitations of 0.025 g and 0.25 g of acceleration at the resonant frequency of 11.5 Hz.

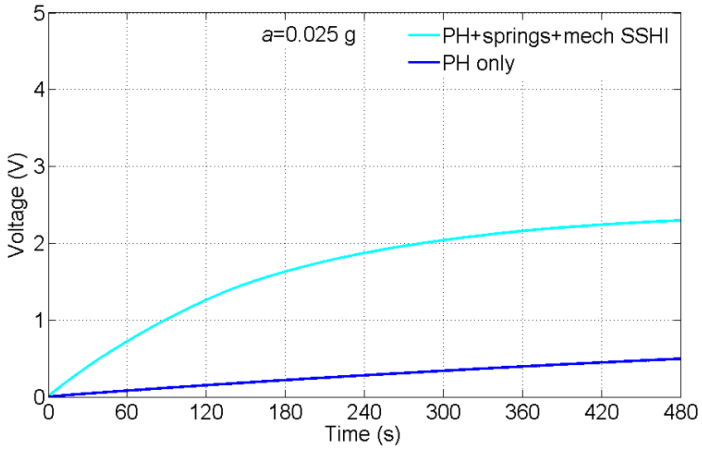

(a)

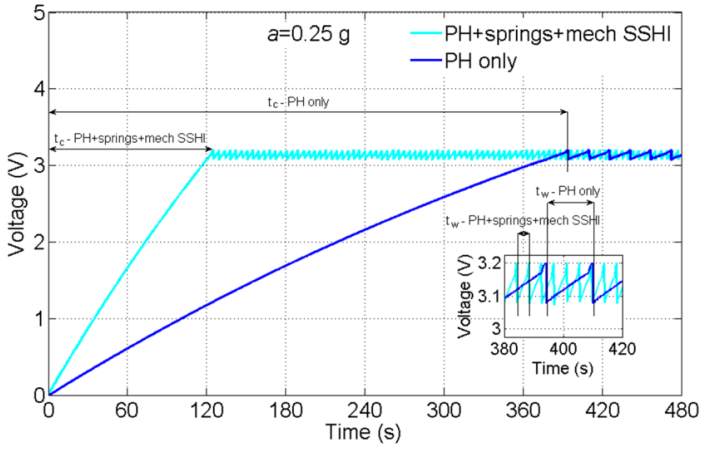

(b)

Figure 6-22 Comparison of the voltage measured across the capacitive energy storage of the implemented wireless sensor system powered by the cantilever-based piezoelectric energy harvester between the configurations without and with interface at the excitations of a) 0.025 g and (b) 0.25 g of acceleration at the resonant frequency of 11.5 Hz

From Figure 6-22(a) it can be observed how, although 480 s are not enough for the cold start of the WSCN, the configuration with the added passive interface including springs and the mechanical SSHI circuit permits to achieve a considerably higher voltage across the capacitive energy storage of the system; namely, the measured values of 2.3 V versus 0.5 V that corresponds to an improvement of 360%. Similarly, from Figure 6-22(b) it can be observed that, under a resonant excitation of 0.25 g, around 124.8 s are needed for the cold start of the WSCN when the passive interface is connected to the harvester rather than the 394.1 s needed by the configuration with the harvester only. The

time for the warm start of the WSCN is also shortened approximately from 15.8 s to 4.2 s. The performance optimisation for the resonant PEH powered wireless sensor system is then equal to 68% and 73% for the cold and warm start of the WSCN, respectively.

6.6 Summary

This chapter has presented typical low power management architectures for EH systems and introduced a novel low power consumption design with an integrated EAI for PEH. With regards to PEH applications, commercially available modules have been shown to have different pro and cons, mainly depending on the implemented energy storage technique. In particular, the use of capacitors results more effective for short term power supply with higher current bursts, offers more flexibility to applications in harsh conditions, and can achieve lower power consumption levels in comparison with rechargeable batteries of the Lithium family for the absence of additional voltage protection circuits. It has been shown that the novel EAI, by wisely monitoring the voltage across the energy storage, permits to reduce the power consumption of PEH systems. Indeed, by use of the EAI, the flow of the harvested energy is delivered to the WSCN through the capacitive energy storage only when this is enough to match the requirements of the end-application. Because there is no additional DC/DC voltage regulation involved and the energy transfer is enabled by the EAI only for a certain time window, there is no additional energy waste. A custom developed low power consumption WSCN, which integrates a thermometer, a light detector, and a 3-axis accelerometer has been also implemented for the realisation of a whole energy-autonomous system-of-systems for online SHM applications. The developed system made of the PMM with the EAI and the WSCN has been tested in connection to both the implemented energy harvesters in resonant and non-resonant conditions under the conditions described by case study 1 and 2. Tests have been performed by measuring the time needed for the cold start of the systems and the time between two consecutive data transmissions as a measure of the alternation intervals between non-active phases and active phases. With regard to case

study 1, a performance comparison has been presented when the system was connected to either a commercially available PMM or the novel implemented design including the EAI. It has been shown that the novel design allows up to 4 times more active cycles during the same time interval compared to tested off-the-shelf modules and that, in both case study 1 and 2, the system is capable to perform active cycles at intervals of seconds or fractions of a second rather than minutes under continuous low-frequency excitation. Such a performance has been further improved by use of the developed passive interfaces, which means that both the time intervals for the cold and warm start of the WSCN have been shortened. This further means that an increased capability to continuously supply power for the intended applications in a truly energy-autonomous manner has been achieved. In particular, under an excitation of 480 με at 10 Hz of frequency, the non-resonant MFC energy harvester was shown to supply power to the connected WSCN at intervals as fast as 0.9 s after a cold start of approximately 26.6 s with a percentage improvement respectively equal to 30% and 36% in comparison with the performance of the originally developed low power management design. By connecting the interface for the mechanically activated series SSHI to the cantilever-based piezoelectric harvester, energy was directly transferred to the capacitive storage of the system at every half a cycle of the excitation input with no further need of rectification. Under an excitation of 0.25 g acceleration at 11.5 Hz, the resonant cantilever-based piezoelectric harvester was shown capable to first activate the WSCN after only 124.8 s and to allow data transmissions afterwards at every 4.2 s. Therefore, an improvement equal to 68% and 73% has been achieved for the cold and warm start of the WSCN, respectively. Upon the integration of the developed passive interfaces, the capability of PEH systems to sustain the power requirements of wireless sensor nodes gets closer to the practical need of real-life applications.

7 CONCLUSIONS AND FUTURE WORK

7.1 Brief summary of the thesis

This research work focussed on enhancing the performance of PEH powered wireless sensor nodes for SHM applications capable to facilitate predictive maintenance of critical components by assessing in real time the health status of a system. Since for practical applications a mismatch exist between the energy harvested by small-scale piezoelectric harvesters under low-frequency conditions and the energy required by wireless sensor nodes, novel interfaces and power management approach have been developed at a system level for: 1) maximising the extraction of the energy harvested by non-resonant and resonant piezoelectric transducers; 2) minimising the power requirements for conditioning and managing the harvested energy flow; 3) optimising the overall energy transfer from the piezoelectric harvester to the electrical load (i.e., the wireless sensor node).

Piezoelectric transducers in the form of non-resonant embeddable patches, based on flexible MFC materials bonded to aluminium and composite substrates, and a resonant cantilever beam, based on PZT material on brass substrate, have been implemented in this research work as vibration energy harvesters. Two low-frequency case studies have been examined as practical applications: 1) patch-like MFC energy harvesters scavenging energy from the mechanical strain of aircraft wing structures in active service for wirelessly monitoring conditions such as the gust loading; and 2) a cantilever-based energy harvester scavenging energy from the resonant excitation of large industrial machinery for wirelessly monitoring bearing or rotor conditions. Theoretical analyses and experimental characterisation have been respectively presented for the MFC harvesters, under applied strain levels between 440 and 1170 με and frequency ≤10 Hz as commonly found on large transport aircraft, and for the cantilever-based harvester, under acceleration levels of 0.025 g and 0.25 g at the resonant frequency of 11.5 Hz as found in the range of vibrations typical on large industrial machinery such as industrial pumps. In order to enhance the energy extraction from the MFC harvesters, a passive CCIM

interface was implemented. The challenge of matching the low capacitance of the harvester in the low-frequency range both practically (in terms of the interface's size) and passively (in terms of the interface's power supply), was addressed by the use of a PC permalloy core toroidal coil with a large initial magnetic permeability of 6×10^4 H/m. Therefore, a large inductance of about 1.6 kH was achieved at 10 Hz but on a centimetre-scaled size (i.e., ~15 cm^3). Being passive, the implemented interface overcomes the power consumption drawbacks of the state-of-the-art impedance matching techniques, does not need any additional power source, and is further easier to be implemented and retrofittable to existing PEH architectures. Passive interfaces were also developed in order to increase the energy harvested by the cantilever-based piezoelectric energy harvester. It was shown that, by using compression springs, the mechanical energy of the cantilever beam is amplified as a result of the additional springs' reactive force against spatially fixed conductive strips. In addion, passive interfaces were developed to implement the SSHI technique through a magnetic or mechanical activation. The deflection of the cantilever beam was exploited so as to avoid the use of specific algorithms or active electronic control circuits as in previous SSHI implementations proposed in the literature, whose power consumption is inevitably high. Reed switches were used for the magnetically activated switch of the harvester's output when the displacement of the cantilever beam reached its extrema whilst compression springs and mechanical contact on conductive strips were used for the mechanically activated SSHI implementation. The interfaces were first tested in connection to resistive loads and experimental results showed significant improvement of the PEH performance, in that higher output powers from the harvesters were achieved in correspondence to electrical loads of smaller impedance. In particular, an increment of the power around 95% was obtained under an excitation of 480 με at 10 Hz in correspondence to a resistive load reduced by over 70% when the passive impedance matching interface was connected in series with the implemented MFC harvester on aluminium substrate. For the implemented cantilever-based harvester, power enhancements up to 359% and 452% were respectively measured across

connected resistive loads of 66 and 61 kΩ at the low resonant frequency of 11.5 Hz and under excitations of 0.025 g and 0.25 g of acceleration. Aiming at delivering a practical PEH system to be used in real-life applications, a PMM and a WSCN were also developed in this research work. A full-wave rectifier, a capacitive energy storage, and a novel EAI were integrated into the PMM for the purpose of managing the flow of the harvested energy towards the WSCN with low power consumption. By use of a voltage sensing device, the implemented EAI allowed monitoring the stored energy and transferring it further only when this was enough to sustain the power requirements of the end-application. This energy was then used by the WSCN to acquire data of temperature, acceleration, and light and to wireless transmit them to a base station via three of the sixteen channels available in the 2.4 GHz range. The PEH systems made by the custom-developed harvesters, PMM, and WSCN were tested under the conditions of the two examined case studies. A performance comparison between the PEH systems integrating the custom-developed PMM and commercially available PMM architectures showed that the novel design with the EAI permits to achieve shorter activation intervals for the WSCN. Indeed, the overall power consumption is reduced through the EAI as the WSCN is electrically disconnected from the rest of the circuit until an amount of energy enough to sustain a whole active cycle of data acquisition and wireless transmission has been harvested and stored in the capacitor bank. Additionally, the EAI permits to avoid the use of DC/DC converters in the PMM, which are typically added cascading the capacitive energy storage to regulate the voltage supply of the connected electrical load. Time intervals of 13.4 and 394 s were respectively measured for the cold start of the WSCN under the highest magnitude of the non-resonant and resonant excitations used for testing of the two case studies. Data transmissions as fast as 0.4 and 15.8 s were also respectively measured. By adding the developed passive interfaces between the harvesters and the novel PMM, further improvements were proved. In particular, the cold start and warm start time intervals of the WSCN were respectively lowered by 30% and 36%, for the non-resonant system powered by the MFC harvester, and up to 68% and 73%, for the resonant cantilever-based

system. In other words, this means that more data could be acquired and transmitted by the developed PEH systems during a certain time interval as more power was extracted from the implemented harvesters and less was consumed to make it usable by the connected WSCN.

The results of this research work indicate the capability to approach continuous power supply to wireless sensor nodes entirely from vibration-harvested energy. By reducing the mismatch between harvested and demanded energy, the presented systems make a step forward towards the widespread of PEH technology and hold a potential for practical energy-autonomous SHM applications.

7.2 Limitations

Enhancing the EH performance of piezoelectric harvesters is a useful prospect as it represents a promise for a wider application potential. This research work has shown the capability to approach continuous power supply to wireless sensor nodes entirely from vibration-harvested energy. Such a capability has been proved to sustain data acquisitions and transmissions at intervals as fast as 0.4 s. This is ideal for many static or slowly changing process monitoring requirements such as for measuring temperature in low fire-hazard environments. Depending upon the application, however, sensors may be required to acquire data continuously during a longer activation interval before the cycle driven by the EAI cuts off the energy transfer from the storage. In the form it has been presented and with the performance it has been shown, the developed system could not be usable for dynamic SHM measurements or simply to supply power to more or more power-hungry sensors than those already integrated. This research work has also considered the vibration source as a simple harmonic motion type of vibration with a single operating frequency and selected acceleration or strain amplitude levels. Such an assumption corresponds to reality for resonant applications featuring a main recurrent frequency and acceleration level. However, non-resonant PEH applications or applications featuring intermittent, variable-frequency, and variable-amplitude vibrations may not lead to the same results achieved herein. In addition, it is

worthwhile to mention that the achieved results are not always based on an optimal systems' implementation with regards to material selection and assembly. This is especially true for the bonding procedure used for the MFC energy harvester and the ceramic element on brass used for the resonant cantilever-based PEH configuration. Although they could both be optimised, a physical limitation remains at a structural level that is the thickness of the adhesive layer between the piezoelectric element and the substrate. Such a layer, in fact, lowers the transducer's electromechanical coupling and causes a not uniform strain distribution. In order to overcome these limitations, an alternative solution can be based on the integration of the piezoelectric material directly into the structure of the substrate. This would eventually address the challenges but move the problem towards the realisation of functional composite materials and electrical connections for extracting and using the harvested power. From a circuital point of view, parameters such as the equivalent series resistance (ESR) of the storage capacitors and the quality factor (Q) of the interfaces' inductors are also limitations of the implemented systems that can be optimised but not eliminated.

7.3 Future work

The PEH circuitry presented herein, with novel interface implementations and power management approach, makes a step further towards compensating the existing mismatch between harvested and demanded energy as it permits an increase in power generation and a decrease in power consumption. Based on the limitations of Paragraph 7.2 and for completion of this research work, several areas have been identified in order to further extend or improve the achieved results:

- Reducing size and power dissipation of the developed systems through an optimal component selection and assembly:

  Performance-grade rather than standard-grade electronic components may be used for future implementations of the presented systems. These will permit a reduction of the systems' size and power consumption. To

further reduce the energy dissipation between connections, on-board circuital integration could be performed by following industrial procedures for PCB fabrication. It is also worth exploring the use of an adfirmed bonding industrial procedure for the implementation of the MFC energy harvester as well as a more efficient piezoelectric element for the resonant cantilever-based PEH configuration. In addition, based on the results reported in [232], it may be worthwhile placing a capacitance across the terminals of the piezoelectric transducer in order to reduce the size of the implemented passive impedance matching coil.

- Increasing the capacity of the energy storage and introducing a timer for a pre-scheduled activation of the WSCN:

  The implemented power management approach makes use of a 2 mF capacitive energy storage. The stored energy is then smartly transferred to the custom developed WSCN when a voltage around 3.2 V is reached across. Substituting the existing storage device with a device of larger capacitance or adding a backup reservoir characterised by higher energy retention (e.g., a rechargeable battery) may represent a significant advantage in case of specific wireless sensor applications. This means that the WSCN could at certain times transmit data without the need to wait for a sufficient electric charge to build up in the energy storage. For that purpose or with the intention of running pre-scheduled operations, a time delay driver can be introduced into the ciruitry of the PMM so that the harvested energy flow may be split at once to two different lines of load or at alternative steps through mutual switching circuits. Keeping the timing control externally from the WSCN, namely without involving the use of a microntroller, may allow reducing the systems' power consumption according to the consideration reported in Paragrapgh 6.2. The time introduced by the delay circuit can be varied in accordance with the EH scenario for a flexible activation of the WSCN.

- Performing analysis and experimental validation with intermittent, variable-frequency, and variable-amplitude vibrations:

Although different case vibration scenarios have been separately examined, it might worth carrying out analysis and experimental validation under an excitation composed of a number of frequencies and amplitudes. Intermittency in the vibration source may also be considered to validate a good PMM performance. In addition, introducing a delay driver circuit into the PMM as proposed above can add reliability to the PEH mechanism in case of discontinuous ambient vibrations according to the considerations reported in Paragraph 6.2.

- Performing statistical analysis and fatigue tests:

  From a comparison of the MFC material characterisation on aluminium and composite substrates under non-resonant vibrations, it has been shown that the EH capability of the composite specimen was slightly higher under a similar excitation input. This suggests that the composite material is more efficient in transferring the applied strain to the attached harvester due to the orientation of the carbon fibres on the top layer. On the other hand, given the critical factor of the thickness of the adhesive layer as a result of the custom sample preparation, performing further experiments on a larger number of samples is recommended to clarify an effective difference between the harvesting performances of the MFC material bonded on aluminium and composite substrates. From a larger amount of data, in fact, a more statistically significant comparison can be derived and potential changes in the specimen implementation taken into account. Another aspect of the research to be considered relates to fatigue testing on the implemented harvester specimens as a prerequisite for integrating the developed systems in a real application environment.

- Implementing a WSN in a real application environment:

  The use of a custom wireless sensor node as the electrical load of the developed PEH systems could be extended to a larger number of nodes with bidirectional wireless communication ability. This can form the basis of a future study aimed at realising an energy-autonomous WSN.

Strategies to further reduce the node's power consumption when integrated into a network may be investigated as such: 1) sharing or transferring the harvested energy in a point common to several neighbour nodes; 2) running periodic self-configuration protocols and collaborative signal processing for the detection/estimation of some events of interest; 3) reducing wireless communications with the base station only to cases when an alert status needs to be reported; and 4) introducing querying capability from an external observer. A standard wireless local area network (WLAN) may also be employed at the receiver-end in order to provide data exchange from multiple local sensing networks over a broad area. Then, data may be addressed from remote by any user on the local area network (LAN) using a standard internet browser.

Moving the developed technology from the laboratory environment to the real-word environment would give an overall insight of the aspects that need further attention before exploitation.

REFERENCES

[1] Akyildiz, I.F., Su, W., Sankarasubramaniam, Y. and Cayirci, E. (2002): “Wireless sensor networks: a survey” *Comput. Netw.*, vol. 38, no. 4, pp. 393–422.

[2] Boisseau, S., Despesse, G. and Ahmed Seddik, B. (2012): *Electrostatic Conversion for Vibration Energy Harvesting, Small-Scale Energy Harvesting*, InTech, Lallart, M. (Ed.), ISBN: 978-953-51-0826-9, DOI: 10.5772/51360.

[3] Stevens, J.W. (1999): "Heat transfer and thermoelectric design considerations for a ground-source thermoelectric generator," Eighteenth International Conference on Thermoelectrics, Baltimore, MD, USA, pp. 68-71.

[4] Mantiply, E D., Pohl, K. R., Poppell, S. W. and Murphy, J. A. (1997): Summary of measured radiofrequency electric and magnetic fields (10 kHto 30 GHz) in thegeneral and work environment, *Bioelectromagnetics*, 1997, Vol. 18, no. 8, pp. 563-577, 0197-8462.

[5] Roundy, S., Wright, P.K. and Rabaey, J. (2003): "A study of low level vibrations as a power source for wireless sensor nodes," *Computer Communications,* vol. 26, pp. 1131-1144.

[6] Roundy, S., Leland, E.S., Baker, J., Carleton, E., Reilly, E., Lai, E., Otis, B., Rabaey, J.M., Wright, P.K. and Sundararajan, V. (2005): "Improving power output for vibration-based energy scavengers," *IEEE Pervasive Computing,* vol. 4, pp. 28-36.

[7] Mitcheson, P.D., Green, T.C., Yeatman, E.M. and Holmes, A.S. (2004): "Architectures for vibration-driven micropower generators," *Journal of Microelectromechanical Systems,* vol. 13, pp. 429-440.

[8] Miyazaki, M., Tanaka, H., Ono, G., Nagano, T., Ohkubo, N., Kawahara, T. and Yano, K. (2003): "Electric-Energy Generation Using Variable-Capacitive Resonator for Power-Free LSI: Efficiency Analysis and Fundamental Experiment," Proceedings of the 2003 International Symposium on Low Power Electronics and Design ISLPED '03. Seoul, South Korea, pp. 193-198.

[9] Torah, R.N., Beeby, S.P., Tudor, M.J., O'Donnell, T. and Roy, S. (2006): "Development of a Cantilever Beam Generator Employing Vibration Energy Harvesting," Proceedings of the 6th International Workshop on Micro and Nanotechnology for Power Generation and Energy Conversion Applications, Berkeley CA, pp. 181-184.

[10] Wang, L. and Yuan, F. G. (2008): Vibration energy harvesting by magnetostrictive material, Smart Mater. Struct., vol. 17, no. 4, 045009 (14pp).

[11] Bottner, H., Nurnus, J., Gavrikov, A., Kuhner, G., Jagle, M., Kunzel, C., Eberhard, D., Plescher, G., Schubert, A. and Schlereth, K.-H. (2004): "New thermoelectric components using microsystems technologies," *Journal of Microelectromechanical Systems,* vol. 13, pp. 414-420.

[12] duToit, N. E., Wardle, B. L. and Kim, S. G. (2005): Design considerations for MEMSscale piezoelectric mechanical vibration energy harvesters. *Integr. Ferroelectr.*, vol. 71, no. 1, pp. 121-160.

[13] Beeby, S. P., Tudor, M. J. and White, N. M. (2006): "Energy harvesting vibration sources for microsystems applications," *Measurement Science and Technology,* vol. 17, pp. 175-195.

[14] Glynne-Jones, P., Beeby, S. P. and White, N. M. (2001): "Towards a piezoelectric vibration-powered microgenerator," *IEE Proceedings: Science, Measurement and Technology,* vol. 148, pp. 68-72.

[15] Sodano, H. A., Lloyd, J. and Inman, D. J. (2006): "An experimental comparison between several active composite actuators for power generation," *Smart Materials and Structures,* vol. 15, pp. 1211-1216.

[16] Kim, H. W., Batra, A., Priya, S., Uchino, K., Markley, D., Newnham, R. E. and Hofmann, H. F. (2004): "Energy harvesting using a piezoelectric "cymbal" transducer in dynamic environment," *Japanese Journal of Applied Physics, Part 1: Regular Papers and Short Notes and Review Papers,* vol. 43, pp. 6178-6183.

[17] Priya, S., Chen, C.-T., Fye, D. and Zahnd, J. (2005): "Piezoelectric Windmill: A novel solution to remote sensing," *Japanese Journal of Applied Physics, Part 2: Letters,* vol. 44, pp. 104-107.

[18] Jeon, Y. B., Sood, R., Jeong, J. H. and Kim, S. G. (2005): "MEMS power generator with transverse mode thin film PZT," *Sensors and Actuators, A: Physical,* vol. 122, pp. 16-22.

[19] Fang, H.-B., Liu, J.-Q., Xu, Z.-Y., Dong, L., Wang, L., Chen, D., Cai, B.-C. and Liu, Y. (2006): "Fabrication and performance of MEMS-based piezoelectric power generator for vibration energy harvesting," *Microelectronics Journal,* vol. 37, pp. 1280-1284.

[20] White, N.M., Glynne-Jones, P. and Beeby, S. P. (2001): "A novel thick-film piezoelectric micro-generator," *Smart Materials and Structures,* vol. 10, pp. 850-852.

[21] Konak, M.J., Powlesland, I.G., van der Velden, S. P. and Galea, S. C. (1997): "Selfpowered discrete time piezoelectric vibration damper," in *Smart Materials, Structures, and Integrated Systems*, Adelaide, Australia, pp. 270-279.

[22] Schmidt, V. H. (1986): "*Theoretical electrical power output per unit volume of PVF2 and mechanical-to-electrical conversion efficiency as functions of frequency*," Bethlehem, PA, USA, pp. 538-542.

[23] Shenck, N. S. and Paradiso, J. A. (2001): "Energy scavenging with shoe-mounted piezoelectrics," *IEEE Micro,* vol. 21, pp. 30-42.

[24] Ottman, G. K., Hofmann, H. F. and Lesieutre, G. A. (2003): "Optimized Piezoelectric Energy Harvesting Circuit Using Step-Down Converter in Discontinuous Conduction Mode," *IEEE Transactions On Power Electronics,* vol. 18.

[25] Elvin, N., Elvin, A. and Choi, D. H. (2003): “A self-powered damage detection sensor,” *J. Strain Analysis*, vol. 38, no. 2, pp. 115–24, Jan 2003.

[26] Lallart, M., Guyomar, D., Jayet, Y., Petit, L., Lefeuvre, E., Monnier, T., Guy, P. and Richard, C. (2008): “Synchronized switch harvesting applied to selfpowered smart systems: piezoactive microgenerators for autonomous wireless receiver,” *Sens. Actuators A: Phys*., vol. 147, no. 1, pp. 263–72, Sept. 2008.

[27] Weiss, D. E. (1972): *“An Advanced Strain Level Counter for Monitoring Aircraft Fatigue”*, Instrument Society of America, ASI 72212, pp. 105-108.

[28] Guyomar, D., Lallart, M., Monnier, T., Wang, X. and Petit, L. (2009): "Passive impact location using piezoelectric sensors," *Struct. Health Monit.,* vol. 8, no. 5, pp. 357–67, Sept 2009.

[29] Lynch, J.P. and Loh, K.J. (2006): "A summary review of wireless sensors and sensor networks for structural health monitoring," *Shock Vib. Digest*, vol. 38, no. 2, pp. 91–128, Mar 2006

[30] Woo, A. L. C. (2004): "Networking support for query processing in sensor networks*", Networking of Sensor System (NOSS) workshop, Communications of the ACM - Wireless sensor networks (CACM) WSN special issue*, vol. 47, Issue 6, June 2004.

[31] Anton, S.R. and Sodano, H.A. (2007): "A review of power harvesting using piezoelectric materials (2003–2006)", *Smart Mater. Struct.,* vol. 16, no. 3, R1–21.

[32] Sodano, H.A., Park, G. and Inman, D.J. (2004): "Estimation of electric charge output for piezoelectric energy harvesting", *Strain,* vol. 40, pp. 49–58

[33] Erturk, A. and Inman, D. (2008): "On mechanical modeling of cantilevered piezoelectric vibration energy harvesters", *J. Intell. Mater. Syst. Struct*., vol. 19, pp. 1311–1325

[34] Zhu, M., Worthington, E. and Njuguna, J. (2009): "Analyses of power output of piezoelectric energy-harvesting devices directly connected to a load resistor using a coupled piezoelectric-circuit finite element method", *IEEE Trans. Ultrason. Ferroelectr. Freq. Control,* vol. 56, pp. 1309–1317.

[35] Stanton, S.C., McGehee, C.C. and Mann, B.P. (2010): "Nonlinear dynamics for broadband energy harvesting: investigation of a bistable piezoelectric inertial generator", *Physica* D, vol. 239, pp. 640–653.

[36] Ottman, G.K., Hofmann, H.F., Bhatt, A.C. and Lesieutre, G.A. (2002): "Adaptive piezoelectric energy harvesting circuit for wireless remote power supply", *IEEE Trans. Power Electron.,* vol. 17, pp. 669–676.

[37] Lefeuvre, E., Badel, A., Richard, C., Petit, L. and Guyomar, D. (2006): "A comparison between several vibration-powered piezoelectric generators for standalone systems", *Sensors Actuators A*, vol. 126, pp. 405–416.

[38] Qiu, J., Jiang, H., Ji, H. and Zhu, K. (2009): “Comparison between four piezoelectric energy harvesting circuits”, *Front. Mech. Eng. China,* vol. 4, pp. 153–159.

[39] Shu, Y.C., Lien, I.C. and Wu, W.J. (2007): “An improved analysis of the SSHI interface in piezoelectric energy harvesting”, *Smart Mater. Struct*., vol. 16, pp. 2253–2264.

[40] Liu, Y., Tian, G., Wang, Y., Lin, J., Zhang, Q. and Hofmann, H.F. (2009): “Active piezoelectric energy harvesting: general principle and experimental demonstration”, *J. Intell. Mater. Syst. Struct*., vol. 20, pp. 575–585.

[41] Liu, W.Q., Feng, Z.H., He, J. and Liu, R.B. (2007): “Maximum mechanical energy harvesting strategy for a piezoelement”, *Smart Mater. Struct*., vol. 16, pp. 2130–2136.

[42] Scruggs, J.T. (2010): “On the causal power generation limit for a vibratory energy harvester in broadband stochastic response” J. Intell. Mater. Syst. Struct., vol. 21, no. 13, 1249-1262, September 2010.

[43] Tang, L., Yang, Y. and Soh, C.K. (2013): Broadband Vibration Energy Harvesting Techniques, Chapter 2, Advances in Energy Harvesting Methods, Elvin, N. and Erturk, A. (eds.), DOI 10.1007/978-1-4614-5705-3 2, Springer Science Business Media New York, pp. 17-61.

[44]. Cottone, F., Vocca, H., Gammaitoni, L. (2009): “Nonlinear Energy Harvesting”, *Phys. Rev. Lett.,* vol. 102, no. 8, 080601.

[45] Whitney, D. E. (2004): *Mechanical Assemblies: Their Design, Manufacture, and Role in Product Development*. New York, NY: Oxford University Press, p. 449.

[46] Wildschek, A. (2009): *An adaptive feed-forward controller for active wing bending vibration alleviation on large transport aircraft*. Munich, Germany: Verlag Dr. Hut, pp 9–22.

[47] Lomax, T. L. (1996): *Structural Loads Analysis for Commercial Transport Aircraft: Theory and Practice*. Reston, VA: AIAA Education Series.

[48] Barrett Jr., R. M. (“Low frequency machinery monitoring measurement considerations,” *Wilcoxon Research, Inc., Meggitt Group*, pp. 1-26.

[49] Zuber, N., Ličen, H. and Klašnja-Miličević, A. (2008): “Remote online condition monitoring of the bucket wheel excavator sr1300 - a case study”, *Facta Universitatis. Series. Working and Living Environmental Protection*, vol. 5.

[50] Saavedra, P. and Estupinan, E. (2002): “Vibration analysis applied to low-speed machines in the pulp and paper industry (Predictive Maintenance)”, Solutions - for People, Processes and Paper, January 1, 2002.

[51] Beeby, S. P., Tudor, M. J. and White, N. M. (2006): “Energy harvesting vibration sources for microsystems applications,” *Meas. Sci. Technol.,* vol. 17, no. 12, pp. R175–95, Dec 2006

[52] Antaki, J. F., Bertocci, G. E., Green, E. C., Nadeem, A., Rintoul, T., Kormos, R. L. and Griffith, B. P. (1995): "Gait-powered autologous battery charging system for artificial organs," *ASAIO Journal,* vol. 41, pp. 588-595.

[53] Barsoum, M. W. (2003): *Fundamentals of Ceramics*. Bristol and Philadelphia: IOP Publishing Ltd.

[54] Piezo System Inc., http://www.piezo.com, accessed on 13 September 2012.

[55] Measurement Specialities, http://www.meas-spec.com/myMeas/default/index.asp, accessed on 13 September 2012.

[56] Tljhen, W., Tamagawa, T., Ye, C.-P., Hsueh, C. C., Schiller, P. and Polla, D. L. (1991): "Properties of piezoelectric thin films for micromechanical devices and systems," *Proceedings of the IEEE Micro Electro Mechanical Systems, MEMS,* 30 January – 2 February 1991, Nara, Japan, pp. 114-119.

[57] Tsuchiya, K., Kitagawa, T., Uetsuji, Y. and Nakamachi, E. (2005): "Fabrication of smart material PZT thin films by RF magnetron sputtering, method in micro actuators," *Nihon Kikai Gakkai Ronbunshu, A Hen/Transactions of the Japan Society of Mechanical Engineers, Part A,* vol. 71, pp. 66-72.

[58] AZoM.com company (2001): Aluminium Nitride / Aluminum Nitride (AIN) - Properties and Applications, http://www.azom.com/Details.asp?ArticleID=610, accessed on 10 June 2011.

[59] Elfrink, R., Kamel, T. M., Goedbloed, M., Matova, S., Hohlfeld, D., Andel, Y. V. and Schaijk, R. V., (2009): “Vibration energy harvesting with aluminum nitride-based piezoelectric devices,” *Journal of Micromechanics and MicroEngineering*, Vol. 19, No. 9, Paper No. 094005.

[60] Kim, H. W., Priya, S., Uchino, K. and Newnham, R. E. (2005): “Piezoelectric energy harvesting under high pre-stressed cyclic Vibrations,” *Journal of Electroceramics*, Vol. 15, No. 1, pp. 27-34.

[61] Li, X., Guo, M. and Dong, S., (2011): “A flex-compressive-mode piezoelectric transducer for mechanical vibration/strain energy harvesting,” *IEEE Transactions on Ultrasonics, Ferroelectrics and Frequency Control*, Vol. 58, No. 4, pp. 698-703.

[62] Adhikari, S., Friswell, M. I. and Inman, D. J. (2009): “Piezoelectric energy harvesting from broadband random vibrations,” *Smart Materials and Structures*, Vol. 18, No. 11, Paper No. 115005.

[63]. Lefeuvre, E., Badel, A., Richard, C., Petit, L. and Guyomar, D., (2006): “A comparison between several vibration-powered piezoelectric generators for standalone systems,” *Sensors and Actuators A: Physical*, Vol. 126, No. 2, pp. 405-416.

[64] Yoon, H. S., Washington, G. and Danak, A., (2005): “Modeling, optimization, and design of efficient initially curved piezoceramic unimorphs for energy harvesting applications,” *Journal of Intelligent Material Systems and Structures*, vol. 16, no. 10, pp. 877-888.

[65] Yoon, H. S., Lee, Y. H., Lee, S. W. and Lee, C., (2008): “Energy Harvesting characteristics of PZT-5A under gunfire shock,” *Materials Letters*, vol. 62, no. 21-22, pp. 3632-3635.

[66] Chen, Z. G., Hu, Y. T. and Yang, J. S., (2007): “Piezoelectric generator based on torsional modes for power harvesting from angular vibrations,” *Applied Mathematics and Mechanics*, vol.28, no. 6, pp. 779-784.

[67] Elvin, N. G., Elvin, A. A. and Spector, M., (2001): “A self-powered mechanical strain energy sensor*,” Smart Materials and Structures*, vol. 10, no. 2, pp. 293-299.

[68] Roundy, S. and Wright, P. K., “A piezoelectric vibration based generator for wireless electronics,” *Smart Materials and Structures*, vol. 13, no. 5, pp. 1131-1142, 2004.

[69] Leland, E. S. and Wright, P. K., (2006): “Resonance tuning of piezoelectric vibration energy scavenging generators using compressive axial preload,” *Smart Materials and Structures*, vol. 15, no. 5, pp. 1413-1420.

[70] Shen, D., Park, J. H., Noh, J. H., Choe, S. Y., Kim, S. H., Wikle, H. C. and Kim, D. J., (2009): “Micromachined PZT cantilever based on SOI structure for low frequency vibration energy harvesting,” *Sensors and Actuators A: Physical*, vol. 154, no. 1, pp. 103-108.

[71] Liu, J., Fang, H., Xu, Z., Mao, X., Shen, X., Chen, D., Liao, H. and Cai, B., (2008): “A MEMS-based piezoelectric power generator array for vibration energy harvesting,” *Microelectronics Journal*, vol. 39, no. 5, pp. 802-806.

[72] Choi, W. J., Jeon, Y., Jeong, J. H., Sood, R. and Kim, S. G., (2006): “Energy harvesting MEMS device based on thin film piezoelectric Cantilevers,” *Journal of Electroceramics*, vol. 17, no. 2-4, pp. 543-548.

[73] *Worthington, E. L. (2010): Piezoelectric Energy Harvesting: Enhancing Power Output by Device Optimisation and Circuit Techniques,* Cranfield University, School of Applied Sciences, Microsystems and Nanotechnology Centre Department of Materials, (PhD Thesis).

[74] Zhu, M., Worthington, E. and Njuguna, J. (2009): “Analyses of power output of piezoelectric energy harvesting devices directly connected to a load resistor using a coupled piezoelectric-circuit finite element method”, *IEEE Trans. Ultrason. Ferroelectr. Freq. Control*, vol. 56, no. 7, pp. 1309-1317.

[75] Roundy, S., Wright, P. K. and Rabaey, J. M. (2004): *Energy Scavenging for Wireless Sensor Networks: With Special Focus on Vibrations*, Boston: Kluwer-Academic.

[76] Beeby, S. P., Tudor, M. J. and White, N. M. (2006): “Energy harvesting vibration sources for microsystems applications”, *Meas. Sci. Technol.*, vol. 17, R175-95.

[77] Tien, C. M. T. and Goo, N. S., (2010): “Use of a piezocomposite generating element in energy harvesting,” *Journal of Intelligent Material Systems and Structures*, vol. 21, no. 14, pp. 1427-1436.

[78] Wilkie, W. K., Bryant, R. G., Fox, R. L., Hellbaum, R. F., High, J. W., Jalink, A. J., Little, B. D., and Mirick, P. H. (2003): “*Piezoelectric macro-fiber composite actuator and method for making same*,” U.S. Patent 6 629 341, March 27, 2003.

[79] FACE International Corporation (2001): Thunder White Paper, www.faceinternational.com, accessed on 22 April 2012.

[80] Tsuchiya, K., Kitagawa, T., Uetsuji, Y. and Nakamachi, E. (2005): "Fabrication of smart material PZT thin films by RF magnetron sputtering, method in micro actuators," *Nihon Kikai Gakkai Ronbunshu, A Hen/Transactions of the Japan Society of Mechanical Engineers, Part A,* vol. 71, pp. 66-72.

[81] Antaki, J. F., Bertocci, G. E., Green, E. C., Nadeem, A., Rintoul, T., Kormos, R. L. and Griffith, B. P. (1995): "Gait-powered autologous battery charging system for artificial organs," *ASAIO Journal,* vol. 41, pp. 588-595.

[82] Sodano, H. A., Park, G. H., Leo, D. J. and Inman, D. J., (2003): “*Electric power harvesting using piezoelectric materials*,” Center for Intelligent Material Systems and Structures, Virginia Polytechnic Institute and State University.

[83] Priya, S. and Inman, D. J. (2009): *Energy Harvesting Technologies*, Springer Science+Business Media LLC, ISBN 978-0-387-76463-4, DOI 10.1007/978-0-387-76464-1.

[84] Sahele, M., H.F., Liu Y. and Hofmann (2005): “Piezoelectric energy harvesting using different approaches including control system”, *NSF EE REU PENN STATE Annual Research Journal*, vol. 3, pp. 134-141.

[85] Tabesh, A. and Fréchette, L.G. (2010): “A low-power stand-alone adaptive circuit for harvesting energy from a piezoelectric micropower generator”, *IEEE Transactions on Industrial Electronics*, vol. 57, no. 3, pp. 840-849.

[86] Umeda, T., Yoshida, H., Sekine, S., Fujita, Y., Suzuki, T., and Otaka, S. (2006): “A 950-MHz rectifier circuit for sensor network tags with 10-m

distance", *IEEE Journal of Solid-State Circuits*, vol. 41, no. 1, pp. 35-41, Jan. 2006

[87] Ghovanloo, M. and Najafi, K. (2004): "Fully integrated wideband high-current rectifiers for inductively powered devices", *IEEE Journal of Solid-State Circuits*, vol. 39, no. 11, pp. 1976-1984.

[88] Lam, Y. H., Ki, W. H. and Tsui, C. Y. (2006): "Integrated low-loss CMOS active rectifier for wirelessly powered devices*", IEEE Trans. Circuits Systems-II:Express Briefs*, vol. 53, pp. 1378-1382.

[89] Lehmann, T. and Moghe, Y. (2005): "On-chip active power rectifiers for biomedical applications", *IEEE Intl. Symp. Circuits Sys. ISCAS*, pp. 732-735.

[90] Cheng, S., Jin, Y., Rao, Y. and Arnold, D. P. (2009): "A bridge voltage doubler AC/DC converter for low-voltage energy harvesting applications", *PowerMEMS*, Washington DC, USA, December 01-04-09, pp. 25-28.

[91] Ghovanloo, M. and Najafi, K. (2004): "Fully integrated wideband high-current rectifiers for inductively powered devices", *IEEE J. Solid-State Circuits*, vol. 39, pp. 1976-84.

[92] Peters, C., Spreemann, D., Ortmanns, M. and Manoli, Y. (2008): "A CMOS integrated voltage and power efficient AC/DC converter for energy harvesting applications", *J. Micromech. Microeng.,* Vol. 18.

[93] Xu, S. and Chung, G-B. (2007): Low Frequency Pulsed Resonant Converter for Energy Harvesting, *IEEE Transactions on power electronics*, Vol. 22, No. 1, pp. 63.

[94] Le, T.T. (2008): *Efficient Power Conversion Interface Circuits for Energy Harvesting Applications*, Oregon State University, ISBN 9780549555285.

[95] Guilar, N. J., Amirtharajah, R. and Hurst, P. J. (2008): "A Full-Wave Rectifier for Interfacing with Multi-Phase Piezoelectric Energy Harvesters", *IEEE Int. Solid State Circ. Conf. (ISSCC) Dig. Tech. Pap*, vol. 615, pp. 302-303.

[96] Ottman, G.K. (2003): "Optimized Piezoelectric Energy Harvesting Circuit Using Step-Down Converter in Discontinuous Conduction Mode", *IEEE Transactions on Power Electronics*, vol. 18, no. 2, pp. 696-703.

[97] Park, J. K., Choi, W. Y. and Kwon, B. H. (2007): “A Step-Up DC–DC Converter With a Resonant Voltage Doubler”, *IEEE Transactions on industrial electronics*, vol. 54, no. 6, pp. 3267-75.

[98] Hyun-Lark Do, H. L. (2012): *Full-Bridge High Step-Up DC-DC Converter with Two Stage Voltage Doubler*, Advances in Electronic Engineering, Communication and Management, D. Jin and S. Lin (Eds.), Springer-Verlag Berlin Heidelberg, vol. 1, LNEE 139, pp. 251–254.

[99] Dickson, J. F. (1976): “On-chip high-voltage generation in MNOS integrated circuits using an improved voltage multiplier technique”, *IEEE Journal of Solid-State Circuits*, vol. 11, no. 3 pp. 374-378, June.

[100] Hara, N., Oota, I., Ueno F. and Inoue, T. (1998): “A ring type step-up switched capacitor DC-DC converter with low inrush current at start-up and low current ripplelin steady state”, *IEICE Trans. C-II*, vol. J81-C-II, no.7, pp.600-612.

[101] Hara, N., Oota, I., Ueno F. Harada, I. and Inoue, T. (1999): “Programable ring type switched capacitor DC-DC converters”, *IEICE Trans. C-II*, vol. J82-C-II, no.2, pp.56-68.

[102] Makowski, M. S. and Maksimovic, D. (1995): “Performance Limits of Switched-Capacitor DC-DC Converters”, *IEEE/PESC*, vol. 2, pp. 1215-1221.

[103] Doms, I., Merken, P. and Van Hoof, C. (2007): “Comparison of DC-DC-converter Architectures of Power Management Circuits for Thermoelectric Generators”, *Proceedings of 2007 European Conference on Power Electronics and Applications*, pp. 1-5.

[104] Lefeuvre, E., Audigier, D., Richard, C. and Guyomar, D. (2007): “Buck-Boost Convereter for Sensorless Power Optimization of Piezoelectric Energy Harvetser”, *IEEE Transactions on Power Electronics*, vol. 22, no. 5, pp. 2018-2025.

[105] Global Battery Markets, Battery University, http://batteryuniversity.com/learn/article/global_battery_markets, accessed on 15 November 2011.

[106] Lithium-based Batteries, Battery University, http://batteryuniversity.com/learn/article/lithium_based_batteries, accessed on 15 November 2011.

[107] Battery Knowledge, AA Portable Power Corp, http://www.batteryspace.com/batteryknowledge.aspx, accessed on 15 November 2011.

[108] Thinergy MEC200 Series, Digi-Key Corporation, http://www.digikey.com/product-highlights/us/en/infinite-power-solutions-thinergy-mec200/1775, accessed on 15 November 2011.

[109] Ottman, G.K., Hofmann, H.F. and Bhatt, A.C. and Lesieutre, G.A. (2002): "Adaptive piezoelectric energy harvesting circuit for wireless remote power supply", *IEEE Transactions on Power Electronics,* vol. 17, no. 5, pp. 669-676.

[110] Sodano, H.A., Inman, D. J. and Park, G. (2005): "Comparison of piezoelectric energy harvesting devices for recharging batteries", 2005, *Journal of Intelligent Material Systems and Structures*, Vol. 16, pp. 799-807.

[111] Chmiola, J., Yushin, G., Gogotsi, Y., Portet, C., Simon, P. and Taberna, P. L. (2006): "Anomalous Increase in Carbon Capacitance at Pore Sizes Less Than 1 Nanometer", *Science*, 10.1126/science.1132195, vol. 313, no. 5794, pp. 1760-1763.

[112] Conway, B.E. (1999): Scientific Fundamentals and Technological Applications in Electrochemical Supercapacitors, Kluwer Academic/Plenum, New York, USA

[113] Battery Developments, Buchmann, Isidor, http://batteryuniversity.com/learn/article/battery_developments, accessed on 15 September 2011.

[114] Switching Regulators, Texas Instruments (2012), http://www.ti.com/lit/an/snva559/snva559.pdf, accessed on 1 June 2013

[115] Bates, J. B., Dudney, N. J., Neudecker, B, Ueda, A. and Evans, C. D. (2000): "Thin-film lithium and lithium-ion batteries", *Solid State Ionics*, vol. 135, pp. 33-45.

[116] Brand, C. (2007): “A micro battery for low power applications”, *Proceedings of nanoPower Forum*, San Jose, USA, June 4-6, 2007.

[117] Nathan, M., Golodnitsky, D., Yufit, V., Strauss, E., Ripenbein, T., Shechtman, I., Menkin, S. and Peled, E. (2005): “Three dimensional (3d) thin film micro batteries”, *Proceedings of Symposium on Design, Test, Integration, Packaging of MEMS/MOEMS*, 2005.

[118] Marquardt, K., Hahn, R., Luger, T. and Reichl, H. (2006): “Assembly of and hermetic Encapsulation of wafer level secondary batteries”, *MEMS2006*, Istanbul, 22-26 January 2006, pp. 954-957.

[119] Hahn, R. (2006): “*Battery, especially a microbattery, and the production thereof using wafer-level technology*”, WO2005036689 (A3).

[120] Wang, W., Wang, N., Vinco, A., Siddique, R., Hayes, M., O`Flynn, B. and O`Mathuna, C. (2013): “Super-capacitor and Thin Film Battery Hybrid Energy Storage for Energy Harvesting Applications”, *PowerMEMS 2013, Journal of Physics: Conference Series* vol. 476, no. 1, 012105.

[121] Ongaro, F., Saggini, S. and Mattavelli, P. (2012): “Li-Ion Battery-Supercapacitor Hybrid Storage System for a Long Lifetime, Photovoltaic-Based Wireless Sensor Network”, *IEEE Transactions on Power Electronics*, vol. 27, no. 9, pp. 3944-3952, ISSN 0885-8993.

[122] Abdelkefi, A., Alothman, A. and Hajj, M. R. (2013): “Performance analysis and validation of thermoelectric energy harvesters”, *Smart Materials and Structures,* vol. 22, no. 9, 095014.

[123] Becker, T., Kluge, M., Schalk, J., Tiplady, K. Paget, C., Hilleringmann, U. and Otterpohl, T. (2009): “Autonomous Sensor Nodes for Aircraft Structural Health Monitoring”, *IEEE Sensors Journal*, vol. 9, no. 12, pp. 1589-1595, ISSN 1530-437X.

[124] Atmel Corporation (2011): ATMega 128, 8-bit Atmel Microcontroller with 128 kBytes In-System Programmable Flash, Revision Letter 2467XS–AVR–06/11, http://www.atmel.com/Images/2467s.pdf, accessed on 7 February 2014.

[125] Texas Instrument Inc. (2014): MSP430™Ultra-Low-Power Microcontrollers Brochure 1H14,

http://www.ti.com/lit/sg/slab034x/slab034x.pdf, accessed on 7 February 2014.

[126] NXP Laboratories UK (2010): JN5148-001-Myy JenNet, ZigBee PRO and IEEE802.15.4 Module, http://www.jennic.com/files/support_files/JN-DS-JN5148MO-1v4.pdf, Rev. JN-DS-JN5148-001-Myy 1v4, accessed on 7 February 2014.

[127] Moser, C., Thiele, L., Brunelli, D. and Benini, L. (2007): "Adaptive power management in energy harvesting systems", *Proceedings - Design, Automation and Test in Europe, DATE*, 2007, pp. 773- 778.

[128] Vigorito, C. M., Ganesan, D. and Barto, A. G. (2007): "Adaptive control of duty cycling in energy-harvesting wireless sensor networks", *4th Annual IEEE Communications Society Conference on Sensor, Mesh and Ad Hoc Communications and Networks, SECON*, 2007, pp. 21-30.

[129] Hsu, J., Zahedi, S., Kansal, A., Srivastava, M. and Raghunathan, V. (2006): "Adaptive duty cycling for energy harvesting systems", *Proceedings of the International Symposium on Low Power Electronics and Design*, 2006, pp. 180-185.

[130] Kansal, A., Hsu, J., Srivastava, M. and Raghunathan, V. (2006): "Harvesting aware power management for sensor networks", *DAC '06 Proceedings of the 43rd annual Design Automation Conference*, pp. 651-656.

[131] Pimentel, D. and Musilek, P. (2010): "Power management with energy harvesting devices", *23rd Canadian Conference on Electrical and Computer Engineering (CCECE)*, 2-5 May 2010, Calgary, AB, pp. 1 – 4.

[132] Min, R., Bhardwaj, M., Cho, S.-H., Shih, E., Sinha, A., Wang, A., Chandrakasan, A. and Sinha, A. (2001): "Low-Power Wireless Sensor Networks", *14th International Conference on VLSI Design*, 3-7 January 2011, Bangalore, pp. 205-210.

[133] Levis, P., Madden, S., Polastre, J., Szewczyk, R., Whitehouse, K., Woo, A., Gay, D., Hill, J., Welsh, M., Brewer, E. and Culler, D. (2005): "TinyOS: An Operating System for Sensor Networks, Part II", *Ambient Intelligence*, Weber, W. et al. (ed.), Springer Berlin Heidelberg, pp. 115-148.

[134] Karl, H. and Willig, A. (2007): *Protocols and Architectures for Wireless Sensor Networks*, John Wiley & Sons, 497, ISBN 0470519231, 9780470519233

[135] Heinzelman, W. R., Chandrakasan, A. and Balakrishnan, H. (2000): “Energy-efficient communication protocol for wireless microsensor networks, System Sciences”, *Proceedings of the 33rd Annual Hawaii International Conference*, 4-7 January 2000

[136] Chang, R.-S. and Kuo, C.-J. (2006): “An energy efficient routing mechanism for wireless sensor networks”, *20th International Conference on Advanced Information Networking and Applications AINA* 18-20 April 2006, vol. 2.

[137] Demirkol, I., Ersoy, C. and Alagoz, F. (2006): “MAC protocols for wireless sensor networks: a survey”, *IEEE Communications Magazine*, vol. 44, no. 4, pp. 115 – 121.

[138] Ahmad, M. R., Dutkiewicz, E. and Huang, X. (2011): *A Survey of Low Duty Cycle MAC Protocols in Wireless Sensor Networks*, Chapter 5, Emerging Communications for Wireless Sensor Networks, Foerster, A. and Foerster, A. (eds.), 7 February 2011,CC BY-NC-SA 3.0 license, ISBN 978-953-307-082-7.

[139] Elson, J. and Estrin, D. (2000): "An address-free architecture for dynamic sensor networks." *Computer Science Department USC, Tech. Rep. 00-724*.

[140] Erturk, A. and Inman, D. (2008): “On mechanical modeling of cantilevered piezoelectric vibration energy harvesters,” *Journal of Intelligent Material Systems and Structures*, vol. 19, no. 11, pp. 1311–25, Apr 2008.

[141] Zhu, M., Worthington, E. and Njuguna, J. (2009): “Analyses of power output of piezoelectric energy-harvesting devices directly connected to a load resistor using a coupled piezoelectric-circuit finite element method,” *IEEE Trans. Ultrason., Ferroelect., Freq. Contr.*, vol. 56, no. 7, pp. 1309–17, Jul 2009.

[142] Andò, B., Baglio, S., Trigona, C., Dumas, N., Latorre, L., Nouet, P. (2010): “Nonlinear mechanism in MEMS devices for energy harvesting pplications”, *J. Micromechan. Microeng.,* vol. 20, no. 12, 125020.

[143] Shu, Y. C., Lien, I. C. and Wu, W. J. (2007): “An improved analysis of the SSHI interface in piezoelectric energy harvesting,” *Smart Mater. Struct.*, vol. 16, no. 6, pp. 2253–64, Dec 2007.

[144] Jackson, H. W. (1959): *Introduction to Electronic Circuits*. Englewood Cliffs, NJ: Prentice-Hall.

[145] Renno, J. M., Daqaq, M. F. and Inman, D. J. (2009): “On the optimal energy harvesting from a vibration source,” *J. Sound Vib.*, vol. 320, no. 1-2, pp. 386–405, Feb 2009.

[146] Brufau-Penella J. and Puig-Vidal, M. (2009): “Piezoelectric energy harvesting improvement with complex conjugate impedance matching,” *J. of Intell. Mater. Syst. and Struct.*, vol. 20, no. 5, pp. 597–608, Mar 2009.

[147] Tellegen, B. D. H. (1948): “The gyrator, a new electronic network element”, *The Netherlands : Philips Research Reports*, vol. 3, pp. 81-101.

[148] Radatz, J. (1997): *The IEEE Standard Dictionary of Electrical and Electronics terms (6th ed.),* Institute of Electrical and Electronics Engineers*,* New York IEEE 1997. ISBN 1-55937-833-6.

[149] Ford, R.L. and Girling, F.E.J. (1966): “Active filters and oscillators using simulated inductance”, *Electronics Letters*, vol. 2, no. 2, p. 52.

[150] Prescott, A.J. (1966): “Loss-compensated active gyrator using differential-input operational amplifiers”*, Electronics Letters*, vol. 2, no. 7, pp. 283-284.

[151] Berndt, D. and Dutta Roy, S.C. (1969): “Inductor simulation using a single unity gain amplifier”*, Journal of Solid-State Circuits (Corresp.)*, vol. 4, no. 3, pp. 161-162.

[152] Keen, A.W. and Peters,J.L. (1967): “Inductance simulation with a single differential-input operational amplifier”, *Electronics Letters*, vol. 3, no. 4, pp. 136-137.

[153] Roy, S.C.D. and Nagarajan, V. (1970): “On inductor simulation using a unity-gain amplifier”, *IEEE Journal of Solid-State Circuits*, vol. 5, no. 3, pp. 95-98.

[154] Riordan, R.H.S. (1967): “Simulated inductors using differential amplifiers”*, Electronics Letters*, vol. 3, no. 2, pp. 50-51.

[155] Antoniou, A. (1967): “Gyrators using operational amplifiers”, *Electronics Letters*, vol. 3, no. 8, pp. 350-352.

[156] Inigo, R.M. (1971): “Gyrator realization using two operational amplifiers”, *IEEE J. Solid-State Circuits*, vol. 6, no. 2, pp. 88-89.

[157] Antoniou, A. and Naidu, K. (1973): “Modeling of a gyrator circuit”, *IEEE Transactions on Circuit Theory*, vol. 20, no. 5, pp. 533-540.

[158] Roy, S.D. (1963): “The Inductive Transistor”, *IEEE Transactions on Circuit Theory*, vol. 10, no. 1, pp. 113-115.

[159] Shenoi, B. (1965): “Practical Realization of a Gyrator Circuit and RC-Gyrator Filters”, *IEEE Transactions on Circuit Theory*, vol. 12, no. 3, pp. 374-380.

[160] . Su, K. L. (1966): “F.E.T.-circuit realisation of the inductance”, *Electronics Letters*, Vol. 2, no. 12, pp. 469-470.

[161] Radhakrishna Rao, K. and Venkateswaran, S. (1970): “Synthesis of inductors and gyrators with voltage-controlled voltage sources”, *Electronics Letters*, vol. 6, no. 2, pp. 29-30.

[162] Patranabis, D. (1970): “Inductor realization with a negative impedance converter”, *Electronics Letters*, vol. 6, no. 13, pp. 415-417.

[163] Patranabis, D. and Paul, A.N. (1980): “Floating inductor with two current conveyors”, *International Journal of Circuit Theory and Applications*, vol. 8, no. 4, pp. 457-461.

[164] Patranabis, D. (1971): “Inductorless modified Colpitts oscillator”, *International Journal of Electronics*, vol. 30, no. 4, pp. 395-399.

[165] Saggini, S., Giro, S., Ongaro, F. and Mattavelli, P. (2010): “Implementation of reactive and resistive load matching for optimal energy harvesting from piezoelectric generators,” *IEEE 12th Workshop on Control and Modeling for Power Electronics (COMPEL)*, 28-30 June 2010, Boulder, CO, pp. 1–6.

[166] Ottman, G. K., Hofmann, H. F., Bhatt, A. C. and Lesieutre, G. A. (2002): “Adaptive Piezoelectric energy harvesting circuit for wireless remote power supply,” *IEEE Trans. Power Electron.*, vol. 17, no. 5, pp. 669–76, Sep 2002.

[167] Ottman, G. K., Hofmann, H. F., Bhatt, A. C. and Lesieutre, G. A. (2003): “Optimized piezoelectric energy harvesting circuit using step-down converter in discontinuous conduction mode,” *IEEE Trans. Power Electron.*, vol. 18, no. 2, pp. 696–703, Mar 2003.

[168] Lefeuvre, E., Audigier, D., Richard, C. and Guyomar, D. (2007): “Buck-boost converter for sensorless power optimization of piezoelectric energy harvester,” *IEEE Trans. Power Electron.*, vol. 22, no. 5, pp. 2018–25, Sep 2007.

[169] Lallart M. and Inman, D. J. (2010): “Low-cost integrable tuning-free converter for piezoelectric energy harvesting optimization,” *IEEE Trans. Power Electron.*, vol. 25, no. 7, pp. 1811–19, Jul 2010.

[170] Xu, S., Ngo, K.D.T., Nishida, T., Gyo-Bum, C. and Sharma, A. (2005): ‘‘Converter and Controller for Micro-power Energy Harvesting,’’ *IEEE Applied Power Electronics Conference and Exposition*, vol.1, pp. 226-230.

[171] Kong, N., Ha, D. S., Erturk, A. and Inman, D. J. (2010): “Resistive impedance matching circuit for piezoelectric energy harvesting,” *J. of Intell. Mater. Syst. and Struct.*, vol. 21, no. 13, pp. 1293–302, Sep 2010.

[172] Kim, H., Priya, S., Stephanou, H. and Uchino, K. (2007): “Consideration of impedance matching techniques for efficient piezoelectric energy harvesting,” *IEEE Trans. Ultrason., Ferroelect., Freq. Contr.*, vol. 54, no. 9, pp. 1851–9, Sep 2007.

[173] Guyomar, D., Sebald, G., Pruvost, S., Lallart, M., Khodayari, A., Richard, C. (2009): “Energy harvesting from ambient vibrations and heat”, *J. Intell. Mater. Syst. Struct.,* vol. 20, pp. 609-624.

[174] Lallart, M., Guyomar, D., Richard, C. and Petit, L. (2010): “Nonlinear optimization of acoustic energy harvesting using piezoelectric devices”, *J. Acoust. Soc. Am.*, vol. 128, pp. 2739-2748.

[175] Ammar Y. and Basrour, S. (2007): “Non-linear techniques for increasing harvesting energy from piezoelectric and electromagnetic micro-power-generators,” *Dans Symposium on Design, Test, Integration and Packaging (DTIP) of MEMS / MOEMS*, Stresa, Italy, 26-28 April 2006, The Computing Research Repository (CoRR), November 2007.

[176] Andò, B., Baglio, S., Trigona, C., Dumas, N., Latorre, L. and Nouet, P. (2010): “Nonlinear mechanism in MEMS devices for energy harvesting applications”, *J. Micromechan. Microeng.*, vol. 20, no. 12, 125020.

[177] Arrieta, A.F., Hagedorn, P., Erturk, A., Inman, D.J. (2010): “A piezoelectric bistable plate for nonlinear broadband energy harvesting”, *Appl. Phys. Lett.*, vol. *97*, no. 10, 104102.

[178] Taylor, G.W., Burns, J.R., Kammann, S.M., Powers, W.B. and Welsh, T.R. (2001): “The energy harvesting eel: A small subsurface ocean/river power generator”, *IEEE J. Ocean. Eng.,* vol. 26, pp. 539-547.

[179] Wu, W.J., Wickenheiser, A.M., Reissman, T. and Garcia, E. (2008): “Modeling and experimental verification of synchronized discharging techniques for boosting power harvesting from piezoelectric transducers”, *Smart Mater. Struct.,* vol. 18, no. 5, 055012.

[180] Erturk, A. and Inman, D.J. (2008): “Issues in mathematical modeling of piezoelectric energy harvesters”, *Smart Mater. Struct.*, vol. 17, no. 6, 065016.

[181] Lallart, M., Garbuio, L., Petit, L., Richard, C. and Guyomar, D. (2008): “Double Synchronized Switch Harvesting (DSSH): A new energy harvesting scheme for efficient energy extraction”, *IEEE Trans. Ultrason. Ferroelectrics Freq. Contr.,* vol. 55, no. 10, pp. 2119-2130.

[182] Shen, H., Qiu, J., Ji, H., Zhu, K. and Balsi, M. (2010): “Enhanced synchronized switch harvesting: A new energy harvesting scheme for efficient energy extraction”, *Smart Mater. Struct.*, vol. 19, no. 11, 115017.

[183] Lallart, M. and Guyomar, D. (2010): “Piezoelectric conversion and energy harvesting enhancement by initial energy injection”, *Appl. Phys. Lett.*, vol. 97, no. 1, 014104.

[184] Lefeuvre, E., Sebald, G., Guyomar, D., Lallart, M. and Richard, C. (2009): “Materials, structures and power interfaces for efficient piezoelectric energy harvesting”, *J. Electroceram*., vol. 22, pp. 171-179

[185] Liu, Y., Tian, G., Wang, Y., Lin, J., Zhang, Q. and Hofman, H.F. (2009): “Active piezoelectric energy harvesting: general principles and experimental demonstration”, *J. Intell. Mater. Syst. Struct.*, vol. *20*, pp. 575-585.

[186] D. Guyomar and M. Lallart, “Recent progress in piezoelectric conversion and energy harvesting using nonlinear electronic interfaces and issues in small scale implementation,” *Micromachines*, vol. 2, no. 2, pp. 274–94, Jun 2011.

[187] Qiu, J., Jiang, H., Ji, H. and Zhu, K. (2009): “Comparison between four piezoelectric energy harvesting circuits”, *Front. Mech. Eng. China*, vol. *4*, pp. 153-159.

[188] Lallart, M., Lefeuvre, E., Richard, C. and Guyomar, D. (2008): “Self-powered circuit for broadband, multimodal piezoelectric vibration control”, *Sens. Actuat. A: Phys.*, vol. 143, pp. 377-382.

[189] Shen, H., Qiu, J., Ji, H., Zhu, K., Balsi, M., Girogio, I. and Dell’Isola, F. (2010): “A low-power circuit for piezoelectric vibration control by synchronized switching on voltage sources”, *Sens. Actuat. A Phys.*, vol. 161, pp. 245-255.

[190] Niederberger, D. and Morari, M. (2006): “An autonomous shunt circuit for vibration damping”, *Smart Mater. Struct.*, vol. 15, pp. 359-364.

[191] Richard C., Guyomar, D. and Lefeuvre, E. (2007): *Self-Powered Electronic Breaker with Automatic Switching by Detecting Maxima or Minima of Potential Difference between Its Power Electrodes*, Patent # PCT/FR2005/003000, Publication number: WO/2007/063194, 7 June 2007.

[192] Xu, S., Ngo K.D.T., Nishida, T., Chung, G.-B. and Sharma, A. (2007): “Low frequency pulsed resonant converter for energy harvesting”, *IEEE Trans. Ultrason. Ferroelectrics Freq. Contr*, vol. 22, pp. 63-68.

[193] Hehn, T., Peters, C., Hagedorn, F., Ortmanns, M. and Manoli, Y. (2008): “A CMOS Integrated Interface for Piezoelectric Generators”, *Technical Digest, PowerMEMS* 2008, Sendai, Japan, November 2008, pp. 457-460.

[194] M. Lallart and D. Guyomar (2008) “An optimized self-powered switching circuit for non-linear energy harvesting with low voltage output,” *Smart. Mater. Struct*., vol. 17, no.3, pp. 035030-035038.

[195] Ferrari, M., Ferrari, V., Guizzetti, M., Andò, B., Baglio, S., Trigona, C. (2010): “Improved energy harvesting from wideband vibrations by nonlinear piezoelectric converters”, *Sens. Actuat. A: Phys.*, vol. 162, pp. 425-431.

[196] D'hulst, R. and Driesen, J. (2008): "Power Processing Circuits for Vibration-based Energy Harvesters: An Integrated Approach", *Technical Digest, PowerMEMS*, Sendai, Japan, November 2008; pp. 453-456.

[197] Garbuio, L., Lallart, M., Guyomar, D., Richard, C. and Audigier, D. (2009): "Mechanical energy harvester with ultralow threshold rectification based on SSHI nonlinear technique", *IEEE Trans. Ind. Electron.*, vol. 56, pp. 1048-1056.

[198] Lallart, M., Richard, C., Garbuio, L., Petit, L. and Guyomar, D. (2010): "High efficiency, wide load bandwidth piezoelectric energy scavenging by a hybrid nonlinear approach", *Sens. Actuat. A: Phys.*, vol. 165, no. 2, pp. 294-302.

[199] Tiwari, R., Ryoo, K., Schlichting, A. and Garcia, E. (2013): "Extremely low-loss rectification methodology for low-power vibration energy harvesters", *Smart Mater. Struct.*, vol. 22, no. 6, 062001.

[200] Kansal, A., Hsu, J., Zahedi, S. and Srivastava, M. B. (2007): "Power management in energy harvesting sensor networks," *ACM Transactions on Embedded Computing Systems*, vol. 6, no. 4.

[201] NASA (2008): Hydrogen research for Spaceport and space-based applications" http://gltrs.grc.nasa.gov/reports/2008/CR-2008-215440-PART2.pdf, accessed on 13 September 2011.

[202] Paradiso, J. A. and Feldmeier, M. (2001): A Compact, Wireless, Self-Powered Pushbutton Controller, *Lecture Notes in Computer Science, MIT Media Laboratory,* Vol. 2201, pp 299-304.

[203] Yuen, S. C. L. (2004): Low Power Wireless Sensor Applications, Department of Computer Science & Engineering, *The Chinese University of Hong Kong,* June, 2004 (PhD Thesis).

[204] Perpetuum (2013): VEH Vibration Energy Harvester Datasheet, 21 October 2013, http://www.perpetuum.com/access.asp?doc=4, accessed on 26 april 2014

[205] Elvin, N., Elvin, A. and Choi, D. H. (2003): "A self-powered damage detection sensor," *J. Strain Analysis*, vol. 38, no. 2, pp. 115–24, Jan 2003.

[206] Lallart, M., Guyomar, D., Jayet, Y., Petit, L., Lefeuvre, E., Monnier, T., Guy, P. and Richard, C. (2008): “Synchronized switch harvesting applied to selfpowered smart systems: piezoactive microgenerators for autonomous wireless receiver,” *Sens. Actuators A: Phys.*, vol. 147, no. 1, pp. 263–72, Sept. 2008.

[207] Churchill, D. L., Hamel, M. J., Townsend, C. P. and Arms, S. W. (2003): “Strain energy harvesting for wireless sensor networks,” *Proc. Smart Struct. Mater. Conf. Proc. SPIE*, vol. 5055, pp. 319–27, Jul 2003.

[208] Arms, S. W., Townsend, C. P., Galbreath, J. H., Churchill, D. L., Augustin, M., Yeary, D., Darden, P. and Phan, N. (2007): “Tracking pitch link dynamic loads with energy harvesting wireless sensors,” *American Helicopter Society 63rd Annual Forum*, Virginia Beach, VA, May 1–3, 2007.

[209] Stupar, S., Simonovic, A. and Jovanovic, M. (2012): “Measurement and analysis of vibrations on the helicopter structure in order to detect defects of operating elements,” *Scientific Technical Review*, vol. 62, no. 1, pp. 58–63, 2012.

[210] Zhu, D., Beeby, S. P., Tudor, M. J. and Harris, N. R. (2011): “A credit card sized self powered smart sensor node,” *Sens. Actuators A: Phys.*, vol. 169, no. 2, pp. 317–25, Oct 2011.

[211] Anton S. R. and Inman, D. J. (2008): “Vibration energy harvesting for unmanned aerial vehicles,” *Proc. of the 15th SPIE Annual International Symposium on Smart Structures and Materials & Nondestructive Evaluation and Health Monitoring*, vol. 6928, pp. 692824-1–12, Apr 2008.

[212] Galea, S. C., Velden, S. V. D., Powlesland, I., Nguyen, Q., Ferrarotto, P. and Konak, M. (2006): “Flight demonstrator of a self-powered SHM system on a composite bonded patch attached to an F/A-18 aileron hinge,” *Asia-Pacific Workshop on Structural Health Monitoring*, 4–6 December 2006, Yokohama, Japan, pp. 146–154.

[213] Farrar, C. R. and Lieven, N. A. J. (2007): “Damage prognosis: the future of structural health monitoring,” *Phil. Trans. R. Soc. A*, vol. 365, pp. 623–32, Feb 2007.

[214] Wilson, W. and Atkinson, G. (2008): “Wireless sensing opportunities for aerospace applications,” *Sens. & Transd. J.*, vol. 94, no. 7, pp. 83–90, Jul 2008.

[215] Yedavalli, R. K. and Belapurkar, R. K. (2011): “Application of wireless sensor networks to aircraft control and health management systems,” *J. Control Theory Appl.*, vol. 9, no. 1, pp. 28–33, Feb 2011.

[216] Pozzi, M., Guo, S. and Zhu, M. (2012): Harvesting energy from the dynamic deformation of an aircraft wing under gust loading, *Proc. SPIE 8348, Health Monitoring of Structural and Biological Systems*, vol. 834831 (April 26, 2012); doi:10.1117/12.917039

[217] Saavedra, P. and Estupinan, E. (2002): “Vibration analysis applied too low-speed machines in the pulp and paper industry,” vol.1, no. 3, pp.5–10, May 2002.

[218] Barrett Jr., R. M. (“Low frequency machinery monitoring measurement considerations,” *Wilcoxon Research, Inc., Meggitt Group*, pp. 1-26.

[219] Zuber, N., Ličen, H. and Klašnja-Miličević, A. (2008): “Remote online condition monitoring of the bucket wheel excavator sr1300 - a case study”, *Facta Universitatis. Series. Working and Living Environmental Protection*, vol. 5.

[220] Saavedra, P. and Estupinan, E. (2002): “Vibration analysis applied to low-speed machines in the pulp and paper industry (Predictive Maintenance)”, Solutions - for People, Processes and Paper, January 1, 2002.

[221] Miller, L. M., Halvorsen, E., Dong, T., and Wright, P. K. (2011): “Modelling and experimental verification of low-frequency MEMS energy harvesting from ambient vibrations”, *J. Micromech. Microeng.*, vol. 21, no. 4, 045029, doi:10.1088/0960-1317/21/4/045029.

[222] Sodano, H. A. (2003): “Macro-Fiber Composites for Sensing, Actuation and Power Generation”, Faculty of the Virginia Polytechnic Institute and State University, Blacksburg, Virginia, July 28, 2003 (PhD Thesis).

[223] Smart Material Corp. (2011): Macro Fiber Composite (MFC) brochure (MFC-V2.0-2011), Sarasota, FL., http://www.smart-material.com/Datasheets.html, accessed on 12 September 2012.

[224] IEEE Standard on Piezoelectricity (1988): ANSI/IEEE Standard 176-1987, NSPEC Accession Number: 3237638.

[225] Timoshenko, S. (2012):"Stress and deformation analysis of linear elastic beams in bending", Chapter 13, *History of Strength of Materials,* pp. 297-356.

[226] HAMLIN Inc. (2008): "Reed Switch and Reed Sensor Activation", HAMLIN Application Note AN104, https://www.sparkfun.com/datasheets/Components/Buttons/AN104.pdf, accessed on 23 October 2012.

[227] HAMLIN Electronics (Europe) Ltd (2002): "Single Pole Form A Proximity Device", 1059600495, http://datasheet.octopart.com/59600-495-Hamlin-datasheet-577996.pdf, accessed on 23 October 2012.

[228] Guyomar, D., Badel, A., Lefeuvre, E. and Richard, C. (2005): "Toward energy harvesting using active materials and conversion improvement by nonlinear processing," *IEEE Trans. Ultrason. Ferroelectr. Freq. Control*, vol. 52, no. 4, pp.584-595.

[229] Lien, I. C., Shu, Y. C., Wu, W. J., Shiu, S. M. and Lin, H. C. (2010): "Revisit of series-SSHI with comparisons to other interfacing circuits in piezoelectric energy harvesting", *Smart Mater. Struct.,* vol. 19, no. 12, 125009, doi:10.1088/0964-1726/19/12/125009.

[230] Physik Instrumente (PI) GmbH & Co. (2012): "Electronic Module for Energy Harvesting Using Piezo Actuators for Energy Generation E-821", R2 12/09/11.02, http://www.piceramic.com/datasheet/E821_Datasheet.pdf, accessed on 28 February 2014.

[231] Marsic, V., Zhu, M. and Williams, S. (2012): "Wireless sensor communication system with low sensor power consumption for integration with energy harvesting technology," *Telfor J.*, vol. 4, no. 2, pp. 89–94.

[232] Fleming, A. J., Behrens, S. and Moheimani, S. O. R. (2003): "Reducing the inductance requirements of piezoelectric shunt damping systems," *Smart Mater. Struct.*, vol. 12, no. 1, pp. 57–64, Feb 2003.